

P881-122525

REPORT NO.  
UCB/EERC-80/04  
FEBRUARY 1980

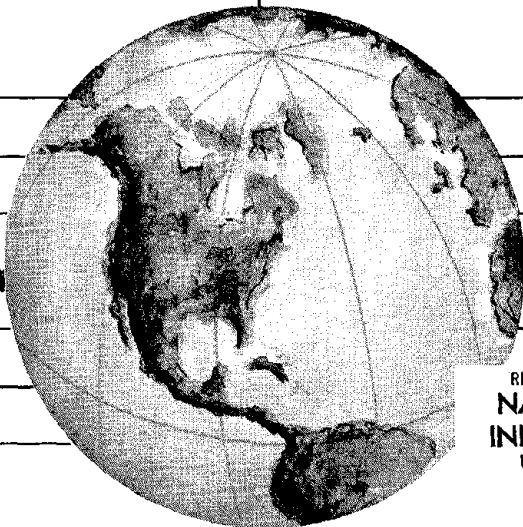
EARTHQUAKE ENGINEERING RESEARCH CENTER

# EFFECTS OF AMOUNT AND ARRANGEMENT OF WALL-PANEL REINFORCEMENT ON HYSTERETIC BEHAVIOR OF REINFORCED CONCRETE WALLS

by

RAMZI ILIYA  
VITELMO V. BERTERO

Report to National Science Foundation



REPRODUCED BY  
**NATIONAL TECHNICAL  
INFORMATION SERVICE**  
U. S. DEPARTMENT OF COMMERCE  
SPRINGFIELD, VA. 22161

COLLEGE OF ENGINEERING

UNIVERSITY OF CALIFORNIA · Berkeley, California



<b>REPORT DOCUMENTATION PAGE</b>	<b>1. REPORT NO.</b> NSF/RA-800191	<b>2.</b>	<b>3. Recipient's Accession No.</b> PB01 12 25 25
<b>4. Title and Subtitle</b> Effects of Amount and Arrangement of Wall-Panel Reinforcement on Hysteretic Behavior of Reinforced Concrete Walls			<b>5. Report Date</b> February 1980
<b>7. Author(s)</b> Ramzi Iliya and Vitelmo V. Bertero			<b>6.</b>
<b>9. Performing Organization Name and Address</b> Earthquake Engineering Research Center University of California, Richmond Field Station 47th and Hoffman Blvd. Richmond, California 94804			<b>8. Performing Organization Rept. No.</b> UCB/EERC-80/04
			<b>10. Project/Task/Work Unit No.</b>
			<b>11. Contract(C) or Grant(G) No.</b> (C) (G) ENV76-04263 PFR-7908984
<b>12. Sponsoring Organization Name and Address</b> National Science Foundation 1800 G. Street, N.W. Washington, D. C. 20550			<b>13. Type of Report &amp; Period Covered</b>
			<b>14.</b>
<b>15. Supplementary Notes</b>			
<b>16. Abstract (Limit: 200 words)</b> This report presents the experimental results obtained in the third phase of an ongoing investigation on the seismic behavior of reinforced concrete walls. The ultimate objectives of this investigation are to find ways of designing and constructing R/C walls with large energy absorption and dissipation capacities under the effects of severe seismic excitations and to develop practical methods for the seismic design of combined wall-frame structural systems. Although the main objective of the studies reported here was to investigate the effects of the amount and arrangement of wall-panel reinforcement on the overall seismic performance of the walls, additional objectives were to study (1) the effectiveness of the epoxy injection technique for repairing damaged walls, (2) methods of strengthening walls after their local failure, and (3) the effects of construction joints.  Two one-third scale models of the three bottom stories of the wall of a ten-story frame-wall R/C building designed according to UBC/73 seismic code requirements were constructed and studied experimentally. In one model equal amounts of horizontal and vertical reinforcement were used in the wall panel, while in the other specimen the panel reinforcement was arranged diagonally at 45°.  Each specimen was subjected to three series of three tests. In the first series, the specimen was loaded under generalized loading (cyclic with full reversals) up to first yielding of all the reinforcing bars at the edge member in tension. Then the specimen was repaired by injecting epoxy in the cracks. In the second series, after being loaded with full deformation reversal cycles up to first yielding, the specimen was loaded with monotonically increasing deformations up to failure, which occurred in the first story. After repairing and strengthening this first story, the model was loaded under cyclic loading, inducing full deformation reversals, up to failure.  The results obtained are evaluated and discussed in detail and then compared with the results from experiments carried out on the six previous specimens studied in the first and second phases of the ongoing investigation.  The report concludes with some recommendations for improving present seismic code provisions and for future research.			
<b>18. Availability Statement:</b>  Release Unlimited	<b>19. Security Class (This Report)</b>	<b>21. No. of Pages</b>	
	<b>20. Security Class (This Page)</b>	<b>22. Price</b>	



EFFECTS OF AMOUNT AND ARRANGEMENT OF WALL-PANEL REINFORCEMENT  
ON HYSTERETIC BEHAVIOR OF REINFORCED CONCRETE WALLS

by

Ramzi Iliya  
Research Assistant  
Department of Civil Engineering  
University of California, Berkeley

Vitelmo V. Bertero  
Professor of Civil Engineering  
University of California, Berkeley

Report to Sponsor:  
National Science Foundation

Report No. UCB/EERC-80/04  
Earthquake Engineering Research Center  
College of Engineering  
University of California  
Berkeley, California

February 1980



## ABSTRACT

This report presents the experimental results obtained in the third phase of an ongoing investigation on the seismic behavior of reinforced concrete walls. The ultimate objectives of this investigation are to find ways of designing and constructing R/C walls with large energy absorption and dissipation capacities under the effects of severe seismic excitations and to develop practical methods for the seismic design of combined wall-frame structural systems. Although the main objective of the studies reported here was to investigate the effects of the amount and arrangement of wall-panel reinforcement on the overall seismic performance of the walls, additional objectives were to study (1) the effectiveness of the epoxy-injection technique for repairing damaged walls, (2) methods of strengthening walls after their local failure, and (3) the effects of construction joints.

Two one-third scale models of the three bottom stories of the wall of a ten-story frame-wall R/C building designed according to UBC/73 seismic code requirements were constructed and studied experimentally. In one model equal amounts of horizontal and vertical reinforcement were used in the wall panel, while in the other specimen the panel reinforcement was arranged diagonally at  $45^{\circ}$ .

Each specimen was subjected to three series of three tests. In the first series, the specimen was loaded under generalized loading (cyclic with full reversals) up to first yielding of all the reinforcing bars at the edge member in tension. Then the specimen was repaired by injecting epoxy in the cracks. In the second series, after being loaded with full deformation reversal cycles up to first yielding, the specimen was loaded with monotonically increasing deformations up to failure, which occurred in the first story. After repairing and strengthening this first story, the model was loaded under cyclic loading, inducing full deformation reversals, up to failure.

The results obtained are presented, evaluated and discussed in detail and then compared with the results from experiments carried out on the six previous specimens studied in the first and second phases

of the ongoing investigation. The conclusion drawn from the evaluation and comparison of these results is that the overall behavior of the specimens tested in this third phase was satisfactory despite the fact that the design of the wall panel against shear did not satisfy present UBC seismic code requirements. The diagonal arrangement of the panel reinforcement resulted in better behavior than the vertical and horizontal reinforcing bar arrangement. While the epoxy injection technique could not completely restore the stiffness of the virgin specimen, stiffness was sufficiently restored to produce acceptable behavior under service as well as yielding load levels. The repair and strengthening techniques used permitted the restored specimen to develop a lateral resistance even larger than that observed in the virgin specimen, but did not restore the ductility of the latter. The construction joint behaved very well although the lap splicing of the reinforcement did not satisfy minimum code requirements.

The report concludes with some recommendations for improving present seismic code provisions and for future research.



## ACKNOWLEDGMENTS

The study reported herein was conducted as part of a larger research project, "Seismic Behavior of Structural Components" (E. P. Popov, Principal Investigator), with financial support provided by the National Science Foundation under Grant No. ENV76-04263, Subproject No. 0-21198, and Grant No. PFR-7908984, Subproject No. 0-22002. However, any opinions, discussions, findings, conclusions, and/or recommendations are those of the authors and do not necessarily reflect the views of the National Science Foundation.

Much of the work reported was undertaken by Ramzi Iliya, under the direction of V. V. Bertero, as CE299, an Individual Study in his Master of Science program of studies. The authors would like to express their gratitude to B. Lotz and D. Clyde who constructed the test specimens and provided valuable assistance in conducting the experiments. Thanks are due also to W. Neighbour for his assistance throughout the experiment, M.C. Randall and E. Matthews who provided editorial assistance, and D. Ullman for preparing the figures.



## TABLE OF CONTENTS

	<u>Page</u>
ABSTRACT . . . . .	i
ACKNOWLEDGMENTS . . . . .	iii
TABLE OF CONTENTS . . . . .	v
LIST OF TABLES . . . . .	xi
LIST OF FIGURES . . . . .	xiii
1. INTRODUCTION . . . . .	1
1.1 General Remarks . . . . .	1
1.2 Review of Available Literature . . . . .	2
1.3 Objectives and Scope . . . . .	4
2. TEST SPECIMENS . . . . .	7
2.1 Selection of Test Specimens . . . . .	7
2.1.1 Prototype Building . . . . .	7
2.1.2 Selection of Test Specimens . . . . .	8
2.2 Review of Specimens Tested up to the Present . . . . .	8
2.2.1 Phase I . . . . .	8
2.2.2 Phase II . . . . .	9
2.2.3 Phase III . . . . .	9
2.3 Design of Specimens SW7 and SW8 . . . . .	9
2.3.1 Wall-Panel Reinforcement . . . . .	9
2.3.1.1 Do Specimens SW1 and SW2 Satisfy the UBC/76? . . . . .	10
2.3.1.2 Wall Reinforcement for Specimens SW7 and SW8 . . . . .	11
2.3.2 Edge Column of Walls . . . . .	17
2.4 Mechanical Characteristics of Model Materials . . . . .	17
2.4.1 Concrete . . . . .	18
2.4.2 Steel Reinforcing Bars . . . . .	18
2.4.2.1 No. 6 Bars . . . . .	18
2.4.2.2 No. 2 Bars . . . . .	18
2.4.2.3 Spiral Reinforcement . . . . .	19
2.5 Fabrication of Specimens . . . . .	19

	<u>Page</u>
3. EXPERIMENTAL SETUP AND TESTING PROCEDURE . . . . .	21
3.1 Selection of Loading Conditions to be Imposed on the Specimen . . . . .	21
3.2 Experimental Setup . . . . .	22
3.2.1 General Setup . . . . .	22
3.3 Specimen Instrumentation and Data Acquisition System .	22
3.3.1 External Instrumentation . . . . .	22
3.3.1.1 Measurement of Lateral Displacement .	22
3.3.1.2 Measurement of Shear Distortion . . .	23
3.3.1.3 Photogrammetric Measurements . . . .	23
3.3.2 Internal Instrumentation . . . . .	23
3.3.3 Data Acquisition System . . . . .	24
3.4 Determination of Total Lateral Load . . . . .	24
4. TEST RESULTS AND THEIR EVALUATION . . . . .	27
4.1 Introductory Remarks . . . . .	27
4.1.1 Loading Histories . . . . .	28
4.1.2 Base Shear vs. Lateral Displacement ( $P_T - \delta_R$ Diagrams) . . . . .	28
4.1.3 Base Shear vs. Shear Distortions ( $P_T - \gamma_R$ Diagrams) . . . . .	29
4.1.4 Flexural Deformation and Fixed-End Rotation . .	29
4.1.5 Maximum Values of Base Shear, Lateral Displacement, and Overturning Moments . . . .	29
4.2 Specimen SW7. . . . .	29
4.2.1 Results of Tests on Virgin Specimen . . . . .	30
4.2.1.1 Base Shear vs. Total Lateral Displacement: Specimen SW7 Virgin . .	30
4.2.1.2 Base Shear vs. Shear Deformation . . .	31
4.2.1.3 Other Sources of Deformation . . . . .	31
4.2.1.4 Concluding Remarks . . . . .	32
4.2.2 Results of Tests on Epoxy-Repaired Specimen, SW7 R <sub>1</sub> . . . . .	32
4.2.2.1 Base Shear vs. Total Lateral Displacement: Specimen SW7 R <sub>1</sub> . . . .	33
4.2.2.2 Base Shear vs. Shear Deformation: Specimen SW7 R <sub>1</sub> . . . . .	35
4.2.2.3 Other Sources of Deformation . . . . .	37

	<u>Page</u>
4.2.2.4 Failure Mechanism . . . . .	37
4.2.2.5 Concluding Remarks . . . . .	38
4.2.3 Results of Tests on Repaired and Strengthened Specimen: SW7 R <sub>2</sub> . . . . .	39
4.2.3.1 Base Shear vs. Total Lateral Displacement: Specimen SW7 R <sub>2</sub> . . . . .	39
4.2.3.2 Base Shear vs. Shear Deformation: Specimen SW7 R <sub>2</sub> . . . . .	42
4.2.3.3 Other Sources of Deformation: Specimen SW7 R <sub>2</sub> . . . . .	44
4.2.3.4 Failure Mode: SW7 R <sub>2</sub> . . . . .	44
4.2.3.5 Concluding Remarks . . . . .	46
4.3 Specimen SW8 . . . . .	46
4.3.1 Results of Tests on the Virgin Specimen: SW8 Virgin . . . . .	47
4.3.1.1 Base Shear vs. Total Lateral Displacement: Specimen SW8 Virgin . . . . .	47
4.3.1.2 Base Shear vs. Shear Deformation: Specimen SW8 Virgin . . . . .	49
4.3.1.3 Other Sources of Deformation: Specimen SW8 Virgin . . . . .	50
4.3.1.4 Concluding Remarks . . . . .	51
4.3.2 Results of Tests on Epoxy-Repaired Specimen: SW8 R <sub>1</sub> . . . . .	51
4.3.2.1 Base Shear vs. Total Lateral Displacement: Specimen SW8 R <sub>1</sub> . . . . .	52
4.3.2.2 Base Shear vs. Shear Deformation: Specimen SW8 R <sub>1</sub> . . . . .	53
4.3.2.3 Other Sources of Deformation: SW8 R <sub>1</sub> . . . . .	55
4.3.2.4 Failure Mode: SW8 R <sub>1</sub> . . . . .	56
4.3.2.5 Concluding Remarks . . . . .	56
4.3.3 Results of Tests on Repaired and Strengthened Specimen: SW8 R <sub>2</sub> . . . . .	57
4.3.3.1 Base Shear vs. Total Lateral Displacement: Specimen SW8 R <sub>2</sub> . . . . .	57
4.3.3.2 Base Shear vs. Shear Deformation: Specimen SW8 R <sub>2</sub> . . . . .	59
4.3.3.3 Other Sources of Deformation: Specimen SW8 R <sub>2</sub> . . . . .	60
4.3.3.4 Failure Mode: SW8 R <sub>2</sub> . . . . .	63
4.3.3.5 Concluding Remarks . . . . .	64

	<u>Page</u>
4.4 Lateral Displacement Components: Comments on the Variation of Displacement Components with Ductility Graphs . . . . .	64
4.4.1 Introductory Remarks . . . . .	64
4.4.2 Specimen SW7 . . . . .	65
4.4.3 Specimen SW8 . . . . .	66
5. REPAIRING AND STRENGTHENING TECHNIQUES . . . . .	67
5.1 Introductory Remarks . . . . .	67
5.2 Damage to Virgin Specimens . . . . .	67
5.3 Damage to Epoxy-Repaired Specimens . . . . .	67
5.3.1 Specimen SW7 R <sub>1</sub> . . . . .	67
5.3.2 Specimen SW8 R <sub>1</sub> . . . . .	68
6. COMPARISON OF BEHAVIOR OF SPECIMENS SW7 and SW8 . . . . .	69
6.1 General . . . . .	69
6.2 Virgin Specimens . . . . .	69
6.3 Epoxy-Repaired Specimens (R <sub>1</sub> ) . . . . .	70
6.4 Twice-Repaired Specimens (R <sub>2</sub> ) . . . . .	72
6.5 Concluding Remarks . . . . .	73
7. COMPARISON OF BEHAVIOR OF SPECIMENS SW7 AND SW8 WITH BEHAVIOR OF PREVIOUSLY TESTED SPECIMENS . . . . .	75
7.1 Introductory Remarks . . . . .	75
7.2 Comparison of Specimens SW7 and SW8 with Specimens SW1 and SW2 . . . . .	75
7.2.1 Monotonically-Loaded Specimens . . . . .	76
7.2.2 Cyclically-Loaded Specimens . . . . .	76
7.3 Comparison of Specimens SW7 and SW8 with Specimens SW3 and SW4 . . . . .	76
7.3.1 Comparison of Specimen SW3 with SW7 R <sub>1</sub> (Monotonic Loading) . . . . .	76
7.3.2 SW4 R vs. SW7 R <sub>1</sub> (Monotonic Loading) . . . . .	77
7.3.3 SW3 vs. SW8 R <sub>1</sub> . . . . .	77
7.3.4 SW3 R vs. SW7 R <sub>2</sub> (Cyclic Loading) . . . . .	78
7.3.5 SW3 R vs. SW8 R <sub>2</sub> (Cyclic Loading) . . . . .	78
7.3.6 SW4 vs. SW7 R <sub>2</sub> and SW8 R <sub>2</sub> . . . . .	78
7.4 SW5 and SW6 vs. SW7 and SW8 . . . . .	78
7.5 Concluding Remarks . . . . .	79

	<u>Page</u>
8. CONCLUSIONS AND RECOMMENDATIONS . . . . .	81
8.1 Conclusions . . . . .	81
8.1.1 Overall Behavior . . . . .	81
8.1.2 Effects of Amount and Arrangement of the Wall-Panel Reinforcement . . . . .	82
8.1.3 Effectiveness of Repair and Strengthening Techniques . . . . .	84
8.1.4 Effectiveness of Construction Joints . . . . .	86
8.2 Recommendations . . . . .	86
8.2.1 Recommendations for Improving Present Seismic Code Provisions . . . . .	86
8.2.2 Recommendations for Future Research . . . . .	87
REFERENCES . . . . .	89
TABLES . . . . .	93
FIGURES . . . . .	103





LIST OF TABLES

<u>Table</u>		<u>Page</u>
1(a)	Mechanical Characteristics of Materials Specimens SW7 and SW8 . . . . .	95
1(b)	Comparison of Experimentally Determined Values of $E_c$ vs. Those Calculated by ACI Empirical Equations .	95
2	Displacement Components--SW7 $R_1$ . . . . .	96
3	Displacement Components--SW7 $R_2$ . . . . .	97
4	Displacement Components--SW8 and SW8 $R_1$ . . . . .	98
5	Displacement Components--SW8 $R_2$ . . . . .	99
6	Comparison of Specimen Results . . . . .	100



LIST OF FIGURES

<u>Figure</u>		<u>Page</u>
1.1	Prototype Building (a) Typical Floor Plan; (b) Elevation . . . . .	105
1.2(a)	Elevation View of SW7 . . . . .	105
1.2(b)	Section Showing Barbell Cross-Sectional Type Specimens SW7 and SW8 . . . . .	105
1.3	Dimensions and Details of SW7 . . . . .	106
1.4	Dimensions and Details of SW8 (a) Elevation of SW8; (b) Section of SW8 . . . . .	106
2.1	Stress-Strain Diagrams for Concrete Specimens-- SW7 and SW8 (First Story) Virgin Specimens . . . . .	107
2.2	Stress-Strain Diagrams for Concrete Specimens-- SW7 (Second and Third Stories) Virgin Specimen . . . . .	107
2.3	Stress-Strain Diagrams for Concrete Specimens-- SW8 (Second and Third Stories) Virgin Specimen . . . . .	107
2.4	Stress-Strain Diagrams of Reinforcement for SW7 and SW8 . . . . .	108
3.1	Shear and Moment Diagrams of a Single N-S Wall When Subjected to One Half the 1.4 (E + Torsion) Code Forces . . . . .	108
3.2	Loading Conditions of Prototype and Model . . . . .	109
3.3	Plan and General View of Testing Facility (a) Plan; (b) General View . . . . .	111
3.4	External Instrumentation of Wall Specimen . . . . .	112
3.5	Error in Lateral Displacement Measurement . . . . .	112
3.6	Grid for Photogrammetric Measurement . . . . .	113
3.7	Internal Instrumentation for Specimen SW7 . . . . .	113
3.8	Internal Instrumentation for Specimen SW8 . . . . .	114
3.9	Horizontal Component of Net Axial Force . . . . .	114
4.1(a)	Loading History--Specimens SW7 Virgin + SW7 Epoxy-Repaired . . . . .	115
4.1(b)	Displacement History--Specimen SW7 Virgin + SW7 Epoxy-Repaired . . . . .	115
4.2	Loading Program--Specimen SW7 R <sub>2</sub> (a) Loading History; (b) Displacement History . . . . .	116
4.3	Total Lateral Load, V, vs. Third-Story Displacement Envelope--Specimen SW7: Virgin, Epoxy-Repaired, Twice-Repaired . . . . .	117

<u>Figure</u>	<u>Page</u>
4.4(a) Total Lateral Load, V, vs. Third-Floor Relative Displacement Diagram, $\delta_{3R}$ --Specimen SW7 Virgin . . . . .	117
4.4(b) Total Lateral Load, V, vs. Third-Floor Relative Displacement Diagram, $\delta_{3R}$ --Specimen SW7 R <sub>1</sub> Epoxy-Repaired . . . . .	117
4.5(a) Total Lateral Load, V, vs. Second-Floor Relative Displacement Diagram, $\delta_{2R}$ --Specimen SW7 Virgin . . . . .	118
4.5(b) Total Lateral Load, V, vs. Second-Floor Relative Displacement Diagram, $\delta_{2R}$ --Specimen SW7 R <sub>1</sub> Epoxy-Repaired . . . . .	118
4.6(a) Total Lateral Load, V, vs. First-Floor Relative Displacement Diagram, $\delta_{1R}$ --Specimen SW7 Virgin . . . . .	119
4.6(b) Total Lateral Load, V, vs. First-Floor Relative Displacement Diagram, $\delta_{1R}$ --Specimen SW7 R <sub>1</sub> Epoxy-Repaired . . . . .	119
4.7 Total Lateral Load, V, vs. Third-Floor Lateral Displacement Diagram, $\delta_{3R}$ --Specimen SW7 R <sub>2</sub> . . . . .	120
4.8 Total Lateral Load, V, vs. Second-Floor Lateral Displacement, $\delta_{2R}$ --Specimen SW7 R <sub>2</sub> . . . . .	120
4.9(a) Total Lateral Load, V, vs. First-Floor Lateral Displacement Diagram, $\delta_{1R}$ --Specimen SW7 R <sub>2</sub> . . . . .	121
4.9(b) Total Lateral Load, V, vs. First-Floor Lateral Displacement Diagram, $\delta_{1R}$ --Specimen SW7 R <sub>2</sub> . . . . .	121
4.10(a) Total Lateral Load, V, vs. Third-Story Shear Distortion, $\gamma_3$ --Specimen SW7 Virgin . . . . .	122
4.10(b) Total Lateral Load, V, vs. Third-Story Shear Distortion, $\gamma_3$ --Specimen SW7 Epoxy-Repaired . . . . .	122
4.11(a) Total Lateral Load, V, vs. Second-Story Shear Distortion, $\gamma_2$ --Specimen SW7 Virgin . . . . .	123
4.11(b) Total Lateral Load, V, vs. Second-Story Shear Distortion, $\gamma_2$ --Specimen SW7 Epoxy-Repaired . . . . .	123
4.12(a) Total Lateral Load, V, vs. First-Story Shear Distortion, $\gamma_1$ --Specimen SW7 Virgin . . . . .	124
4.12(b) Total Lateral Load, V, vs. First-Story Shear Distortion, $\gamma_1$ --Specimen SW7 Epoxy-Repaired . . . . .	124
4.13 Total Lateral Load, V, vs. Third-Story Shear Distortion, $\gamma_3$ --Specimen SW7 R <sub>2</sub> . . . . .	125
4.14 Total Lateral Load, V, vs. Second-Story Shear Distortion, $\gamma_2$ --Specimen SW7 R <sub>2</sub> . . . . .	125

<u>Figure</u>	<u>Page</u>
4.15	Total Lateral Load, V, vs. First-Story Shear Distortion, $\gamma_1$ --Specimen SW7 R <sub>2</sub> . . . . . 126
4.16	Loading Program--Specimen SW8 Virgin + SW8 Epoxy-Repaired (a) Loading History; (b) Displacement History . . . . . 127
4.17	Loading Program--Specimen SW8 R <sub>2</sub> (a) Loading History; (b) Displacement History . . . . . 128
4.18	Total Lateral Load, V, vs. Third-Floor Relative Displacement Envelope, $\delta_{3R}$ --Specimen SW8: Virgin, Epoxy-Repaired, Twice-Repaired . . . . . 129
4.19	Total Lateral Load, V, vs. Third-Floor Relative Displacement, $\delta_{3R}$ --Specimen SW8: Virgin + Epoxy-Repaired . . . . . 129
4.20	Total Lateral Load, V, vs. Second-Floor Relative Displacement, $\delta_{2R}$ --Specimen SW8: Virgin + Epoxy-Repaired . . . . . 130
4.21	Total Lateral Load, V, vs. First-Floor Relative Displacement, $\delta_{1R}$ --Specimen SW8: Virgin + Epoxy-Repaired . . . . . 130
4.22	Total Lateral Load, V, vs. Third-Floor Relative Displacement, $\delta_{3R}$ --Specimen SW8 R <sub>2</sub> . . . . . 131
4.23	Total Lateral Load, V, vs. Second-Story Relative Displacement, $\delta_{2R}$ --Specimen SW8 R <sub>2</sub> . . . . . 131
4.24	Total Lateral Load, V, vs. First-Story Lateral Displacement, $\delta_{1R}$ --Specimen SW8 R <sub>2</sub> . . . . . 132
4.25	Total Lateral Load, V, vs. First-Story Shear Distortion, $\gamma_1$ --Specimen SW8 Virgin . . . . . 132
4.26	Total Lateral Load, V, vs. Second-Story Shear Distortion, $\gamma_2$ --Specimen SW8: Virgin + Epoxy-Repaired . . . . . 133
4.27	Total Lateral Load, V, vs. First-Story Shear Distortion, $\gamma_1$ --Specimen SW8: Virgin + Epoxy-Repaired . . . . . 133
4.28	Total Lateral Load, V, vs. Third-Story Shear Distortion, $\gamma_3$ --Specimen SW8 R <sub>2</sub> . . . . . 134
4.29	Total Lateral Load, V, vs. Second-Story Shear Distortion, $\gamma_2$ --Specimen SW8 R <sub>2</sub> . . . . . 134
4.30	Total Lateral Load, V, vs. First-Story Shear Distortion, $\gamma_1$ --Specimen SW8 R <sub>2</sub> . . . . . 135

<u>Figure</u>	<u>Page</u>
4.31	Variation of Displacement Components with Ductility (Third Story)--Specimen SW7 Virgin . . . . . 135
4.32	Variation of Displacement Components with Ductility (Second Story)--Specimen SW7 Virgin . . . . . 135
4.33	Variation of Displacement Components with Ductility (First Story)--SW7 Virgin . . . . . 136
4.34	Variation of Displacement Components with Ductility (Third Story)--SW7 Virgin and SW7 Epoxy-Repaired . . 136
4.35	Variation of Displacement Components with Ductility (Second Story)--Specimens SW7 Virgin and SW7 Epoxy- Repaired . . . . . 137
4.36	Variation of Displacement Components with Ductility (First Story)--Specimens SW7 Virgin and SW7 Epoxy- Repaired . . . . . 137
4.37	Variation of Displacement Components with Ductility (Third Story)--Specimen SW7 R <sub>2</sub> . . . . . 138
4.38	Variation of Displacement Components with Ductility (Second Story)--Specimen SW7 R <sub>2</sub> . . . . . 138
4.39	Variation of Displacement Components with Ductility (First Story)--Specimen SW7 R <sub>2</sub> . . . . . 138
4.40	Variation of Displacement Components with Ductility (Third Story)--Specimen SW8 Virgin . . . . . 138
4.41	Variation of Displacement Components with Ductility (Second Story)--Specimen SW8 Virgin . . . . . 139
4.42	Variation of Displacement Components with Ductility (First Story)--Specimen SW8 Virgin . . . . . 139
4.43	Variation of Displacement Components with Ductility (Third Story)--Specimen SW8 Virgin + SW8 Epoxy- Repaired . . . . . 139
4.44	Variation of Displacement Components with Ductility (Second Story)--Specimen SW8 Virgin and SW8 Epoxy- Repaired . . . . . 140
4.45	Variation of Displacement Components with Ductility (First Story)--Specimen SW8 Virgin and SW8 Epoxy- Repaired . . . . . 140
4.46	Variation of Displacement Components with Ductility (Third Story)--Specimen SW8 R <sub>2</sub> . . . . . 140
4.47	Variation of Displacement Components with Ductility (Second Story)--Specimen SW8 R <sub>2</sub> . . . . . 141

<u>Figure</u>	<u>Page</u>
4.48	Variation of Displacement Components with Ductility (First Story)--Specimen SW8 R <sub>2</sub> . . . . . 141
4.49	Excessive Cracking at First-Story Level of Specimen SW7 Epoxy-Repaired. LP 904, $\mu_{\delta} = 3$ . . . . . 141
4.50	Crushing of Concrete in the North Corner of First-Story Wall Panel of Specimen SW7 Epoxy-Repaired. LP 1145, $\mu_{\delta} = 6.4$ . . . . . 142
4.51	Crack at Base of Second-Story South Column of Specimen SW7 R <sub>2</sub> . LP 125, $\delta_{3R} = 1''$ . . . . . 142
4.52	Diagonal Cracks in Second-Story Wall Panel of Specimen SW7 R <sub>2</sub> . LP 125, $\delta_{3R} = 1''$ . . . . . 142
4.53	Diagonal Cracking and Localized Concrete Crushing of Third-Story Wall Panel of Specimen SW7 R <sub>2</sub> . LP 159, $\delta_{3R} = 1''$ . . . . . 142
4.54	Diagonal Cracking and Localized Concrete Crushing of Second-Story Wall Panel of Specimen SW7 R <sub>2</sub> . LP 310, $\delta_{3R} = 1\ 1/2''$ , $\mu_{\delta} = 2$ . . . . . 143
4.55	Cracks Extending from Upper North Corner of Third-Story Wall Panel to Face of Second-Story Slab of Specimen SW7 R <sub>2</sub> . LP 450 . . . . . 143
4.56	Spalling of Crushed Concrete in Upper North Corner of Third-Story Wall Panel of Specimen SW7 R <sub>2</sub> . LP 450 . . . . . 143
4.57	Failure Zone: Third-Story Wall Panel of Specimen SW7 R <sub>2</sub> . Excessive Crushing of Concrete and Buckling of Panel Reinforcement. LP 547, $\mu_{\delta} = 3$ . . . . . 143
4.58	Failure Zone: Third-Story Wall Panel of Specimen SW7 R <sub>2</sub> . Exposed and Buckled Panel Reinforcement. End of Test . . . . . 144
4.59	Wide Cracks in the First-Story Level of the South Column of Specimen SW8 R <sub>1</sub> . LP 701, $\delta_{3R} = 3.7''$ , $\mu_{\delta} = 5.9$ . . . . . 144
4.60	Further Widening of Cracks in First-Story Level of South Column of Specimen SW8 R <sub>1</sub> . Propagation of Cracks into Wall Panel. LP 766, $\delta_{3R} = 6''$ , $\mu_{\delta} = 9.75$ . 144
4.61	Crushing of Concrete at Base of First-Story North Column of Specimen SW8 R <sub>1</sub> . LP 766, $\delta_{3R} = 6''$ , $\mu_{\delta} = 9.75$ . . . . . 144
4.62	Loading to the South after Failure of Specimen SW8 R <sub>1</sub> . Crushing of Concrete Cover at Base of First-Story South Column. Buckling of Wall-Panel Reinforcement and Fracture of Spiral. LP 800. End of Experiment . 145

<u>Figure</u>	<u>Page</u>
4.63	Appearance of First Major Cracks at Second-Story Level of South Column of Specimen SW8 R <sub>2</sub> . LP 142, $\mu_{\delta} = 1$ . . . . . 145
4.64	Diagonal Cracking in Second-Story Wall Panel of Specimen SW8 R <sub>2</sub> . LP 142, $\mu_{\delta} = 1$ . . . . . 145
4.65	Localized Crushing of Concrete and Buckling of Reinforcement in Third-Story Wall Panel of Specimen SW8 R <sub>2</sub> . LP 247, $\mu_{\delta} = 2$ . . . . . 146
4.66	Failure of Concrete Cover at Top of First-Story South Column of Specimen SW8 R <sub>2</sub> . LP 361 . . . . . 146
4.67	Specimen SW8 R <sub>2</sub> . LP 383, $\mu_{\delta} = 2.18$ . (a) Wide Crack Initiated at Base of South Column due to Tension Failure of Longitudinal Reinforcement; (b) Propagation of Crack into First-Story Wall Panel Adjacent to Foundation . . . . . 147
4.68	Increased Localized Crushing of Concrete in Third-Story Wall Panel, Accompanied by Buckling of Wall-Panel Reinforcement of Specimen SW8 R <sub>2</sub> . LP 383, $\mu_{\delta} = 2.18$ . . . . . 148
4.69	Specimen SW8 R <sub>2</sub> after Failure, LP 558. Failure of Longitudinal Reinforcement at Base of First-Story South Column as well as Failure of First-Story Wall-Panel Reinforcement . . . . . 148
5.1	Dowels Originally Placed at First-Story Level to Facilitate Strengthening of Specimen SW7 . . . . . 149
5.2	First-Story Repairs on Specimen SW7 after Failure of Specimen SW7 Epoxy-Repaired . . . . . 149
5.3	Section X'-X (Fig. 5.2)--Splice Detail Showing First-Story Column Repairs on Specimen SW7 after Failure of Specimen SW7 Epoxy-Repaired . . . . . 150
5.4	Stress-Strain Diagrams for Concrete Specimens--Specimen SW7 R <sub>2</sub> (Repaired) . . . . . 150
5.5	View Showing Placement of Repair Steel at First-Story Level--Specimen SW8 Virgin . . . . . 151
5.6	Stress-Strain Diagrams for Concrete Specimens--Specimen SW8 R <sub>2</sub> (Repaired) . . . . . 151
5.7	Repairing and Strengthening Techniques for First Stories of Specimens SW7 R <sub>1</sub> and SW8 R <sub>1</sub> . . . . . 152
5.8	Repairing and Strengthening Techniques for Specimens SW7 and SW8 (Welded Splice of Longitudinal Reinforcement in First-Story Columns) . . . . . 152



<u>Figure</u>		<u>Page</u>
5.9	Repairing and Strengthening Techniques for Specimens SW7 and SW8 (Two No. 9 Bars Butt Welded on Outer Edges at Base of First-Story Columns; Bars Extend to First-Floor Slab) . . . . .	153
5.10	Repairing and Strengthening Techniques for Specimens SW7 and SW8 . . . . .	153
6.1	Effect of Arrangement of Wall Reinforcement on the Load-Displacement Relationship-- Monotonic Loading. Specimens SW7 and SW8 Epoxy-Repaired . . . . .	154
6.2	Effect of Arrangement of Reinforcement on Amount of First-Story Shear Distortion. Specimens SW7 and SW8 Virgin . . . . .	154
6.3	Effect of Arrangement of Reinforcement on Amount of First-Story Shear Distortion-- Monotonic Loading. Specimens SW7 R <sub>1</sub> and SW8 R <sub>1</sub> . . . . .	155
6.4	Effect of Arrangement of Reinforcement on Load-Displacement Relationship--Cyclic Loading. Specimens SW7 R <sub>2</sub> and SW8 R <sub>2</sub> . . . . .	155
6.5	Effect of Arrangement of Reinforcement on Amount of Third-Story Shear Distortion--Cyclic Loading. Specimens SW7 R <sub>2</sub> and SW8 R <sub>2</sub> . . . . .	156
6.6	Effect of Arrangement of Reinforcement on the Amount of Second-Story Shear Distortion--Cyclic Loading. Specimens SW7 R <sub>2</sub> and SW8 R <sub>2</sub> . . . . .	156



## 1. INTRODUCTION

### 1.1 General Remarks

Due to uncertainties regarding the magnitude and characteristics of future earthquakes, it is seldom economically feasible to design structures to resist major earthquake shaking elastically [1,2,3]. According to present design philosophy, a building should be able to:

- (a) Resist frequent minor earthquake ground shaking without undergoing structural or nonstructural damage;
- (b) Resist occasional moderate earthquake shaking with only minor nonstructural damage;
- (c) Resist rare major earthquake shaking without suffering serious damage or collapse.

To be more specific, a structural system must be able to provide the building with sufficient stiffness under service loading, as well as sufficient strength and energy absorption and dissipation capacities, to withstand severe seismic excitations.

Many structures of low and medium height consist of ductile moment-resistant frames. However, as the height of the structure increases--for example, to more than 10 stories [4,5]--it is more efficient to provide the building with the required lateral strength and stiffness by means of a frame system interacting with structural walls. Because they are designed to resist the total lateral shear forces, these walls are referred to as "shear walls." However, a wall could be designed such that its failure mechanism will be controlled by flexural behavior, thereby providing a considerable amount of energy absorption and dissipation capacities. Such a wall must have a large length-to-depth ratio (greater than two for a cantilever wall loaded in the top [6]) and can be referred to as a "flexural wall."

In order to study the behavior of structures using shear or flexural walls as their main lateral force-resisting element under major earthquake excitations, it is essential to have information on the hysteretic behavior of such walls.

**Preceding page blank**

## 1.2 Review of Available Literature

Although wall systems have been used extensively in actual buildings, information on their hysteretic behavior is sparse, especially for medium- and high-rise walls. According to damage studies of past earthquakes [7-11], some structures with wall elements performed very well. Other structures with similar wall elements collapsed or suffered heavy damage during severe earthquakes. Damage to the latter was primarily due to poor design or poor construction and not due to the inadequacy of the wall-frame system itself.

Various studies on the seismic behavior of shear walls and wall-frame systems have been performed, as well as studies on the damage to existing structures from severe earthquakes [12-16]. In the past 25 years, most experimental data have been obtained from tests of one- and two-story reinforced concrete walls which were subjected to simplified loading conditions. These "squat" walls had rectangular cross-sections [17], I-sections [18], or wall panels with boundary elements [19-22].

Cardenas and Magura [17] tested several rectangular high-rise walls under static loading conditions and found that, depending on the percentage and distribution of the vertical reinforcement, the behavior of this kind of wall is controlled by either shear or flexure. It was also found that, to achieve large ductility, it is necessary to concentrate the vertical reinforcement near the outer vertical edges of the wall cross-section. It is also necessary to provide good confinement for the concrete near the edges of the wall and to prevent buckling of the vertical reinforcement at the same locations.

There is a lack of reliable data regarding the behavior of tall slender (flexural) walls. These walls have the potential for providing high strength, stiffness, and energy absorption and dissipation capacities. In 1972, therefore, it was decided to conduct an investigation of such walls at the University of California, Berkeley. The study reported herein is part of this ongoing research. The aim of the investigation begun at Berkeley was to determine the effects of several parameters on the mechanical behavior of reinforced concrete

walls. These parameters include: (a) loading history; (b) cross-section type (whether barbell or rectangular); (c) wall reinforcement (amount and arrangement); (d) shear stress; (e) methods of concrete confinement at edge members; and (f) flexibility of the foundation.

The investigation was broken down into several phases, starting with analysis of available data, planning of the research program, design and fabrication of test facilities, and analytical and experimental studies. The experimental studies began with two framed walls (of barbell cross-section) with spirally reinforced edge-columns labeled specimens SW1 and SW2. These walls were designed according to the 1973 Uniform Building Code [23]. This part of the study was carried out by Wang [24].

The second series of experiments dealt with four walls (specimens SW3 through SW6), and were carried out by Vallenias [25]. Specimens SW3 and SW4 were framed walls (barbell cross-section) with stirrups providing the concrete confinement in the edge columns. The amount of wall-panel reinforcement in specimens SW3 and SW4 was identical to that of wall-panel reinforcement for specimens SW1 and SW2.

Thus, the parameters studied in the first two series of experiments were: the shape (cross-section) of the walls; the types of edge-column confinement; the shear stress; and the effect of loading history programs (whether cyclic or monotonic). In both series, special emphasis was placed upon the effects of the above parameters on the stiffness, strength, plastic hinge rotation, ductility, and energy dissipation capacity of the walls, as well as on their modes of failure. The variations in the critical damping ratio and in the frequency of the wall with degree of damage induced in the walls were also studied by measuring these values after the specimens were subjected to different levels of loading and damage. The effectiveness of present methods of repairing structures was a secondary objective.

The third series of experiments dealt with two framed walls with spiral reinforcement at the edge columns (specimens SW7 and SW8), and is the series reported herein. Specimen SW7 differed from specimens SW1 and SW2 only in that its wall panel contained one-half the amount of

reinforcement that existed in specimens SW1 and SW2. Specimen SW8 contained the same amount of wall-panel reinforcement as that of specimen SW7, but it was differently arranged (diagonally at  $45^{\circ}$ ). In this series, emphasis was placed on the effect of the amount and arrangement of the wall-panel reinforcement on the mechanical behavior of the walls.

Further research is needed before knowledge about the behavior of walls or wall-frame systems under seismic excitations is complete. The ultimate objectives of the general investigation are: (a) to discover whether it is possible to design and construct walls that allow ductile behavior under severe seismic excitations; and, if so, (b) to use these walls in complete wall-frame systems; and (c) to develop practical methods for the seismic design of these combined wall-frame structural systems. The objective and scope of the studies follow.

### 1.3 Objectives and Scope

The main objective of the research reported herein is to investigate the effects of the amount and arrangement of wall-panel reinforcement on the behavior of walls when subjected to seismic loading conditions. Three secondary objectives have been the study of the effectiveness of the epoxy-injection technique for repairing damaged walls, methods of strengthening the wall after failure, and the effects of construction joints.

To attain the main objective, two framed wall specimens (SW7 and SW8) were designed, constructed, and tested (Figs. 1.1 to 1.4). Comparison is made of their behavior and that of the previously tested specimens (SW1 through SW6). The effect of the amount of wall-panel reinforcement was investigated by comparing the results of specimen SW7 with those of SW1 and SW2 which were studied by Wang et al. [24]. The effect of the diagonal arrangement of wall-panel reinforcement was studied by comparing the results of specimen SW8 with specimen SW7.

In this report, special emphasis is placed on a discussion of the overall performance of each of the specimens and of their strength and deformation capacities, as well as on a comparison with predicted values. A detailed comparison is made of the measured values of the

lateral displacement at each story level, and the contribution of the flexural deformation, the shear distortion, and the fixed-end rotation to the total measured displacement in the two walls studied with those results obtained in previous studies. The different modes of failure are also discussed in detail.

Finally, after drawing some conclusions, recommendations for future research are offered.





## 2. TEST SPECIMENS

### 2.1 Selection of Test Specimens

#### 2.1.1 Prototype Building

A 10-story reinforced concrete building was designed with a lateral force resisting system consisting of two framed walls running along the E-W direction. The floor plan and elevation of the building are shown in Fig. 1.1. The building is symmetric with respect to both directions, minimizing the torsional force that could develop during an earthquake.

The N-S walls were selected for study [24,25]. Although the present study only utilizes two structural walls, it is usually desirable to have a larger number. For example, the same prototype building designed according to AIJ code specifications [26] would have a minimum of four walls. (For a detailed discussion of the prototype building, see Section 2.1 of Ref. 24.) A summary of the design criteria and procedure follows.

The panels of the N-S walls are 12 inches thick, and those of the E-W walls are 8 inches thick. The floor diaphragm consists of an 8-inch thick flat slab. The exterior columns of the prototype building, including the boundary columns of the E-W walls, are all 20 inches by 20 inches. All the interior columns are 24 inches by 24 inches. The exterior columns are further interconnected with 12-inch wide and 16-inch deep spandrel beams.

The prototype building was designed according to the third category specified in Table 23.1 of the 1973 Uniform Building Code (UBC) [23]; that is, the horizontal force factor,  $k$ , of Eq. 14-1, Chapter 23 of the UBC, was selected to be 0.8. The building was assumed to be located in Seismic Zone No. 3 (this corresponds to Zone 4 in the 1976 UBC). Therefore, the value of  $z$  in this equation was 1.0. The specified yield strength of the reinforcement was 60 ksi, and the specified concrete compressive strength was 4 ksi.

Using the TABS computer program, analyses were made of the prototype building's dynamic response to the N-S component of the 1940

El Centro earthquake and to the S-16 -E component of the derived Pacoima base rock motion from the 1971 San Fernando earthquake [24]. From these analyses, a critical induced shear-to-moment ratio was obtained. Specimens SW1, SW2 [24]; SW3, SW4, SW5, SW6 [25]; SW7, and SW8 were tested under different loading histories to study the effect of this primary parameter on their behavior.

### 2.1.2 Selection of Test Specimens

In the selection of specimens SW1 through SW8, it was necessary to determine, first, the basic subassemblage for which a study could supply the required information for the whole structure and, second, the model scale for reproducing this subassemblage.

The selection of the subassemblage is discussed in Section 2.3.1 of Ref. 24. It was based upon determination of where the yield zone or "critical region" would occur. This region was assumed to occur in the first two stories. However, simulation of boundary conditions (force applications) demanded the selection of at least a three-story assemblage. The selection of the model scale is also discussed in Section 2.3.1 of Ref. 24. The final specimen selected for the investigation was a three-story scale subassemblage model shown in Fig. 1.2.

Except for the slab thickness, the dimensions of the specimen correspond exactly to one-third the dimensions of the prototype. The dimensions of specimens SW7 and SW8 are shown in Figs. 1.2 through 1.4.

## 2.2 Review of Specimens Tested up to the Present

### 2.2.1 Phase I

A series of tests were conducted on two one-third scale component models of the bottom three stories of the 10-story, frame-wall building. The tests are reported in Ref. 24, and the specimens were labeled as specimens SW1 and SW2. The overall dimensions and reinforcement of the edge columns of these specimens were the same as those indicated in Fig. 1.2. The specimens were framed walls (barbell cross-section). The wall panel was 4 inches thick with a reinforcement of No. 2 bars placed 3 inches center-to-center at each face of the panel and in both vertical and horizontal directions. The 10-inch, square-edge column

reinforcement consisted of eight No. 6 bars arranged in a circle with a 0.205-inch diameter spiral at a 0.833-inch pitch.

### 2.2.2 Phase II

The second stage of the investigation consisted of a series of tests on four specimens SW3, SW4, SW5, and SW6. The results are reported in Ref. 25. Specimens SW3 and SW4 were framed walls (barbell cross-section), and specimens SW5 and SW6 were rectangular. The arrangement and amount of reinforcement in the wall panels, and the dimensions of specimens SW3 and SW4 were the same as those of specimens SW1 and SW2. The only differences between specimens SW3 and SW4 and specimens SW1 and SW2 were the type of confinement used and the arrangement of longitudinal reinforcement in the edge columns. The longitudinal reinforcement in each of the columns of SW3 and SW4 consisted of eight No. 6 bars distributed equally on the four faces and confined by square ties.

### 2.2.3 Phase III

In the third phase of the investigation, a series of tests were conducted on two additional specimens--SW7 and SW8. The design, testing, and behavior of these two specimens are discussed in detail in this report.

## 2.3 Design of Specimens SW7 and SW8

The same design criteria were used for specimens SW7 and SW8 as for specimens SW1 and SW2 [24]. However, the design of specimens SW7 and SW8 was based on the 1976 edition of the UBC [23] and the 1974 edition of the SEAOC [27].

### 2.3.1 Wall-Panel Reinforcement

In specimens SW1 and SW2, the design of the wall-panel reinforcement was based upon Section 2611(q) of the 1973 edition of the UBC. Reference 24 shows that, using UBC Section 2611, Eq. 11-33, the horizontal wall-panel reinforcement could be spaced at 9 inches ( $\rho_n = 0.0082$ ) in the prototype building (corresponding to 3-inch spacing in the specimens). The same amount of reinforcement was used in the vertical direction.

It was decided that perhaps less wall-panel reinforcement could be used in specimens SW7 and SW8 by designing their reinforcement according to the UBC/76 and the SEAOC/74. The design for specimens SW7 and SW8 is presented in the following section. In this same section, SW1 and SW2 are investigated to determine if they satisfy the 1976 UBC and 1974 SEAOC recommendations.

### 2.3.1.1 Do Specimens SW1 and SW2 Satisfy the UBC/76?

According to the UBC/76, walls acting independently of the ductile moment-resisting portion of space frames should be capable of resisting the total required lateral forces (Table 23-I, Item 3, of the UBC). According to Section 2312(d) of the UBC/76, Eqs. 12-3A, 12-2, and 12-1:

$$T = \frac{0.05 h_n}{\sqrt{D}} = \frac{0.05 \cdot 93}{\sqrt{61}} = 0.595 \text{ seconds}$$

$$C = \frac{1}{15\sqrt{T}} = 0.0864$$

$$V = ZIKCSW = 1.0 \cdot 1.0 \cdot 0.8 \cdot .0864 \cdot 1.0 \cdot 19988 = 1382 \text{ kips}$$

The estimation of the total weight of building  $W = 19988$  kips is given in Ref. 24, Appendix A.

Section 2312(e), Item 5, of the UBC/76 requires that walls be able to resist a minimum torsional moment equal to the story shear acting with an eccentricity of 5 percent of the maximum building dimension at that level. This is computed to be:

$$M_t = 0.05 \cdot 180 \cdot 1382 = 12438.0 \text{ K-ft.}$$

Thus, the total base shear per wall is  $1382/2 + 12483/140 = 780$  kips, where 140 feet is the distance between the walls. This assumes that all the torsional moments are resisted by the N-S walls of the building alone which is a conservative assumption.

Section 2627(a) of the UBC/76 and Section 3(A) of the SEAOC/74

specify a load factor of 2.0 for calculating shear stresses in shear walls of buildings without 100 percent moment-resisting space frames. For shear, the  $\phi$  factor is equal to 0.85. Thus,

$$\frac{V_u}{\phi} = \frac{2.0(780)}{0.85} = 1835 \text{ kips}$$

Using a 12-inch thick wall panel,  $h$ , and taking the effective depth,  $d$ , of the wall as the code specified value of  $0.8 \ell_w = 226$  inches, the nominal shear stress,  $v_u$ , is computed by Eq. 11-31 of UBC/76 Section 2611(q), i.e.,

$$v_u = \frac{V_u}{\phi h d} = \frac{1835 \cdot 10^3}{12 \cdot 226} = 680 \text{ psi}$$

According to Section 2611(q) of the UBC/76,  $v_u$  shall be less than  $10\sqrt{f'_c} = 633$  psi. However, the value of  $d$  taken as  $0.8 \ell_w$  is conservative in this case since the framed wall is designed such that most of its vertical reinforcement is concentrated at its edge columns. For instance, if no vertical reinforcement is provided for the wall panel, the value of  $d$ --being the distance between the extreme compression fiber and the centroid of the tension column--becomes equal to 267 inches. In Ref. 24, when the  $d$  value of the specimen is the distance from the extreme compression fiber to the centroid of the area of the rebars in tension,  $d$  is equal to 78.3 inches for the specimen and 235 inches for the corresponding prototype. If this value is adopted,  $v_u = 650$  psi  $= 10.6\sqrt{f'_c}$  which is still larger than  $10\sqrt{f'_c} = 633$  psi; therefore, a 12-inch thick wall does *not* meet the UBC/76 recommendations.

#### 2.3.1.2 Wall Reinforcement for Specimens SW7 and SW8

According to the behavior of the specimens observed in the first two phases of the investigation, i.e., specimens SW1 through SW6, it was felt that a  $v_u = 10.6\sqrt{f'_c}$  could be accepted for barbell cross-sections which were the sections used in this phase of the investigation--i.e., specimens SW7 and SW8. Thus it was decided to estimate the amount of wall-panel reinforcement required using  $h = 12$  inches.

(a) Horizontal Wall-Panel Reinforcement.

Using Eq. 11-33 of Section 2611(q) of the UBC/76,

$$v_c = 0.6\sqrt{f'_c} + \frac{\left(\ell_w \cdot 1.25\sqrt{f'_c} + 0.2 \frac{N_u}{\ell_w h}\right)}{\frac{M_u}{V_u} - \frac{\ell_w}{2}} > 2\sqrt{f'_c} = 127 \text{ psi}$$

where

$$\frac{N_u}{\ell_w h} = \frac{195 \text{ kips}}{282 \cdot 12} = 58 \text{ (compression)}$$

However, according to this same code section, for buildings located in Seismic Zone No. 4,  $N_u$  when in compression shall be taken as zero. Hence,

$$v_c = 0.6 \cdot 63.3 + 282 \frac{(1.25 \cdot 63.3 + 0.2 \cdot 0)}{788 - 141} = 73 \text{ psi}$$

Thus,  $v_c$  can be taken as  $2\sqrt{f'_c} = 127 \text{ psi}$  when  $N_u$  is in compression.

Using No. 6 rebars in a double layer (in the prototype):

$$s = \frac{A_v f_y}{(v_u - v_c) b_w} = \frac{0.88 \cdot 60,000}{(680 - 127) \cdot 12} = 7.96 \text{ inches} \approx 8 \text{ inches}$$

The spacing could be increased to 8.4 inches if the more realistic value of  $d = 235$  inches is used in computing  $v_u$ . If  $s = 8$  inches is used,

$$\rho_h = \frac{0.88}{8 \cdot 12} = 0.00917$$

(b) Vertical Wall-Panel Reinforcement

According to Eq. 11-34, Section 2611 of the UBC/76, vertical shear reinforcement shall not be less than

$$\rho_n = 0.0025 + 0.5 \left(2.5 - \frac{h_w}{\ell_w}\right) (\rho_h - 0.0025) = 0.0023$$

or 0.0025, but need not be greater than  $\rho_h$ . According to the SEAOC recommendation [27], however, the value of  $\rho_n$  should be the same as that for  $\rho_h$ , i.e., equal to 0.00917.

Although the above results indicate that the UBC/76 requires even

more wall reinforcement than the UBC/73, in view of the excellent performance of wall specimens SW1 through SW4 it was decided to use less reinforcement, increasing the spacing of the No. 2 bars to the maximum acceptable by code.

According to the UBC/76, the ratio,  $\rho_h$ , of horizontal shear reinforcement area to the gross concrete area of vertical sections shall be at least 0.0025. The spacing of horizontal shear reinforcement shall not exceed  $\ell_w/5$ ,  $3h$ , nor 18 inches. According to the SEAOC/74, the minimum reinforcing ratio,  $\rho$ , for walls designed to resist seismic forces acting parallel to the walls should be 0.0025 each way. The maximum spacing of reinforcement shall not exceed  $d/3$  nor 18 inches--whichever is smaller--where  $d$  is the dimension of the wall element parallel to the shear force. That portion of the wall reinforcement required to resist design shears should be uniformly distributed.

Upon calculating the above values, it was found that  $\ell_w/5 = 56.5$  inches in the prototype (18.8 inches in the model specimen), and that  $3h = 36$  inches in the prototype (12 inches in the model specimen), and 18 inches in the prototype (6 inches in the model specimen). Therefore, the maximum spacing allowed by the UBC/76 and SEAOC/74 was 18 inches in the prototype (6 inches in the model). Thus, the use of No. 2 bars at a 6-inch, center-to-center spacing in both the horizontal and vertical directions was acceptable since the requirements for minimum  $\rho_h$ ,  $\rho_n$ , and for spacing were all met. The value of  $\rho_h$  becomes

$$\rho_h = \frac{0.05 \cdot 2}{4 \cdot 6} = 0.0041 > 0.0025$$

where 0.05 is the area in square inches of a No. 2 bar. The same value of  $\rho_h$  is found for the prototype, if No. 6 bars are used at  $s = 18$  inches:

$$\rho_h = \frac{0.44 \cdot 2}{12 \cdot 18} = 0.0041 > 0.0025$$

It must be noted that, according to the previous computation, the required  $s$  for a 12-inch thick wall to resist the total base shear per wall computed according to the UBC/76 was about 8 inches. Thus, the above values of spacing,  $s = 18$  inches, do not satisfy Eq. 13-11, Section

2611, of the UBC/76. If the space  $s = 18$  inches is used, the required  $A_v$  would be:

$$A_v = \frac{(v_u - v_c) b_w s}{f_y} = \frac{(680 - 127) \cdot 12 \cdot 18}{60,000} = 1.99 \text{ in.}^2$$

for the prototype, corresponding to  $0.22 \text{ in.}^2$  in the specimen. This value of  $A_v$  is greater than that provided by two No. 2 bars for the model specimen.  $A_v$  provided =  $2 \cdot 0.05 = 0.10 < A_v$  specified. In spite of this, and in view of the results obtained in the previous investigations of specimens SW1 to SW4, it was decided to check the behavior of walls with wall-panel reinforcement that does not satisfy present code provisions.

(c) Specimen SW7 Reinforcement

The wall-panel reinforcement for specimen SW7 consisted of No. 2 bars spaced every 6 inches on both sides of the wall in both the vertical and horizontal directions. This value corresponds to the maximum spacing allowed by the UBC/76 and SEAOC/74. The dimensions of the wall and the details of the reinforcement can be seen in Figs. 1.2 and 1.3.

A 9-inch splice was used for the vertical bars of the wall panel of SW7 at the bottom of the second-story level in order to determine the effect of the construction joint on the behavior of the wall and whether the joint would create a "weak" zone in the panel. This is a more realistic approach than that used for specimens SW1 and SW2 where the reinforcement ran all the way from the first- to the third-story levels without any splicing. The length of the splice was calculated according to Sections 2612(f) and 2607(g) of the UBC/76.

According to Section 2612(f) of the UBC/76, the development length,  $\ell_d$ , for a No. 6 bar in the prototype can be calculated as

$$\ell_d = 0.04 A_b f_y / \sqrt{f'_c} = \frac{0.04 \cdot 0.44 \cdot 60,000}{\sqrt{4000}} = 16.70 \text{ in.}$$

but larger than  $0.0004 d_b f_y = 18 \text{ in.}$  According to Section 2607(g) of the UBC/76, the wall panel splice length for a class C splice can be calculated as



$$\text{splice length} = 1.7 \ell_d = 1.7 \cdot 18 = 30.6 \text{ in.}$$

for the prototype. Although this corresponds to 10 inches in the specimen, a 9-inch length was adopted. Note that, if the specimen is considered as a prototype rather than a model, the 9-inch length will not satisfy the code provision 2607(g) which requires that the minimum length of lap for tension lap splice be not less than 12 inches.

In the edge members (i.e., columns), the splice length was calculated according to Sections 2607(h) and 2612(g) of the UBC/76. It should be noted that according to Sections 2627(c) and 2626(f), the lap splices should be made within the center half of the column, and the splice length should not be less than 30 bar diameters. According to Section 2612(g), the development length for a No. 18 bar\* (in the prototype column) should be computed as  $\ell_d = 0.02 f_y d_b / \sqrt{f'_c}$  but not less than  $0.0003 f_y d_b$  nor 8 inches. The first two values can be calculated as 42.9 and 40.7 inches. According to Section 2607(h), however, the splice length should not be less than  $0.0005 f_y d_b$  for  $f_y$  of 60,000 or less. This is calculated to be 67.80 inches for a No. 18 bar (in the prototype) which corresponds to 22.6 inches in the model.\*\*

If, on the other hand, the specimen is considered as a prototype rather than a model, the development length for a No. 6 bar in compression, according to Section 2612(g) of the UBC/76, should be the greater of 14.2 inches, 13.5 inches, and 8 inches. However, according to 2607(h), the splice length is calculated to be 22.5 inches.\*\*

From the above, it can be concluded that a splice length of 22.5 inches would satisfy the UBC/76 conditions for both the prototype and the model, and thus it was used for the edge members (columns) for specimen SW7. The splice location was at the bottom of the second-story level.

The locations of both wall panel and column splicing are presented in Fig. 1.2(a).

---

\* According to the UBC/76, Section 2607(f), and the ACI-77, Section 12.15.2, lap splices should not be used for bars larger than No. 11.

\*\* Because reinforcement is enclosed by spirals, the development length could be reduced by 25 percent [UBC/76, Sections 2612(g) and 2607(h)].

(d) Specimen SW8 Reinforcement

The wall-panel reinforcement was placed diagonally at an angle of  $45^\circ$  along both directions (Fig. 1.4). The reason for this arrangement was to study the behavior of walls with diagonal reinforcement and compare it with that of regularly reinforced walls (i.e., to see whether the diagonal reinforcement could create an effective shear-resisting mechanism).

The amount of reinforcement consisted of two layers of No. 2 bars placed diagonally at a center-to-center spacing of 6 inches measured perpendicular to the longitudinal direction of the bars. This amount of reinforcement, however, is not in accordance with Eq. 11-14, Section 2611, of the UBC/76. According to Section 11-4, when inclined stirrups are used the required area should not be less than

$$A_v = \frac{(v_u - v_c) b_w s}{f_y (\sin \alpha + \cos \alpha)} = \frac{(680 - 127) \cdot 12 \cdot 18}{60,000 (\sin 45^\circ + \cos 45^\circ)} = 1.41 \text{ in.}^2$$

This value of  $A_v = 1.41 \text{ in.}^2$  is larger than the value of the shear reinforcement area provided by the inclined reinforcement, i.e., for the prototype building

$$A_{v \text{ provided}} = 0.44 \cdot 2 = 0.88 \text{ in.}^2 < A_{v \text{ specified}} = 1.41 \text{ in.}^2$$

However, minimum spacing requirements of the UBC/76 and SEAOC/74 are met as well as the minimum reinforcement ratio,  $\rho_h = 0.0025$ . The spacing provided corresponds to a ratio,  $\rho_h = 0.0041$ , when calculated in a direction perpendicular to the direction of the bars. This value of  $\rho = 0.0041$  is the same as that used for specimen SW7.

As in specimen SW7, a splice was used for wall-panel as well as edge-member (column) reinforcement for specimen SW8. All bars were spliced at the bottom of the second-story level. The splice length for the wall-panel reinforcement was 9 inches measured along the bars, while that of the column reinforcement was 22.5 inches. The splice positions as well as their lengths are presented in Fig. 1.4(a).

(e) Comparison of Volume of Steel, SW7 vs. SW8

The total volume of steel used in the wall panel of specimen SW7 was calculated to be around 380 in<sup>3</sup>. The total volume of steel used in the wall panel of specimen SW8 was around 390 in.<sup>3</sup>, which is very close to that of SW7. However, the cost of constructing diagonally-reinforced walls is higher because the bars must be cut at varying lengths and because the placing and anchorage of these bars is more difficult than that of vertical and horizontal bars. Therefore, in general, construction of diagonally-reinforced walls is more complicated and time-consuming than the construction of walls where reinforcement bars are placed vertically and horizontally.

2.3.2 Edge Column of Walls

According to Section 2627(c) of the UBC/76, edge columns should be designed to carry all vertical stresses resulting from wall loads in addition to tributary dead and live loads and from the specified horizontal earthquake forces. The design of the edge-column reinforcement was the same as that for specimens SW1 and SW2 and can be obtained from Section 2.2.1, Ref. 24. In this case, the specified yield strength of the reinforcement was also the same as in the case of specimens SW1 and SW2, i.e., 60 ksi, and the specified concrete compressive strength was 4 ksi.

The amount and arrangement of edge-column reinforcement were identical for all four specimens, SW1, SW2, SW7, and SW8, and consisted of eight No. 6 bars arranged in a circular manner. The spiral was No. 7 gauge wire with a diameter of 0.205 inches. The pitch used for the spiral confinement was 0.83 inches. The details of the edge-column reinforcement for both specimens SW7 and SW8 can be seen in Figs. 1.2 through 1.4.

2.4 Mechanical Characteristics of Model Materials

The prototype wall structure was designed on the basis of an  $f'_c = 4$  ksi and  $f_y = 60$  ksi. Thus, similar design strengths were adopted for the model materials.

#### 2.4.1 Concrete

The specified 28-day strength of the concrete was 4000 psi. The specimens were cast story by story. On the day of testing, the strength reached 5910 psi for the first stories of both specimens SW7 and SW8. The stress-strain curves for each individual story of the two specimens are given in Figs. 2.1 to 2.3, and the mechanical characteristics are given in Table 1(a).

The secant moduli of concrete  $E_c$  at  $0.45 f'_c$  were calculated and compared to the values calculated according to ACI (UBC) empirical equation,  $E_c = 57,000 \sqrt{f'_c}$  [23]. For the first stories of both specimens SW7 and SW8, the measured secant modulus at  $0.45 f'_c$  is equal to 3325 ksi. This value is considerably lower than the values calculated according to the ACI empirical equation. The results are compared in Table 1(b).

#### 2.4.2 Steel Reinforcing Bars

Each of the stress-strain curves for the different reinforcing bars of specimens SW7 and SW8 are shown in Fig. 2.4 were obtained by averaging the curves of two similar test specimens.

##### 2.4.2.1 No. 6 Bars

The stress-strain diagram of the No. 6 rebars is shown in Fig. 2.4. Although the specified yield strength of the reinforcement was 60 ksi, the measured stress-strain relationships for the No. 6 rebars showed an upper yield stress of 81.5 ksi and a lower yield stress of 75 ksi. Thus, even the lower yield strength was 25 percent higher than the specified one. The strain hardening of the rebars began when their strain reached 0.016. The initial strain hardening modulus was about 2000 ksi. The tensile strength, i.e., the maximum nominal stress, was 109 ksi, reached at a strain of 0.24.

Both No. 6 rebars were machined down from their original size for the purpose of fitting them in the testing machine. The two machined rebars that were tested had diameters of 0.4 inches each.

##### 2.4.2.2 No. 2 Bars

Figure 2.4 also shows the stress-strain diagram of the No. 2 rebars.

Their yield strength reached 70 ksi, and their strain hardening modulus was about 700 ksi. The tensile strength, i.e., the maximum nominal stress, was 95 ksi and was reached at a strain of 0.145.

#### 2.4.2.3 Spiral Reinforcement

Number 7 gauge wire was used as spiral reinforcement. The stress-strain diagram for this reinforcement is shown in Fig. 2.4. No clear plastic plateau can be seen on the stress-strain curve of the spiral. Thus, the yield stress determined for this wire was 85 ksi, based on ASTM standards to determine the yielding strength. However, the maximum stress reached was 92.1 ksi, and the ultimate strain of the spirals was 0.024.

It is clear that the wire used for the spiral was considerably less ductile than the deformed No. 2 and No. 6 bars. In practice, it would be desirable to use more ductile steel bars for the spiral.

#### 2.5 Fabrication of Specimens

In order to simulate construction procedure in the field, the specimens were cast story by story in their vertical position. The steel cages for the edge columns and the wall panel up to the second story were ready at the time that the footing was cast. Three days after each casting, the formwork for the next story was placed. The period between each casting was 13 days.

Following this procedure, the specimens had four construction joints-- a concrete construction joint at each story level, and a steel splice construction joint at the bottom of the second-story level (Figs. 1.2 and 1.4). These construction joints, however, did not influence the strength or failure mode of the specimens.

Specimens SW7 and SW8 were cast simultaneously to have a similar quality of concrete to eliminate variation in this parameter when their performance under similar loading programs is compared. During casting, the concrete was compacted with a high-frequency vibrator and cured by covering with wet sacks under a plastic cover for one week. The forms of the lower stories were not removed until fabrication of the entire specimen was completed.

The forms were stripped 10 days after casting, and the specimen was transferred from its cast position to its horizontal test position by a pick-up frame. The specimen was then tied to reaction blocks by means of twenty prestressing rods of 1-3/8 inch-diameter in the longitudinal direction and by four similar rods in the horizontal direction. Each of these rods was prestressed to 120 kips.

### 3. EXPERIMENTAL SETUP AND TESTING PROCEDURE

#### 3.1 Selection of Loading Conditions to be Imposed on the Specimen

The framed-wall prototype was designed for the UBC-specified critical load combination of gravity loads and lateral forces. This combination is shown in Fig. 3.1. Unfortunately, this loading combination does not simulate the actual loading condition of the framed wall even when subjected to seismic excitations of the intensity specified by the UBC. The influence of the interacting frames and higher modes of vibration is not accounted for properly by the adopted UBC distribution of the total base shear. An attempt has been made to find a more realistic and more critical loading condition (as far as the maximum shear acting at the critical region of the wall is concerned) when the whole building is subjected to severe seismic excitations. The results are discussed in detail in Chapter 3 of Ref. 24 and summarized here.

According to the discussion in Chapter 3 of Ref. 24, the actual shear force that can be developed in the wall could be considerably higher than the unfactored UBC specified shear force. This is because the amount of shear force that can be developed would be controlled by the actual flexural strength of the wall and affected by the interaction between the walls and the frames and by the higher modes of vibration. The different loading conditions are shown in Figs. 3.2(1) to 3.2(5). The most critical loading condition is shown in Fig. 3.2(4); this was the condition selected for use in the tests. Using this loading condition, the shear force of 2,187 kips--which is equal to  $9 \times 243$  kips--that could have developed in the prototype wall during ground accelerations of the 1940 El Centro earthquake is 4.08 times the unfactored UBC force of 536 kips [ $1.0 \times (E + \text{torsion})$ , Section 2.2, Ref. 24]. Although the UBC/73 specifies a load factor of 2.8 in designing against shear and diagonal tensions, this load factor--together with the code strength-reduction factor,  $\phi$ --is apparently not large enough to give a realistic estimation of the actual shear that could be induced in the wall when the flexural strength of the wall is developed.

Except in research work where some advanced methods such as the nonlinear finite element-analysis technique are used, the shear strength

of reinforced concrete members is still most often estimated using empirical formulas. These formulas, however, are not very reliable and usually result in conservative values. More specifically, the actual shear capacity of the wall may be larger than that estimated, and this larger value of shear capacity might prevent brittle shear failure from occurring. However, because there is currently a lack of reliable test data, there is no guarantee that walls designed according to UBC/76 specifications will not undergo brittle shear failure despite the higher specified load factor of 2.0 for shear design. Therefore, a more rational design method is necessary.

### 3.2 Experimental Setup

#### 3.2.1 General Setup

The experimental setup, including the wall specimen and the testing facility, is shown in Fig. 3.3. As indicated, the specimen is tested in the horizontal position. The testing facility consists of reaction blocks, loading devices, ancillary devices, and instrumentation using a data-acquisition system. These are discussed in detail in Chapter 4 of Ref. 24.

### 3.3 Specimen Instrumentation and Data Acquisition System

#### 3.3.1 External Instrumentation

The schematic plan for external instrumentation is shown in Fig. 3.4. This instrumentation was designed to obtain data on lateral displacements, curvature, story shear distortions, and steel and concrete strains using electronic and mechanical transducers as well as photogrammetric readings.

##### 3.3.1.1 Measurement of Lateral Displacement

The lateral displacement of the specimen was measured by four linear potentiometers. The first three potentiometers were placed at each floor level and are marked as  $\delta_3$ ,  $\delta_2$ , and  $\delta_1$  in Fig. 3.4. The fourth potentiometer was placed mid-depth at the first story and is marked as  $\delta_4$  in Fig. 3.4. The measurements were based on the assumption that the slabs and the walls between the edge columns cannot be extended laterally so that the lateral displacement measured at the right and left sides of the specimen has the same value.



Although several cracks were found in the slabs during the tests, these occurred after large deflections had been measured. Thus, it appears that the amount of slab extension is very small compared with the total value of lateral displacement. As shown in Fig. 3.5, another source of error in the measurement of the lateral displacement was due to the effect of axial deformation of the specimens. This error is also negligible. For instance, at LP 310 for specimen SW7 R2, the total extension of the right (south) column was 0.65 inches, which introduced an error of 0.0094 inches in the measurement of  $\delta_3$ . This error was only 0.62 percent of the  $\delta_3$  value at that load point.

#### 3.3.1.2 Measurement of Shear Distortion

The average shear distortion of the wall panel in each story was measured by a pair of linear potentiometers placed diagonally across from each other. The principle of relating the measurement of the relative movement of two diagonally oriented points to the average shear distortion is discussed in Ref. 28.

#### 3.3.1.3 Photogrammetric Measurements

After the specimen was placed in position for testing, its upper surface was whitewashed and then marked with a rectangular grid as shown in Fig. 3.6. This grid was used to obtain the deformation pattern of the specimen's upper surface through a photogrammetric technique. Two stretched wires running completely independently of the specimen served as reference lines. Targets were attached at every intersection of the grid lines and at several points along the reference lines to assist with the subsequent data reduction. Supported by a rigid independent steel frame, two cameras were fixed 11 feet above the specimen for taking photographs.

#### 3.3.2 Internal Instrumentation

Several microdot strain gauges were welded on the first- and second-story reinforcement and on the part of this reinforcement embedded in the footing. This positioning was used because most of the damage was expected in the first two stories. The exact location of these gauges is shown in Figs. 3.7 and 3.8. These gauges permit: (1) determination of the first yielding of the specimen; (2) recording

of the strain history of the different reinforcements at some important locations so that the stress history of the reinforcements at those locations can be estimated and compared with the predicted values in order to study the effectiveness of the different reinforcements;

(3) studying the anchorage effectiveness of the vertical reinforcement; and (4) studying the possibility of a sliding shear failure in the splicing at the construction joint.

### 3.3.3 Data Acquisition System

To have a clear idea of how the behavior of the specimen changed as the test progressed and, therefore, to be able to control the test, it would be ideal to continuously record the output from all transducers by X-Y or X-Y-Y' recorders. However, only 16 to 18 Y and Y' channels were available during the tests. These channels were used to record the histories of the following: the two axial forces; the lateral displacements,  $\delta_3$ ,  $\delta_2$ , and  $\delta_1$ ; curvature; shear distortion,  $\gamma_1$  and  $\gamma_2$ ; and the steel reinforcement strain values at the most important locations (Figs. 3.7 and 3.8). Each X channel of these recorders was connected in series to the lateral load transducer to create plots of each of the main parameters versus the lateral load. The output from the rest of the transducers was read at selected stages of the test directly through a high-speed, data-acquisition system which is based on the use of a NOVA minicomputer.

### 3.4 Determination of Total Lateral Load

Due to the lateral movement of the specimen, the net axial force provided by the hydraulic jacks, P, has a horizontal components,  $\Delta P$ , acting on the specimen as shown in Fig. 3.9. The distance between the hinge on the clevis-mounted jack and the hinge at the clevis attachment at the tip of the column is 83 inches when the specimen does not undergo axial deformation. When the specimen undergoes axial deformation, this distance varies as a function of the angle  $\alpha$  and the lateral displacement  $\delta_3$  (Fig. 3.9). Because this variation is small, the distance between those two hinges is taken as constant, 83 inches, and the load correction,  $\Delta P$ , can be computed according to the following:

$$\Delta P = (\Sigma P) \cdot \sin \alpha = (\Sigma P) \cdot \frac{\delta_3}{83} \quad \therefore \Delta P = (P_1 + P_2) \cdot \frac{\delta_3}{83}$$

where  $\Delta P$  is in kips, and  $\delta_3$ --the total lateral displacement of the specimen at the level of the third floor--is in inches.

The total lateral force,  $P_T$ , or the total shear of the specimen, can be computed as follows:

$$P_T = P + \Delta P$$

where  $P$  is the force applied by the lateral loading jack. The maximum value of  $\Delta P$  at LP 310 of specimen SW7 R2 was equal to 3.5 kips or 1.4 percent of the  $P$  value at that load point.

The vertical component of the lateral force  $P$ , due to the axial deformation of the specimen, was always less than 2 percent of the net axial force. Since the response of the specimen was not sensitive to small variation of the net axial force, this vertical component of  $P$  was neglected.



## 4. TEST RESULTS AND THEIR EVALUATION

### 4.1 Introductory Remarks

The series of tests conducted on specimens SW7 and SW8 were divided into three phases for each specimen. These three phases were denoted as: (a) virgin specimen; (b) epoxy-repaired specimen ( $R_1$  specimen); and (c) twice-repaired specimen ( $R_2$  specimen). One of the main reasons for carrying out all of the tests on each specimen was economic, i.e., because of the high cost of fabrication, it was necessary to make the most use of each specimen.

The virgin specimen (SW7 Virgin or SW8 Virgin) was cyclically loaded up to the first yield of the column steel corresponding to a ductility of  $\mu = 1$ . The test was then halted and all the flexural cracks in the columns and the diagonal cracks in the wall panels that could be injected with epoxy were repaired in this way. The reason for the epoxy repair was to study (1) the effectiveness of epoxy injection after mild seismic excitations, and (2) the behavior of the wall when subsequently subjected to service lateral loading as well as to large lateral inelastic deformations.

The epoxy-repaired specimen ( $R_1$ ) was then monotonically loaded, with a few intermediate cycles, up to failure. Most of the damage was concentrated in the first story. The specimen was then not only repaired, but the first story was strengthened as well. This specimen, denoted as  $R_2$ , was tested again. The reason for this repairing and strengthening was to study the effectiveness of the strengthening techniques and also the behavior of the  $R_2$  specimen when subjected to cyclic loadings at large ratios of  $V_u/M_u$ . The twice-repaired specimen was cyclically loaded until failure, thus ending the series of tests conducted on specimens SW7 and SW8. The details of the repairing and strengthening techniques used for each specimen are discussed in detail in Chapter 5 of this report.

The main parameters considered in evaluating the behavior of the tested specimen in each of the three phases were:

- (1) the loading history;
- (2) the relationship between the total lateral force  $P_T$ , i.e.,

- base shear, and the value of the lateral displacement at each story level (presented in the form of  $P_T - \delta_R$  diagrams);
- (3) the relationship between  $P_T$  and the story shear distortion at each story level (presented as  $P_T - \gamma_R$  diagrams);
  - (4) the amount of flexural deformation (at each story level) at each loading stage;
  - (5) the amount of fixed-end rotation at the foot of the columns in each specimen at each loading stage;
  - (6) the maximum values of lateral displacement, ductility, total base shear, and overturning moment in each of the three phases of the testing;
  - (7) the mode of failure of the specimen in each phase of the testing.

#### 4.1.1 Loading Histories

The experiments were conducted under controlled third-story lateral displacement,  $\delta_{3R}$ , as well as cycling under specific predetermined loads such as a service or working load,  $P$ , of 90 kips. The loading histories of each specimen are presented in the form of loading-history diagrams which depict the amount of third-story lateral displacement,  $\delta_{3R}$ ; the value of the lateral load; and the number of cycles under the prescribed conditions of loading and displacement. Figures 4.1 and 4.2 show the loading history diagrams for specimen SW7. The loading history diagrams for specimen SW8 are shown in Figs. 4.16 and 4.17.

#### 4.1.2 Base Shear vs. Lateral Displacement ( $P_T - \delta_R$ Diagrams)

The relative lateral displacements at the mid-depth of each floor slab are denoted as  $\delta_{3R}$ ,  $\delta_{2R}$ ,  $\delta_{1R}$  corresponding to the third, second, and first stories, respectively. These terms refer to the displacements with respect to the footing of the specimen. Specifically, the lateral displacements caused by the rigid body translation and rotation have been excluded. The manner in which  $\delta_{3R}$ ,  $\delta_{2R}$ , and  $\delta_{1R}$  are obtained is described in Section 3.3.

The total lateral force (i.e., base shear) versus the individual story lateral displacements is plotted for each of the three testing phases. Plots for specimen SW7 are given in Figs. 4.3 to 4.9. Plots for

specimen SW8 are given in Figs. 4.18 to 4.24.  $P_T$  is given in KN and  $\delta_i$ 's are in millimeters. The displacement ductility factor,  $\mu_\delta$ , is defined as  $\delta_{3R}/\delta_{3Y}$  where  $\delta_{3Y}$  is the value of  $\delta_{3R}$  at the first-yield load. The stiffness of the specimen against lateral movements is defined by the slope of the  $P_T - \delta_{3R}$  diagram.

#### 4.1.3 Base Shear vs. Shear Distortions ( $P_T - \gamma_R$ Diagrams)

Angular distortions due to shear in each of the three-story wall panels are denoted by  $\gamma_3$ ,  $\gamma_2$ , and  $\gamma_1$ , and the displacements due to shear by  $\delta\gamma_3$ ,  $\delta\gamma_2$ , and  $\delta\gamma_1$ , respectively, going from the third-story to the first-story levels. The manner in which the shear distortions and deformations are obtained is described in Section 3.3.

Plots of the total lateral load-shear distortion relationships (i.e., base shear vs. shear displacement) are given in Figs. 4.10 to 4.15 for specimen SW7 and Figs. 4.25 to 4.30 for specimen SW8.  $P_T$  is given in KN,  $\gamma_i$  in radians, and  $\delta\gamma_i$  in millimeters.

#### 4.1.4 Flexural Deformation and Fixed-End Rotation

The amount of flexural deformation and fixed-end rotation were measured at each of the loading points throughout the testing of the specimens. The contribution of these components to the total lateral displacement depends on the slenderness of the specimen. The more slender the specimen, the more significant the flexural deformation and the fixed-end rotation. Graphical information on the contribution of these two components to the total lateral displacement, as well as the contribution of the shear distortion, is given in Figs. 4.31 through 4.48, and values are given in Tables 2 to 5.

#### 4.1.5 Maximum Values of Base Shear, Lateral Displacement, and Overturning Moments

Maximum values were determined for base shear, lateral displacement, and overturning moment for each of the three phases (Virgin,  $R_1$ ,  $R_2$ ) during the testing of specimens SW7 and SW8. Most of these values, as well as the modes of failure, are given in Table 6.

#### 4.2 Specimen SW7

In the first phase of the testing, specimen SW7 Virgin was subjected to several working-load cycles, the maximum of which was 90 kips, and then

displaced to first-yield ductility ( $\mu_\delta = 1$ ), corresponding to  $\delta_{3R} = 0.72$  inches.

The specimen was then epoxy-repaired. After a few cycles at lateral loads smaller and/or equal to service load, the specimen was loaded monotonically up to a certain level of deformation, then unloaded and subjected to cycles at service loads. The specimen was loaded again monotonically up to a new and larger predetermined deformation, and the former process was repeated to a ductility of  $\mu_\delta = 6.4$  where the first-story wall panel failed. The third-story lateral displacement at that point was  $\delta_{3R} = 4.61$  inches (117 mm), and the maximum base shear was  $P_T = 227$  kips (1010 KN). The specimen was then repaired and strengthened at the first-story level and was cyclically loaded up to failure. The maximum cyclic displacement ductility was  $\mu_\delta = 2.1$ , corresponding to a positive displacement  $\delta_{3R} = 1.5$  inches (38 mm). The total base shear reached at that point was  $P_T = 278$  kips (1231 KN).

A more detailed discussion of each of the series of tests follows.

#### 4.2.1 Results of Tests on Virgin Specimen

The load history graph for specimen SW7 Virgin is given in Fig. 4.1.  $P - \delta_T$  graphs are given in Figs. 4.4 to 4.6, and  $V - \gamma$  diagrams are given in Figs. 4.10 to 4.12.

Specimen SW7 Virgin was initially loaded up to 10 kips (45 KN) at LP 10 and cycled once. Then it was loaded up to 25 kips (111 KN) at LP 16 and cycled once, then up to a working load of 90 kips (400 KN) and subjected to four loading reversals from LP 37 to LP 263. The specimen was then loaded up to 125 kips (556 KN) at LP 347, unloaded to zero, brought up to 171.5 kips (763 KN) at LP 410, and cycled once at that load to LP 470. The specimen was taken up to a ductility,  $\mu_\delta = 1$ , corresponding to a  $\delta_{3R} = 0.72$  inches (18.3 mm) and a load  $P_T = 197$  kips (877 KN) at LP 552. It was subjected to one load reversal at the  $\mu_\delta = 1$  level. The test was then halted and the specimen was epoxy-repaired at LP 663.

##### 4.2.1.1 Base Shear vs. Total Lateral Displacement: Specimen SW7 Virgin

In the first part of the test before LP 37, the amount of total third-story lateral displacement,  $\delta_{3R}$ , was very small. At LP 37,  $\delta_{3R}$  reached a value equal to 0.18 inches (4.5 mm) (Fig. 4.4a). No significant



loss of stiffness can be seen during reversals at working load levels (LP 37 and LP 263). At LP 347,  $\delta_{3R} = 0.26$  inches (6.73 mm), and at LP 410,  $\delta_{3R} = 0.50$  inches (12.8 mm). At the point of first yield (LP 552), the three measured lateral displacements were as follows:  $\delta_{3R} = 0.72$  inches (18.3 mm);  $\delta_{2R} = 0.47$  inches (12 mm); and  $\delta_{1R} = 0.20$  inches (5.0 mm).

#### 4.2.1.2 Base Shear vs. Shear Deformation

Up to LP 347, the amount of shear deformation in the specimen as a whole contributed to about 32 percent of the total lateral displacement, 16 percent of which was due to the shear deformation in the first story and about 8 percent to each of the other two stories (Figs. 4.10 - 4.12).

Between LP 347 and LP 410, there was an increase in the amount of shear deformation. The amounts measured at LP 410 were:  $\delta_{\gamma_3} = 0.07$  inches (1.89 mm);  $\delta_{\gamma_2} = 0.06$  inches (1.43 mm); and  $\delta_{\gamma_1} = 0.10$  inches (2.52 mm). These amounts add up to 46 percent of the total lateral displacement,  $\delta_{3R}$ . The amount contributed by the third, second, and first stories was equal to 14 percent, 12 percent, and 20 percent, respectively.

Between LP 410 and LP 552, further increase is observed in the amount of shear deformation. At LP 552, the measured amounts of shear deformation were as follows:  $\delta_{\gamma_3} = 0.11$  inches (2.80 mm);  $\delta_{\gamma_2} = 0.08$  inches (2.0 mm); and  $\delta_{\gamma_1} = 0.12$  inches (2.9 mm). These amounts add up to a total of 45 percent of the total lateral displacement,  $\delta_{3R}$ . The amounts contributed by the third, second, and first stories were equal to 12 percent, 16 percent, and 17 percent, respectively.

Comparison of the above values shows that the amount of displacement contributed by shearing deformation is higher in the first story than in the upper two stories. Furthermore, the rate of shear deformation increased as the shear load was increased, indicating shear deterioration, particularly at the first story.

#### 4.2.1.3 Other Sources of Deformation

Other sources of deformation measured during the testing were the fixed-end rotation and the deflection due to flexure. At LP 347, the total amount of contribution of fixed-end rotation is very small, i.e.,

less than 5 percent. At this loading stage, the total amount of flexure deformation is about 60 percent of the total displacement,  $\delta_{3R}$ .

The maximum contribution of the fixed-end rotation was at LP 552; it amounted to 11 percent of the total lateral displacement,  $\delta_{3R}$ , at that point. The measured amount of flexural deformation at that point was about 38 percent of the total deformation, and was mostly concentrated at the first-story level (19 percent at the first-story level, 14.5 percent at the second-story level, and 4.5 percent at the third-story level).

#### 4.2.1.4 Concluding Remarks

The previous data show that, for specimen SW7 Virgin, the maximum displacement,  $\delta_{3R}$ , reached was 0.72 inches (18.3 mm). Of this displacement, 45 percent was due to shear distortion, 38 percent was due to flexural deformation, 11 percent was due to fixed-end rotation, and the rest was due to the deformation of the foundation and errors in instrumentation. It was observed that most of the shear distortion was concentrated in the first story (17 percent) and most of the flexural deformation was also in the first story (19 percent). No major failure mechanism was observed in the specimen at this phase of testing.

#### 4.2.2 Results of Tests on Epoxy-Repaired Specimen, SW7 R<sub>1</sub>

The load history diagram for Specimen SW7 R<sub>1</sub> is given in Fig. 4.1.  $P_T - \delta$  graphs are given in Figs. 4.4 to 4.6.  $V - \gamma$  diagrams are given in Figs. 4.10 to 4.12.

Specimen SW7 R<sub>1</sub> was initially at LP 663. It was first loaded to 10 kips (45 KN) and cycled once, then to 25 kips (111 KN) and cycled once, and then to a working load of 90 kips (400 KN) and subjected to three loading cycles from LP 685 to LP 736.

The specimen was taken up to a ductility,  $\mu_\delta = 1$ , corresponding to  $\delta_{3R} = 0.72$  inches (18.3 mm) and cycled three times from LP 762 to LP 868. The maximum load carried during these cycles was 183 kips (815 KN). Specimen SW7 R<sub>1</sub> was then taken up to a ductility,  $\mu_\delta = 3$ , at LP 907 corresponding to  $\delta_{3R} = 2.16$  inches (54.9 mm). The load carried by the specimen at that point was 208 kips (925 KN). The specimen was then

unloaded to a zero load at LP 927. The recorded permanent deflection,  $\delta_{3R}$ , at that point was 1.38 inches (35 mm) (Fig. 4.4b).

The specimen was loaded up to a working load of 90 kips (400 KN) and subjected to four loading cycles from LP 942 to LP 1032. Next, it was taken up to a ductility,  $\mu_{\delta} = 5$ , corresponding to  $\delta_{3R} = 3.6$  inches (91.4 mm) at LP 1071, and brought back to a zero load at LP 1088. The total load resisted by the specimen at LP 1071 was  $P_T = 227$  kips (1010 KN) and the recorded permanent displacement at LP 1088 was  $\delta_{3R} = 2.75$  inches (69.9 mm). The specimen was then subjected to two cycles at a load of 25 kips (111 KN), from LP 1098 to LP 1119, and, subsequently, loaded up to failure. Failure occurred at LP 1145 corresponding to a ductility  $\mu_{\delta} = 6.4$  and  $\delta_{3R} = 4.61$  inches (117 mm). The maximum load observed was 227.5 kips (1010 KN).

Specimen SW7 R<sub>1</sub> was then loaded and subjected to two cycles at a load of 65 kips (289 KN) from LP 1175 to LP 1247. In the second cycle, however, the specimen could not reach the 65-kip load and at the maximum deflection imposed, LP 1233, the resistance was 25 kips (111 KN). The specimen was loaded with a 10-kip (45 KN) load at LP 1259 and then the load was reversed. The maximum load that the failed specimen could resist during this loading reversal was 117 kips (524 KN) at LP 1273. The experiment was stopped at LP 1298 and the specimen removed for repairs.

#### 4.2.2.1 Base Shear vs. Total Lateral Displacement: Specimen SW7 R<sub>1</sub>

In the first part of the test before LP 685, the amount of total third-story lateral displacement is very small. At LP 685,  $\delta_{3R}$  reached a value equal to 0.33 inch (8.38 mm) (Figs. 4.4b, 4.5b and 4.6b). No significant loss of stiffness can be seen at the working load reversals between LP 685 and LP 736. At the point of first yield, i.e., LP 762, the three measured lateral displacements were as follows:  $\delta_{3R} = 0.72$  inches (18.3 mm);  $\delta_{2R} = 0.52$  inches (13.21 mm); and  $\delta_{1R} = 0.27$  inches (6.79 mm) (Figs. 4.4b, 4.5b, and 4.6b). No significant loss of stiffness can be observed in the specimen during the three cycles at first yield.

At LP 907 corresponding to  $\mu_{\delta} = 3$ , the measured lateral displacements for the third-, second-, and first-story levels were  $\delta_{3R} = 2.16$  inches (54.9 mm),  $\delta_{2R} = 1.38$  inches (35.0 mm), and  $\delta_{1R} = 0.72$  inches (18.30 mm).

The specimen was then unloaded to a zero load at LP 927. The permanent displacements measured were as follows:  $\delta_{3R} = 1.24$  inches (31.5 mm);  $\delta_{2R} = 0.87$  inches (22.1 mm);  $\delta_{1R} = 0.41$  inches (10.53 mm). At LP 942, the measured deflections were  $\delta_{3R} = 1.57$  inches (40.0 mm),  $\delta_{2R} = 1.09$  inches (27.8 mm), and  $\delta_{1R} = 0.49$  inches (12.4 mm).

Upon reversal of the 90-kip (400 KN) working load from LP 942 to LP 958, the specimen underwent a change of lateral displacement in the third-story amounting to 1.33 inches (33.8 mm). At LP 958, the measured lateral displacements for the third, second, and first stories were  $\delta_{3R} = 0.24$  inches (6.07 mm),  $\delta_{2R} = 0.16$  inches (4.02 mm), and  $\delta_{1R} = 0.07$  inches (1.71 mm), respectively.

As can be seen from Fig. 4.4b, the three working load cycles from LP 958 to LP 1032 show a maximum variation of lateral displacement in the third story equal to 0.93 inches (23.53 mm) per load reversal (i.e., between LP 1019 and LP 1032). This was 3.76 times the change in displacement which occurred previously under the same working load cycles. For example, the net change in  $\delta_{3R}$  between LP 726 and LP 736 was 0.25 inches (6.25 mm). It can therefore be concluded that there has been significant loss of stiffness and a significant amount of shear deterioration due to the large displacement ductility to which the specimen was subjected,  $\mu_{\delta} = 3$ .

The specimen was then loaded until it reached  $\mu_{\delta} = 5$  at LP 1071 corresponding to  $\delta_{3R} = 3.6$  inches (91.44 mm) and, subsequently, brought back to a zero load at LP 1088. At LP 1088, the recorded permanent deflections for the third, second, and first stories were  $\delta_{3R} = 2.7$  inches (68.4 mm),  $\delta_{2R} = 1.82$  inches (46.2 mm), and  $\delta_{1R} = 1.39$  inches (35.2 mm), respectively.

The specimen was subjected to two 25-kip (111 KN) loading cycles and subsequently displaced until failure occurred in the first-story panel at LP 1145, corresponding to  $\mu_{\delta} = 6.4$  and  $\delta_{3R} = 4.61$  inches (117 mm). The second- and first-story deflections at that point were as follows:  $\delta_{2R} = 3.15$  inches (80.0 mm) and  $\delta_{1R} = 2.24$  inches (57.0 mm). The above values show that the amount of first-story displacement,  $\delta_{1R}$ , contributed to about 50 percent of the total lateral displacement,  $\delta_{3R}$ .

After failure, the specimen continued to deflect laterally until  $\delta_{3R}$  reached a value of 4.72 inches (120.0 mm) at LP 1152. The load carried by the specimen at that point was 87.9 kips (391 KN).

At the two 65-kip (289 KN) cycles, from LP 1175 to LP 1247, the specimen displays an increasing loss of stiffness. This can be deduced from the large increase in the value of lateral displacement from LP 1198 to LP 1233. This increase was measured to be 0.30 inches (7.60 mm) for both the third and the first story. This shows that the loss in stiffness (which caused increased lateral displacement under the same 65-kip load) was concentrated in the first story due to the shear damage at this story.

Under the 10-kip (45 KN) load at LP 1259, the third-story lateral displacement,  $\delta_{3R}$ , was 4.56 inches (115.7 mm). Under the negative 117-kip (524 KN) load, the first-story lateral displacement at LP 1273 is negative [ $\delta_{1R} = -0.60$  inches (-15.27 mm)] even though the third-story displacement is positive [ $\delta_{3R} = 0.25$  inch (6.25 mm)]. This is due to the excessive damage in the first-story wall panel which caused the specimen to lose much of its stiffness.

The experiment was stopped at LP 1298.

#### 4.2.2.2 Base Shear vs. Shear Deformation: Specimen SW7 R<sub>1</sub>

Up to LP 685, the total amount of shear deformation in the specimen as a whole contributed to about 32 percent of the total lateral displacement, 13 percent of which was due to the shear distortion in the first story, 10 percent to the second, and 9 percent to the third-story shear distortion (Figs. 4.10b, 4.11b and 4.12b).

Between LP 685 and LP 762, there was an increase in shear deformation in each of the three stories. At LP 762 the amount of shear deformation contributed to about 46 percent of the total lateral displacement. The measured deformations for the third, second, and first stories were  $\delta_{\gamma_3} = 0.106$  inches (2.68 mm),  $\delta_{\gamma_2} = 0.090$  inches (2.28 mm), and  $\delta_{\gamma_1} = 0.138$  inches (3.51 mm), respectively. The amount of deformation contributed by each story was 14.6 percent, 12.5 percent, and 19 percent for the third, second, and first stories, respectively. These data show that, upon cycling at first yield, the contribution of shear distortion

in the first story is 19 percent of the total lateral displacement.

Between LP 762 and LP 907, there is a decrease in the contribution of shear deformation for the specimen as a whole. The amounts measured at LP 907 (i.e., corresponding to  $\mu_\delta = 3$ ) were  $\delta_{\gamma_3} = 0.127$  inches (3.22 mm),  $\delta_{\gamma_2} = 0.113$  inches (2.86 mm), and  $\delta_{\gamma_1} = 0.465$  inches (11.81 mm). These amounts add up to 32.6 percent of the total lateral displacement,  $\delta_{3R}$ . The amounts contributed by the third-, second-, and first-story wall panels were 5.9 percent, 5.2 percent, and 21.5 percent, respectively. Even though the contribution of the specimen as a whole has decreased, the first-story contribution of shear deformation has increased by 2.5 percent.

For the working load cycles between LP 927 and LP 1032, there is a significant increase in first-story shear deformation, as can be seen by the pinching effect of the hysteretic loops on the lateral displacement and shear deformation graphs (Figs. 4.6b and 4.12b). The measured amount of first-story deformation was  $\delta_{\gamma_1} = 0.261$  inches (6.62 mm) or about 24 percent of the total lateral displacement at LP 998. The contributions of the second and third stories are much less, adding up to 11 percent of the total displacement at that point.

At LP 1071, there is a slight decrease in the shear contribution of the specimen as a whole. The measured amounts were  $\delta_{\gamma_3} = 0.161$  inches (4.10 mm),  $\delta_{\gamma_2} = 0.162$  inches (4.11 mm), and  $\delta_{\gamma_1} = 0.729$  inches (18.52 mm) for the third, second, and first stories, respectively. These amounts add up to 30 percent of the total lateral displacement at that point, 4.1 percent of which was contributed by the third story, 4.0 percent by the second, and 21.9 percent by the first. For the first story alone, the contribution of shear to the first-story lateral displacement,  $\delta_{1R}$ , was about 42 percent.

Under the 25-kip (111 kN) cycles, between LP 1098 and LP 1119, there is a significant increase in the first-story shear deformation. The largest measured amount was  $\delta_{\gamma_1} = 0.602$  inches (15.23 mm) or about 22 percent of the total displacement,  $\delta_{3R}$ , under that load.

At LP 1145, the measured amounts of shear deformation were  $\delta_{\gamma_3} = 0.18$  inches (4.6 mm),  $\delta_{\gamma_2} = 0.19$  inches (4.8 mm), and  $\delta_{\gamma_1} = 1.05$  inches (26.6 mm). These sum to 1.42 inches (36.0 mm) or 30 percent of the total

lateral displacement,  $\delta_{3R}$ . Upon failure of the specimen at LP 1145, there is a marked increase of shear deformation in the first-story wall panel which continues until LP 1152. At LP 1152,  $\delta_{\gamma 1}$  was equal to 1.47 inches (37.4 mm) or 32 percent of the total lateral displacement,  $\delta_{3R}$ , at that point and 56 percent of the total first-story lateral displacement,  $\delta_{1R}$ .

Under the 65-kip (289 KN) cycles, a large loss of stiffness is apparent in the first-story wall panel between LP 1175 and LP 1247. This can be seen from the hysteretic behavior and the increased shear deformation between these load points (Fig. 4.12b). This loss of stiffness is much less for the second and third stories (Figs. 4.10b and 4.11b), as no shear failure and no excessive shear damage (cracking) had occurred in the upper two stories.

#### 4.2.2.3 Other Sources of Deformation

The other displacement components measured during the testing were those due to the fixed-end rotation and to flexural deformation. Exact values of the contribution of these sources of deformation for each story level and at certain important load points are given in Table 2. Graphic interpretation of these sources is also given in Figs. 4.34 to 4.36.

Up to LP 685, the contribution of the fixed -end rotation is very small (less than 8 percent) and the total amount of flexural deformation is the largest during this testing phase. Its calculated value was about 54 percent.

As the loading program is carried out, there is a gradual increase in the contribution of the fixed-end rotation. However, the contribution of the flexural deformation decreases. The greatest amount of decrease is at the first-story level where there is the largest amount of shear deformation due to the failure of the wall panel. The minimum value of flexural deformation at the first story was about 30 percent, corresponding to 47 percent shear deformation at LP 1145.

#### 4.2.2.4 Failure Mechanism

During the testing of specimen SW7 R<sub>1</sub>, the failure mode was initiated

by the crushing of the first-story wall panel. This crushing practically eliminated one of the main sources of a shear-resisting mechanism in the specimen. Buckling of the wall panel reinforcement in both directions could also be observed when the loose concrete pieces fell out. According to these observations, the first-story wall panel could have failed in one of two mechanisms. The wall-panel reinforcement could have buckled first and then damaged the concrete cover of that panel (for the reinforcement to buckle first, wide cracks must open up or the cover must split at that level of reinforcement), or the wall-panel concrete could have crushed first, thereby reducing the constraint of the wall-panel reinforcement and precipitating buckling.

Upon observing the failure sequence of the specimen, it was observed that widening and propagation of cracks that had already been formed in the virgin specimen (SW7 Virgin) occurred between LP 851 and LP 907 (see Fig. 4.49). As the specimen was displaced up to a ductility,  $\mu_\delta = 5$ , at LP 1071, wide cracks appeared at the base of the south column (first-story level) and loose pieces of concrete came off the edge of the column. As the cycling continued and the specimen displaced up to a ductility,  $\mu_\delta = 6.4$ , at LP 1145, there was buckling of the wall-panel reinforcement and crushing of the concrete (see Fig. 4.50). The crack at the base of the south column widened and propagated deeply into the wall panel. Upon further cycling, there was excessive damage in the wall panel as well as failure of both the longitudinal and transverse column reinforcement.

The failure was thus a flexure-shear failure that originated in the crushing of both column and wall panel concrete, reducing the constraint of the reinforcement and precipitating buckling.

#### 4.2.2.5 Concluding Remarks

The previous data show that, for the repaired specimen, SW7 R<sub>1</sub>, the maximum lateral displacement,  $\delta_{3R}$ , reached was 4.61 inches (117 mm), corresponding to an overall ductility,  $\mu_\delta = 6.4$ . The  $\mu_\delta$  for the first story was 8.4. Of the total  $\delta_{3R} = 4.6$  inches displacement, 30 percent was due to shear deformation, 42 percent was due to flexural deformation, and 25 percent was due to fixed-end rotation; the rest was due to the



deformation of the foundation and errors in instrumentation. It was observed that most of the shear distortion was concentrated in the first story (23 of the total 30 percent).

#### 4.2.3 Results of Tests on Repaired and Strengthened Specimen: SW7 R<sub>2</sub>

After the crushing of the first-story wall panel of SW7 R<sub>1</sub>, the specimen was repaired. The wall panel and both edge members of the first-story level were strengthened. Details of the repairing and strengthening techniques are discussed in Chapter 5. The loading history graph for SW7 R<sub>2</sub> is given in Fig. 4.2, P<sub>T</sub> -  $\delta$  graphs are given in Figs. 4.7 through 4.9, and V -  $\gamma$  diagrams are given in Figs. 4.13 through 4.15.

Specimen SW7 R<sub>2</sub> was subjected to cyclic loading up to failure. It was initially loaded up to 10 kips (45 KN) and cycled once, then loaded up to 25 kips (111 KN) and cycled once, and finally loaded up to 50 kips (222 KN) and subjected to three loading cycles from LP 20 to LP 47. The specimen was next subjected to three 90-kip (400 KN) working load cycles from LP 53 to LP 97, and then taken to a displacement corresponding to  $\delta_{3R} = 1.0$  inches (25.4 mm) and subjected to three loading cycles between LP 125 and LP 274. The displacement was increased until the specimen reached a ductility,  $\mu_{\delta} = 2.1$ , corresponding to a lateral displacement,  $\delta_{3R}$ , equal to 1.51 inches (38.4 mm) at LP 310. It was subjected to three loading reversals at this displacement (from LP 310 to LP 450). The specimen was then unloaded and subjected to three 50-kip (222 KN) cycles from LP 465 to LP 505. It was cycled once at a 90-kip (400 KN) load cycle from LP 512 to LP 520 and, finally, it was taken up to a lateral displacement,  $\delta_{3R} = 2.53$  inches (64.38 mm) and cycled three times from LP 552 to LP 609. After this, the specimen was unloaded and the experiment was halted.

##### 4.2.3.1 Base Shear vs. Total Lateral Displacement: Specimen SW7 R<sub>2</sub> (Figs. 4.7 - 4.9)

(1) In the initial part of the experiment before LP 20, the deformations in the three stories were found to be very small [less than 0.17 inches (4.32 mm)]. No significant deterioration or loss of stiffness can be observed in the specimen.

(2) Under the 90-kip (400 KN) working load cycles (from LP 53 to

LP 97) the total observed lateral displacement was 0.30 inches (7.67 mm). No significant deterioration can be observed since the hysteretic loops are very stable at that load level.

(3) Under controlled displacement cycling, corresponding to  $\delta_{3R} = 1.0$  inches (25.4 mm) from LP 125 to LP 274, the maximum load resisted was equal to  $P_T = 257.4$  kips (1145 KN). A drop in load resistance capacity of 17 kips (75 KN) can be observed from the drop in the maximum load at LP 125 to the maximum load at LP 193. This drop is accompanied by a loss of stiffness which stabilized in the third cycle at LP 252 where the total lateral load was only 3.1 kips (14 KN) less than that at LP 193.

The above loss of stiffness was attributed to the formation of significant cracks. One crack at the base of the south column at the second-story level was estimated to be 0.1 inches (2.54 mm) wide. A significant amount of cracking was also observed between LP 97 and LP 125 in the first-story wall panel. At LP 125, the measured story deflections were  $\delta_{3R} = 1.03$  inches (26.16 mm),  $\delta_{2R} = 0.58$  inches (14.57 mm); and  $\delta_{1R} = 0.24$  inches (6.2 mm) for the third, second, and first stories, respectively.

(4) Under controlled lateral displacement cycling at a ductility  $\mu_\delta = 2.1$ , corresponding to  $\delta_{3R} = 1.51$  inches (38.4 mm), from LP 310 to LP 450, the maximum load carried by the specimen was  $P_T = 278$  kips (1233 KN). The following large decreases in load capacity were observed: 31.7 kips (141 KN) between LP 310 and LP 388; 20.2 kips (89 KN) between LP 388 and LP 414; and 72.8 kips (324 KN) between LP 414 and LP 450. These decreases in the load-bearing capacity of the specimen were accompanied by a considerable loss in stiffness and large amounts of shear resistance and stiffness deterioration. This can be seen from the pinching in the  $P_T - \delta$  diagrams.

This loss of stiffness and increased deterioration was caused by excessive diagonal cracking in the wall panels as well as the buckling of some of the longitudinal reinforcement in the columns at the base of the second-story columns. The pinching effect is much more apparent in the second- and third-story wall panels than it is in the first,

which indicates that the shear deterioration is greater in the second and third stories than it is in the first. The measured lateral displacements at LP 310 were  $\delta_{3R} = 1.51$  inches (38.4 mm),  $\delta_{2R} = 0.89$  inches (22.7 mm), and  $\delta_{1R} = 0.37$  inches (9.5 mm) for the third, second, and first stories, respectively.

(5) Under the three 50-kip (222 KN) loading cycles from LP 465 to LP 505, more shear deterioration is observed from the pinching of the  $P_T - \delta$  curves. A considerable loss of stiffness is noticeable in the first 50-kip (222 KN) loading cycles between LP 20 and LP 47. The measured amount of total lateral displacement,  $\delta_{3R}$ , at LP 465 is 0.42 inches (10.6 mm), which is 2.45 times the measured deflection at LP 20. The measured lateral displacements at LP 476 were  $\delta_{3R} = -0.42$  inches (-10.63 mm),  $\delta_{2R} = -0.39$  inches (-9.85 mm), and  $\delta_{1R} = -0.10$  inches (-2.65 mm).

(6) Under the 90-kip (400 KN) working load cycle from LP 512 to LP 520, more shear deterioration is observed. This deterioration is mainly concentrated in the second and third stories of the specimen. The measured lateral displacements at LP 512 were  $\delta_{3R} = 0.76$  inches (19.4 mm),  $\delta_{2R} = 0.54$  inches (13.6 mm), and  $\delta_{1R} = 0.15$  inches (3.89 mm). The value of total lateral displacement,  $\delta_{3R}$ , was measured to be 2.53 times the value measured under the same 90-kip (400 KN) working load at LP 53. This result is consistent with the value obtained in item (5) of this section when the behavior of the specimen under the 50-kip (222 KN) loading cycles was studied.

(7) Under controlled lateral displacement cycling at  $\delta_{3R} = 2.53$  inches (64.3 mm), between LP 520 and LP 609, a great reduction in stiffness is observed in the specimen. This is mainly due to diagonal shear failure of the third-story wall panel between LP 539 and LP 552. The loading capacity decreases by 80 kips (352 KN) between LP 539 [where the maximum load carried was 183 kips (815 KN)] and LP 552. This is accompanied by an increase of lateral deformation,  $\delta_{3R}$ , of 1.08 inches (27.5 mm).

As the cycling continues after LP 552, large pinching is observed in the hysteretic loops of the third-story level. This behavior is not the same for the lower two stories which are now much stiffer than the third one. The loss of stiffness in the third story is accompanied by a

decrease in load-resistance capacity of 46.3 kips (206 KN) between LP 552 and LP 600. The measured lateral displacements at LP 552 were  $\delta_{3R} = 2.54$  inches (64.5 mm),  $\delta_{2R} = 0.84$  inches (21.3 mm), and  $\delta_{1R} = 0.20$  inches (5.1 mm) for the third, second, and first stories, respectively.

The specimen was then unloaded and the experiment was halted at LP 618.

#### 4.2.3.2 Base Shear vs. Shear Deformation: Specimen SW7 R<sub>2</sub> (Figs. 4.13 - 4.15)

(1) In the initial stage of the experiment before LP 20, the shear deformations in the three stories were calculated to be very small. At LP 20, the total amount of shear deformation for the three stories was 0.117 inches (2.97 mm). This value is about 68 percent of the total displacement at that point.

(2) Under the 90-kip (400 KN) working load cycles, from LP 53 to LP 97, the total measured shear deformation was 0.19 inches (4.89 mm) which is about 64 percent of the total lateral displacement. The amounts measured for each story separately were  $\delta_{\gamma_3} = 0.098$  inches (2.50 mm),  $\delta_{\gamma_2} = 0.085$  inches (2.15 mm), and  $\delta_{\gamma_1} = 0.0094$  inches (0.240 mm). The amount contributed by the third story alone at LP 53 was 32 percent of the total lateral displacement,  $\delta_{3R}$ .

(3) Under controlled displacement cycling, corresponding to  $\delta_{3R} = 1.0$  inches (25.4 mm), from LP 125 to LP 274, significant pinching and shear deterioration were visible on the shear deformation curves for the second and third stories. The measured amounts for each story at LP 125 were  $\delta_{\gamma_3} = 0.22$  inches (5.57 mm),  $\delta_{\gamma_2} = 0.237$  inches (6.023 mm), and  $\delta_{\gamma_1} = 0.099$  inches (2.54 mm) for the third, second, and first stories, respectively. These add up to 0.555 inches (14.10 mm) which is about 54 percent of the total displacement,  $\delta_{3R}$ , at that point.

At LP 252, the measured shear deformations were  $\delta_{\gamma_3} = 0.235$  inches (5.97 mm),  $\delta_{\gamma_2} = 0.258$  inches (6.56 mm), and  $\delta_{\gamma_1} = 0.091$  inches (2.32 mm), for the third, second and first stories, respectively. These add up to 0.58 inches (14.85 mm) which is about 58 percent of the total lateral displacement,  $\delta_{3R}$ , at that point. A comparison of the results at LP 125 and LP 252 shows a 4 percent increase in the contribution of shear

deformation to the total displacement between these two points.

(4) Under controlled displacement cycling at a ductility,  $\mu_\delta = 2.1$ , from LP 310 to LP 450, the amount of shear deterioration in all three stories increases. The measured deformations at LP 310 were  $\delta_{\gamma_3} = 0.284$  inches (7.22 mm),  $\delta_{\gamma_2} = 0.343$  inches (8.71 mm), and  $\delta_{\gamma_1} = 0.169$  inches (4.31 mm) for the third, second, and first stories, respectively. These total 0.796 inches (20.21 mm) or about 51 percent of the total lateral load at that point. The reasons for the slight decrease in the contribution of the shear as a source of deformation (51 percent vs. 54 percent) were the buckling of the longitudinal reinforcement in the columns and a flexural-type failure in the tension column just prior to LP 310. This failure contributed to the flexural deformation, thus decreasing the percentage of the shear deformation contribution.

In the negative parts of the hysteretic loops, the shear deformation graphs show large deteriorations accompanied by very little change in loads. This is especially true for the second and third stories, at LP 354 and just prior to LP 450, respectively. The measured deformations at LP 449 were  $\delta_{\gamma_3} = -0.67$  inches (-17.15 mm),  $\delta_{\gamma_2} = -0.438$  inches (-11.13 mm), and  $\delta_{\gamma_1} = -0.089$  inches (-2.27 mm) for the third, second, and first stories, respectively. These add up to -1.19 inches (-30.5 mm) which is about 95 percent of the total lateral displacement,  $\delta_{3R}$ , at that point.

(5) Under the three 50-kip (222 KN) loading cycles from LP 465 to LP 505, more shear deterioration is observed from the pinching of the shear deformation curves.

(6) Between LP 520 and LP 609, and under controlled lateral displacement cycling at  $\delta_{3R} = 2.53$  inches (64.3 mm), great shear deterioration is observed in the third-story wall panel. This shear deterioration is due to a shear failure in the third-story panel at LP 539. Similar failure was observed in the second-story panel, although it was not as extensive. The measured values for shear deformation at LP 539 were  $\delta_{\gamma_3} = 0.455$  inches (11.56 mm),  $\delta_{\gamma_2} = 0.313$  inches (7.94 mm), and  $\delta_{\gamma_1} = 0.110$  inches (2.78 mm) for the third, second and first stories, respectively. Together these total 0.878 inches (22.29 mm) or 60 percent of the total lateral displacement,  $\delta_{3R}$ , at that point. The amount contributed by the third-story wall panel alone is about 31 percent of  $\delta_{3R}$ .

At LP 552, after the excessive shear failure along the diagonal of the third-story wall panel and the localized crushing of concrete in the second-story wall panel, the measured shear deformation values were  $\delta_{\gamma 3} = 1.64$  inches (41.81 mm),  $\delta_{\gamma 2} = 0.319$  inches (8.09 mm), and  $\delta_{\gamma 1} = 0.088$  inches (2.23 mm) for the third, second, and first stories, respectively. These total 2.08 inches (52.73 mm) or about 82 percent of the total lateral displacement at that point.

Between LP 539 and LP 552, when the failure of the specimen had occurred, there was a total shear deformation increase of 1.20 inches (30.43 mm), corresponding to an increase of about 22 percent in the contribution of shear to the total lateral deformation. Of this, the contribution of the third story alone was 1.19 inches (30.18 mm) which corresponds to almost all of the total increase in deformation; the rest was contributed by the second-story wall panel. The specimen was then unloaded and the experiment was halted at LP 618.

#### 4.2.3.3 Other Sources of Deformation: Specimen SW7 R<sub>2</sub>

The other displacements measured during the testing were due to the fixed-end rotation and the deflection due to the flexural deformation. Table 3 gives exact values of the contribution of these sources for each story level and at certain important load points. Graphic interpretation of these sources is given in Figs. 4.37 to 4.39.

At LP 53, the total contribution of fixed-end rotation amounted to about 5 percent of the total lateral deformation. The total contribution of flexural deformation was about 24 percent. At LP 125, there was a decrease of fixed-end rotation, and a large increase of flexural deformation to about 40 percent of the total lateral displacement,  $\delta_{3R}$ . The maximum recorded fixed-end rotation was about 0.102 inches (2.58 mm), or about 7 percent of the total lateral displacement, at LP 310. The maximum of the total of the flexural deformations for the three stories was about 40 percent of the lateral displacement,  $\delta_{3R}$ , at LP 125. This corresponded to a total of 0.41 inches (10.49 mm) for the three story levels.

#### 4.2.3.4 Failure Mode: SW7 R<sub>2</sub>

During the testing of SW7 R<sub>2</sub>, the following observations were made in relation to the mode of failure:

(1) Before the 90-kip (400 KN) load cycles from LP 53 to LP 97, only hairline cracks were observed in the second- and third-story wall panels. The first-story wall panel was virtually uncracked.

(2) As the specimen was displaced to  $\delta_{3R} = 1.0$  inches (25.4 mm) at LP 125, more pronounced cracks could be observed. The largest cracks were in the south column both at the middle and the base of the second story (see Fig. 4.51). Many cracks running along the diagonal from the upper south corners of the second- and third-story wall panels appeared and widened (see Fig. 4.52).

As the load was reversed between LP 125 and LP 159, cracking and localized crushing of concrete appeared along the other diagonal (from the upper north corner of the third and second stories) (see Fig. 4.53). Several cracks were also observed in the north column at the second-story level.

(3) As the specimen was subjected to further cycling and taken up to ductility  $\mu_{\delta} = 2$  at LP 310, the cracks in the second- and third-story wall panels became wider and the crushed concrete zones became more extensive. The cracks in the second-story column also became wider and extended into the wall panel. A large crack was observed at the top of the second story between the column and the second-floor slab (see Fig. 4.54).

As the cycling continued between LP 310 and LP 450, a major zone of crushed concrete appeared in the upper north corner of the specimen at the third-story level (see Fig. 4.55). Crushing was also observed along the face of the crack running diagonally to the second-floor slab and reaching the bottom third-story corner in the south side. Between LP 449 and LP 450, the crushed concrete in the upper corner (see Fig. 4.56) was raised up by the buckling of the wall-panel reinforcement in this zone.

(4) As the specimen was subjected to further loading reversals, huge concrete pieces came loose and excessive wall-panel reinforcement buckling was observed. The largest concentration of damage occurred between LP 539 and LP 552, where the failure zone covered a large portion of the third-story wall panel (see Fig. 4.57).

(5) As the cycling continued to LP 609, the loose concrete pieces fell, exposing the heavily buckled wall-panel reinforcement (see Fig. 4.58).

#### 4.2.3.5 Concluding Remarks

The previous data show that for the repaired specimen, SW7 R<sub>2</sub>, the maximum positive displacement,  $\delta_{3R}$ , reached before failure was 1.51 inches (38.35 mm) at LP 310, which corresponds to an overall nominal ductility  $\mu_{\delta} = 2.1$ . The maximum negative displacement was -1.55 inches (-39.26 mm), corresponding to a ductility  $\mu_{\delta} = 2.15$ . These total 3.06 inches (77.61 mm) which corresponds to a cyclic ductility of 3.1.

Of the positive displacement, 53 percent was due to shear distortion in the three wall panels, and 36 percent to the flexural deformation in the three stories. Of the negative displacement, 69 percent was due to shear distortion in the three wall panels, and 24 percent to the flexural deformation in the three stories.

It was observed that most of the shear distortion was concentrated in the second- and third-story wall panels due to failure zones which developed in those wall panels. The overall actual failure, however, occurred in the third-story wall panel around LP 539 where crushing of concrete and buckling of panel reinforcement was observed across the whole panel.

The maximum load carried by the specimen before failure was 275 kips (1215 KN) which corresponds to a nominal shear stress

$$v_{\max} = 12.2 \sqrt{f'_c} \text{ (psi) or } 1.01 \sqrt{f'_c} \text{ (MPa)}$$

#### 4.3 Specimen SW8

(a) Virgin phase. As illustrated in Fig. 4.16, in this first phase of the testing, SW8 Virgin was subjected to several working load cycles, the maximum of which was 90 kips (400 KN) and then displaced to first yield (ductility  $\mu_{\delta} = 1$ ), corresponding to  $\delta_{3R} = 0.62$  inches (15.75 mm). It was also displaced to yield in the negative direction and then subjected to a cycle of loading reversal. The specimen was then subjected to several working load cycles.



(b) Epoxy-repaired phase. As indicated in Fig. 4.16, the specimen was epoxy repaired at LP 325 and, after several cycles of loading reversals at yielding, it was loaded monotonically to failure with some unloading and intermediate cycling. A displacement ductility of  $\mu_{\delta} = 9.75$  was reached at the point of failure of the first-story wall panel. The third-story lateral displacement at that point was  $\delta_{3R} = 6.04$  inches (153.6 mm), and the maximum base shear was  $P_T = 234$  kips (1040 KN).

(c) Twice-repaired phase. The specimen was repaired and strengthened at the first-story level, and cyclically loaded up to failure (Fig. 4.17). The maximum shear resisted was 277 kips (1231 KN), and the maximum positive ductility reached when failure started was  $\mu_{\delta} = 2.3$ , corresponding to a positive displacement  $\delta_{3R} = 1.65$  inches (41.9 mm).

Each of the above three phases is discussed in detail below.

#### 4.3.1 Results of Tests on the Virgin Specimen: SW8 Virgin

The loading history for specimen SW8 Virgin is given in Fig. 4.16.  $P_T - \delta$  graphs are given in Figs. 4.18 through 4.21, and  $V - \gamma$  diagrams are given in Figs. 4.25 through 4.27.

As indicated in Fig. 4.16, specimen SW8 was initially loaded up to 10 kips (45 KN) and cycled once, then up to 25 kips (111 KN) at LP 16, cycled once, and then subjected to three cycles at a working load of 90 kips (400 KN) between LP 34 and LP 106. The specimen was displaced until first yield,  $\mu_{\delta} = 1$ , corresponding to  $\delta_{3R} = 0.62$  inches (15.75 mm) at LP 155. It was unloaded and subjected to two 25-kip (111 KN) cycles from LP 170 to LP 184 before it was taken to first yield in the negative direction, corresponding to  $\delta_{3R} = 0.53$  inches (13.46 mm) at LP 218. It was then unloaded and subjected to one 25-kip loading reversal between LP 233 and LP 237, after which it was taken again to first yield and subjected to one load cycle from LP 257 to LP 284. Finally, it was subjected to two 25-kip cycles from LP 300 to LP 314. The test was then halted, and the specimen was epoxy repaired.

##### 4.3.1.1 Base Shear vs. Total Lateral Displacement: Specimen SW8 Virgin (Figs. 4.19 - 4.21)

(1) In the initial part of the experiment before LP 34, the deformations in all three stories were found to be very small, i.e., less than 0.14 inches (3.56 mm). No significant deterioration or loss of

stiffness can be observed in the specimen.

(2) Under the 90-kip working load cycles, from LP 34 to LP 106, the total observed lateral displacement was 0.15 inches (3.68 mm). No significant deterioration can be observed, since the hysteretic loops are very stable at that load level.

(3) Under controlled displacement loading at the point of first yield corresponding to  $\delta_{3R} = 0.62$  inches (15.75 mm) at LP 155, the total lateral load carried by the specimen was 196 kips (872 KN).

(4) Under the 25-kip (111 KN) loading cycles from LP 170 to LP 184, the maximum total lateral displacement measured was 0.16 inches (4.07 mm), which is 6.4 times the displacement measured under the same load at LP 19. The permanent displacement under zero load was measured as  $\delta_{3R} = 0.13$  inches (3.25 mm) at LP 182.

(5) Under controlled displacement to the point of first yield in the negative direction corresponding to  $\delta_{3R} = -0.53$  inches (-13.46 mm) at LP 218, the total lateral load resisted by the specimen was 199 kips (887 KN).

(6) Under the 25-kip (111 KN) loading cycle from LP 233 to LP 237, the maximum measured lateral displacement was 0.034 inches (0.86 mm).

(7) Under controlled displacement loading at ductility  $\mu_{\delta} = 1$  from LP 257 to LP 284, the maximum total lateral load measured was 183 kips (816 KN) in the positive direction and 196 kips (873 KN) in the negative direction. Both values are lower than the previous ones at the same displacement, which can be attributed to a loss of stiffness in the specimen due to the cracking in the wall panels. The drop in load values is no more than 7 percent.

(8) Under the two 25-kip (111 KN) load cycles between LP 300 and LP 314, the maximum measured lateral displacement was 0.063 inches (1.60 mm), which is about 1.8 times the value measured under the same load at LP 233. This was caused by the loss of stiffness in the specimen when taken to first yield.

The specimen was then unloaded and epoxy repaired at LP 325.

4.3.1.2 Base Shear vs. Shear Deformation: Specimen SW8 Virgin  
(Figs. 4.25 - 4.27)

(1) In the initial part of the experiment, before LP 34, the shear deformation in the three-story wall panels was calculated to be very small. At LP 34, the total amount of shear deformation for the three stories was 0.017 inches (0.43 mm), or about 12 percent of the total deformation.

(2) Under the 90-kip working load cycles, from LP 34 to LP 106, the maximum total measured shear deformation was 0.022 inches (0.57 mm), which is about 15 percent of the total displacement at that point.

(3) At the point of first yield at LP 155, the measured amounts of shear deformation were  $\delta_{\gamma_3} = 0.066$  inches (1.68 mm),  $\delta_{\gamma_2} = 0.059$  inches (1.5 mm), and  $\delta_{\gamma_1} = 0.092$  inches (2.34 mm) for the third, second, and first stories, respectively. These add up to a total of 0.217 inches (5.52 mm) which is about 35 percent of the total lateral displacement,  $\delta_{3R}$ , at that point.

(4) Under the 25-kip loading cycles from LP 170 to LP 184, the largest measured shear deformations were  $\delta_{\gamma_3} = 0.013$  inches (0.32 mm),  $\delta_{\gamma_2} = 0.017$  inches (0.42 mm), and  $\delta_{\gamma_1} = 0.024$  inches (0.62 mm), for the third, second, and first stories, respectively. These total 0.053 inches (1.34 mm), or about 32 percent of the total lateral displacement  $\delta_{3R}$  at that point.

(5) Under controlled displacement to the point of first yield in the negative direction at LP 218, the measured shear deformations were  $\delta_{\gamma_3} = -0.054$  inches (-1.37 mm),  $\delta_{\gamma_2} = -0.056$  inches (-1.48 mm), and  $\delta_{\gamma_1} = -0.095$  inches (-2.42 mm) for the third, second, and first stories, respectively. These add up to -0.207 inches (-5.27 mm) which is about 38 percent of the total lateral displacement at that point.

(6) Under controlled displacement loading at ductility  $\mu_\delta = 1$  from LP 257 to LP 284, the measured shear deformations were  $\delta_{\gamma_3} = 0.050$  inches (1.25 mm),  $\delta_{\gamma_2} = 0.058$  inches (1.46 mm), and  $\delta_{\gamma_1} = 0.096$  inches (2.42 mm) for the third, second, and first stories, respectively. These add up to a total of 0.202 inches (5.13 mm) which is about 33 percent of the total displacement at that point.

#### 4.3.1.3 Other Sources of Deformation: Specimen SW8 Virgin

The other displacements measured during the testing were those due to fixed-end rotation and to the flexural deformation. Graphic interpretation of the contributions of these sources is given in Figs. 4.40 to 4.42. Exact values of the contribution of these sources for each story level and at certain important points are given in Table 4.

(1) Before LP 34 the total amount of flexural deformation for the three stories was 0.091 inches (2.3 mm) which is about 64 percent of the total lateral displacement. The measured fixed-end rotation was 0.014 inches (0.35 mm) or about 10 percent of the total deformation.

(2) Under the 90-kip working load cycles from LP 34 to LP 106, the total measured flexural deformation for the specimen was 0.095 inches (2.4 mm), and the fixed-end rotation was 0.015 inches (0.389 mm). These values correspond to 65 and 11 percent of the total deflection at that point.

(3) At the point of first yield at LP 155, the measured flexural deformation and fixed-end rotation were 0.33 inches (8.38 mm) and 0.056 inches (1.42 mm), respectively. These values correspond to 53 and 9 percent of the total lateral displacement at that load point.

(4) Under the 25-kip loading cycles from LP 170 to LP 184, the measured flexural deformation and fixed-end rotation were 0.088 inches (2.24 mm) and 0.016 inches (0.407 mm), respectively. These values correspond to about 55 and 10 percent of the total lateral displacement at that point.

(5) At LP 218, corresponding to the point of first yield in the negative direction, the measured flexural deformation and fixed-end rotation were -0.25 inches (-6.37 mm) and -0.063 inches (-1.59 mm). These amount to 47 and 12 percent of the total lateral displacement at that point.

(6) Under controlled displacement loading at ductility  $\mu_{\delta} = 1$  from LP 257 to LP 284, the largest measured flexural deformations and fixed-end rotation were 0.367 inches (9.32 mm) and 0.0275 inches (0.698 mm), respectively. These values correspond to 59 and 4 percent of the total lateral displacement at that point.

#### 4.3.1.4 Concluding Remarks

The previous data show that for the virgin specimen, SW8 Virgin, the maximum displacement,  $\delta_{3R}$ , reached was 0.62 inches (15.75 mm). Of this displacement, 33 percent was due to shear distortion, 59 percent to flexural deformation, 4 percent to the fixed-end rotation, and the rest to the deformation of the foundation and the errors in instrumentation. It was observed that most of the shear distortion (15 percent of total  $\delta_{3R}$ ) and flexural deformation (23 percent of total  $\delta_{3R}$ ) were concentrated in the first story.

The maximum load carried by the specimen was 199 kips (887 KN) at LP 218. No indication of a failure mechanism was observed in the specimen at this phase of testing.

#### 4.3.2 Results of Tests on Epoxy-Repaired Specimen: SW8 R<sub>1</sub>

The loading history for specimen SW8 Epoxy-Repaired is given in Fig. 4.16.  $P_T - \delta$  graphs are given in Figs. 4.18 through 4.21, and  $V - \gamma$  diagrams are given in Figs. 4.26 and 4.27.

Epoxy-repaired specimen SW8 was initially loaded and cycled once at 10 kips (45 KN) and 25 kips (111 KN). Then it was subjected to three 90-kip working load cycles from LP 351 to LP 403. After this, it was displaced up to the value at which the first yield was originally observed in the virgin specimen SW8, i.e., to a  $\delta_{3R} = 0.62$  inches (15.75 mm). It was cycled three times from LP 426 to LP 544 and was then displaced up to a ductility,  $\mu_\delta = 3.0$ , corresponding to  $\delta_{3R} = 2.16$  inches (54.8 mm) at LP 593. The specimen was unloaded to a zero load at LP 604 and subjected to three 90-kip working load cycles from LP 612 to LP 668, after which it was displaced up to a ductility,  $\mu_\delta = 5.93$ , at LP 702, corresponding to a lateral displacement  $\delta_{3R} = 3.68$  inches (93.40 mm). The specimen was unloaded to a zero load and cycled twice under a 25-kip (111 KN) load from LP 710 to LP 727. It was then displaced up to failure, which occurred at LP 755. The maximum lateral displacement reached at LP 755 was 6.05 inches (153.62 mm), corresponding to a ductility of  $\mu_\delta = 9.75$ . The specimen was then unloaded, repaired, and strengthened at the first-story level.

4.3.2.1 Base Shear vs. Total Lateral Displacement: Specimen SW8 R<sub>1</sub>  
(Figs. 4.18 - 4.21)

(1) In the initial part of the experiment, under the 90-kip (400 KN) working load cycles between LP 351 and LP 403, the third-story lateral displacement was 0.21 inches (5.31 mm). This value is about 1.4 times that of the virgin specimen under the same load cycles.

(2) Under cycling at a displacement corresponding to first yield of the virgin specimen, i.e., between LP 426 and LP 544, the maximum total lateral load resisted by the specimen was 192.4 kips (856 KN), which was about 3 percent less than that at which first yielding occurred in the virgin specimen, 196 kips (872 KN). The measured lateral displacements at that point were  $\delta_{3R} = 0.62$  inches (15.75 mm),  $\delta_{2R} = 0.41$  inches (10.31 mm), and  $\delta_{1R} = 0.23$  inches (5.78 mm), for the third, second, and first stories, respectively.

(3) At a displacement of  $\delta_{3R} = 2.16$  inches (54.86 mm) corresponding to  $\mu_{\delta} = 3.5$  at LP 593, the maximum load carried by the specimen was  $P_T = 216.3$  kips (962 KN). The measured lateral displacements at that point were  $\delta_{2R} = 1.46$  inches (37.10 mm) and  $\delta_{1R} = 0.84$  inches (21.25 mm) for the second and first stories, respectively.

(4) The specimen was then unloaded to a zero load at LP 604. The permanent deflection,  $\delta_{3R}$ , at LP 604 was 1.35 inches (34.20 mm). Under the 90-kip (400 KN) working load cycles, between LP 623 and LP 668, the largest displacement,  $\delta_{3R}$ , was 0.95 inches (24.02 mm), which is about 4.5 times the value under the same load at LP 351.

(5) At a displacement,  $\delta_{3R} = 3.68$  inches (93.40 mm), corresponding to a ductility  $\mu_{\delta} = 5.9$  at LP 702, the maximum load,  $P_T$ , carried by the specimen was 231 kips (1026 KN). The second- and first-story displacements measured at that point were  $\delta_{2R} = 2.52$  inches (63.98 mm) and  $\delta_{1R} = 1.43$  inches (36.34 mm), respectively.

(6) The specimen was then unloaded to a zero load at LP 710. The permanent lateral displacements at that point were  $\delta_{3R} = 2.82$  inches (71.61 mm),  $\delta_{2R} = 1.98$  inches (50.36 mm), and  $\delta_{1R} = 1.15$  inches (29.28 mm) for the third, second, and first stories, respectively.

(7) At a displacement,  $\delta_{3R} = 6.05$  inches (153.6 mm), corresponding

to a ductility,  $\mu_\delta = 9.75$ , the maximum total lateral load carried by the specimen was  $P_T = 234$  kips (1041 KN). The measured second- and first-story displacements at that point were  $\delta_{2R} = 4.14$  inches (105.08 mm) and  $\delta_{1R} = 2.35$  inches (59.71 mm), respectively.

(8) The specimen was then unloaded and removed for repairs.

#### 4.3.2.2 Base Shear vs. Shear Deformation: Specimen SW8 R<sub>1</sub> (Figs. 4.26 and 4.27)

(1) Under the 90-kip (400 KN) working load cycles, between LP 351 and LP 403, the measured shear deformations for the three stories were  $\delta_{\gamma 3} = 0.023$  inches (0.572 mm),  $\delta_{\gamma 2} = 0.027$  inches (0.686 mm), and  $\delta_{\gamma 1} = 0.035$  inches (0.880 mm) for the third, second, and first stories, respectively. These amounts total 0.084 inches (2.14 mm), or about 40 percent of the total lateral displacement at that loading level.

(2) Under cycling, at a displacement corresponding to first yield in SW8 Virgin between LP 426 and LP 544, the measured shear deformations were  $\delta_{\gamma 3} = 0.063$  inches (1.60 mm),  $\delta_{\gamma 2} = 0.070$  inches (1.78 mm), and  $\delta_{\gamma 1} = 0.113$  inches (2.88 mm) for the third, second, and first stories, respectively. These values add up to 0.247 inches (6.26 mm), or about 40 percent of the total lateral displacement at that loading level. The shear deformation is mostly concentrated at the first-story level, where the contribution is about 18 percent of the total displacement.

(3) As the specimen is displaced to a ductility,  $\mu_\delta = 3.5$  at LP 593, the measured shear deformations were  $\delta_{\gamma 3} = 0.076$  inches (1.94 mm),  $\delta_{\gamma 2} = 0.0806$  inches (2.05 mm), and  $\delta_{\gamma 1} = 0.445$  inches (11.31 mm) for the third, second and first stories, respectively, a total of 0.602 inches (15.28 mm) or about 28 percent of the total lateral displacement at that point. This value shows a decrease of about 12 percent in the contribution of shear deformation from the value at LP 426. The contribution of first-story shear deformation has, however, increased by about 2 percent.

(4) Under zero load, at LP 604, the measured shear deformations were  $\delta_{\gamma 3} = 0.018$  inches (0.457 mm),  $\delta_{\gamma 2} = 0.023$  inches (0.572 mm), and  $\delta_{\gamma 1} = 0.312$  inches (7.92 mm) for the third, second, and first stories, respectively. These values total 0.352 inches (8.95 mm) which is about 26 percent of the total permanent displacement at that point.

Under the 90-kip (400 KN) working load cycles between LP 623 and LP 668, the largest measured shear deformations were  $\delta_{\gamma_3} = 0.027$  inches (0.686 mm),  $\delta_{\gamma_2} = 0.034$  inches (0.857 mm), and  $\delta_{\gamma_1} = 0.208$  inches (5.28 mm) for the third, second, and first stories, respectively, or a total of 0.269 inches (6.82 mm) which is about 28 percent of the total lateral displacement at that load level. This increased amount of shear deformation is primarily due to an increase in the shear deterioration in the first-story wall panel, as can be deduced from an analysis of the hysteretic behavior of the load-shear deformation diagram for the first-story level between LP 630 and LP 647, as well as from the fact that the contribution of the first-story wall panel is about 15 percent of the total lateral displacement,  $\delta_{3R}$ .

(5) As the specimen was displaced up to a ductility,  $\mu_{\delta} = 5.9$  at LP 702, the measured values of shear deformation were  $\delta_{\gamma_3} = 0.090$  inches (2.28 mm),  $\delta_{\gamma_2} = 0.134$  inches (3.41 mm), and  $\delta_{\gamma_1} = 0.789$  (20.04 mm) for the third, second, and first stories, respectively. These values total 1.01 inches (25.73 mm) or about 27.5 percent of the total lateral displacement at that point. The contribution of the first-story shear deformation was about 21.5 percent of the total lateral displacement, leaving only 6 percent for the second and third stories.

(6) Under zero load, at LP 710, the measured shear deformations were  $\delta_{\gamma_3} = 0.056$  inches (1.42 mm),  $\delta_{\gamma_2} = 0.068$  inches (1.75 mm), and  $\delta_{\gamma_1} = 0.606$  inches (15.40 mm) for the third, second, and first stories, respectively. These values total 0.731 inches (18.57 mm) or about 26 percent of the total permanent lateral displacement,  $\delta_{3R}$ .

Under 25-kip (111 KN) load cycling between LP 715 and LP 727, the total contribution of shear deformation for the three stories was about 27 percent of the total lateral displacement,  $\delta_{3R}$ .

(7) As the specimen is displaced up to a ductility,  $\mu_{\delta} = 9.75$  (LP 755), the largest shear deformations were  $\delta_{\gamma_3} = 0.180$  inches (4.57 mm),  $\delta_{\gamma_2} = 0.225$  inches (5.72 mm), and  $\delta_{\gamma_1} = 1.34$  inches (33.94 mm) for the third, second, and first stories, respectively. These values add up to 1.75 inches (44.33 mm) which is about 29 percent of the total lateral displacement at that point. The first-story shear deformation



contribution at the point of failure is about 22 percent of the total lateral displacement,  $\delta_{3R}$ .

#### 4.3.2.3 Other Sources of Deformation: SW8 R<sub>1</sub>

The other displacements measured during the testing were those due to fixed-end rotation and the deflection due to the flexural deformation. Graphic interpretation of the contributions of these sources is given in Figs. 4.43 to 4.45. Exact values of the contribution of these sources for each story level and at certain important load points are given in Table 4.

(1) Under the 90-kip (400 KN) working load cycles, between LP 351 and LP 403, the total measured amount of flexural deformation was 0.11 inches (2.82 mm) which is about 53 percent of the total lateral displacement. The measured amount of fixed-end rotation was 0.014 inches (0.354 mm) which is about 7 percent of the total lateral deformation at that point.

(2) Under cycling at first yield, between LP 426 and LP 544, the total measured flexural deformation and fixed-end rotation were 0.341 inches (8.66 mm) and 0.0279 inches (0.709 mm), respectively. These amounts are about 55 and 5 percent of the total lateral displacement, respectively.

(3) At a ductility  $\mu_{\delta} = 3.5$  at LP 593, the measured amounts of total flexural deformation and fixed-end rotation were 1.23 inches (31.30 mm) and 0.168 inches (4.25 mm), respectively. These values are about 57 and 8 percent of the total lateral displacement at that point.

(4) Under zero load at LP 604, the measured amounts of total flexural deformation and fixed-end rotation were 0.935 inches (23.75 mm) and 0.098 inches (2.48 mm), respectively. These values are about 69 and 6 percent of the total lateral displacement.

Under the 90-kip (400 KN) working load cycles, between LP 623 and LP 668, the measured total flexural deformation and fixed-end rotation were 0.598 inches (15.20 mm) and 0.056 inches (1.42 mm), respectively. These values are about 63 and 6 percent of the total lateral deformation,  $\delta_{3R}$ .

(5) At a displacement corresponding to  $\mu_{\delta} = 5.9$  at LP 702, the measured amounts of total flexural deformation and fixed-end rotation were 2.28 inches (58.05 mm) and 0.423 inches (10.74 mm), respectively. These are about 62 and 11 percent of the total lateral displacement at that point.

(6) Under zero load, at LP 710, the measured amounts of total flexural deformation and fixed-end rotation were 1.86 inches (47.43 mm) and 0.900 inches (2.29 mm). These values are about 66 and 3.2 percent of the total lateral displacement,  $\delta_{3R}$ .

(7) At a displacement  $\delta_{3R}$  of 6.05 inches (153.6 mm) corresponding to  $\mu_{\delta} = 9.75$  at LP 755, the measured total flexural deformation and fixed-end rotation were 3.93 inches (99.87 mm) and 0.139 inches (3.54 mm),\* respectively. These values are about 65 and 2 percent of the total lateral displacement,  $\delta_{3R}$ .

#### 4.3.2.4 Failure Mode: SW8 R<sub>1</sub>

During the testing of specimen SW8 R<sub>1</sub>, it was observed that the failure mode was initiated by the considerable widening of horizontal cracks which opened at the first-story south column (see Fig. 4.59). These cracks then propagated into the first-story wall panel (see Fig. 4.60). Crushing of concrete and initiation of buckling of column reinforcement in the lower north corner of the first-story columns were also observed (see Fig. 4.61).

After failure, when the specimen was loaded to the south (i.e., between LP 755 and LP 791), buckling of the first-story wall-panel reinforcement as well as crushing of the concrete cover at the base of the south column could be seen (Fig. 4.62). A large number of ties were broken. In the edge column, the region where the concrete crushed extended from the base of the south column to about 20 inches above (508 mm).

#### 4.3.2.5 Concluding Remarks

The previous data show that for the epoxy-repaired specimen, SW8 R<sub>1</sub>, the failure mode was that of a combined flexure-shear type. The maximum displacement,  $\delta_{3R}$ , reached before the failure of the specimen, was 6.05 inches (153.6 mm), corresponding to a displacement ductility of 9.75 at LP 755. Of this maximum displacement, 29 percent was due to the effect

---

\*It is suspected that this value has been incorrectly measured.

of shear deterioration in the three wall panels, 65 percent to flexural deformation, 2 percent to fixed-end rotation, and the rest to the deformation of the foundation and the errors in the instrumentation at large values of ductility.

It was observed that most of the flexural and shear deformations were concentrated at the first-story levels, and thus the failure zone was at that level. The contributions of shear and flexural deformations in the first story were 22 and 24 percent of the total lateral displacement,  $\delta_{3R}$ , respectively.

The maximum load carried by the specimen before failure was 234 kips (1041 KN) at LP 755.

#### 4.3.3 Results of Tests on Repaired and Strengthened Specimen: SW8 R<sub>2</sub>

The loading history for specimen SW8 R<sub>2</sub> is given in Fig. 4.17.  $P_T - \delta$  graphs are given in Figs. 4.22 through 4.24, and  $V - \gamma$  diagrams are given in Figs. 4.28 through 4.30.

Specimen SW8, twice repaired and with its first story strengthened, was initially loaded and cycled once at 10 kips (45 KN) and once at 25 kips (111 KN). Then it was subjected to three 50-kip (222 KN) cycles between LP 31 and LP 57, and to three 90-kip (400 KN) cycles between LP 64 and LP 92 before it was subjected to a load of 185 kips (823 KN) at LP 105. After these series of tests, the specimen was subjected to three loading cycles between LP 132 and LP 170 at a ductility  $\mu_\delta = 1$  (based on the first yield observed in this specimen). Then it was displaced to a ductility  $\mu_\delta = 2$  and subjected to three loading cycles between LP 193 and LP 292, after which it was subjected to three 50-kip load cycles between LP 302 and 328 and to one cycle at a load of 90 kips (LP 337 and LP 343). Finally, the specimen was displaced up to a ductility  $\mu_\delta = 2.3$  and subjected to four cycles between LP 367 and LP 587 during which failure occurred. The specimen was then unloaded and the experiment was halted.

##### 4.3.3.1 Base Shear vs. Total Lateral Displacement: Specimen SW8 R<sub>2</sub> (Figs. 4.22 - 4.24)

(1) In the initial part of the experiment before the 50-kip (222 KN) load cycles, i.e., before LP 31, the largest measured lateral displacements

were  $\delta_{3R} = 0.112$  inches (2.84 mm) and  $\delta_{2R} = 0.048$  (1.23 mm) for the third and second stories, respectively. The first-story displacement was negligible.

(2) Under the 90-kip (400 KN) loading cycles between LP 64 and LP 92, the measured largest lateral displacements were  $\delta_{3R} = 0.214$  inches (5.44 mm) and  $\delta_{2R} = 0.105$  inches (2.66 mm) for the third and second stories, respectively. The first-story lateral displacement was also negligible i.e., less than 0.039 inches (1.0 mm).

(3) Under the 185-kip (823 KN) load at LP 105, the measured lateral displacements were  $\delta_{3R} = 0.554$  inches (14.08 mm) and  $\delta_{2R} = 0.301$  inches (7.64 mm) for the third and second stories. The first-story lateral displacement was still negligible [0.07 inches (1.77 mm)].

(4) As the specimen was displaced up to a first yield,  $\mu_{\delta} = 1$ , corresponding to  $\delta_{3R} = 0.72$  inches (18.29 mm) and subjected to three cycles between LP 132 and LP 170, the largest measured lateral displacements were  $\delta_{3R} = 0.75$  inches (19.13 mm),  $\delta_{2R} = 0.422$  inches (10.71 mm), and  $\delta_{1R} = 0.121$  inches (3.08 mm) for the third-, second-, and first-floor levels, respectively. The maximum load,  $P_T$ , resisted by the specimen was 241 kips (1073 KN) at LP 132.

(5) As the specimen was displaced up to a ductility  $\mu_{\delta} = 2$ , corresponding to  $\delta_{3R} = 1.44$  inches (36.58 mm), and subjected to three loading cycles between LP 193 and LP 292, the maximum measured lateral displacements were  $\delta_{3R} = 1.52$  inches (38.53 mm),  $\delta_{2R} = 0.901$  inches (22.81 mm), and  $\delta_{1R} = 0.324$  inches (8.23 mm) for the third, second and first stories, respectively. The maximum load resisted by the specimen was 277 kips (1231 KN) at LP 209. The maximum negative load was 256 kips (1138 KN) at LP 193.

(6) Under the three 50-kip (222 KN) load cycles from LP 302 to LP 328, the largest measured lateral displacements were  $\delta_{3R} = -0.679$  inches (-17.19 mm) and  $\delta_{2R} = -0.353$  inches (-8.97 mm) for the third and second stories. The positive first-story displacement under these loading cycles was 0.027 inches (0.7 mm), and the negative one was 0.14 inches (3.5 mm).

(7) Under the 90-kip (400 KN) working load cycle, from LP 337 to LP 343, the largest measured lateral displacements were  $\delta_{3R} = -0.724$  inches (-18.39 mm),  $\delta_{2R} = -0.375$  inches (-9.52 mm), and  $\delta_{1R} = -0.16$  inches

(-4 mm) for the third, second and first stories, respectively. These values were measured at LP 343. The largest positive values measured were  $\delta_{3R} = 0.293$  inches (7.44 mm),  $\delta_{2R} = 0.223$  inches (5.66 mm) and  $\delta_{1R} = 0.072$  inches (1.81 mm) at LP 337.

(8) As the specimen was displaced up to a ductility  $\mu_{\delta} = 2.3$ , corresponding to  $\delta_{3R} = 1.65$  inches (41.88 mm) and subjected to four loading cycles between LP 367 and LP 587, the maximum positive load resisted by the specimen was 257 kips (1145 KN) at LP 367. At this LP,  $\delta_{2R} = 1.02$  inches (25.82 mm) and  $\delta_{1R} = 0.278$  inches (6.95 mm) for the second and first stories, respectively. The maximum negative load resisted by the specimen was 236 kips (1051 KN) at LP 417. The measured lateral displacements at that point were  $\delta_{3R} = -2.15$  inches (-54.66 mm),  $\delta_{2R} = -1.32$  inches (-33.41 mm) and  $\delta_{1R} = -0.454$  inches (-11.52 mm) for the third, second and first stories, respectively.

The maximum positive ductility reached during the testing was  $\mu_{\delta} = 2.3$ . The maximum negative ductility reached was  $\mu_{\delta} = 3.0$ . The total cyclic ductility was 4.3.

(9) The specimen was then unloaded and the experiment was halted.

#### 4.3.3.2 Base Shear vs. Shear Deformation: Specimen SW8 R<sub>2</sub> (Figs. 4.28 - 4.30)

(1) In the initial part of the experiment before the 50-kip (222 KN) load cycles, i.e., before LP 54, the largest measured shear deformations were  $\delta_{\gamma 3} = 0.050$  inches (1.27 mm) and  $\delta_{\gamma 2} = 0.014$  inches (0.354 mm) for the third and second stories, respectively. The first-story shear distortion was negligible.

(2) Under the 90-kip (400 KN) loading cycles between LP 64 and LP 92, the largest measured values of shear deformation were  $\delta_{\gamma 3} = 0.0707$  inches (1.79 mm),  $\delta_{\gamma 2} = 0.033$  inches (0.846 mm) and  $\delta_{\gamma 1} = 0.002$  inches (0.050 mm) for the third, second and first stories, respectively.

(3) Under the 185-kip (823 KN) load at LP 105, the measured values of shear deformation were  $\delta_{\gamma 3} = 0.132$  inches (3.36 mm),  $\delta_{\gamma 2} = 0.089$  inches (2.26 mm) and  $\delta_{\gamma 1} = 0.0346$  inches (0.879 mm) for the third, second and first stories, respectively.

(4) As the specimen was displaced up to a ductility  $\mu_\delta = 1$ , corresponding to  $\delta_{3R} = 0.72$  inches (18.29 mm), and subjected to three loading cycles between LP 132 and LP 170, the largest measured values of shear deformation were  $\delta_{\gamma_3} = 0.180$  inches (4.57 mm),  $\delta_{\gamma_2} = 0.162$  inches (4.11 mm), and  $\delta_{\gamma_1} = 0.0396$  inches (1.01 mm), for the third, second and first stories, respectively.

(5) As the specimen was displaced up to a ductility  $\mu_\delta = 2$ , corresponding to  $\delta_{3R} = 1.44$  inches (36.58 mm), and subjected to three loading cycles between LP 193 and LP 292, the largest measured values of shear deformation were  $\delta_{\gamma_3} = 0.212$  inches (5.37 mm),  $\delta_{\gamma_2} = 0.279$  inches (7.09 mm) and  $\delta_{\gamma_1} = 0.164$  inches (4.17 mm), for the third, second and first stories, respectively.

(6) Under the 50-kip (222 KN) load cycles between LP 302 and LP 328, the largest measured values of shear deformation were  $\delta_{\gamma_3} = -0.156$  inches (-4.00 mm),  $\delta_{\gamma_2} = -0.212$  inches (-5.38 mm) and  $\delta_{\gamma_1} = -0.0297$  inches (0.75 mm) for the third, second and first stories, respectively.

(7) Under the 90-kip (400 KN) working load cycle, from LP 337 to LP 343, the largest measured shear deformations were  $\delta_{\gamma_3} = -0.163$  inches (-4.15 mm),  $\delta_{\gamma_2} = -0.205$  inches (-5.21 mm) and  $\delta_{\gamma_1} = -0.058$  inches (-1.48 mm) for the third, second and first stories, respectively. These values were measured at LP 343. The largest positive values were  $\delta_{\gamma_3} = 0.052$  inches (1.33 mm),  $\delta_{\gamma_2} = 0.066$  inches (1.67 mm) and  $\delta_{\gamma_1} = 0.050$  inches (1.28 mm) at LP 337.

(8) As the specimen was displaced up to a ductility  $\mu_\delta = 2.3$  and subjected to four cycles between LP 367 and LP 587, the largest measured positive shear deformations before failure were  $\delta_{\gamma_3} = 0.212$  inches (5.37 mm),  $\delta_{\gamma_2} = 0.366$  inches (9.29 mm) and  $\delta_{\gamma_1} = 0.168$  inches (4.27 mm) for the third, second and first stories, respectively.

#### 4.3.3.3 Other Sources of Deformation: Specimen SW8 R<sub>2</sub>

The other displacements that were measured during the testing were those due to the fixed-end rotation and the deflection due to flexural deformation. Exact values of the contribution of these sources of deformations for each story level and at certain important load points are given in Table 5. Graphic interpretation of these sources is given in Figs. 4.46 to 4.48.

(1) In the initial part of the experiment, before the 50-kip (222 KN) loading cycles (i.e., before LP 54), the largest measured total flexural deformation and fixed-end rotation were 0.043 inches (1.01 mm) and 0.004 inches (0.114 mm), respectively. These values correspond to 38 and 4 percent of the total lateral displacement at that point.

(2) Under the 90-kip (400 KN) loading cycles, between LP 64 and LP 92, the largest measured total flexural deformation and fixed-end rotation were 0.098 inches (2.48 mm) and 0.011 inches (0.272 mm), respectively, or about 46 and 5 percent of the total lateral displacement at that point.

(3) At LP 105, under the 185-kip (823 KN) load, the measured values for total flexural deformation and fixed-end rotation were 0.249 inches (6.32 mm) and 0.0499 inches (1.26 mm), respectively, or about 45 and 9 percent of the total lateral displacement at that point.

(4) At LP 143, corresponding to  $\mu_{\delta} = 1$ , the measured total flexural deformation and fixed-end rotation were 0.282 inches (7.17 mm) and 0.086 inches (2.18 mm), respectively, or about 38 and 11 percent of the total lateral displacement at that point.

(5) At LP 209, corresponding to  $\mu_{\delta} = 2$ , the measured values for total flexural deformation and fixed-end rotation were 0.695 inches (17.65 mm) and 0.090 inches (2.28 mm), respectively, or about 46 and 6 percent of the total lateral displacement at that point.

(6) Under the three 50-kip (222 KN) load cycles from LP 302 to LP 328, the largest measured total flexural deformation and fixed-end rotation were -0.274 inches (-6.95 mm) and -0.004 inches (-0.106 mm), respectively, or about 40 and 1 percent of the total relative displacement at LP 328.

(7) Under the 90-kip working load cycle from LP 337 to LP 343, the largest positive measured total flexural deformation and fixed-end rotation were 0.125 inches (3.18 mm) and 0.010 inches (0.248 mm), respectively, or about 43 and 3 percent of the total lateral displacement at that point.

(8) When the specimen was displaced up to a ductility  $\mu_{\delta} = 2.3$  and subjected to four cycles between LP 367 and LP 587, the total measured

values of flexural deformation and fixed-end rotation at LP 367 were 0.855 inches (21.72 mm) and 0.032 inches (0.815 mm), respectively. These values are about 52 and 2 percent of the total lateral displacement at that point.

Between LP 367 and LP 386, there was a marked increase in the contribution of the fixed-end rotation. This was attributed to the failure of the south column at the base of the first-story level. A large crack at the base of the column exposed the reinforcement which had apparently ruptured. The crack propagated into the wall panel along the footing. The largest value for the fixed-end rotation measured at that point was  $\theta_F = 0.0033$  radians which amounts to a third-story deformation of about 0.460 inches (11.69 mm). This value is 21 percent of the total lateral displacement at LP 386. The total amount of flexural deformation at that point was 1.39 inches (35.34 mm) or about 64 percent of the total lateral displacement.

At LP 417, as the largest negative load (to the south) was reached, the fixed-end rotation decreased to  $\theta_F = 0.0014$  radians. This amounts to a third-story deformation of 0.195 inches (4.9 mm) in the positive direction. The measured total flexural deformation at that point was -1.17 inches (-29.66 mm). The flexural deformation amounted to 53 percent of the total lateral displacement. The remaining deformation was attributed to the contribution of the buckling of some of the wall panel reinforcement at both the third- and second-story levels, thus adding to the shear deformation.

As the maximum displacement to the north was reached at LP 459 (see Fig. 4.22), there was a failure in the reinforcement in the south column at the base of the second-story level, thus decreasing the effect of fixed-end rotation. The value reached at LP 459 was  $\theta_F = 0.0025$  radians, which amounts to a third-story deformation of 0.349 inches (8.86 mm). This value is 16 percent of the total lateral displacement at that point. The drop in load resistance at this LP 459 was attributed to the failure of the column reinforcement at the base of the second-story level.

As the cycling continued, the effect of both the flexural deformation and the fixed-end rotation was decreased as the main source of deformation



became the opening of the crack due to reinforcement failure in the south column at the base of the second-story level.

#### 4.3.3.4 Failure Mode: SW8 R<sub>2</sub>

During the testing of specimen SW8 R<sub>2</sub>, the following observations were made in relation to the mode of failure:

(1) The first major cracks appeared in the south column at the second-story level around LP 142 which was closed to LP 143 corresponding to  $\mu_\delta = 1$  (see Fig. 4.63). The widest crack developed at the base of the second-story level and extended to about the middle of the column. Some wide diagonal cracks were also observed in the third- and second-story wall panels (see Fig. 4.64).

(2) Around LP 209, corresponding to  $\mu_\delta = 2$ , there was a widening of these cracks, as well as more cracks in both third- and second-story wall panels. A wide crack also opened at the base of the south column at the first-story level.

(3) As the specimen was cycled at a ductility of 2, some local buckling, together with crushing of the concrete, was observed in the third-story wall-panel reinforcement. This, however, was observed to have occurred at one or two bars only (see Fig. 4.65).

(4) As the ductility of the specimen was increased to a value of 2.3 at LP 367, the concrete cover at the top of the first-story south column spalled (Fig. 4.66). At the same time, a crack in the first-story column developed at the foundation and propagated into the wall panel. This crack became widest at LP 383, where the fixed-end rotation reached a value of  $\theta_F = 0.0033$  radians. This was due to the failure of the column longitudinal reinforcement at that level (see Fig. 4.67a and b).

More extensive cracking was observed in the third-story wall panel, as well as increased localized buckling of the panel reinforcement (see Fig. 4.68).

(5) As the cycling continued at a maximum displacement corresponding to a ductility  $\mu_\delta = 2.3$ , there was a great drop in the load resistance between LP 367 and LP 558. This was attributed to the failure of the south column reinforcement at the base (see Fig. 6.69). As the load was

reversed (i.e., as the specimen was loaded to the south), similar behavior was observed in the north column at the base of the second-story level. This, however, was not nearly as extensive as that of the south column, and the drop in load resistance when the specimen was loaded to the south was much less (see Fig. 4.22).

#### 4.3.3.5 Concluding Remarks

The previous data show that, for the twice-repaired specimen SW8 R<sub>2</sub>, the failure mode was mainly of a flexural type which took place in the south column at the base of the first-story level, as well as at the base of the second-story level, though to a smaller extent. Although initiation of crushing of the concrete at the wall panel was detected, there was no extensive buckling of wall-panel reinforcement and thus no excessive shear failure in either of the three wall panels. This can also be seen from the hysteretic loops of both the lateral displacement and shear-distortion graphs where the pinching effects are not as excessive as those of specimen SW7 R<sub>2</sub>. (Compare Figs. 4.13 to 4.15 with Figs. 4.28 to 4.30.)

The maximum positive displacement,  $\delta_{3R}$ , obtained before the failure of the specimen was 1.65 inches (41.88 mm), corresponding to a ductility of  $\mu_{\delta} = 2.3$ . Of this displacement, 52 percent was due to flexural deformation, 45 percent was due to shear distortion, and about 2 percent was due to fixed-end rotation.

The maximum load resisted by the specimen was 277 kips at  $\mu_{\delta} = 2$ , and just before failure, at  $\mu_{\delta} = 2.3$ , it was 257 kips (1145 KN).

#### 4.4 Lateral Displacement Components: Comments on the Variation of Displacement Components with Ductility Graphs

##### 4.4.1 Introductory Remarks

The sources for the lateral displacement can be grouped into three categories of components: those resulting from (1) flexural deformation, (2) shear distortion, and (3) fixed-end rotation. The amounts of contribution of each of these components to the total lateral displacement depends on the slenderness of the specimen. The more slender the specimen, the more significant the flexural deformation and the fixed-end rotation. Graphic information of the variation of the three components of lateral

displacements at the three floor levels for each of the specimens prior to failure is given in Figs. 4.31 to 4.48. Exact values of the contribution of each of the components are given in Tables 2 to 5.

The flexural deformation and shear distribution of specimens SW7 Virgin, SW7 R<sub>1</sub>, SW7 R<sub>2</sub>, SW8 Virgin, SW8 R<sub>1</sub>, and SW8 R<sub>2</sub> were measured over the entire length of the specimens. If no errors were committed in calibrating the instrumentation, and if the assumptions used in reducing these data are realistic (such as assuming linear strain variations along a section and uniformly distributed curvature over a region), then the lateral displacement measured by the linear potentiometers mounted at the mid-depth of each floor slab should be equal to the sum of its three components. Since the errors shown in the graphs are minor for most of the load points, the experimental data appear excellent.

From the above data and for each of the specimens tested, some significant observations can be made. These are discussed in the following sections.

#### 4.4.2 Specimen SW7

(1) SW7 Virgin: The graphs depicting the variation of the displacement components for SW7 Virgin are given in Figs. 4.31 to 4.33. Except for  $\mu_\delta \leq 1$ , the component contributed by the shear distortion is dominant for the lateral displacement at the level of the three stories throughout the test.

(2) SW7 R<sub>1</sub>: Graphic interpretation of the variation of the displacement components for SW7 R<sub>1</sub> is given in Figs. 4.34 to 4.36. Except for  $\mu_\delta \leq 1$ , the component contributed by the shear distortion is dominant for the lateral displacement at each of the three floor levels throughout the test. However, a marked increase of the component contributed from the fixed-end rotation can be observed.

(3) SW7 R<sub>2</sub>: Graphic interpretation of the variation of the displacement components for SW7 R<sub>2</sub> is given in Figs. 4.37 to 4.39. The component contributed from the shear is also dominant for the lateral displacement at each of the three floor levels. However, at the third-

story level, while the shear contribution when maximum resistance was reached was of the order of 50 percent, after failure it reached a value of 81 percent of the total displacement (Table 3). This is in agreement with the fact that the failure mode of the specimen SW7 R<sub>2</sub> was a shear failure in the wall panel at the third story.

It is observed that the error in the first story is relatively large (up to 9 percent). This error is believed to be caused by a malfunction of the instrumentation.

#### 4.4.3 Specimen SW8

(1) SW8 Virgin: Graphic interpretation of the variation of the displacement components of SW8 Virgin is given in Figs. 4.40 to 4.42. The components contributed from the two sources of lateral displacement, shear and flexure, are almost equally dominant, with a slight dominance of flexure over shear.

(2) SW8 R<sub>1</sub>: The component contributed from the flexural deformation is dominant for the lateral displacement at the level of the second and third stories. However, the component contributed from the shear distortion is dominant at the first-story level (Figs. 4.43 to 4.45).

(3) SW8 R<sub>2</sub>: The components contributed from the two sources of lateral displacement, shear and flexure, are almost equally dominant for the three-story levels. At the first- and second-story levels, the shear component is the larger of the two, the difference being slight in both cases. At the third-story level, the two components are almost equal (Figs. 4.46 to 4.48).

For all three floor levels, the contribution of fixed-end rotation to the lateral displacement, although significant, was considerably less than the contributions of the shear and flexural deformations.

## 5. REPAIRING AND STRENGTHENING TECHNIQUES

### 5.1 Introductory Remarks

As noted previously, the series of tests conducted on specimens SW7 and SW8 were divided into three phases for each specimen which required the repair of the specimen after each series of tests. This extensive testing of the same specimens was done in order to study economically the effectiveness of available repairing and strengthening techniques. A brief description of the damages and the repair techniques follows.

### 5.2 Damage to Virgin Specimens

Both specimens SW7 and SW8 were tested in the virgin states up to a ductility  $\mu_\delta = 1$ , corresponding to first yield in the column steel. No excessive damage was observed, except for narrow cracks in the columns and the wall panels. Most of the flexural cracks in the columns and the diagonal cracks in the wall panels were injected with epoxy. After epoxy repair the specimens were denoted as specimens  $R_1$  or epoxy-repaired.

### 5.3 Damage to Epoxy-Repaired Specimens

The epoxy specimens were loaded up to failure by subjecting them to large inelastic deformations. Most of the damage was concentrated in the first story of each specimen. The specimens were repaired and strengthened as follows.

#### 5.3.1 Specimen SW7 $R_1$

Excessive damage was observed in the first-story wall panel and the first-story columns. Crushing of the first-story wall panel and buckling of the first-story wall reinforcement occurred, in addition to spalling of the concrete cover and buckling of the reinforcement at the base of both first-story columns. Some of the concrete inside the confined core of the first-story columns was also crushed.

After removing all the concrete in the first-story wall panel and the crushed concrete in the confined core of each of the first-story columns, all the buckled reinforcement was repaired. In the wall panel the buckled reinforcement which had become elongated was cut, strengthened, and butt welded.

A new outer mat of steel was placed on each side of the wall. This was done by welding the new reinforcement to #2 dowels that had originally been placed in the columns and the footing when the specimen was constructed (Figs. 5.1 and 5.2). Thus, the reinforcement in the first-story wall panel was doubled. Fresh concrete was poured over both steel mats, doubling the original thickness of the wall panel at the first-story level as well. The concrete compressive strength averaged 7.45 ksi.

In the columns, the buckled reinforcement was cut, and the crushed concrete core was removed. The reinforcement was straightened and lap welded (Fig. 5.3). Two #9 bars were butt welded on the outer side of each column extending from the edge of the footing to the first-story floor slab. The spiral was repaired where broken; and, in addition, 1/4" non-deformed wire lap-welded ties were placed around the column core and the #9 bars @ 6" o.c. (Fig. 5.3). Fresh concrete with an average compressive strength of 7.45 ksi was then poured (the concrete stress-strain diagram is given in Fig. 5.4).

### 5.3.2 Specimen SW8 R<sub>1</sub>

As in shear wall SW7, excessive damage was observed in the first-story wall panel and the first-story columns. However, there was no crushing of the confined concrete core in the north column. The repairs were similar to those of shear wall SW7 (Fig. 5.5) except that the fresh concrete had a compressive strength of 7.20 ksi (Fig. 5.6).

Photographs showing important stages of the repairing and strengthening techniques used on the failed specimens SW7 R<sub>1</sub> and SW8 R<sub>1</sub> are given in Figs. 5.7 through 5.10.

## 6. COMPARISON OF BEHAVIOR OF SPECIMENS SW7 AND SW8

### 6.1 General

Specimens SW7 and SW8 were subjected to similar loading patterns. The loading histories are discussed in Chapter 4 of this report. Load-deflection and load-shear distortion diagrams were plotted, and a comparison of the mechanical behavior of the specimens is discussed in this chapter. The main reason for the comparison is to determine the effect of the arrangement of the wall-panel reinforcement on the behavior of the specimens under both monotonic and cyclic loading programs and particularly on the failure mode of the specimens.

The wall-panel reinforcement of specimen SW7 consisted of two layers of #2 bars spaced at 6 inches and placed in both the vertical and the horizontal directions near each of the two faces of the wall. In specimen SW8, the wall-panel reinforcement was similar to that of specimen SW7 except that it was arranged diagonally at angles of  $45^{\circ}$ . The column reinforcement was identical in both specimens (Figs. 1.2 - 1.4).

The comparison of the behavior of the two specimens is made considering each of the three different tests to which they were subjected: (1) virgin specimen; (2) epoxy-repaired; and (3) twice-repaired and strengthened.

### 6.2 Virgin Specimens

At the initial loading stages of the virgin specimens, SW7 and SW8 displayed very similar behavior (even though SW7 deflected slightly more than SW8). Under cycling at the 90-kip working load, they have almost the same lateral displacement,  $\delta_{3R}$  [specimen SW7 averaged 0.144 inches (3.67 mm) while that of SW8 averaged 0.139 inches (3.53 mm)]. Neither specimen showed any significant loss of strength or increased shear deterioration in this phase of the experiment. At the point of first yield, corresponding to a ductility,  $\mu_{\delta} = 1$ , the load carried by specimen SW8 was practically the same as that carried by specimen SW7. The average value of the total lateral load at  $\mu_{\delta} = 1$  was 197 kips (877 KN) for specimen SW7 and 196 kips (872 KN) for specimen SW8. The above comparisons are illustrated in Figs. 6.1 and 6.2. In Fig. 6.2, which combines the results presented in Figs. 4.12a and 4.25, it is apparent that the amount of shear distortion in the

first-story wall panel of specimen SW7 at the point of first yield is about 0.12 inches (3.0 mm) which is 30 percent higher than the amount of shear distortion observed in the first-story wall panel of specimen SW8 at the same loading stage of  $\delta_{3R} = 0.09$  inches (2.3 mm). In both specimens, the only damage was narrow flexural cracks through the columns and flexural-shear cracks at the panels. The widest cracks occurred at the first story.

### 6.3 Epoxy-Repaired Specimens ( $R_1$ )

The epoxy-repaired specimens, SW7  $R_1$  and SW8  $R_1$ , were both subjected to similar loading programs consisting of a general monotonic loading pattern with intermediate cycling at various stages. At the initial loading stages of this phase of the experiment, the behavior of the two specimens is similar. However, as the deflection,  $\delta_{3R}$ , or the load is increased, specimen SW8 shows somewhat higher strength and less shear distortion than specimen SW7 (especially in the first-story wall panel). This is evident in Fig. 6.3 where the first-story wall panel shear distortions are compared.

In the initial phase of the testing, i.e., before a ductility,  $\mu_\delta = 1$ , the behavior of the specimens was very similar. At the point of first yield, the following comparisons can be made. The lateral displacement,  $\delta_{3R}$ , for specimen SW7  $R_1$  was 0.72 inches (18.3 mm), while that for specimen SW8  $R_1$  was 0.62 inches (15.75 mm). The total lateral load resisted at first yield by specimen SW7  $R_1$  was 183 kips (815 KN), while that resisted by specimen SW8  $R_1$  was 192 kips (856 KN). Thus it can be concluded that SW8  $R_1$  yielded at a lower displacement and resisted a higher load than specimen SW7  $R_1$ .

At a ductility  $\mu_\delta = 3$  for specimen SW7  $R_1$  and  $\mu_\delta = 3.5$  for specimen SW8  $R_1$ , the third-story lateral displacements were equal to 2.16 inches (54.9 mm) each. The first-story displacements were also very similar [0.72 inches (18.3 mm) for SW7  $R_1$  and 0.83 inches (21.2 mm) for SW8  $R_1$ ]. The amount of first-story shear deformation was also similar for the two specimens. The measured values of  $\delta_{Y1}$  were 0.46 inches (11.8 mm) for SW7  $R_1$  and 0.44 inches (11.3 mm) for SW8  $R_1$ . Thus it can be deduced that the contribution of first-story shear distortion at the first-story level is slightly higher for SW7  $R_1$ . The load resisted by SW7  $R_1$  at  $\mu_\delta = 3$  was



208 kips (925 KN), while that resisted by specimen SW8 R<sub>1</sub> at  $\mu_\delta = 3.5$  was 216 kips (962 KN).

At a ductility  $\mu_\delta = 5$  for specimen SW7 R<sub>1</sub> and  $\mu_\delta = 5.9$  for specimen SW8 R<sub>1</sub>, the third-story lateral displacements were very similar (Fig. 6.1). From Tables 2 and 4 it can be seen that the total contribution of shear deformation is higher for specimen SW7 R<sub>1</sub>, that of flexural deformation is higher for SW8 R<sub>1</sub>, and that for fixed-end rotation is considerably higher for SW7 R<sub>1</sub>. The total lateral load,  $P_T$ , resisted by SW7 R<sub>1</sub> at  $\mu_\delta = 5$  was 227 kips (1010 KN), while that resisted by SW8 R<sub>1</sub> at  $\mu_\delta = 5.9$  was 231 kips (1026 KN).

As the specimens were taken up to higher values of ductility, specimen SW7 R<sub>1</sub> reached a displacement,  $\delta_{3R}$ , equal to 4.61 inches (117 mm) before failure corresponding to a ductility,  $\mu_\delta = 6.4$ . However, specimen SW8 R<sub>1</sub> reached a lateral displacement,  $\delta_{3R}$ , equal to 6.04 inches (153.6 mm) before failure. This corresponds to a ductility of 9.75. When the total contribution (i.e., the sum of the contribution of the three stories) from all the sources of deformation is taken into account, it was observed that the percentage contribution of shear was greater for SW7 R<sub>1</sub>, while that for flexure was greater for SW8 R<sub>1</sub>. The percentage of contribution of the fixed-end rotation in specimen SW7 R<sub>1</sub> was considerably higher than that in specimen SW8 R<sub>1</sub>. (Although the value recorded for SW7 R<sub>1</sub> is eight times that of SW8 R<sub>1</sub>, it is believed that the value for SW8 R<sub>1</sub> has not been correctly measured.) In specimen SW8 R<sub>1</sub>, the contribution of each of the sources of displacement were: (a) flexural, 65 percent; (b) shear, 29 percent; and (c) fixed-end rotation, 2 percent.\* In specimen SW7 R<sub>1</sub> the similar contributions were: (a) flexural, 42 percent; (b) shear, 31 percent; and (c) fixed-end rotation, 25 percent.

When the first story of each specimen is taken separately, it is seen that the largest contribution, in both specimens, is that of shear deformation (up to 64 percent for SW7 R<sub>1</sub> and 57 percent for SW8 R<sub>1</sub>). This shows that, at the first-story level where most of the damage occurred, the contribution of shear deformation was the largest. This was caused by the

---

\*It is believed that this value has not been correctly measured.

shearing forces in the wall panel. In the upper two stories, the effect of flexure increases in importance.

The maximum total lateral load resisted by specimen SW7 R<sub>1</sub> before failure was P<sub>T</sub> = 227.5 kips (1010 KN). That resisted by SW8 R<sub>1</sub> was P<sub>T</sub> = 234 kips (1041 KN), i.e., 3 percent larger than that of SW7 R<sub>1</sub>.

#### 6.4 Twice-Repaired Specimens (R<sub>2</sub>)

The twice-repaired specimens, SW7 R<sub>2</sub> and SW8 R<sub>2</sub>, were subjected to similar loading programs consisting of cyclic loading at a ratio of M<sub>u</sub>/V<sub>u</sub>, smaller than 173 inches (2.3 d or 1.84 ℓ<sub>w</sub>) (Figs. 3.2.4d). The reason for this was to study the effectiveness of the repairing and strengthening techniques as well as to study the behavior of the specimen under that ratio of M<sub>u</sub>/V<sub>u</sub>.

At the initial loading stages of this phase, the behavior of the specimens is similar. However, as the deflection, δ<sub>3R</sub>, or the load is increased, specimen SW8 R<sub>2</sub> shows higher strength and less shear deterioration than specimen SW7 R<sub>2</sub>. Under the 90-kip (400 KN) working load, the total lateral displacement for SW7 R<sub>2</sub> is slightly higher than that for SW8 R<sub>2</sub> [0.30 inches (7.67 mm) vs. 0.21 inches (5.44 mm)].

At a ductility μ<sub>δ</sub> = 2.1, the maximum load resisted by specimen SW8 R<sub>2</sub> was 277 kips (1231 KN), while that resisted by SW7 R<sub>2</sub> was 275 kips (1221 KN). The major difference between the two specimens, however, lies in the amount of shear distortion, shear resistant deterioration with cyclic loading, and loss of stiffness in each of them. From Fig. 6.4, it can be observed that specimen SW8 R<sub>2</sub> is somewhat stiffer than specimen SW7 R<sub>2</sub>, and thus has deteriorated less under cyclic loading. This is specifically true for the third-story wall panel of specimen SW7 R<sub>2</sub> where the amount of shear distortion is about 1.4 times that of SW8 R<sub>2</sub> [0.284 inches (7.22 mm) vs. 0.206 inches (5.23 mm)]. This can be seen in Fig. 6.5.

At higher values of ductility, there is a larger increase in the difference of shear deformation between the two specimens. This difference manifests itself in the failure mode of each of the specimens. In SW7 R<sub>2</sub>, where the failure was caused by excessive shear damage and therefore shear distortion of the third-story wall panel, the percentage of contribution of shear was about 60 percent prior to failure and 81 percent just after

failure. In SW8 R<sub>2</sub>, the maximum shear contribution reached was about 45 percent and that of flexural deformation about 52 percent (see Tables 3 and 5). This difference in shear distortion is also obvious from Fig. 6.5. At the second-story level, specimen SW7 R<sub>2</sub> displays more shear stiffness and shear resistance deterioration than SW8 R<sub>2</sub>. This can be observed from the pinching effect of the V-γ<sub>2</sub> diagram presented in Fig. 6.6. The difference in the maximum amount of deterioration at this second story, however, is far less than that at the third-story level.

The failure mode of the specimens can be inferred from analysis of the contribution of each of the different sources of displacement. These different contributions were influenced by the arrangement of the wall-panel reinforcement. The smaller contribution of shear to the failure mode of SW8 R<sub>2</sub> can only be attributed to the diagonally arranged reinforcement, which formed 45° compression and tension diagonals that were effective in resisting the shear stresses.

The maximum positive ductility, μ<sub>δ</sub>, attained by SW8 R<sub>2</sub> before failure was 2.3; that reached by SW7 R<sub>2</sub> was equal to 2.0. The cyclic ductility reached by SW8 R<sub>2</sub> was 4.3, while that for SW7 R<sub>2</sub> was 3.1.

#### 6.5 Concluding Remarks

In general, the mechanical behavior of specimen SW8 is slightly better than that of SW7. In terms of the maximum lateral load resisted by each specimen, the difference is very small. The major difference, however, was in the failure mode of each specimen as well as in the ductility value reached before failure. The previous comparisons are summarized in Table 6. The values of the maximum nominal shear stress, v<sub>max</sub>, are also given in Table 6. They were computed using the formula:

$$v_{\max} = \frac{V_{\max}}{0.8 \ell_w d}$$

For example, for specimen SW7 Virgin,

$$v_{\max} = \frac{197 \cdot 1000}{0.8 \cdot 94 \cdot 4} = 654.9 \text{ psi}$$

Because for this specimen  $f'_c = 5682$  psi,

$$v_{\max} = \frac{654.9 \text{ psi}}{\sqrt{5682}} \sqrt{f'_c} = 8.68 \sqrt{f'_c} \text{ in psi} = 0.72 \sqrt{f'_c} \text{ (MPa)}$$

From Table 6 it can be seen that for specimens SW7 R<sub>2</sub> and SW8 R<sub>2</sub> the maximum  $v_{\max}$  they could resist were  $12.2 \sqrt{f'_c}$  (psi) and  $12.97 \sqrt{f'_c}$  (psi), respectively. These are considerably larger than the maximum value allowed by present ACI and UBC codes which is

$$v_u = \frac{V_u}{\phi \cdot 0.8 \ell_w d} \leq 10 \sqrt{f'_c} \text{ (psi)} = 0.83 \sqrt{f'_c} \text{ (MPa)}$$

Including the  $\phi$  factor which is 0.85, the values obtained for the SW7 R<sub>2</sub> and SW8 R<sub>2</sub> are  $14.4 \sqrt{f'_c}$  (psi) and  $15.3 \sqrt{f'_c}$  (psi), i.e., about 50 percent larger than the ultimate value accepted by code. In evaluating the implications of this observed overstrength, it should be kept in mind that neither one of the wall-panel reinforcements used in these two specimens satisfied minimum code requirements, i.e., they were smaller than the minimum reinforcements required by the code-computed design shear forces (see Section 2.3.1). For example, it can be shown that, according to the UBC/76 code, the maximum nominal shear stress that the second and third stories of specimen SW7 could have resisted was

$$v_u = \phi \left[ v_c + \frac{A_v f_y}{b_w s} \right] = \phi \left[ 2\sqrt{5682} + \frac{0.10 \cdot 60000}{12 \cdot 18} \right] = \phi [429 \text{ psi}]$$

or  $v_u = \phi [5.69 \sqrt{f'_c} \text{ (psi)}]$

which, when considering the code-recommended  $\phi$  of 0.85, becomes  $v_u = 4.8 \sqrt{f'_c}$  (psi) =  $0.4 \sqrt{f'_c}$  (MPa) which is only 39 percent of the nominal shear stress resisted by the SW7 specimen.

## 7. COMPARISON OF BEHAVIOR OF SPECIMENS SW7 AND SW8 WITH BEHAVIOR OF PREVIOUSLY TESTED SPECIMENS

### 7.1 Introductory Remarks

In this chapter the mechanical behavior of specimens SW7 and SW8 is compared with the behavior of previously tested specimens, i.e., specimens SW1 through SW6.

As was discussed in Sections 1.2 and 1.3 of this report, the ongoing investigation at Berkeley was broken down into three phases. The first phase dealt with two framed walls (specimens SW1 and SW2) with spirally reinforced edge columns. Details concerning the amount and arrangement of the reinforcement are given in Section 2.2.1 of this report. This first phase is discussed in detail in Ref. 24.

The second phase of the investigation dealt with four specimens (SW3, SW4, SW5, SW6). Details of the investigation are given in Ref. 25. Specific information regarding the type of reinforcement used is given in Section 2.2.2 of this report.

The main results obtained in the experiments conducted on specimens SW1 through SW8 are summarized in Table 6.

### 7.2 Comparison of Specimens SW7 and SW8 with Specimens SW1 and SW2

In specimens SW1 and SW2, the design of the wall-panel reinforcement was based upon Section 2611(q) of the 1973 edition of the UBC. The horizontal wall-panel reinforcement was spaced at three inches (corresponding to  $\rho = 0.0082$ ). The same amount of reinforcement was used in the vertical direction.

In specimen SW7, the horizontal and vertical reinforcement was spaced at six inches (corresponding to  $\rho = 0.0042$ ). This reinforcement was not enough to resist the code-designed shear force.

In specimen SW8, the reinforcement was diagonally arranged with a spacing of six inches along both diagonals (corresponding to  $\rho = 0.0042$ ). As in the case of SW7, the wall reinforcement did not satisfy code requirements.

The columns of specimens SW1, SW2, SW7 and SW8 were identically reinforced.

### 7.2.1 Monotonically-Loaded Specimens

The largest of the maximum values of lateral load resisted by the monotonically-loaded specimens (namely SW1 Virgin, SW2 R, SW7 R<sub>1</sub>, SW8 R<sub>1</sub>) was that of SW1 Virgin. This value of 248 kips (1104 KN), however, is only about 6 percent larger than the value reached by SW8 R<sub>1</sub> and about 9 percent larger than that reached by SW7 R<sub>1</sub>. It should be noted that the specimen SW1 Virgin was actually subjected to some loading with partial reversals of deformations beyond the working load level. It is possible that these deformation reversals could affect the maximum deformation capacity of SW1 [24,25].

### 7.2.2 Cyclically-Loaded Specimens

The largest maximum value of lateral load resisted by the cyclically-loaded specimens (SW1 R, SW2, SW7 R<sub>2</sub>, SW8 R<sub>2</sub>) was that of SW8 R<sub>2</sub> [277 kips (1231 KN)]. This was due to the diagonally-arranged reinforcement that could resist the shear stress effectively, as well as to the strengthening of the first-story level where the value of  $M_u/V_u$  is largest.

The largest maximum displacement reached by specimen SW2 before failure was 2.95 inches (75 mm). This value is about double that of SW7 R<sub>2</sub> and 1.6 times that of SW8 R<sub>2</sub>. However, the comparison is not fair because specimen SW2 was a virgin specimen while specimens SW7 R<sub>2</sub> and SW8 R<sub>2</sub> were repaired after being loaded up to a significant decrease in strength (failure).

## 7.3 Comparison of Specimens SW7 and SW8 with Specimens SW3 and SW4

### 7.3.1 Comparison of Specimen SW3 with SW7 R<sub>1</sub> (Monotonic Loading)

As previously noted, the displacement component contributed by the shear distortion to the deformation of the first story is dominant for SW7 R<sub>1</sub>. For SW3 (virgin specimen) under monotonic loading, the component contributed by flexural deformation is dominant (being about 60 percent of the total lateral displacement). Noting the difference in the amount of wall-panel reinforcement as well as in the type of column confinement used (ties for SW3 vs. spirals for SW7 and SW8), the results appear logical.

Although specimen SW3 displayed somewhat larger load resistance capacity, 245 kips vs. 227 kips (1090 KN vs. 1010 KN), it showed a considerably larger lateral deformation capacity, 7.3 inches vs. 4.6 inches

(185 mm vs. 117 mm), than SW7 R<sub>1</sub> (see Table 6). However, it should be noted that specimen SW7 R<sub>1</sub> was subjected to cyclic loading with reversals up to yielding before it was repaired. From these results, it can be concluded that, while doubling the amount of reinforcement in the wall panel did not result in any significant increase in strength, it increased significantly the deformation capacity (ductility of the specimen under monotonic loading).

### 7.3.2 SW4 R vs. SW7 R<sub>1</sub> (Monotonic Loading)

The amount and arrangement of the reinforcement used in SW4 R is identical to that of SW3. The difference between them is that SW4 R had already been tested under cyclic conditions (SW4), repaired (SW4 R), and subjected to a monotonic loading program. In SW4 R, the displacement component contributed from the shear distortion under failure load is about 55 percent. This value is significantly larger than that of SW7 R<sub>1</sub>, even though the maximum displacements at that point are almost the same.

Specimen SW4 R displayed a larger lateral resistance capacity, 292 kips vs. 227 kips (1297 KN vs. 1010 KN), as well as a larger maximum lateral displacement than SW7 R<sub>1</sub>, 5.0 inches vs. 4.6 inches (128 mm vs. 117 mm).

### 7.3.3 SW3 vs. SW8 R<sub>1</sub>

The total contribution of flexure for SW8 R<sub>1</sub> under the failure load was about 65 percent and that of shear about 29 percent. The values obtained for SW3 at the same story level were about 60 percent for flexure and 30 percent for shear. When the results obtained for specimens SW3, SW7 R<sub>1</sub> and SW8 R<sub>1</sub> are compared, it can be concluded that the arrangement of the wall-panel reinforcement has a significant effect on the behavior of the specimen, mainly that the 45° arrangement is the desirable one.

The total contribution of shear deformation in specimen SW3 was about 2.19 inches (55.5 mm) and in SW8 R<sub>1</sub> about 1.75 inches (44.33 mm). The maximum displacement for SW3 under failure load was 7.28 inches (185 mm); for SW8 R<sub>1</sub> it was 6.05 inches (153.6 mm). The maximum load resisted by SW3 was 245 kips (1090 KN), and that resisted by SW8 R<sub>1</sub> was 234 kips (1040 KN). This shows that SW8 R<sub>1</sub>, which had about half the volume of wall panel steel as SW3, was almost as strong and only slightly less ductile than SW3, despite the fact that SW8 R<sub>1</sub> was subjected to cyclic loading with reversals up to yielding before being repaired.

#### 7.3.4 SW3 R vs. SW7 R<sub>2</sub> (Cyclic Loading)

In comparing these two specimens, it should be kept in mind that both were repaired and strengthened at the first-story level. SW3 R resisted a slightly higher load just prior to failure, 293 kips vs. 275 kips (1300 KN vs. 1221 KN), i.e., about 6.5 percent higher. SW3 R had a significantly higher lateral displacement capacity and thus a larger ductility under failure load. Due to the high nominal shear stress ( $13.4 \sqrt{f'_c}$  (psi) for SW3 R and  $12.2 \sqrt{f'_c}$  (psi) for SW7 R<sub>2</sub>), the failure mode was controlled by shear and consisted of the crushing of the second-story wall panel in SW3 R and the third-story wall panel in SW7 R<sub>2</sub>.

#### 7.3.5 SW3 R vs. SW8 R<sub>2</sub> (Cyclic Loading)

The comparison of SW3 R to SW8 R<sub>2</sub> under cyclic loading is similar to the comparison of SW3 R with SW7 R<sub>2</sub> with the behavior of SW8 R<sub>2</sub> being better than that of SW7 R<sub>2</sub> and therefore closer to that of SW3 R. The behavior of SW3 R is slightly better (both in maximum lateral load and displacement) than the behavior of SW8 R<sub>2</sub>. The failure modes are different in that there was no excessive crushing of the wall panel of SW8 R<sub>2</sub> at the point of failure. Specific values of maximum load and displacement as well as the mode of failure are compared in Table 6.

#### 7.3.6 SW4 vs. SW7 R<sub>2</sub> and SW8 R<sub>2</sub>

The mechanical behavior of SW4 was better than that of specimens SW7 R<sub>2</sub> and SW8 R<sub>2</sub>, particularly because SW4 dissipated more energy through larger deformation. This result is logical since SW4 was a virgin specimen while the other two were repaired specimens. Furthermore, SW4 had more wall-panel reinforcement than the other two specimens, and was subjected to less shear force.

#### 7.4 SW5 and SW6 vs. SW7 and SW8

Specimens SW5 and SW6 had rectangular cross-sections [25]. The wall-panel reinforcement consisted of No. 2 bars at a spacing of 4 inches both horizontally and vertically.

When SW5 and SW6 are compared with specimens SW7 and SW8 under both monotonic and cyclic loading conditions, certain general observations can be made. Specimens SW7 and SW8 are generally stronger and more



ductile than SW5 and SW6. This was attributed to the cross-section of the specimens.

The barbell cross-section can be considered to be a better section for strength and displacement ductility than a rectangular cross-section of equal and even larger (to a certain extent) amount of reinforcement. Exact values of maximum loads and maximum displacements, as well as the modes of failure, are compared in Table 6.

### 7.5 Concluding Remarks

From the evidence presented in this chapter, it can be concluded that specimens SW7 and SW8 were generally very similar in their mechanical behavior to the previously tested specimens SW1, SW2, SW3 and SW4. The values of maximum loads resisted just prior to failure differed at most by 9 percent. This difference is not enough to justify the use of more reinforcement than that of SW7 and SW8. It must also be noted that, although the previously tested specimens were generally more ductile than specimens SW7 and SW8, the difference again was not very large. Comparing the strength and deformation capacity as well as the modes of failure of each of the specimens, it appears that in the range of panel reinforcement used (0.0042 to 0.0082) the most important detail seems to be the use of barbell cross-section with well-confined edge members rather than the amount of wall-panel reinforcement.

Analysis and comparison of the results obtained also show that the shear resistance and deformation capacities of walls are significantly affected by the loading conditions and that, for a given wall, they are inversely related, i.e., the larger the shear resistance developed, the smaller the deformation capacity (ductility). Regarding the effect of loading conditions, it should be noted that it involves not only the type of time history, i.e., cyclic vs. monotonic, but also the distribution of forces through the height of the wall, that is, the  $M_u/V_u$  ratio. The smaller the value of this ratio, the larger the ductility. Present code provisions do not include the above effects; thus there is a need for improving these provisions.



## 8. CONCLUSIONS AND RECOMMENDATIONS

### 8.1 Conclusions

From the experimental results and their evaluation, the following conclusions have been drawn regarding the overall behavior of the specimens studied, the effects of the amount and arrangement of the wall-panel reinforcement on such behavior, the effectiveness of the repair and strengthening techniques used, and the effectiveness of the construction joints.

#### 8.1.1 Overall Behavior

1.-- The overall behavior of the specimens tested has been excellent despite the fact that the design of the wall panel against shear did not satisfy present UBC seismic code requirements. This conclusion is based on the following results:

Behavior under service loading. Specimens SW7 and SW8 resisted several cycles at the maximum working load (90 kips = 400 KN), showing a stable behavior and offering a stiffness higher than that required by present codes. (The maximum story drift index was 0.0015 which is smaller than that specified by present codes--0.0025.)

Behavior at first yielding. The experimentally obtained first yielding strengths for both specimens--197 kips (877 KN) and 196 kips (872 KN) for SW7 and SW8, respectively--are in good agreement with the analytically predicted values, 184 kips (818 KN). The lateral yielding strength is more than twice the maximum lateral working load. The maximum lateral displacement recorded at first yielding was 0.72 inches (18.3 mm) for a drift index of 0.006 which is acceptable by present codes.

Maximum lateral strength. The maximum strengths recorded--227 kips (1010 KN) and 234 kips (1040 KN) for specimens SW7  $R_1$  and SW8  $R_1$ , respectively--are in good agreement with analytically predicted values, 227 kips (1010 KN) and 213 kips (946 KN). Note that the maximum recorded strengths are equivalent to a nominal shear strength  $v_{\max}$  of

10.0  $\sqrt{f'_c}$  and 11.0  $\sqrt{f'_c}$ , respectively (note that no  $\phi$  factor was used in evaluating these values), and are larger than the acceptable code maximum value of  $\phi(10 \sqrt{f'_c})$ .

Maximum lateral deformation capacity and ductility ratio.

(a) Under monotonic loading. The maximum recorded lateral deformations under monotonically increasing lateral load were 4.6 inches (117 mm) and 6.0 inches (154 mm) for SW7 R<sub>1</sub> and SW8 R<sub>1</sub>, respectively, which corresponded to lateral displacement ductility ratios of 6.4 and 9.75, respectively. Considering these two specimens were subjected to cyclic loading with full reversals at yielding level before monotonically increasing the loading, the results clearly show that both specimens, but particularly SW8 R<sub>1</sub>, had excellent ductile behavior under this kind of loading.

(b) Under cyclic loading. No test on a virgin specimen has been conducted under this type of loading, but, based on the difference between the results obtained under monotonic and cyclic loading (e.g., Wang and Vallenias [24,25]), it appears that specimens like SW7 and SW8 can have good hysteretic behavior even under cyclic loading with full reversals of deformation. This conclusion is supported by the results obtained in the experiments conducted on the SW7 R<sub>2</sub> and SW8 R<sub>2</sub> specimens. Although the second and third stories of these specimens were damaged during the monotonic loading up to failure conducted on specimens SW7 R<sub>1</sub> and SW8 R<sub>1</sub>, they were able to resist several cycles of full deformation reversals at a ductility larger than 2 under a lateral load producing a  $v_{\max}$  of 12.2  $\sqrt{f'_c}$  (psi) and 13.0  $\sqrt{f'_c}$  (psi) which, when one considers the shear strength reduction factor  $\phi = 0.85$ , is considerably higher than the UBC and ACI code maximum acceptable value of  $\phi(10 \sqrt{f'_c})$ .

The maximum cyclic ductility ratio obtained was 4.3 (specimen SW8 R<sub>2</sub>) which is excellent because this was obtained after cycling the specimen with 3 cycles at  $\mu_\delta = \pm 1$ , 3 cycles at  $\mu_\delta = \pm 2$ , and 1 cycle to a  $\mu_\delta = +2.3$  and  $\mu_\delta = -3$ .

8.1.2 Effects of Amount and Arrangement of the Wall-Panel Reinforcement

2.--For the same type of wall reinforcement arrangement, the larger the amount, and particularly the closer the spacing, of the wall-panel reinforcement, the better the behavior of the whole wall. However, the

degree of improvement is not in direct proportion to the amount of panel reinforcement, but is smaller.

3.-- The diagonal arrangement of the reinforcement (i.e., inclined at  $45^\circ$ ) resulted in better behavior than the vertical and horizontal reinforcing bar arrangement.

These two conclusions are supported by the following results. Conclusion 2 is based on comparing results obtained on the following experiments.

Under monotonic loading: SW7 R<sub>1</sub> vs. SW3. The behavior of these two specimens were very similar, with the exception of the lateral deformation capacity (lateral displacement ductility); while the maximum strength of SW3 was 245 kips (1090 KN), that of SW7 R<sub>1</sub> was 227 kips (1010 KN), i.e., less than 8 percent difference. The maximum lateral displacement of SW3 was 7.2 inches (185 mm) with a  $\mu_\delta = 10$ , while that of SW7 R<sub>1</sub> was 4.6 inches (117 mm) with a  $\mu_\delta = 6.4$ . This means a decrease in ductility of 36 percent for a decrease in wall reinforcement of 50 percent (0.0082 vs. 0.0041).

Under cyclic loading: SW7 R<sub>2</sub> vs. SW3 R and SW2. From comparison of the behavior of SW7 R<sub>2</sub> and SW3 R, it becomes evident that the only significant difference was that of maximum lateral displacement ductility or energy dissipation capacity. While SW7 R<sub>2</sub> was able to deform up to 1.54 inches (39 mm) (which corresponds to a  $\mu_\delta = 2.1$ ), specimen SW3 R deformed up to 3.2 inches (83 mm) with a  $\mu_\delta = 4.4$ . However, the cyclic displacement ductility ratios were closer --  $\mu_{\delta cy} = 3.1$  for SW7 R<sub>2</sub> vs. 5.6 for SW3 R. Although these results are not a real representation of what we can expect from virgin specimens, it appears that the amount of reinforcement has more effect on the ductility of cyclically loaded specimens than on the monotonically loaded ones. The crack pattern in the wall panel seems to be affected by the larger spacing of the wall-panel reinforcement. The cracks in SW7 were few in number but wider than in SW2 and SW3.

Conclusion 3 is based on the results obtained in the following experiments.

Under monotonic loading: SW7 R<sub>1</sub> vs. SW8 R<sub>1</sub>. The behavior of these two specimens was very similar except that the lateral deformation capacity of the specimen with wall-panel reinforcement arranged at 45° (SW8 R<sub>1</sub>) was 33 percent larger than that of the specimen with horizontal and vertical arrangement (SW7 R<sub>1</sub>). While specimen SW8 R<sub>1</sub> was capable of supporting a lateral load of about 234 kips (1040 KN) up to a lateral displacement of 6.1 inches (154 mm), specimen SW7 R<sub>1</sub> resisted a maximum lateral load of about 227 kips (1010 KN) up to a lateral displacement of 4.6 inches (117 mm).

Under cyclic loading: SW7 R<sub>2</sub> vs. SW8 R<sub>2</sub>. Specimen SW8 R<sub>2</sub> shows better hysteretic behavior than SW7 R<sub>2</sub>. Although the strength of SW8 R<sub>2</sub> was slightly larger--277 kips (1231 KN) vs. 275 kips (1221 KN)--the maximum lateral displacement cyclic ductility of SW8 R<sub>2</sub> was higher, 4.3 vs. 3.1, and the amount of dissipation of energy of SW8 R<sub>2</sub> was higher (see Fig. 6.4).

The results obtained indicated that the 45° arrangement of the wall reinforcing bars is more effective in resisting the effect of shear reversals, i.e., there is less stiffness deterioration with displacement reversals. It is also noted that, even though both specimens had practically the same reinforcement volumes, the failure modes and cracking patterns were significantly different. In SW7 R<sub>2</sub>, most of the failure was due to diagonal cracking at the third-story wall panel. In SW8 R<sub>2</sub>, the failure was largely flexural (i.e., wide cracks in the columns). This can be attributed to the 45° arrangement of the wall-panel reinforcement in SW8 R<sub>2</sub> which formed a more effective shear resisting mechanism.

#### 8.1.3 Effectiveness of Repair and Strengthening Techniques

4.-- If a wall is loaded up to first yielding of its steel reinforcing bars, although the epoxy injection technique will not completely restore the stiffness of the virgin specimen, it will be sufficiently restored to give an acceptable behavior under service as well as yielding load levels.

5.-- The repair and strengthening technique applied to the specimens

loaded monotonically to failure, while permitting them to develop a lateral load resistance even larger than that observed in the virgin specimen, did not restore the ductility of the specimen. Significantly more brittle failure was observed.

Conclusion 4 was drawn from a comparison of the results obtained in the experiments carried out on SW7 vs. SW7 R<sub>1</sub> and SW8 vs. SW8 R<sub>1</sub> under the following load levels.

Service loads. While the tests carried out on SW7 and SW8 under a lateral load of 90 kips (400 KN) showed maximum lateral displacements of 0.18 inches (4.5 mm) and 0.15 inches (3.7 mm), respectively, the similar tests conducted on SW7 R<sub>1</sub> and SW8 R<sub>1</sub> revealed maximum lateral displacements of 0.33 inches (8.4 mm) and 0.21 inches (5.3 mm), respectively. While the observed stiffness of SW7 R<sub>1</sub> was only 55 percent of the virgin specimen SW7, the larger of the drift indices, i.e.,  $0.33/120 = 0.0027$ , can be considered as acceptable. The main reasons for the incomplete recovery of the stiffness was that it was not possible to inject very small narrow cracks, and that bond was not restored.

First yielding loads. For all practical purposes, the loads required for specimens SW7 R<sub>1</sub> and SW8 R<sub>1</sub> to induce a lateral displacement equal to that at which first yielding of the steel was observed in the virgin specimens SW7 and SW8 were the same, as was expected. It should be noted that, although some of the cracks that were present in the virgin specimen reopened, in most of the cases the cracks in the repaired walls formed in new places.

Conclusion 5 is supported by the following observations. The removal of the first-story panel and recast of a thicker panel with practically a double amount of reinforcement, and the addition of reinforcing bars at the edges of the first story, led to the switch of the critical region to the second or third story. As this new region was subjected to relatively greater shear stresses (because of a larger  $V_u/M_u$  ratio), its stiffness and strength had to deteriorate at a higher rate. Also, the welding of high strength reinforcing bars, rather than helping, made these bars brittle. Thus, caution should be exercised in trying to strengthen a damaged wall by

simply increasing the strength of the damaged story and/or using welding for connecting additional reinforcing bars.

#### 8.1.4 Effectiveness of Construction Joints

6.--The construction joint behaved very well in spite of the fact that the lap splicing of the wall reinforcement did not satisfy minimum code requirements. It should be noted that the splice lengths used were those corresponding to the bars used in the model and not those corresponding to the prototype. No significant movement at this joint was observed. It is believed that the care with which this construction joint was cast and the fact that the splicing of the bars of the edge members was done in well-confined concrete were the main reasons for the excellent behavior of this joint. Very few narrow cracks were observed along the length of the edge columns where the lap splicing was made.

#### 8.2 Recommendations

During the review of previous work in this area as well as during the studies reported herein, it becomes evident that the soundness of some present code provisions regarding the analysis and design of shear walls against seismic excitations is questionable and should be reviewed and improved, and that there are gaps in present knowledge about the real behavior of such structural elements. Some recommendations for improving this situation have already been offered in Refs. 24 and 25. Following are some recommendations pertinent to the problems encountered in the investigation reported herein.

##### 8.2.1 Recommendations for Improving Present Seismic Code Provisions

1.-- Present UBC/76 requirements that the total nominal design shear

stress  $v_u = \frac{V_u}{\phi h (0.8 \ell_w)}$  at any section shall not exceed  $10 \sqrt{f'_c}$  appear

to be conservative for barbell cross-section walls. All available data on the seismic behavior of this type of shear wall should be analyzed, and further experiments should be conducted to determine (1) the soundness of the present equation for estimating  $v_u$ , and (2) the validity of the upper bound  $10 \sqrt{f'_c}$ , and its relationship with the values of the ratio  $M_u/V_u$  and of the expected or required ductility.



Meanwhile, it is suggested that for barbell cross-section walls this upper limit of  $v_u$  be increased to  $12 \sqrt{f'_c}$ .

2.--The present UBC/76 code requirements regarding tension lap splices of wall reinforcement appear to be conservative when applied to barbell cross-section walls, particularly when the reinforcing bars are of small size. Therefore, studies should be conducted to find out whether it is possible to relax the present minimum length of lap for tension splices in walls.

3.-- Seismic code provisions should emphasize the desirability (in the case of seismic shear wall construction) of using small-sized reinforcing bars closely spaced rather than larger-sized bars at the largest spacing presently permitted.

#### 8.2.2 Recommendations for Future Research

Besides the studies indicated above for improving present seismic codes, further studies in the following areas are suggested.

1. Experimental. To investigate (1) the contributions of the confined edge members to the shear resistance of barbell cross-section walls; (2) the optimum thickness of the wall panel (to avoid early crushing of concrete); (3) the optimum amount (size and spacing) of panel steel; (4) the optimum arrangement of steel (vertical and horizontal,  $45^\circ$ , use of special bands of steel bars located along the diagonals of the panels); (5) the effect of different values of axial force on the behavior (strength and deformation capacity) of the walls (tests where the compressive as well as tensile axial force remain constant throughout as well as fluctuation between tension and compression should be considered); and (6) techniques for improving the repair and retrofitting of walls.

2. Analytical. To develop mechanical models that will enable more reliable predictions of the overall behavior (with emphasis on the prediction of deformations) as well as of local behavior, i.e., the mechanisms of stiffness and strength degradation and of the final failure of R/C walls under cyclic combinations of flexural, shear and axial forces. To develop procedures (computer programs) that will enable prediction of the effect that the observed large concentrated shear deformations occurring at the critical regions of the walls would have on the overall seismic response of frame-wall structural systems.



## REFERENCES

1. ACI Committee 442, "Response of Buildings to Lateral Forces," ACI Journal, Proceedings, Vol. 68, February 1971, pp. 81-106.
2. Blume, J. A., Newmark, N. M., and Corning, L. H., Design of Multistory Reinforced Concrete Buildings for Earthquake Motions, Portland Cement Association, Skokie, Illinois, 1961, 318 pp.
3. Fintel, M., "Resistance to Earthquakes - Philosophy, Ductility and Details," ACI Publication SP-36, 1973, pp. 75-91.
4. Derecho, A. T., "Frames and Frame-Shear Wall Systems," ACI Publication SP-36, 1973, pp. 13-37.
5. Khan, F. R., and Iyengar, H. S., "Optimization Approach for Concrete High-Rise Buildings," ACI Publication SP-36, 1973, pp. 61-74.
6. Paulay, T. A., "Some Aspects of Shear Wall Design," Bulletin of the New Zealand Society for Earthquake Engineering, Vol. 5, No. 3, September 1972, pp. 89-105.
7. Fergus, J. W., The Prince William Sound, Alaska, Earthquake of 1964 and Aftershocks, U. S. Department of Commerce, Environmental Science Services Administration, Vol. 2, Part A, 1967, 392 pp.
8. Earthquakes, American Iron and Steel Association, Washington, D.C., 1975, 319 pp.
9. Jennings, P. C. (Ed.), "Engineering Features of the San Fernando Earthquake: February 9, 1971," Report EERL 71-02, Earthquake Engineering Research Laboratory, California Institute of Technology, June 1971, 512 pp.
10. Clarkson, W. P., "A Review of the Repair of Two Concrete Buildings Damaged by the San Fernando Earthquake," ACI Journal, Proceedings, Vol. 70, No. 25, March 1973, pp. 237-241.
11. Berg, G. V., and Degenkolb, H. J., "Engineering Lessons from Managua Earthquake," Conference Proceedings on the Managua, Nicaragua, Earthquake of Dec. 23, 1972, Engineering Research Institute, Vol. 2, San Francisco, November 29 and 30, 1973.
12. Bertero, V. V., "Seismic Performance of Reinforced Concrete Structures," Anales de la Academia Nacional de Ciencias Exactas, Físicas y Naturales, Buenos Aires, 1979, Tomo 31, pp. 75-144.

13. Bertero, V. V., Popov, E. P., Wang, T. Y., and Vallenias, J. M. "Seismic Design Implications of Hysteretic Behavior of Reinforced Concrete Structural Walls," Preprints of the Sixth World Conference on Earthquake Engineering, New Delhi, January 1977, pp. 5.159-5.165.
14. Shiga, T., Shibata, A., and Takashi, T., "Earthquake Damage and Wall Modulus of Reinforced Concrete Building," Report No. 12, Totoku Branch, Architecture Institute of Japan, December 1968, pp. 29-32 (in Japanese).
15. Bertero, V. V., and Collins, R. G., "Investigation of Failures of the Olive View Stairtowers during the San Fernando Earthquake and their Implications in Seismic Design," Report No. EERC 73-26, Earthquake Engineering Research Center, University of California, Berkeley, 1973.
16. Weigel, R. L. (Ed.), Earthquake Engineering, Prentice-Hall, Inc., 1970, 518 pp.
17. Cardenas, A., and Magura, D., "Strength of High-Rise Shear Walls - Rectangular Cross Section," ACI Publication SP-36, 1973, pp. 119-150.
18. Barda, F., "Shear Strength of Low-Rise Walls with Boundary Elements," Ph.D. Dissertation, Department of Civil Engineering, Lehigh University, 1972, 265 pp.
19. Benjamin, J., and Williams, H., "The Behavior of One-Story Reinforced Concrete Shear Walls," Journal of the Structural Division, ASCE, Vol. 83, No. ST. 3, May 1957, pp. 1254.1-1254.49.
20. Galletly, G. D., "Behavior of Reinforced Concrete Shear Walls Under Static Load," Department of Civil and Sanitary Engineering, Massachusetts Institute of Technology, Cambridge, August, 1952.
21. Antebi, J., Utki, S., and Hansen, R. J., "The Response of Shear Walls to Dynamic Loads," Department of Civil and Sanitary Engineering, Massachusetts Institute of Technology, Cambridge, August 1960.
22. Cervenka, V., and Gerstle, K. H., "Inelastic Analysis of Reinforced Concrete Panels: Experimental Verification and Application," IABSE Publication 32-II, 1972, pp. 25-38.
23. Uniform Building Code, International Conference of Building Officials, Pasadena, 1973 Edition.
24. Wang, T. Y., Bertero, V. V., and Popov, E. P., "Hysteretic Behavior of Reinforced Concrete Framed Walls," Report No. EERC 75-23, Earthquake Engineering Research Center, University of California, Berkeley, December 1975.

25. Vallenias, J. M., Bertero, V. V., and Popov, E. P., "Hysteretic Behavior of Reinforced Concrete Structural Walls," Report No. EERC-79/20, Earthquake Engineering Research Center, University of California, Berkeley, August 1979.
26. Building Code and Commentary for Reinforced Concrete Structures, Architectural Institute of Japan, 1971 (in Japanese).
27. Seismology Committee, Recommended Lateral Force Requirements and Commentary, Structural Engineers Association of California, San Francisco, 1974.
28. Bertero, V. V., Popov, E. P., and Wang, T. Y., "Hysteretic Behavior of Reinforced Concrete Flexural Members with Special Web Reinforcement," Report No. EERC 74-9, Earthquake Engineering Research Center, University of California, Berkeley, August 1974.



T A B L E S





TABLE 1(a) MECHANICAL CHARACTERISTICS OF MATERIALS  
SPECIMENS SW7 AND SW8

MECHANICAL CHARACTERISTICS		AVERAGE STRENGTH AT TIME OF TESTING	
		Specimen SW7	Specimen SW8
Concrete Compressive Strength, $f'_c$ , MPa, (psi)	1st story	40.75, (5910)	40.75, (5910)
	2nd story	39.20, (5690)	39.41, (5720)
	3rd story	39.20, (5690)	38.58, (5600)
Wall Steel (#2 Bars) MPa, (psi)	$f_y$	482.70, (70,000)	482.70, (70,000)
	$f_{max}$	655.20, (95,000)	655.20, (95,000)
Col. Long. Steel (#6 Bars) MPa, (psi)	$f_y$ upper	562.10, (81,500)	562.10, (81,500)
	$f_y$ lower	510.30, (74,000)	510.30, (74,000)
	$f_{max}$	751.70, (109,000)	751.70, (109,000)
Col. Transverse Steel ( $\phi = 0.205''$ ) MPa, (psi)	$f_y$	586.20, (85,000)	586.20, (85,000)
	$f_{max}$	635.30, (92,120)	635.30, (92,120)

TABLE 1(b) COMPARISON OF EXPERIMENTALLY DETERMINED VALUES OF MODULUS OF ELASTICITY  $E_c$  VS. THOSE CALCULATED BY ACI EMPIRICAL EQUATION

Story Level	Specimen SW7		Specimen SW8	
	Secant Mod. at $0.45 f'_c$ , MPa, (ksi)	ACI modulus MPa, (ksi)	Secant Mod. at $0.45 f'_c$ , MPa, (ksi)	ACI modulus MPa, (ksi)
1st story	22909, (3325)	30378, (4409)	22909, (3325)	30378, (4409)
2nd story	22875, (3320)	29861, (4334)	24597, (3570)	29696, (4310)
3rd story	22875, (3320)	29861, (4334)	24597, (3570)	29691, (4310)

TABLE 2 DISPLACEMENT COMPONENTS--SW7 R<sub>1</sub>

	Load Point	1 Fixed End Rotation in, (mm)	$\frac{1}{5}$ %	2 $\delta_{\text{Flexure}}$ in, (mm)	$\frac{2}{5}$ %	3 $\delta_{\text{Shear}}$ in, (mm)	$\frac{3}{5}$ %	4 $\delta_{\text{T}} =$ $\Sigma 1,2,3$ in, (mm)	5 Relative Lateral Displacement in, (mm)	6 Error $\frac{5-4}{5}$ %	7 $\mu_{\delta}^* =$ $\frac{\delta_{1R}}{\delta_{1y}}$
Displacement of Third Floor	685	0.026, (0.666)	8.0	0.177, (4.49)	54	0.105, (2.67)	32	0.308, (7.82)	0.33, (8.38)	6.7	0.46
	851	0.072, (1.83)	10.0	0.280, (7.10)	38.8	0.333, (8.47)	46	0.685, (17.40)	0.72, (18.30)	4.9	1.0
	907	0.390, (9.88)	18.0	1.04, (26.35)	48	0.704, (17.89)	33	2.13, (54.14)	2.16, (54.9)	1.4	3.0
	1071	0.792, (20.12)	22.1	1.68, (42.67)	46.7	1.05, (26.73)	30	3.52, (89.52)	3.60, (91.44)	1.0	5.0
	1145	1.150, (29.25)	24.9	1.92, (48.75)	41.6	1.42, (35.97)	31	4.49, (113.9)	4.61, (117.02)	2.6	6.4
Displacement of Second Floor	685	0.009, (0.219)	4.8	0.090, (2.28)	50	0.075, (1.91)	42	0.174, (4.41)	0.180, (4.56)	3.3	0.35
	851	0.047, (1.19)	9.0	0.208, (5.28)	40	0.228, (5.79)	44	0.480, (12.27)	0.520, (13.21)	7.2	1.0
	907	0.289, (7.35)	21.1	0.427, (10.85)	31.1	0.577, (14.67)	42	1.29, (32.87)	1.38, (35.01)	6.3	2.65
	1071	0.536, (13.62)	21.0	1.02, (26.01)	40.1	0.891, (22.63)	35	2.18, (62.29)	2.55, (64.88)	4.0	4.91
	1145	0.671, (16.94)	21.2	1.11, (28.08)	35.1	1.24, (31.40)	39	3.02, (76.58)	3.15, (80.04)	4.4	6.06
Displacement of First Floor	685	0.008, (0.198)	5.2	0.088, (2.26)	59.4	0.043, (1.09)	29	0.138, (3.53)	0.150, (3.80)	7.1	0.56
	851	0.028, (0.706)	10.4	0.087, (2.24)	32.2	0.138, (3.51)	52	0.253, (6.44)	0.270, (6.79)	5.2	1.0
	907	0.139, (3.52)	19.2	0.079, (2.01)	11.1	0.465, (11.81)	64	0.683, (17.35)	0.720, (18.29)	5.2	2.69
	1071	0.281, (7.14)	16.6	0.675, (17.16)	39.9	0.729, (18.52)	43	1.68, (42.80)	1.69, (43.11)	0.7	6.35
	1145	0.409, (10.38)	18.2	0.685, (17.40)	30.5	1.05, (26.60)	47	2.14, (54.39)	2.24, (57.02)	4.7	8.4

\* These values are based on the values of  $\delta_{1y}$  at which first yielding was observed in the virgin specimen SW7.

TABLE 3 DISPLACEMENT COMPONENTS--SW7 R<sub>2</sub>

	Load Point	1 Fixed End Rotation in, (mm)	$\frac{1}{5}$ %	2 $\delta_{Flexure}$ in, (mm)	$\frac{2}{5}$ %	3 $\delta_{Shear}$ in, (mm)	$\frac{3}{5}$ %	4 $\delta_T =$ $\Sigma 1,2,3$ in, (mm)	5 Relative Lateral Displacement in, (mm)	6 Error $\frac{5-4}{5}$ %	7 $\mu_{\delta}^* =$ $\frac{\delta_{iR}}{\delta_{iy}}$
Displacement of Third Floor	53	0.0147, (0.374)	4.9	0.083, (2.11)	23.5	0.192, (4.89)	63.8	0.290, (7.37)	0.302, (7.67)	3.9	0.42
	125	0.007, (0.189)	0.72	0.413, (10.49)	40.1	0.557, (14.15)	53.9	0.978, (24.83)	1.03, (26.16)	5.1	1.43
	310	0.102, (2.58)	6.7	0.544, (13.81)	36.0	0.796, (20.23)	52.8	1.44, (36.60)	1.51, (38.35)	4.5	2.09
	539	0.087, (2.22)	5.9	0.404, (10.27)	27.7	0.878, (22.29)	60.1	1.36, (34.78)	1.46, (37.08)	6.1	2.03
	552	0.069, (1.76)	2.7	0.233, (5.92)	9.17	2.05, (52.13)	80.8	2.35, (59.81)	2.54, (64.51)	7.3	3.53
Displacement of Second Floor	53	0.0096, (0.246)	6.2	0.034, (0.876)	21.1	0.095, (2.40)	60.3	0.153, (3.88)	0.156, (3.97)	2.3	0.30
	125	0.0051, (1.25)	0.86	0.200, (5.09)	34.9	0.337, (8.56)	58.5	0.541, (13.75)	0.575, (14.57)	5.7	1.10
	310	0.068, (1.75)	7.74	0.258, (6.55)	28.9	0.513, (13.02)	57.4	0.839, (21.32)	0.894, (22.70)	6.1	1.72
	539	0.059, (1.50)	7.3	0.273, (6.93)	33.8	0.423, (10.73)	52.1	0.754, (19.16)	0.811, (20.59)	6.9	1.56
	552	0.047, (1.19)	5.6	0.328, (8.35)	39.2	0.406, (10.32)	48.4	0.781, (19.84)	0.839, (21.31)	6.8	1.61
Displacement of First Floor	53	0.0046, (0.119)	11.0	0.025, (0.639)	54.2	0.009, (0.240)	22.2	0.039, (0.998)	0.043, (1.08)	7.6	0.17
	125	0.0026, (0.066)	1.1	0.121, (3.08)	49.7	0.099, (2.54)	41.0	0.228, (5.65)	0.244, (6.20)	8.9	1.01
	310	0.036, (0.918)	9.6	0.192, (4.88)	32.5	0.169, (4.31)	45.3	0.348, (8.84)	0.374, (9.51)	7.0	1.5
	539	0.031, (0.786)	11.8	0.101, (2.56)	38.6	0.110, (2.78)	42.0	0.241, (6.14)	0.261, (6.62)	7.3	1.07
	552	0.024, (0.623)	12.2	0.073, (1.86)	36.5	0.088, (2.23)	43.7	0.186, (4.72)	0.201, (5.10)	7.4	0.82

\* These values are based on the values of  $\delta_{iy}$  at which first yielding was observed in the specimen SW7 R<sub>2</sub>.

TABLE 4 DISPLACEMENT COMPONENTS--SW8 AND SW8 R<sub>1</sub>

	Load Point	1 Fixed End Rotation in, (mm)	$\frac{1}{5}$ %	2 $\delta$ Flexure in, (mm)	$\frac{2}{5}$ %	3 $\delta$ Shear in, (mm)	$\frac{3}{5}$ %	4 $\delta_T =$ $\Sigma 1,2,3$ in, (mm)	5 Relative Lateral Displacement in, (mm)	6 Error $\frac{5-4}{5}$ %	7 $\mu_{\delta}^* =$ $\frac{\delta_{iR}}{\delta_{iy}}$
Displacement of Third Floor	257	0.0275, (0.698)	4.4	0.367, (9.32)	59.2	0.202, (5.13)	32.6	0.596, (15.15)	0.620, (15.75)	3.8	1.0
	426	0.028, (0.709)	4.5	0.341, (8.66)	55.0	0.247, (6.26)	39.8	0.615, (15.62)	0.620, (15.75)	0.8	1.0
	593	0.168, (4.25)	7.8	1.23, (31.30)	57.1	0.602, (15.28)	27.8	2.00, (50.83)	2.16, (54.86)	7.3	3.5
	702	0.423, (10.74)	11.5	2.28, (58.05)	62.2	1.013, (25.73)	27.6	3.72, (94.52)	3.68, (93.40)	-1.2	5.9
	755	0.139, (3.54)	2.3 <sup>+</sup>	3.93, (99.87)	65.0	1.75, (44.33)	28.9	5.5 (147.74)	6.05, (153.60)	3.8	9.75
Displacement of Second Floor	257	0.018, (0.473)	4.7	0.210, (5.33)	53.1	0.152, (3.88)	38.7	0.381, (9.68)	0.395, (10.03)	3.6	0.97
	426	0.019, (0.480)	4.7	0.192, (4.88)	47.3	0.183, (4.65)	45.1	0.395, (10.01)	0.411, (10.31)	2.9	1.0
	593	0.113, (2.88)	7.8	0.714, (18.12)	48.8	0.526, (13.35)	36.0	1.35, (34.35)	1.46, (37.10)	7.4	3.6
	702	0.286, (7.27)	11.4	1.361, (34.57)	54.0	0.923, (23.44)	36.6	2.57, (65.28)	2.52, (63.98)	-2.0	6.2
	755	0.094, (2.40)	2.3 <sup>+</sup>	2.32, (58.90)	56.1	1.56, (39.75)	37.8	3.98, (101.04)	4.14, (105.08)	3.8	10.2
Displacement of First Floor	257	0.010, (0.248)	4.7	0.093, (2.37)	45.1	0.096, (2.42)	46.1	0.198, (5.04)	0.207, (5.25)	4.0	.91
	426	0.010, (0.252)	4.4	0.080, (2.04)	35.3	0.113, (2.88)	49.8	0.204, (5.17)	0.228, (5.78)	10.6	1.0
	593	0.059, (1.51)	7.1	0.269, (6.84)	32.2	0.445, (11.31)	53.2	0.774, (19.66)	0.837, (21.25)	7.5	3.7
	702	0.150, (3.81)	10.5	0.533, (13.54)	37.3	0.789, (20.04)	55.2	1.47, (37.39)	1.43, (36.34)	-2.9	6.3
	755	0.049, (1.26)	2.1 <sup>+</sup>	0.875, (22.21)	37.2	1.34, (33.94)	56.8	2.26, (57.41)	2.35, (59.71)	3.8	10.3

\* These values are computed on the basis of the values of  $\delta_{iy}$  at which first yielding was observed in the virgin specimen SW8.

<sup>+</sup>It is believed that this value is not correct.

TABLE 6 (CONT.) COMPARISON OF SPECIMEN RESULTS

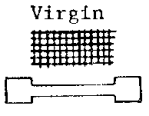

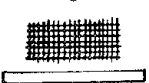

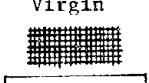
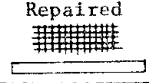

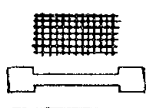
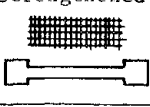
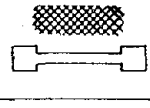
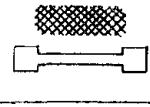
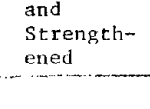
-Specimen, SW -Arrangement of Wall Reinforcement -Cross Section Type		Loading Program	Max.+ve Load-- Kips (KN)	Max.-ve Load-- Kips (KN)	Max.+ve Disp. in (mm)	Max.-ve Disp. in (mm)	Max. Nominal Shear Stress psi (MPa)	Failure Mode
4	Virgin 	Cyclic	227 (1008)	-222 (-987)	2.83 (72)	-2.87 (-73)	$10.55\sqrt{f'_c}$ ( $0.876\sqrt{f'_c}$ )	Flexural-shear cracking and crushing of concrete at first-story wall panel.
4 R	Repaired and Strengthened 	Monotonic	292 (1297)	-205 (-914)	5.04 (128)	3.02 (-76.7)	$13.43\sqrt{f'_c}$ ( $1.12\sqrt{f'_c}$ )	Rupture of tension reinforcement at base of second-story column, buckling of compression reinforcement at same level, and crushing of third-story panel. Failure at third-floor slab.
5	Virgin 	Monotonic	206 (916)	-190 (-847)	3.18 (80.7)	-2.25 (-57.1)	$8.54\sqrt{f'_c}$ ( $0.711\sqrt{f'_c}$ )	Local buckling at base of north edge with rupture of ties and buckling of main reinforcing bars.
5 R	Repaired and Strengthened 	Cyclic	239 (1065)	-231 (-1027)	1.99 (50.6)	-1.98 (-50.2)	$8.51\sqrt{f'_c}$ ( $0.707\sqrt{f'_c}$ )	Rupture of tension reinforcement at south edge member at top of first story.
6	Virgin 	Cyclic	192 (856)	-196 (-870)	1.98 (50.2)	-2.06 (-52.2)	$8.11\sqrt{f'_c}$ ( $0.670\sqrt{f'_c}$ )	Buckling at base of south edge member, including part of panel.
6 R	Repaired 	Monotonic	261 (1162)	-260 (-1158)	2.50 (634)	-2.44 (-62.0)	$9.43\sqrt{f'_c}$ ( $0.783\sqrt{f'_c}$ )	Rupture of tension reinforcement at first- and second-story wall panel.

TABLE 6 (CONT.) COMPARISON OF SPECIMEN RESULTS

-Specimen, SW -Arrangement of Wall Reinforcement -Cross Section Type		Loading Program	Max.+ve Load-- Kips (KN)	Max.-ve Load-- Kips (KN)	Max.+ve Disp. in (mm)	Max.-ve Disp. in (mm)	Max. Nominal Shear Stress psi (MPa)	Failure Mode
7	Virgin 	Cyclic up to first yielding	197.3 (877)	-197.0 (-876)	0.72 (18.29)	-0.68 (-17.2)	$8.68\sqrt{f'_c}$ ( $0.720\sqrt{f'_c}$ )	Loaded up to a ductility $\mu_{\delta} = 1$ , cracks in wall panels and columns (mainly first story). No failure.
7 R <sub>1</sub>	Epoxy- Repaired 	Monotonic	227 (1010)	196 (-872)	4.61 (117.0)	-0.63 (-16.0)	$10.0\sqrt{f'_c}$ ( $0.831\sqrt{f'_c}$ )	Crushing of first-story wall panel and buckling of first-story panel and column reinforcement. Failure of south column at base of first story.
7 R <sub>2</sub>	Twice Repaired and Strengthened 	Cyclic	275 (1221)	-277 (-1233)	1.46 (37.1)	-1.54 (-39.1)	$12.2\sqrt{f'_c}$ ( $1.01\sqrt{f'_c}$ )	Crushing of concrete and buckling of reinforcement in third-story wall panel. Shear failure of third-story wall panel.
8	Virgin 	Cyclic up to first yielding	196 (872)	-199 (-887)	0.62 (15.75)	-0.61 (-15.49)	$9.34\sqrt{f'_c}$ ( $0.775\sqrt{f'_c}$ )	Loaded up to a ductility $\mu_{\delta} = 1$ , cracks in wall panels and columns (concentrated at first-story level). No failure.
8 R <sub>1</sub>	Epoxy- Repaired 	Monotonic	234 (1040)	-212 (-942)	6.05 (153.6)	-0.57 (-14.39)	$10.96\sqrt{f'_c}$ ( $0.911\sqrt{f'_c}$ )	Widening of horizontal cracks in first-story south column, propa- gation of cracks into wall panel. Crushing of north column concrete at base and initiation of buckling of north column reinforcement base.
8 R <sub>2</sub>	Twice- Repaired and Strength- ened 	Cyclic	277 (1231)	256 (-1138)	1.65 (41.88)	-2.25 (-57.2)	$12.97\sqrt{f'_c}$ ( $1.08\sqrt{f'_c}$ )	Some crushing of concrete and buck- ling at second- and third-story wall-panel reinforcement. Failure of south column reinforcement at base of first story.

F I G U R E S





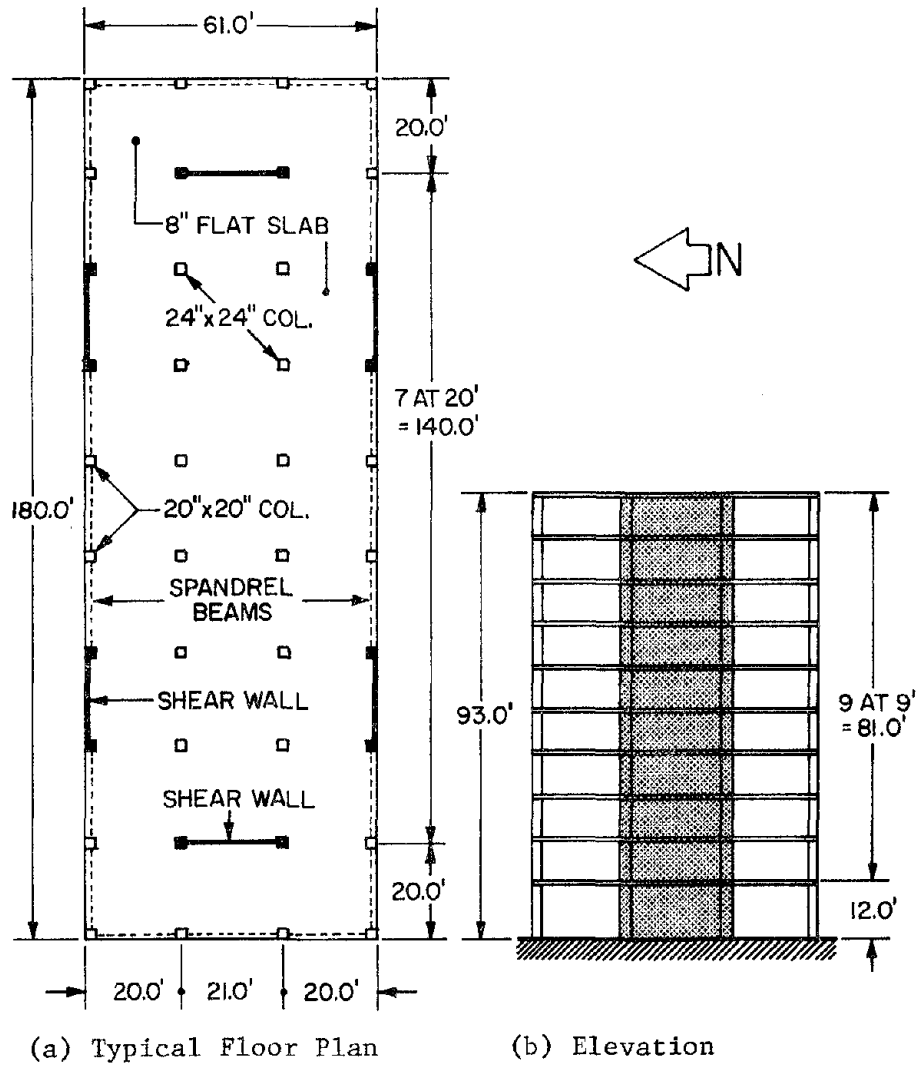


FIG. 1.1 PROTOTYPE BUILDING

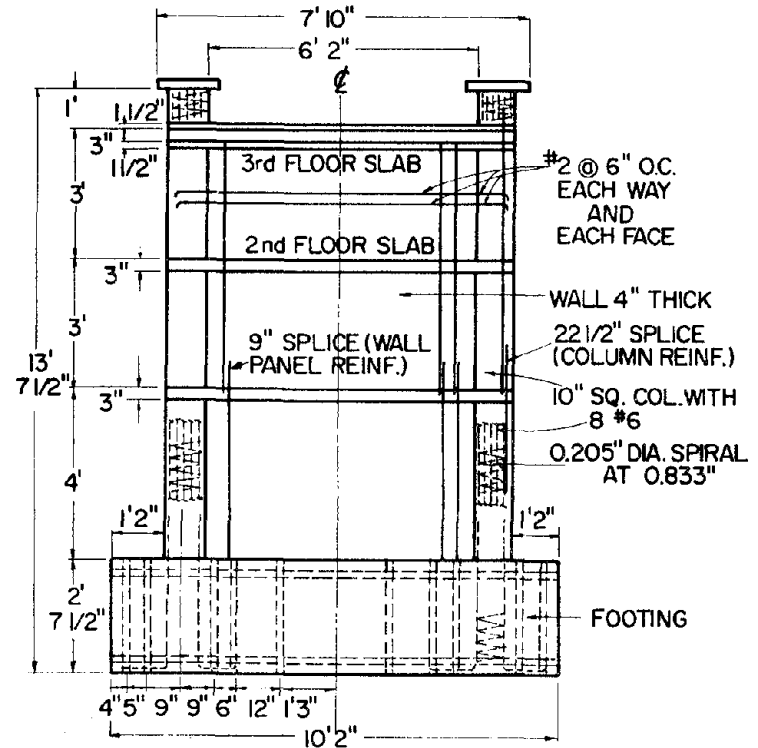
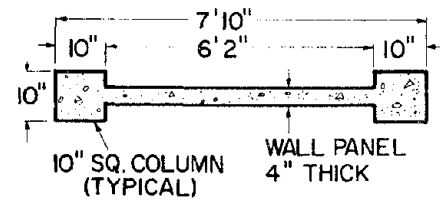


FIG. 1.2(a) ELEVATION VIEW OF SW7



NOTE: REINF. DETAILS NOT SHOWN

FIG. 1.2(b) SECTION SHOWING BARBELL CROSS-SECTIONAL TYPE. SPECIMENS SW7 AND SW8.

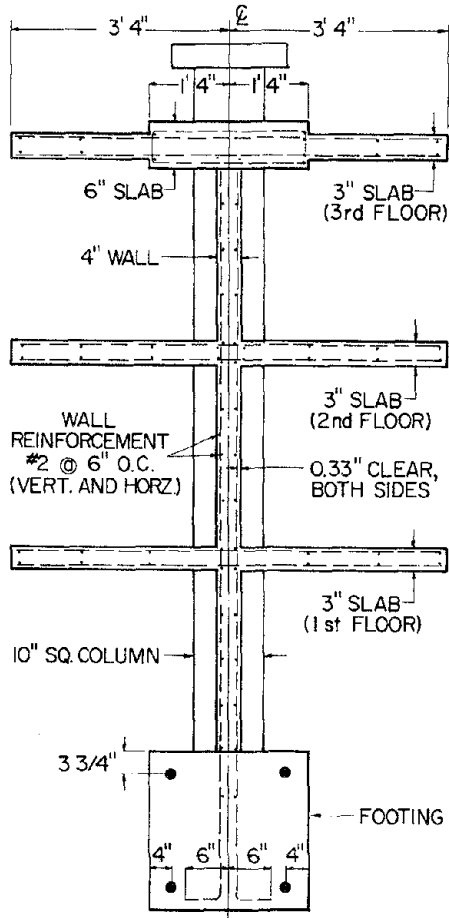
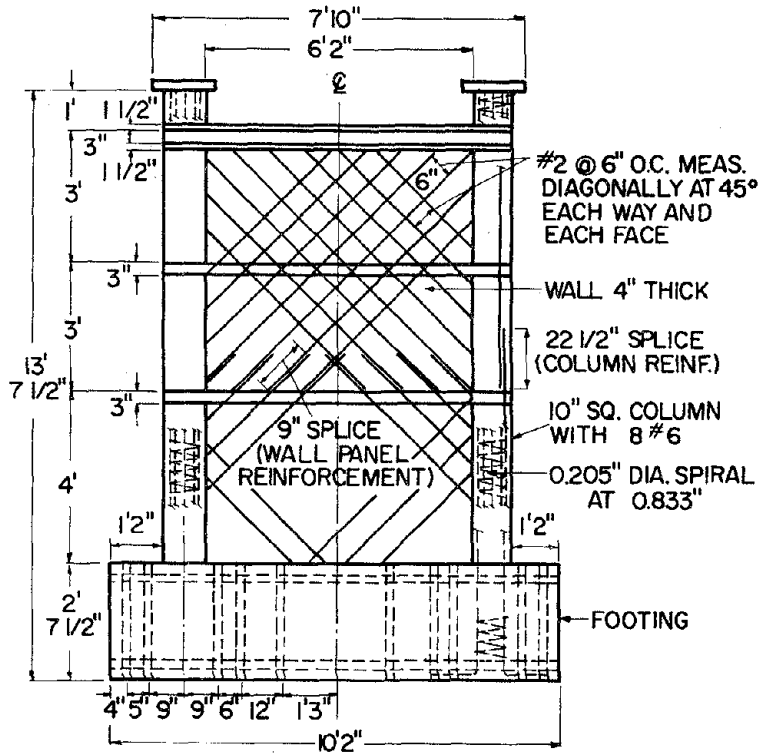
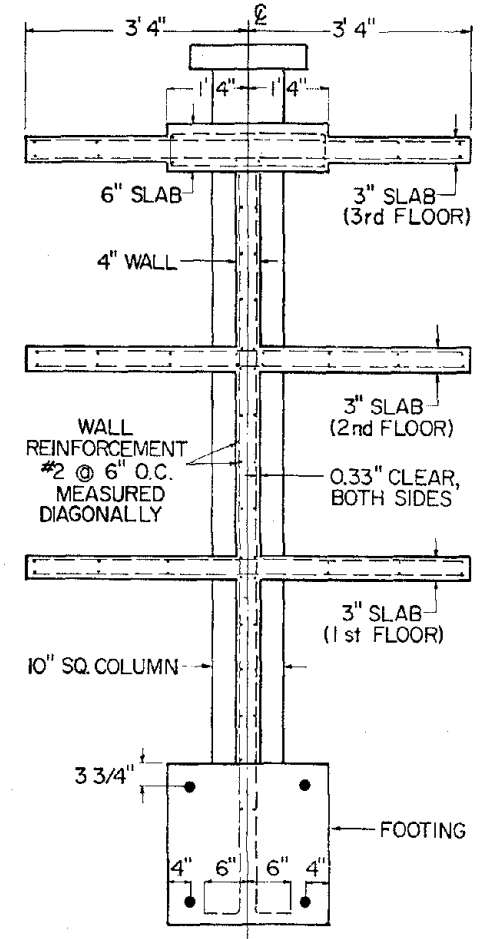


FIG. 1.3 DIMENSIONS AND DETAILS OF SW7



(a) ELEVATION OF SW8



(b) SECTION OF SW8

FIG. 1.4 DIMENSIONS AND DETAILS OF SW8

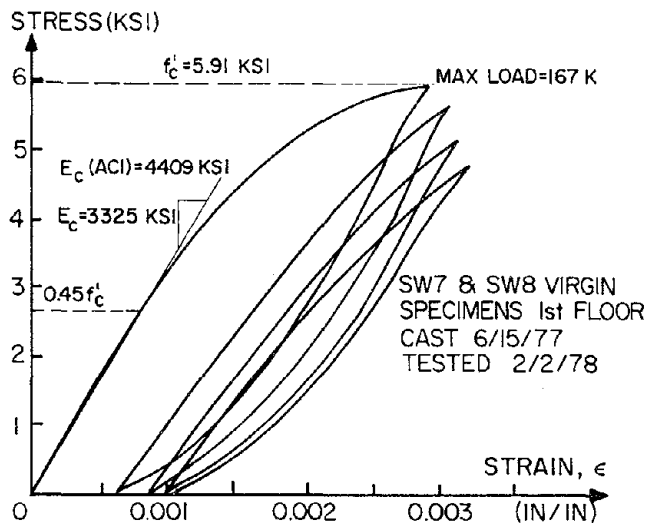


FIG. 2.1 STRESS-STRAIN DIAGRAMS FOR CONCRETE SPECIMENS--SW7 AND SW8 (FIRST STORY) VIRGIN SPECIMENS

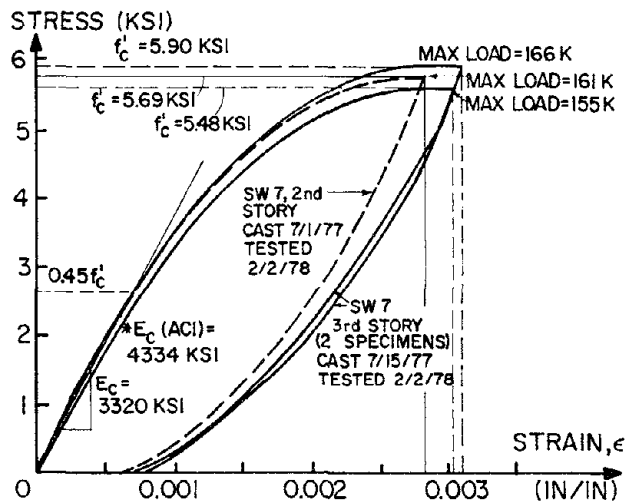


FIG. 2.2 STRESS-STRAIN DIAGRAMS FOR CONCRETE SPECIMENS--SW7 (SECOND AND THIRD STORIES) VIRGIN SPECIMEN

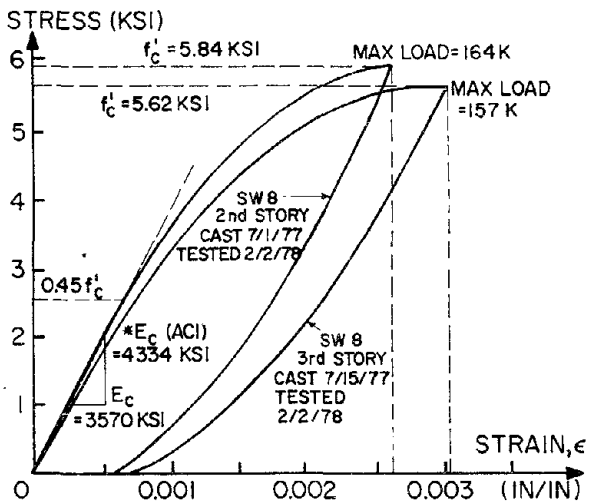


FIG. 2.3 STRESS-STRAIN DIAGRAMS FOR CONCRETE SPECIMENS--SW8 (SECOND AND THIRD STORIES) VIRGIN SPECIMEN

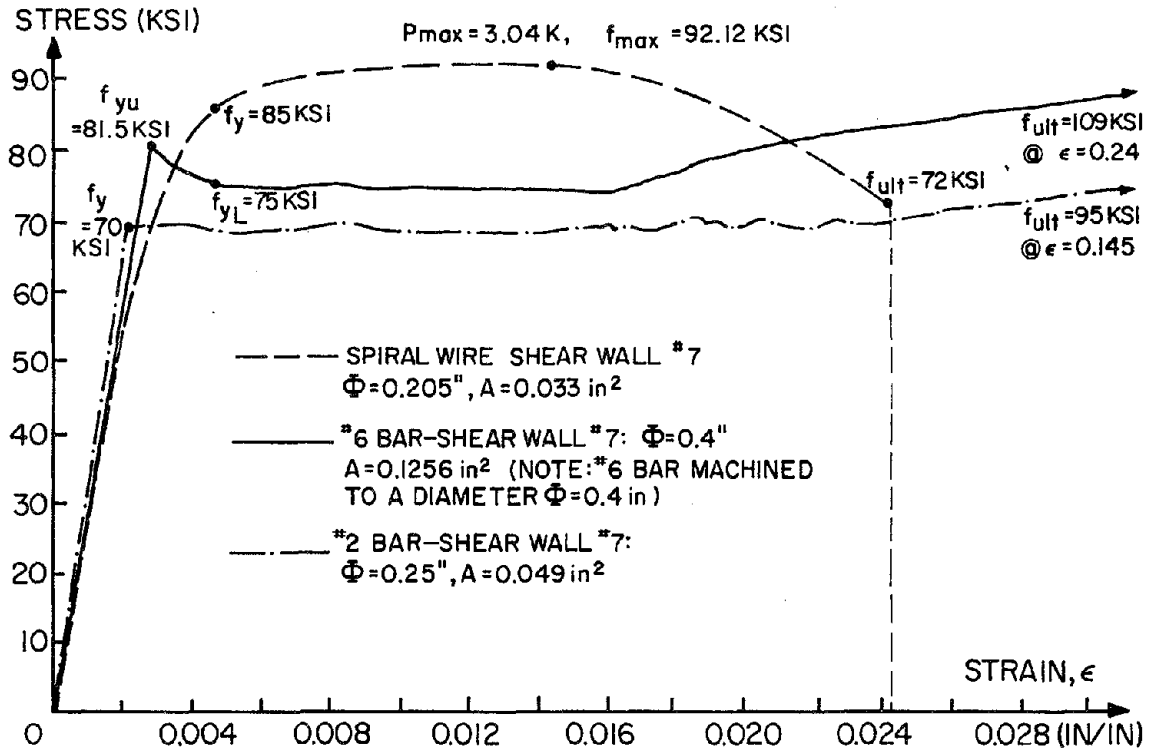


FIG. 2.4 STRESS-STRAIN DIAGRAMS OF REINFORCEMENT FOR SW7 AND SW8

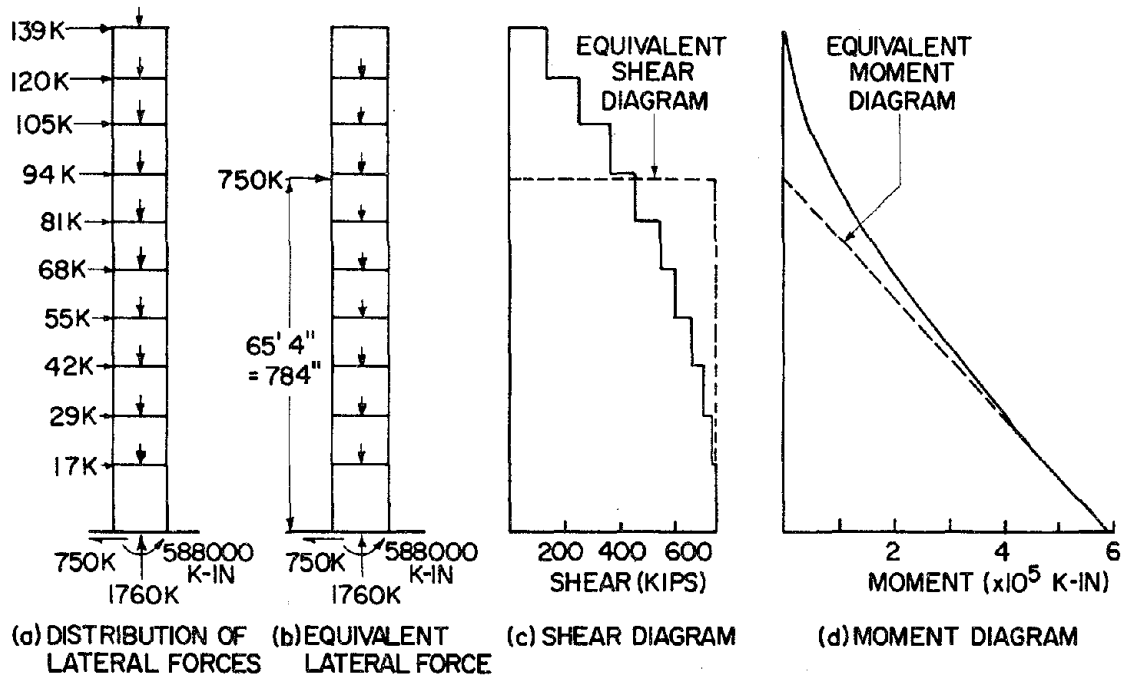
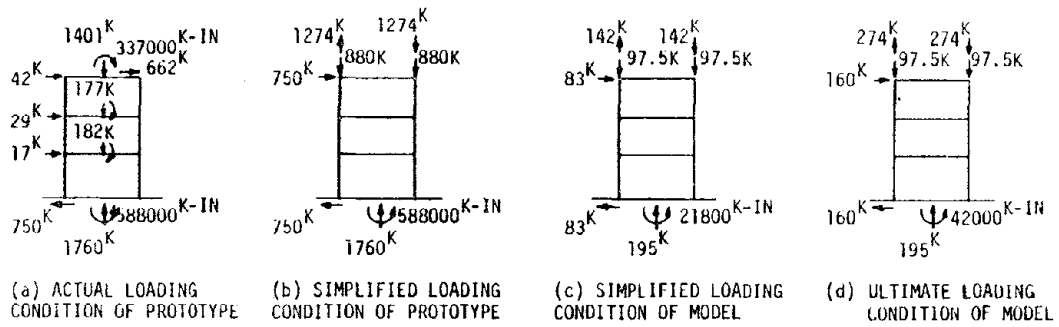
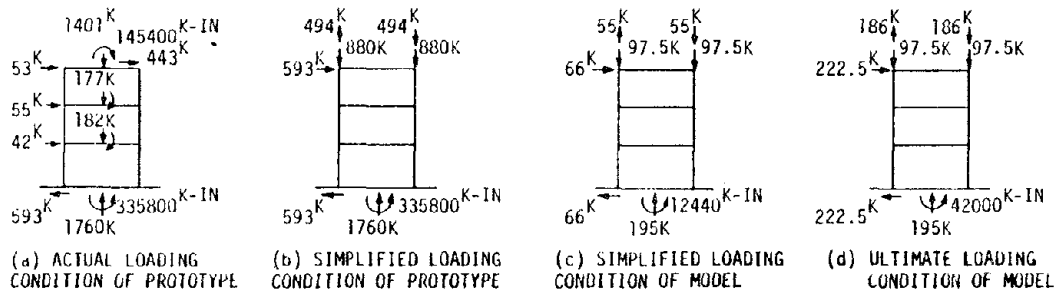


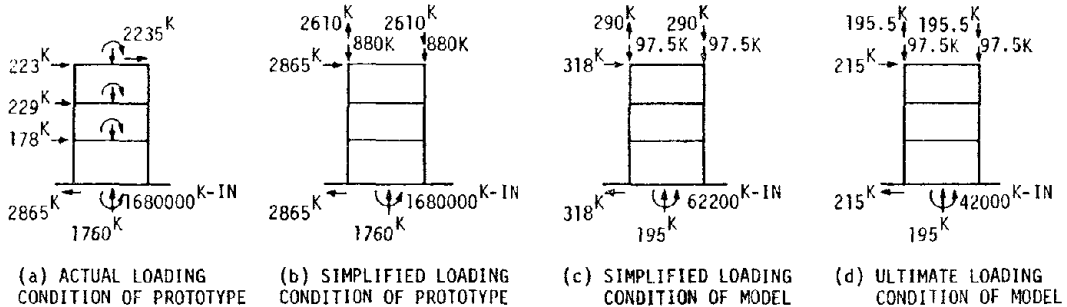
FIG. 3.1 SHEAR AND MOMENT DIAGRAMS OF A SINGLE N-S WALL WHEN SUBJECTED TO ONE HALF THE 1.4 (E + TORSION) CODE FORCES



(1) TWO WALLS RESIST TOTAL EARTHQUAKE LOAD AND TORSION SPECIFIED BY UBC

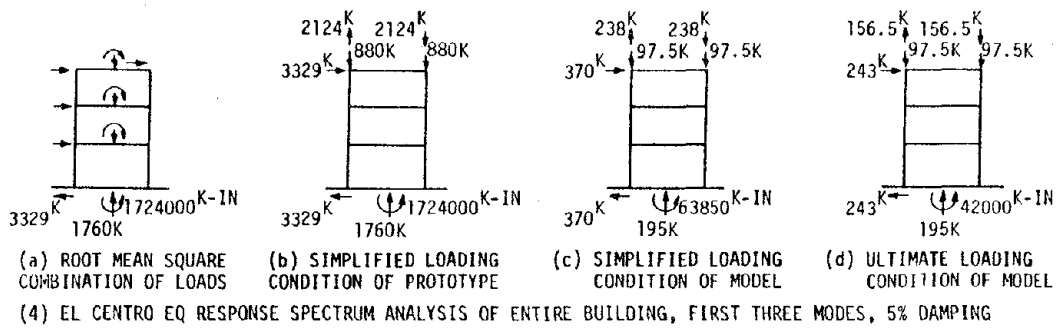


(2) WALLS AND FRAMES ACTING TOGETHER TO RESIST TOTAL EARTHQUAKE LOAD SPECIFIED BY UBC

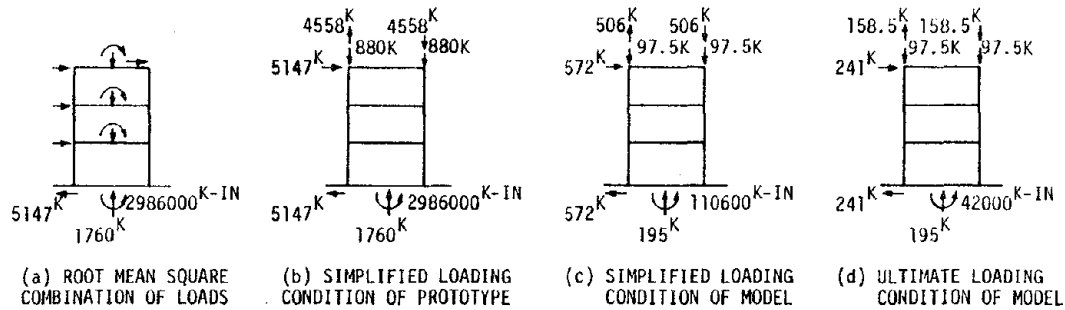


(3) EL CENTRO EQ RESPONSE SPECTRUM ANALYSIS OF ENTIRE BUILDING, FIRST MODE ONLY, 5% DAMPING

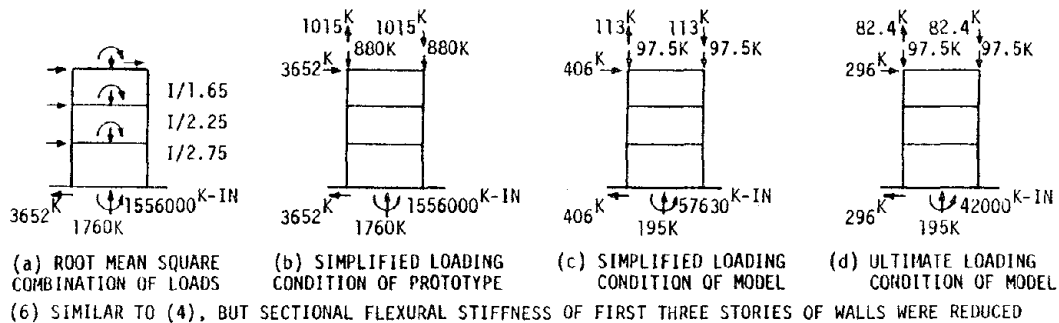
FIG. 3.2 LOADING CONDITIONS OF PROTOTYPE AND MODEL



(4) EL CENTRO EQ RESPONSE SPECTRUM ANALYSIS OF ENTIRE BUILDING, FIRST THREE MODES, 5% DAMPING

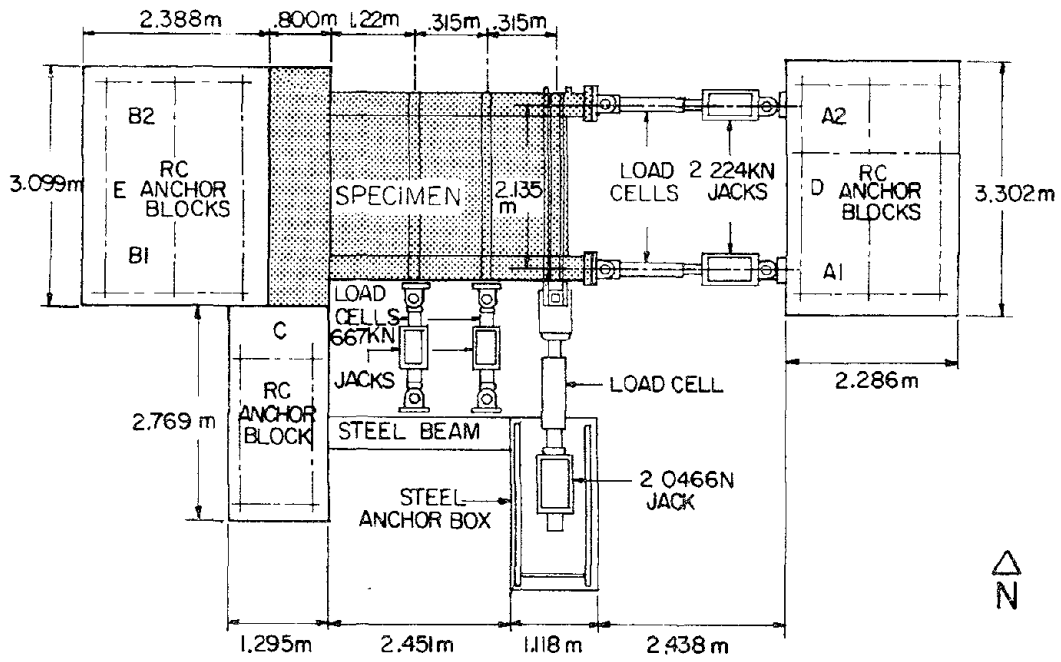


(5) SAN FERNANDO EQ RESPONSE SPECTRUM ANALYSIS OF ENTIRE BUILDING, FIRST THREE MODES, 5% DAMPING

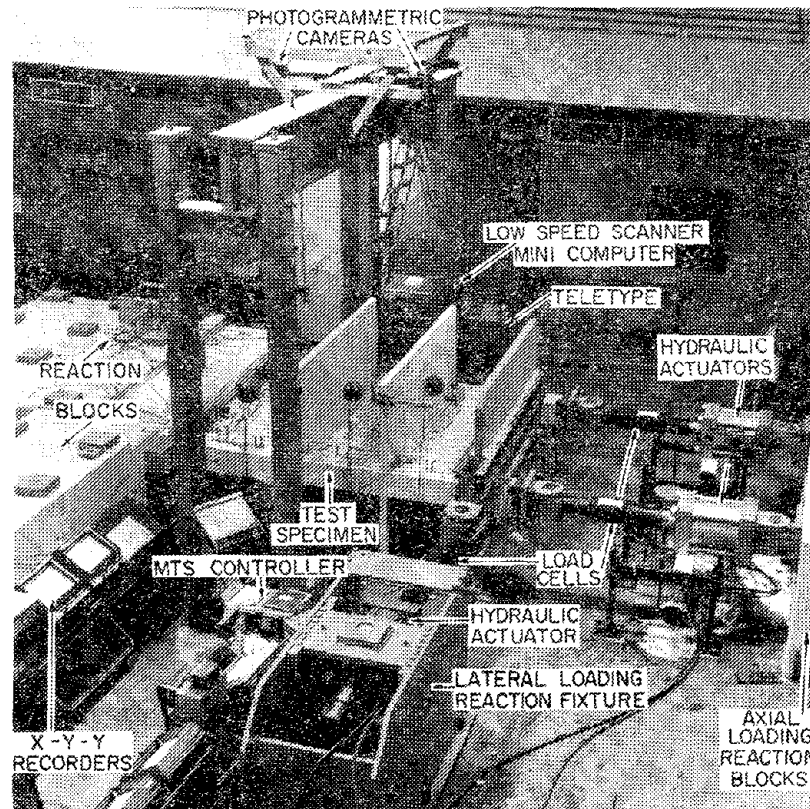


(6) SIMILAR TO (4), BUT SECTIONAL FLEXURAL STIFFNESS OF FIRST THREE STORIES OF WALLS WERE REDUCED

FIG. 3.2 (CONT.)



(a) Plan



(b) General View

FIG. 3.3 PLAN AND GENERAL VIEW OF TESTING FACILITY

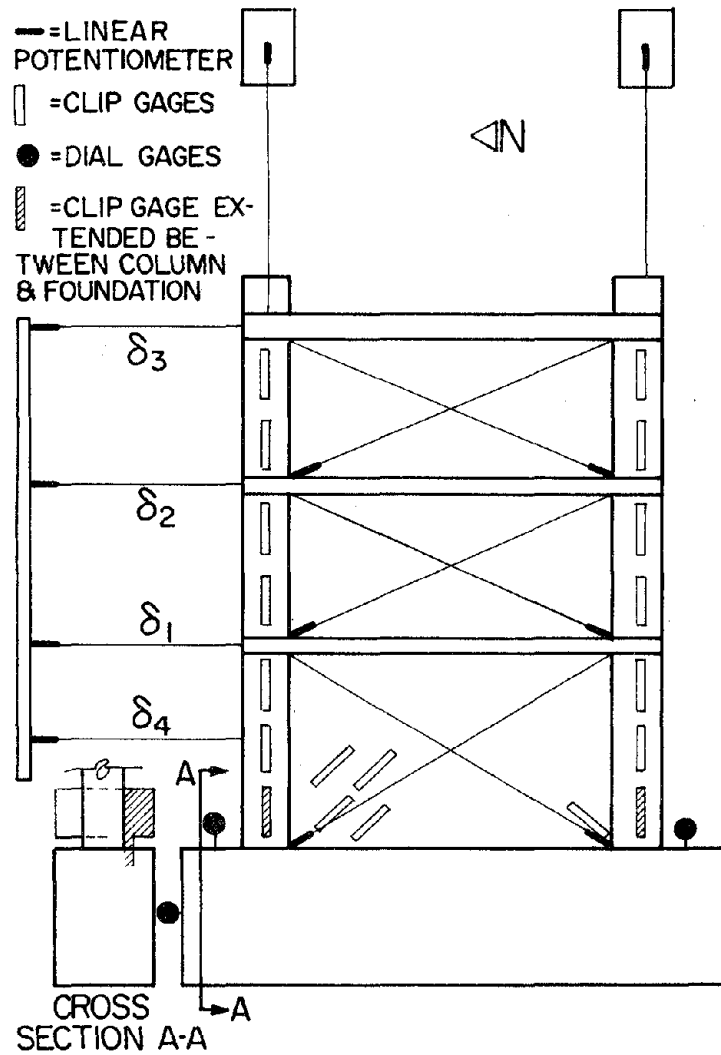


FIG. 3.4 EXTERNAL INSTRUMENTATION OF WALL SPECIMEN

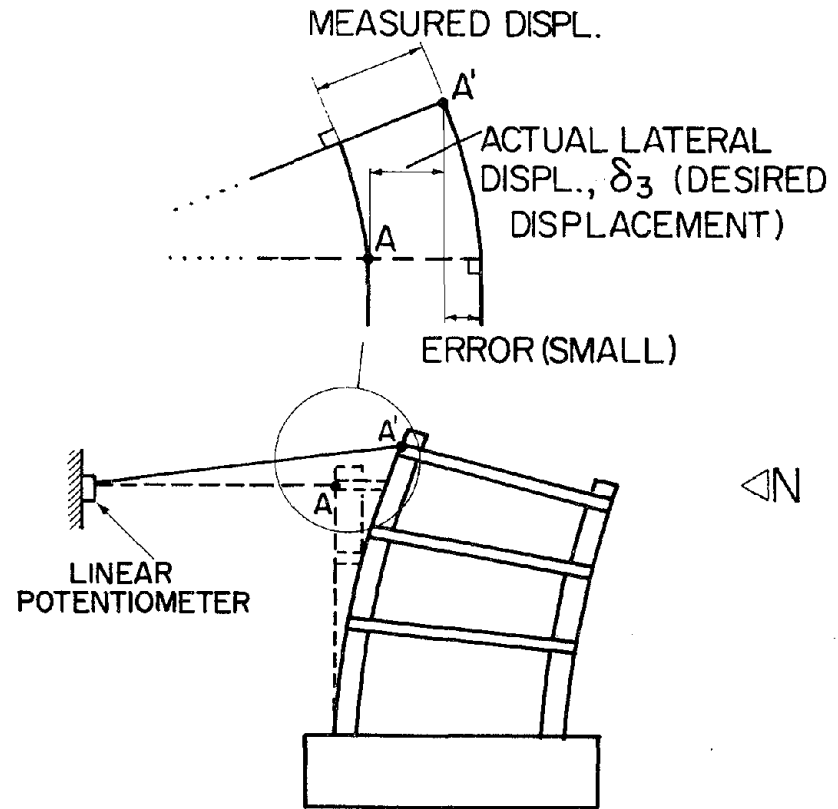


FIG. 3.5 ERROR IN LATERAL DISPLACEMENT MEASUREMENT



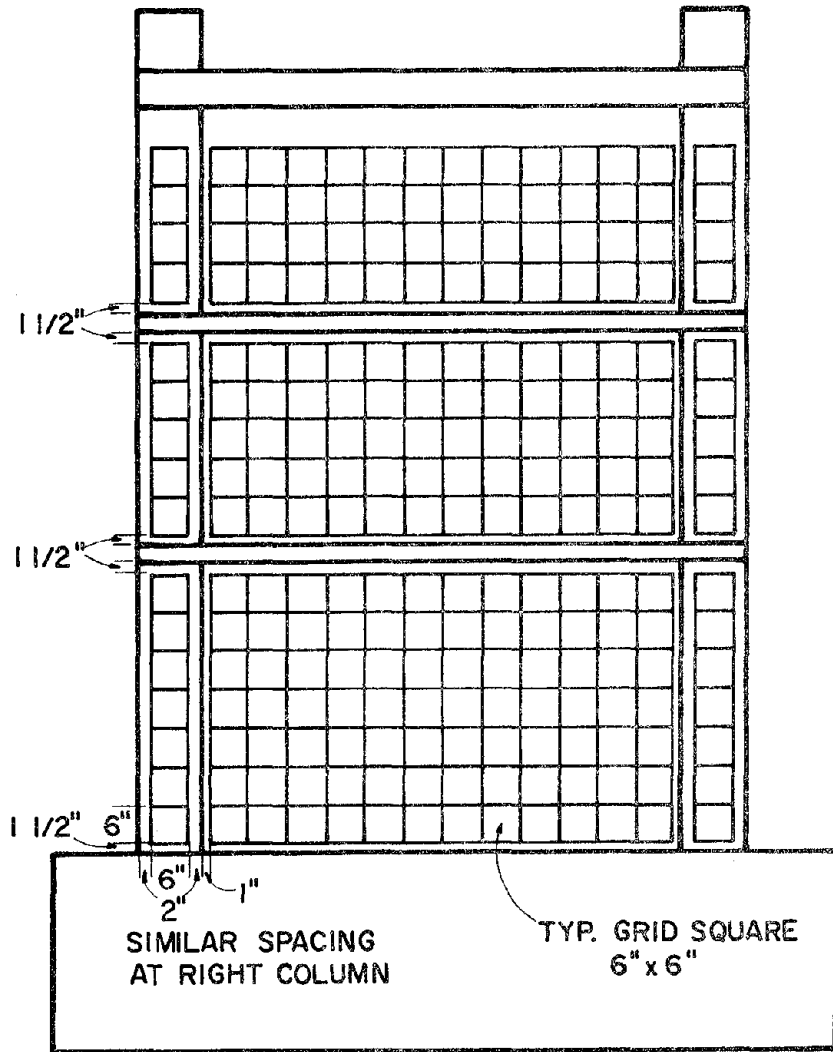


FIG. 3.6 GRID FOR PHOTOGRAMMETRIC MEASUREMENT

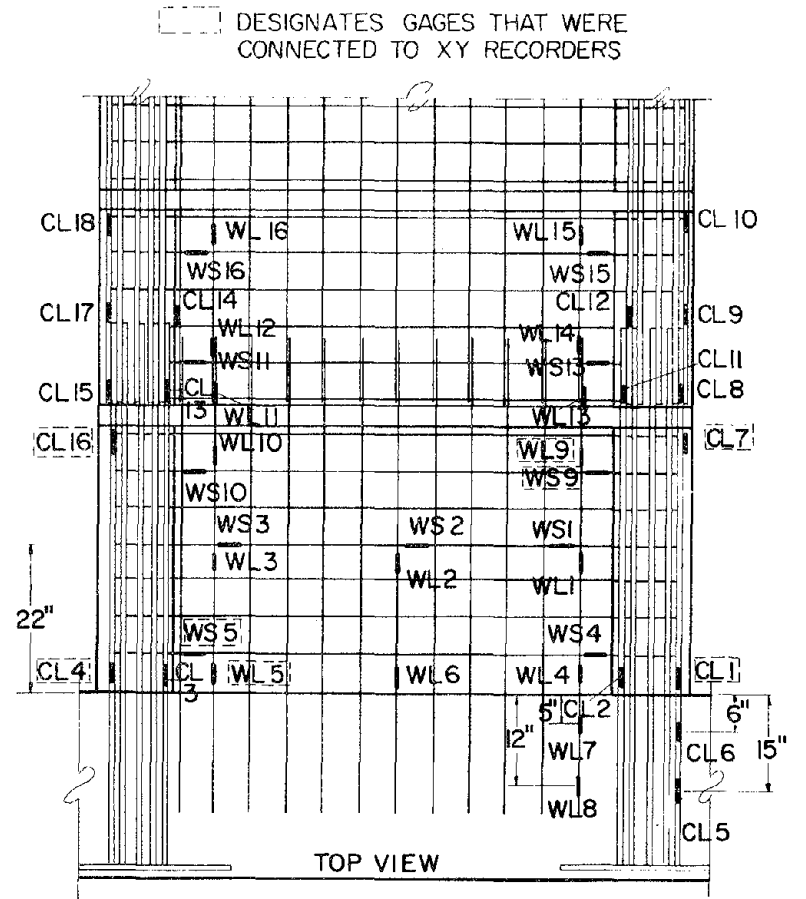


FIG. 3.7 INTERNAL INSTRUMENTATION FOR SPECIMEN SW7

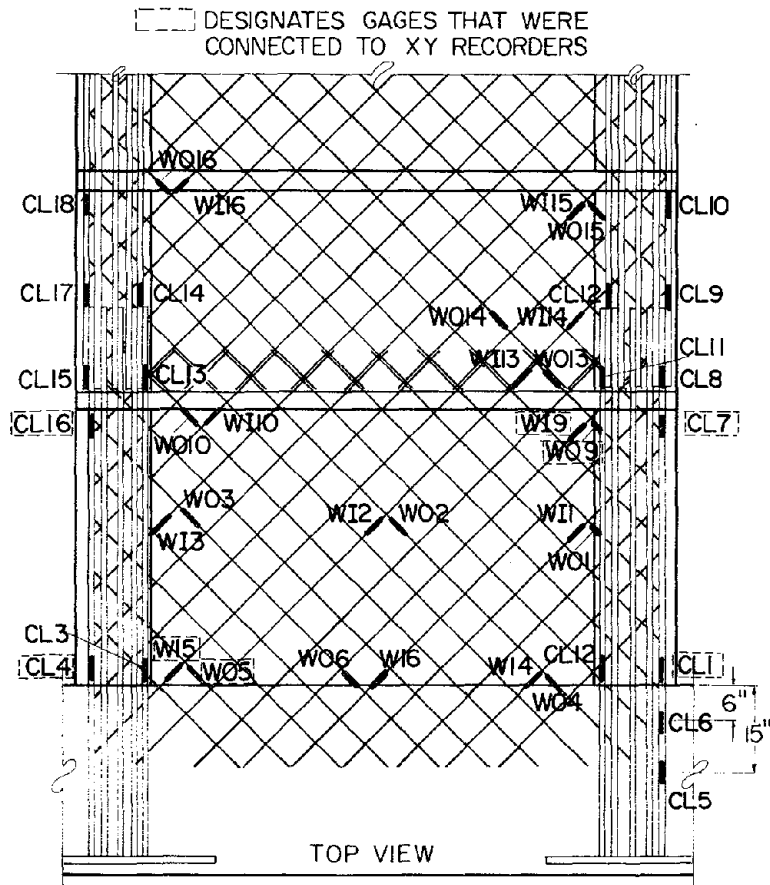


FIG. 3.8 INTERNAL INSTRUMENTATION FOR SPECIMEN SW8

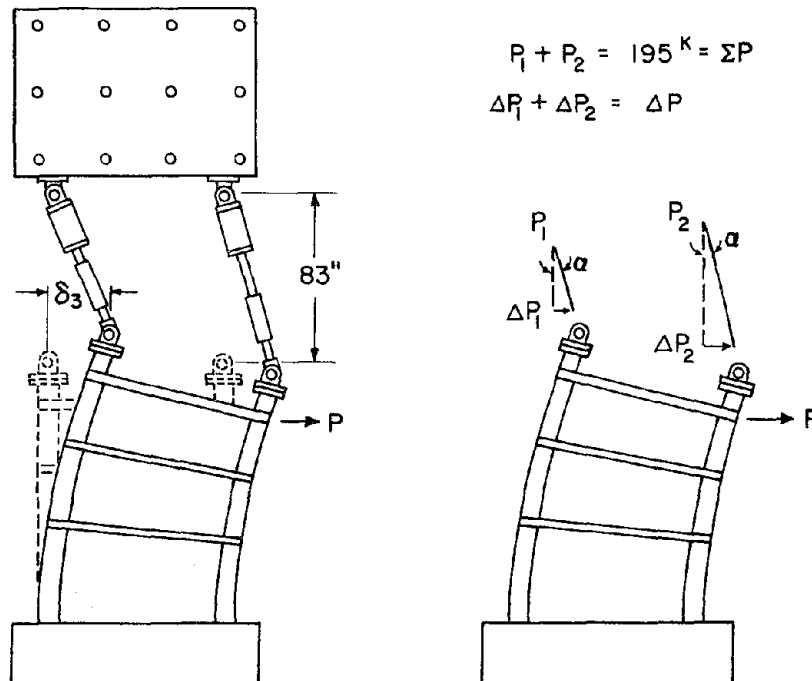


FIG. 3.9 HORIZONTAL COMPONENT OF NET AXIAL FORCE

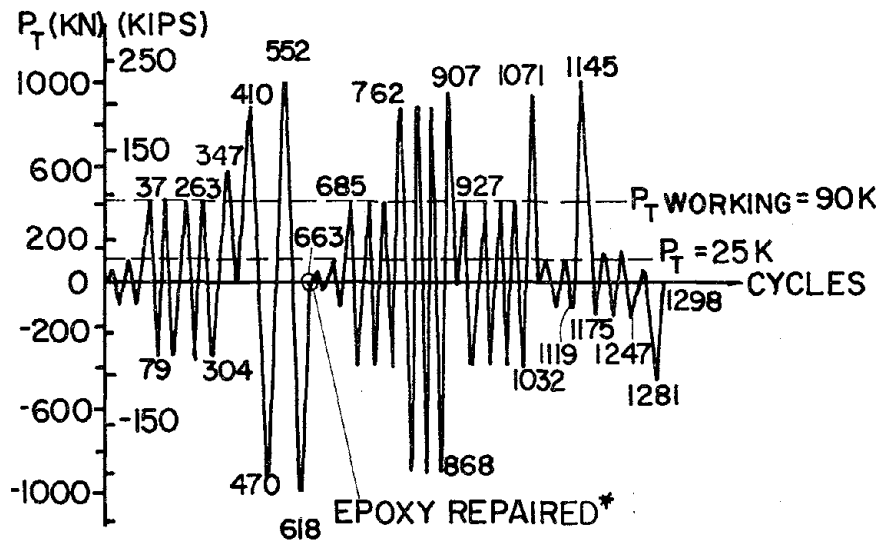


FIG. 4.1(a) LOADING HISTORY--SPECIMENS SW7 VIRGIN + SW7 EPOXY-REPAIRED\*

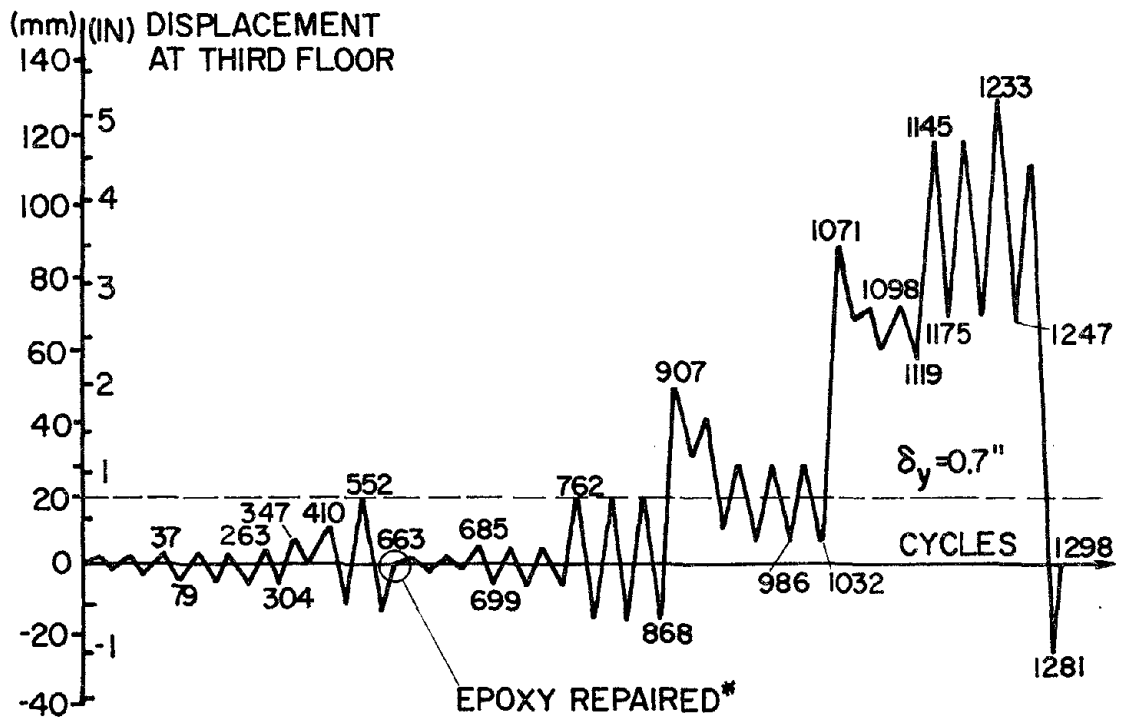
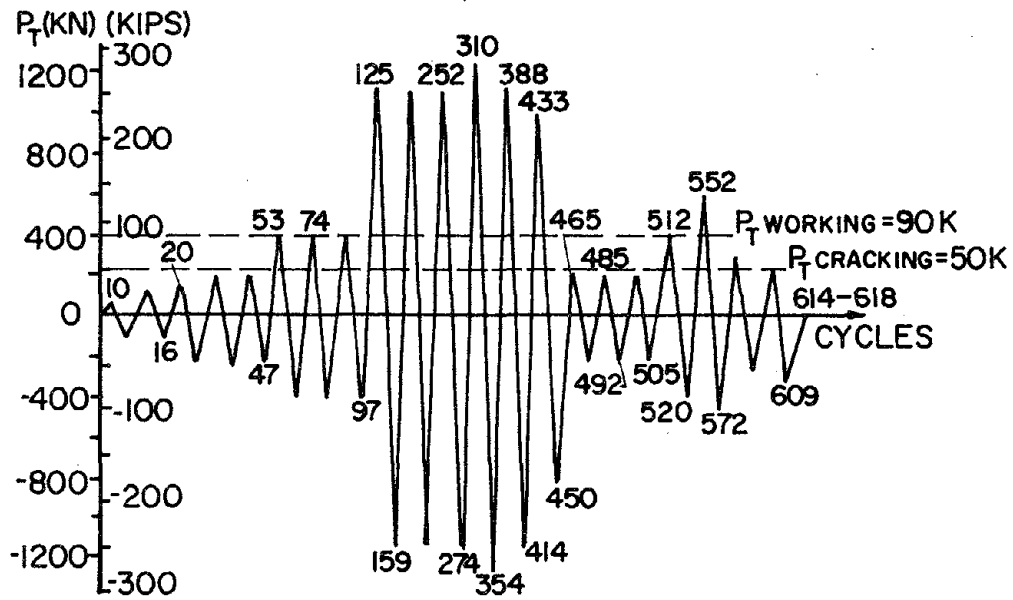
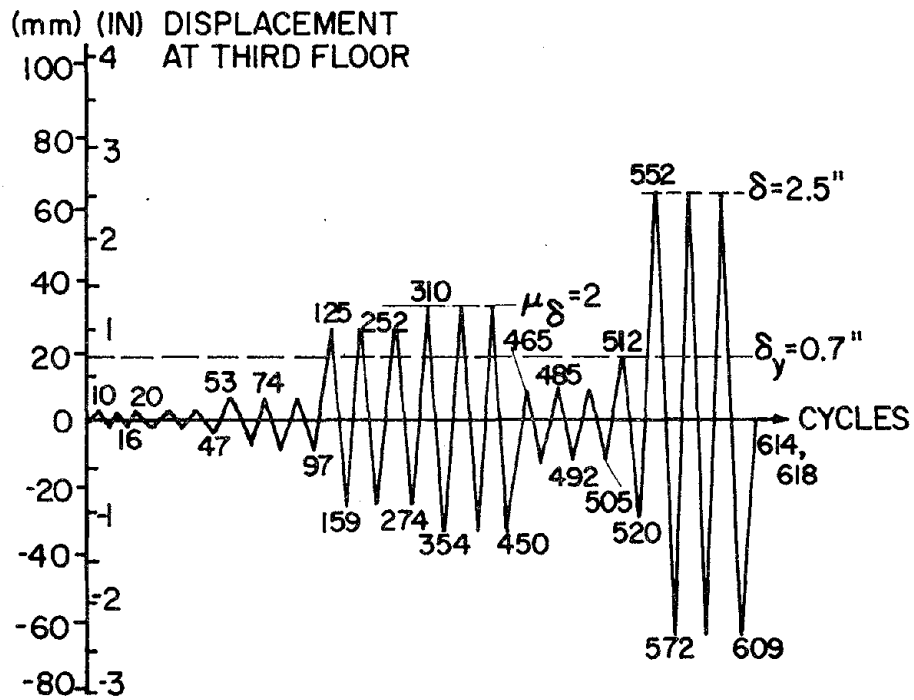


FIG. 4.1(b) DISPLACEMENT HISTORY--SPECIMEN SW7 VIRGIN + SW7 EPOXY-REPAIRED\*



(a) Loading History



(b) Displacement History

FIG. 4.2 LOADING PROGRAM--SPECIMEN SW7 R<sub>2</sub>

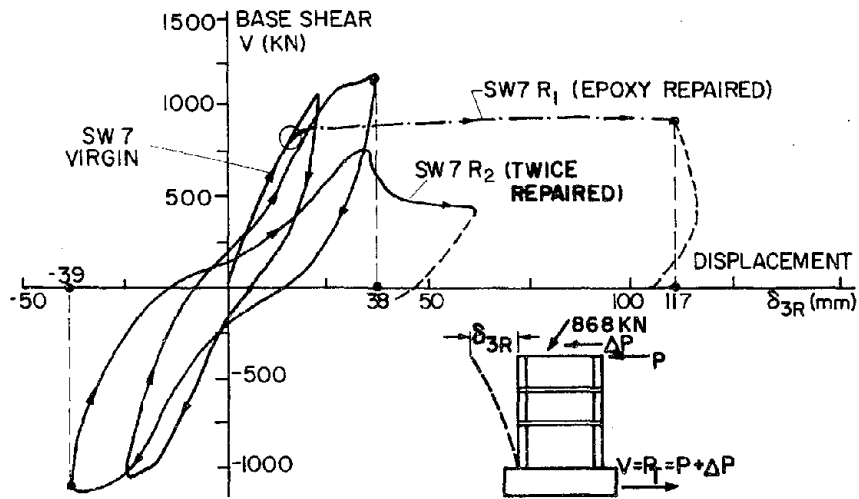


FIG. 4.3 TOTAL LATERAL LOAD,  $V$ , VS. THIRD-STORY DISPLACEMENT ENVELOPE --SPECIMEN SW7: VIRGIN, EPOXY-REPAIRED, TWICE-REPAIRED

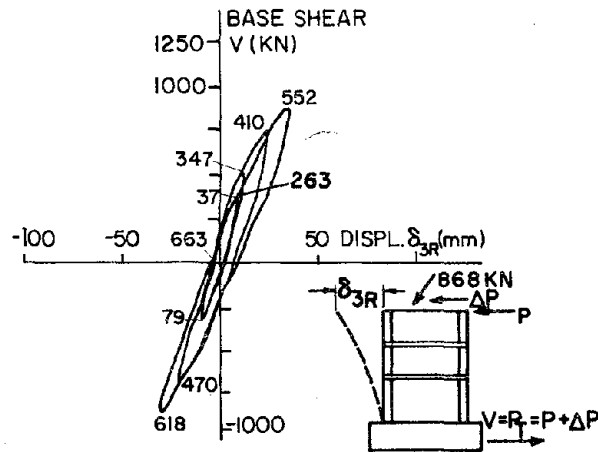


FIG. 4.4(a) TOTAL LATERAL LOAD,  $V$ , VS. THIRD-FLOOR RELATIVE DISPLACEMENT DIAGRAM,  $\delta_{3R}$  --SPECIMEN SW7 VIRGIN

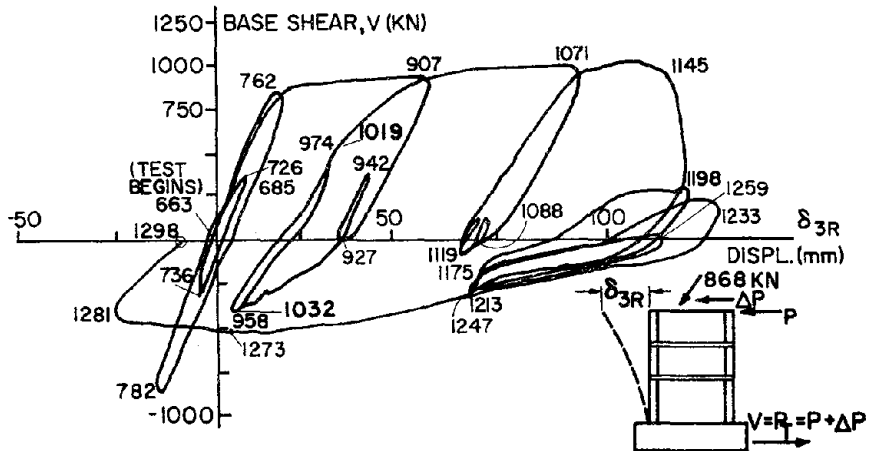


FIG. 4.4(b) TOTAL LATERAL LOAD,  $V$ , VS. THIRD-FLOOR RELATIVE DISPLACEMENT DIAGRAM,  $\delta_{3R}$  --SPECIMEN SW7 R<sub>1</sub>, EPOXY-REPAIRED

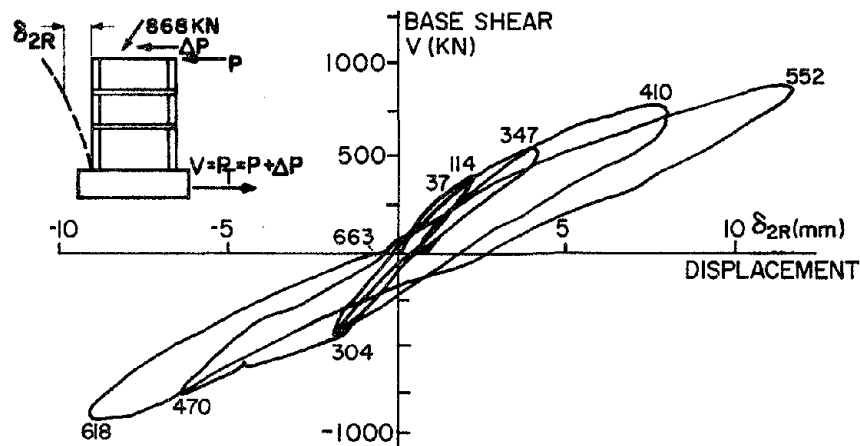


FIG. 4.5(a) TOTAL LATERAL LOAD,  $V$ , VS. SECOND-FLOOR RELATIVE DISPLACEMENT DIAGRAM,  $\delta_{2R}$ --SPECIMEN SW7 VIRGIN

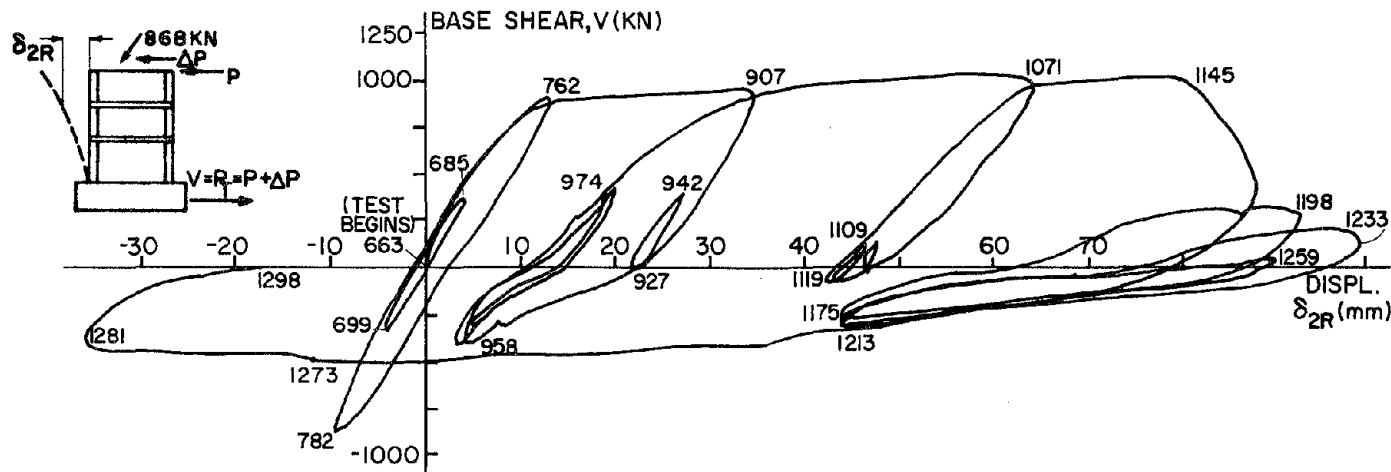


FIG. 4.5(b) TOTAL LATERAL LOAD,  $V$ , VS. SECOND-FLOOR RELATIVE DISPLACEMENT DIAGRAM,  $\delta_{2R}$ --SPECIMEN SW7 R<sub>1</sub> EPOXY-REPAIRED

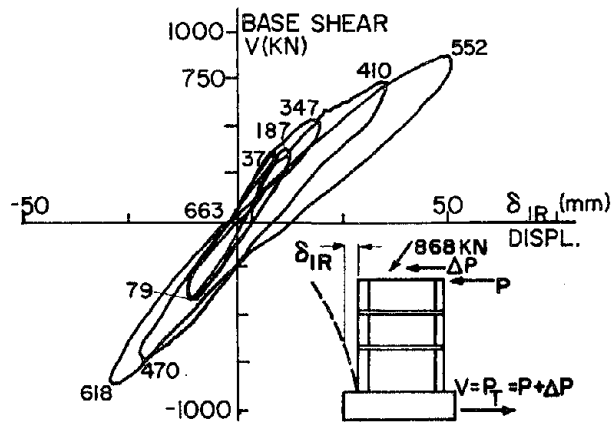


FIG. 4.6(a) TOTAL LATERAL LOAD, V, VS. FIRST-FLOOR RELATIVE DISPLACEMENT DIAGRAM,  $\delta_{1R}$ --SPECIMEN SW7 VIRGIN

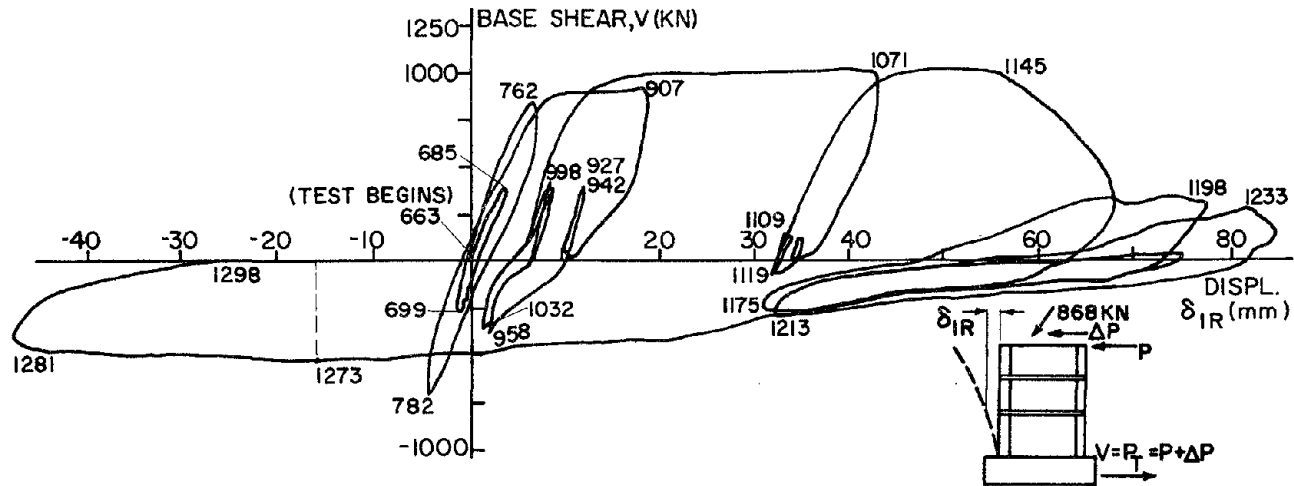


FIG. 4.6(b) TOTAL LATERAL LOAD, V, VS. FIRST-FLOOR RELATIVE DISPLACEMENT DIAGRAM,  $\delta_{1R}$ --SPECIMEN SW7 R<sub>1</sub> EPOXY-REPAIRED

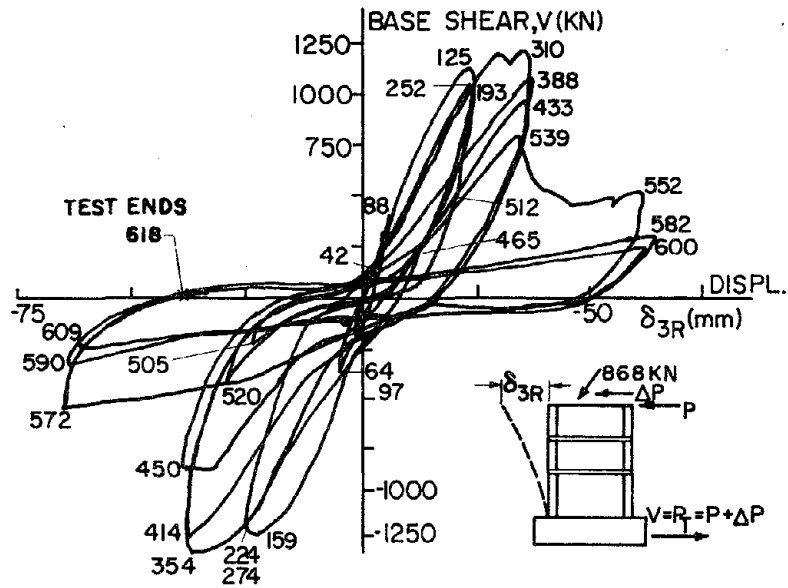


FIG. 4.7 TOTAL LATERAL LOAD, V, VS. THIRD-FLOOR LATERAL DISPLACEMENT DIAGRAM,  $\delta_{3R}$ --SPECIMEN SW7 R<sub>2</sub>

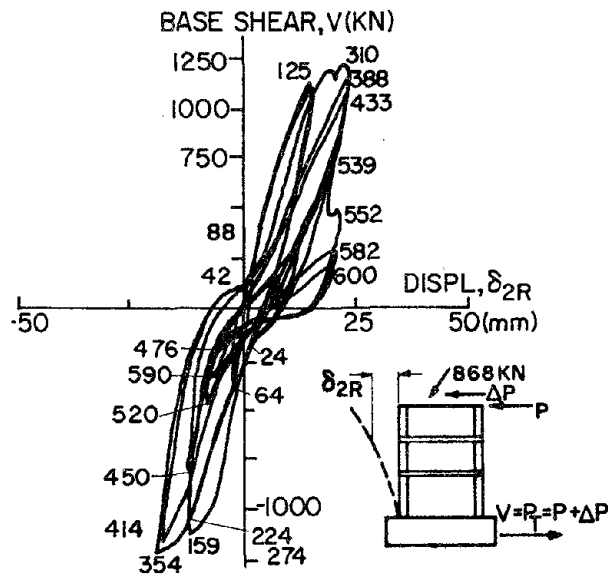


FIG. 4.8 TOTAL LATERAL LOAD, V, VS. SECOND-FLOOR LATERAL DISPLACEMENT DIAGRAM,  $\delta_{2R}$ --SPECIMEN SW7 R<sub>2</sub>



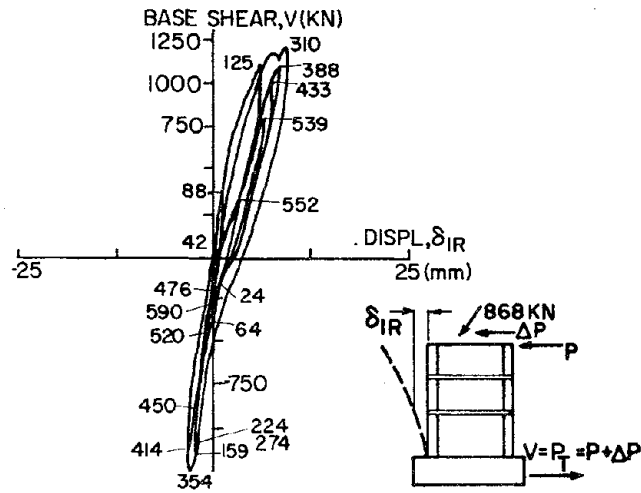


FIG. 4.9(a) TOTAL LATERAL LOAD, V, VS. FIRST-FLOOR LATERAL DISPLACEMENT DIAGRAM,  $\delta_{1R}$ —SPECIMEN SW7 R<sub>2</sub>

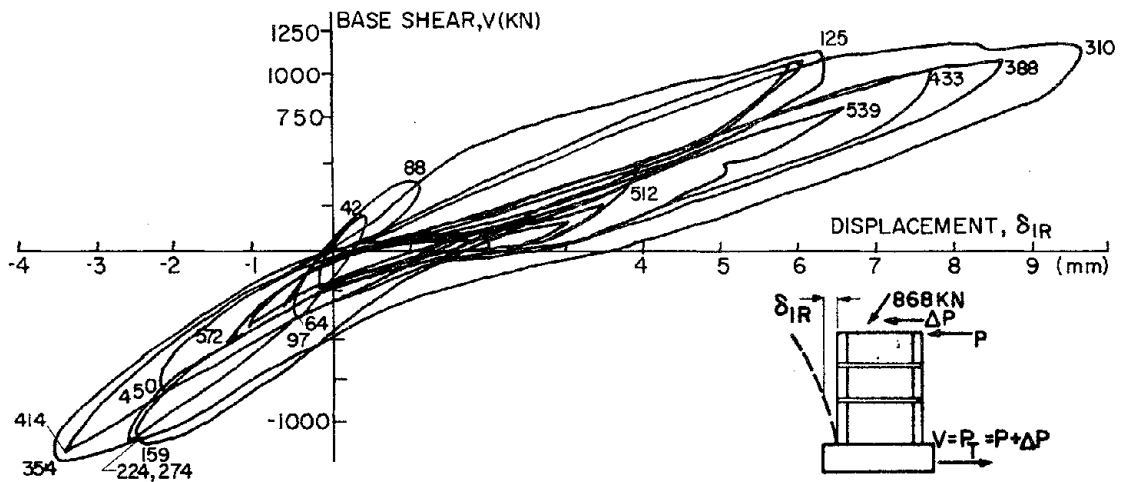


FIG. 4.9(b) TOTAL LATERAL LOAD, V, VS. FIRST-FLOOR LATERAL DISPLACEMENT DIAGRAM,  $\delta_{1R}$ —SPECIMEN SW7 R<sub>2</sub>

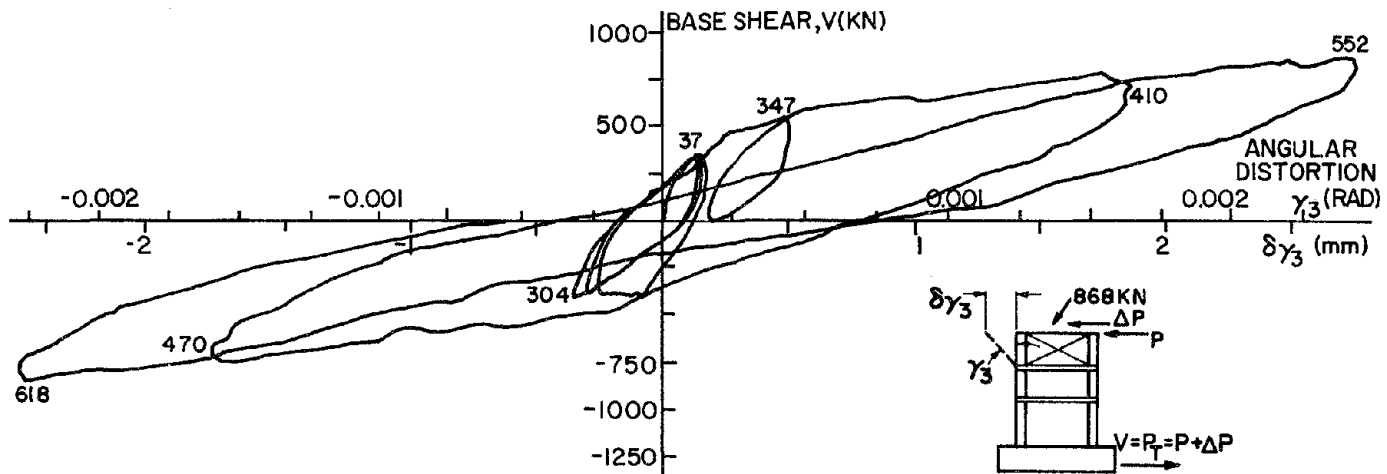


FIG. 4.10(a) TOTAL LATERAL LOAD,  $V$ , VS. THIRD-STORY SHEAR DISTORTION,  $\gamma_3$ -- SPECIMEN SW7 VIRGIN

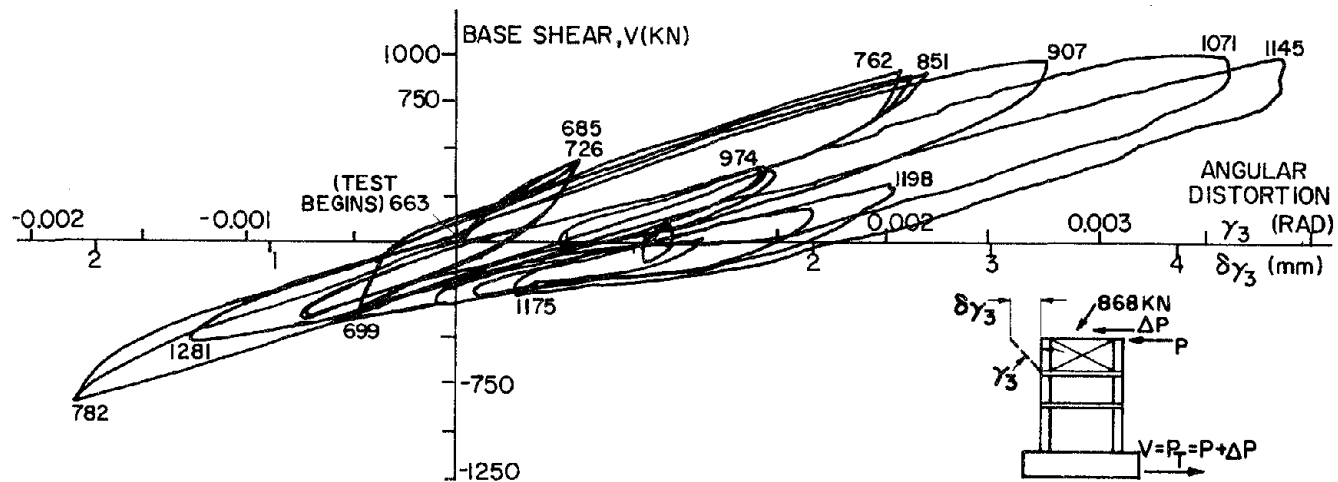


FIG. 4.10(b) TOTAL LATERAL LOAD,  $V$ , VS. THIRD-STORY SHEAR DISTORTION,  $\gamma_3$ -- SPECIMEN SW7 EPOXY-REPAIRED

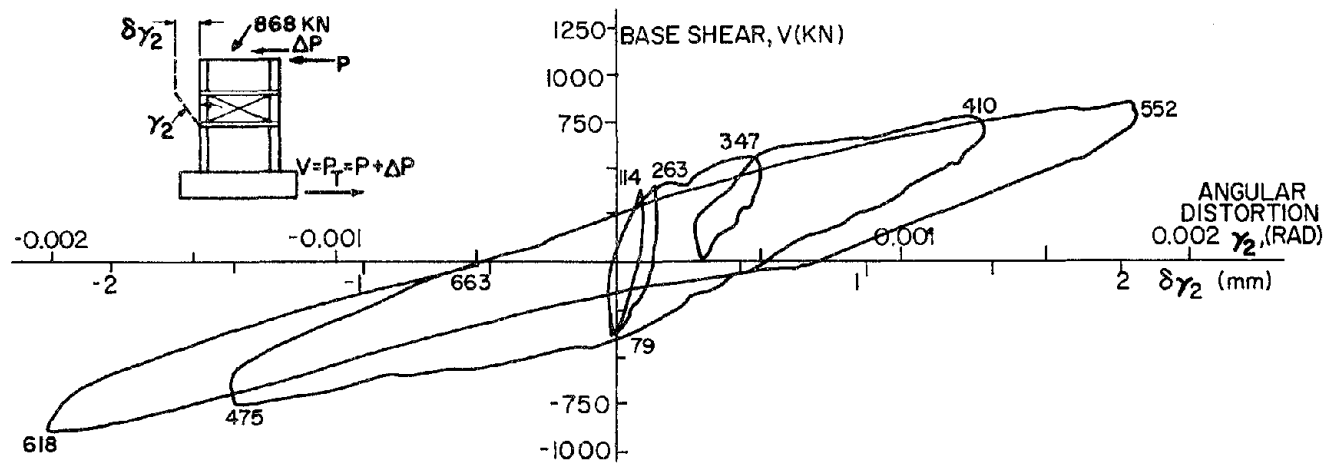


FIG. 4.11(a) TOTAL LATERAL LOAD, V, VS. SECOND-STORY SHEAR DISTORTION,  $\gamma_2$ -- SPECIMEN SW7 VIRGIN

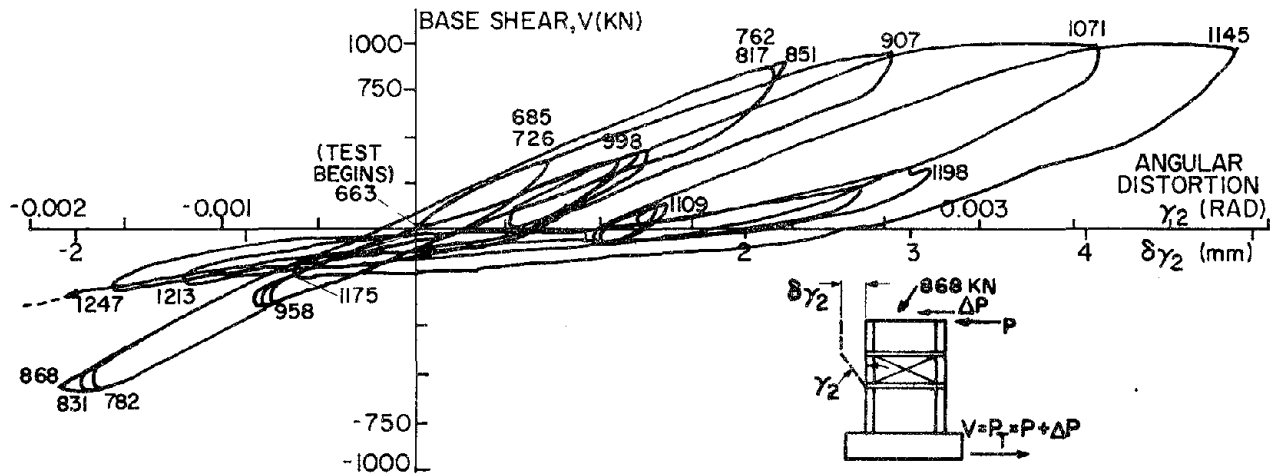


FIG. 4.11(b) TOTAL LATERAL LOAD, V, VS. SECOND-STORY SHEAR DISTORTION,  $\gamma_2$ -- SPECIMEN SW7 EPOXY-REPAIRED

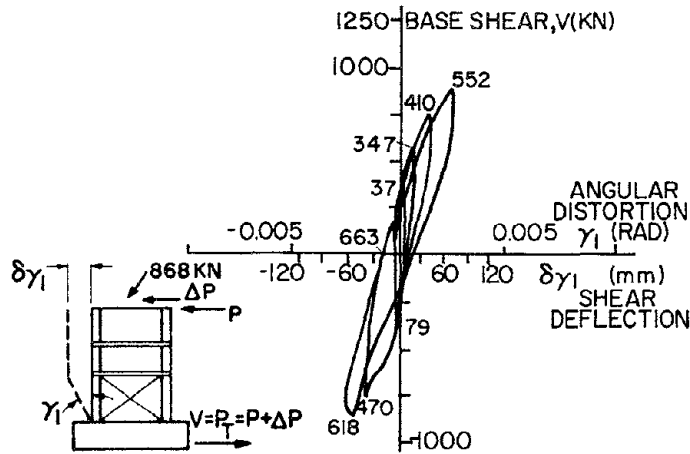


FIG. 4.12(a) TOTAL LATERAL LOAD,  $V$ , VS. FIRST-STORY SHEAR DISTORTION,  $\gamma_1$ --SPECIMEN SW7 VIRGIN

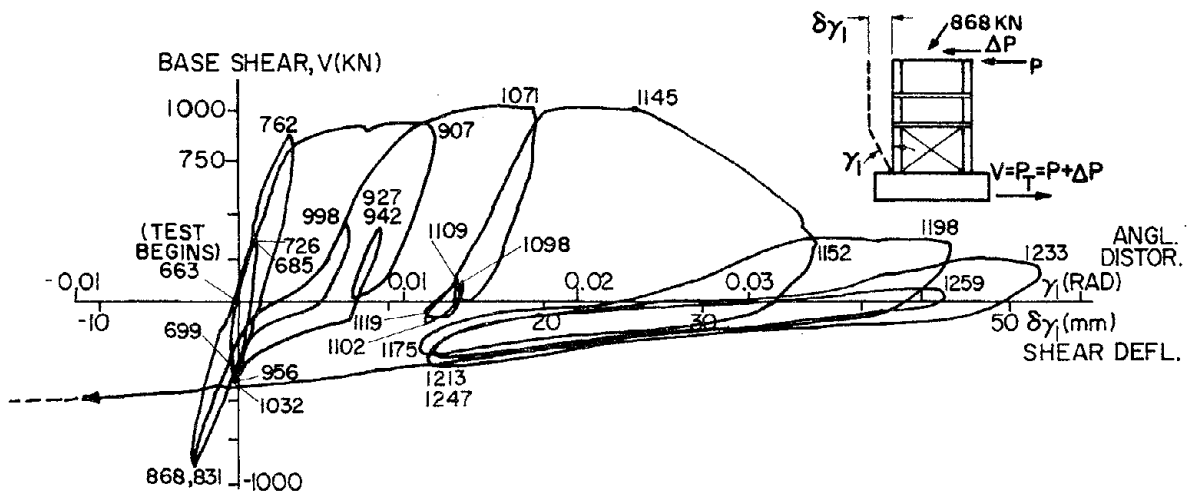


FIG. 4.12(b) TOTAL LATERAL LOAD,  $V$ , VS. FIRST-STORY SHEAR DISTORTION,  $\gamma_1$ --SPECIMEN SW7 EPOXY-REPAIRED

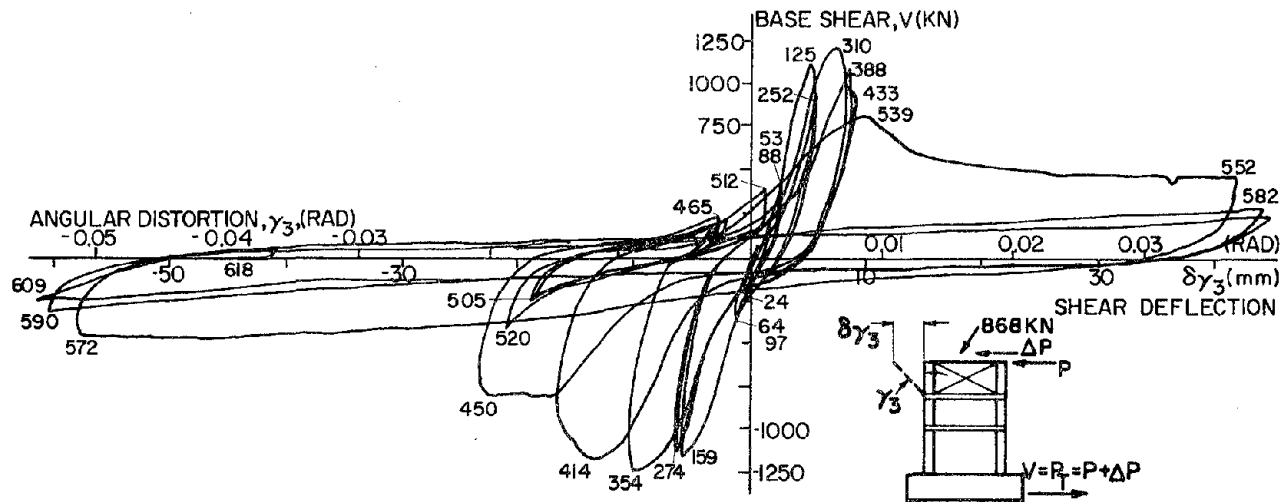


FIG. 4.13 TOTAL LATERAL LOAD, V, VS. THIRD-STORY SHEAR DISTORTION,  $\gamma_3$ -- SPECIMEN SW7 R<sub>2</sub>

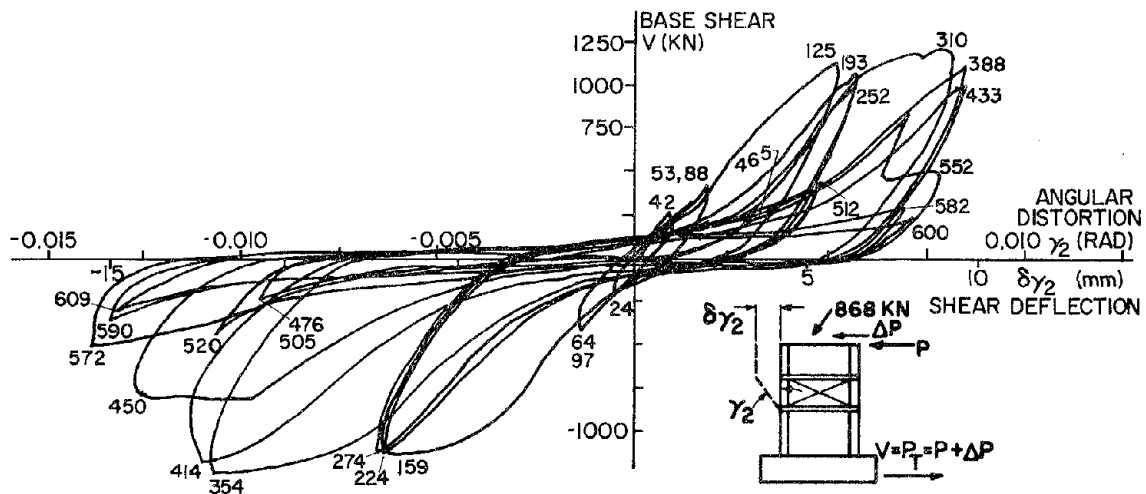


FIG. 4.14 TOTAL LATERAL LOAD, V, VS. SECOND-STORY SHEAR DISTORTION,  $\gamma_2$ -- SPECIMEN SW7 R<sub>2</sub>

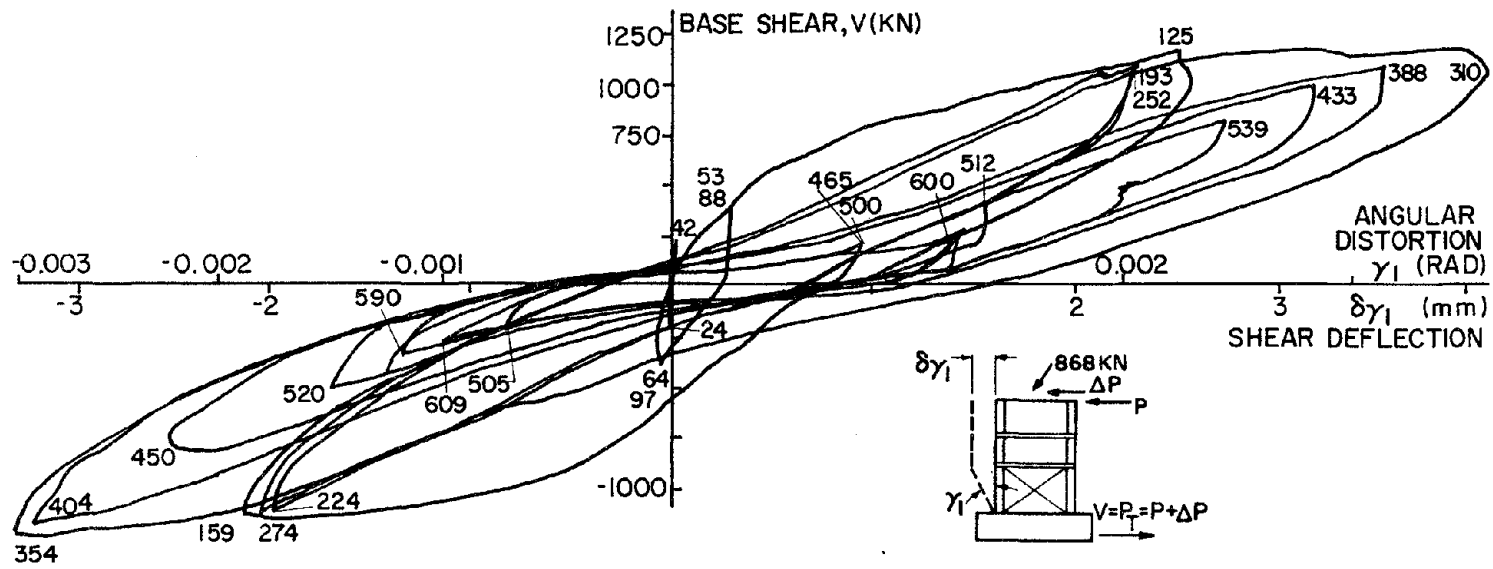
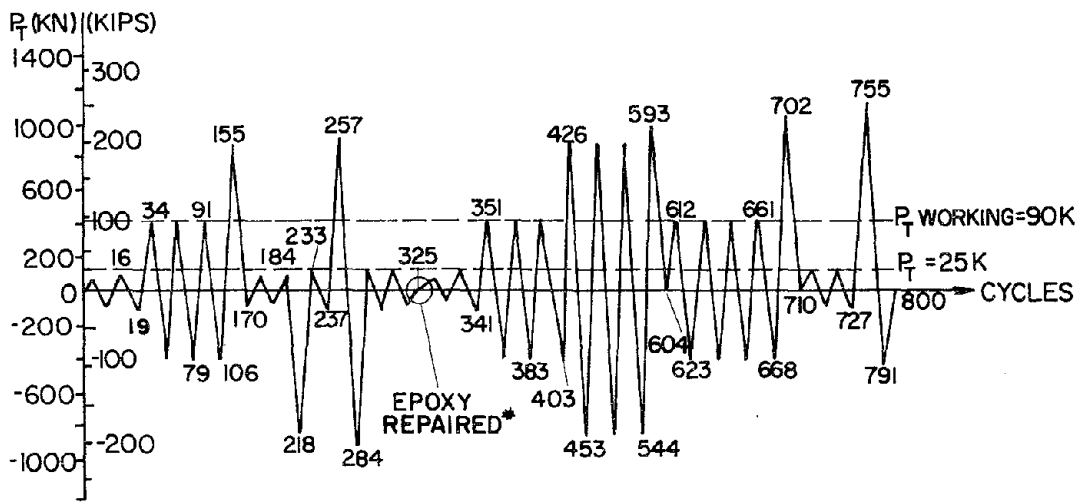
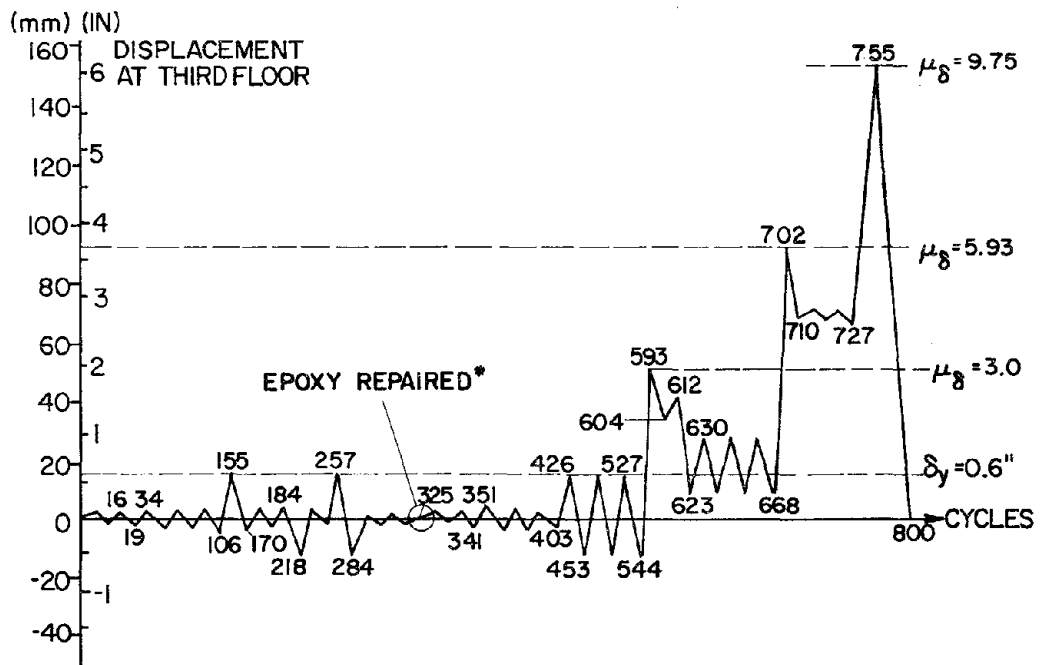


FIG. 4.15 TOTAL LATERAL LOAD, V, VS. FIRST-STORY SHEAR DISTORTION,  $\gamma_1$  -- SPECIMEN SW7 R<sub>2</sub>

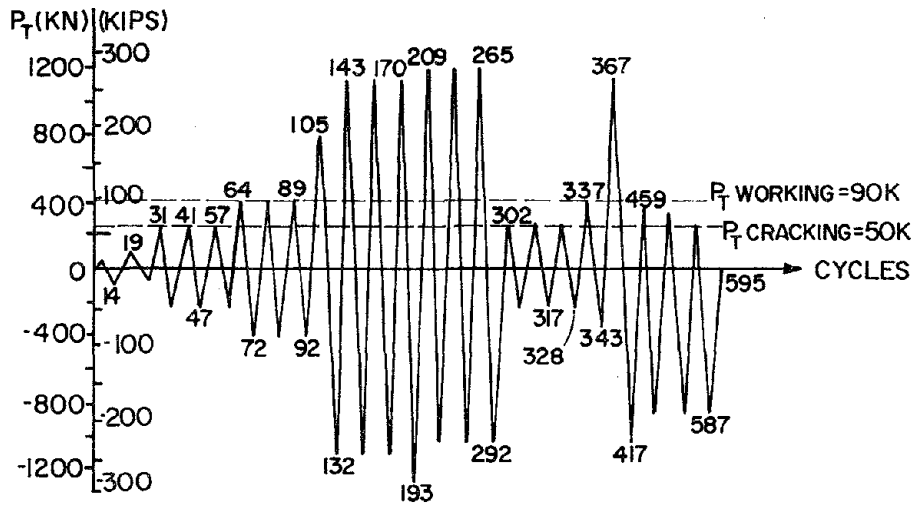


(a) Loading History

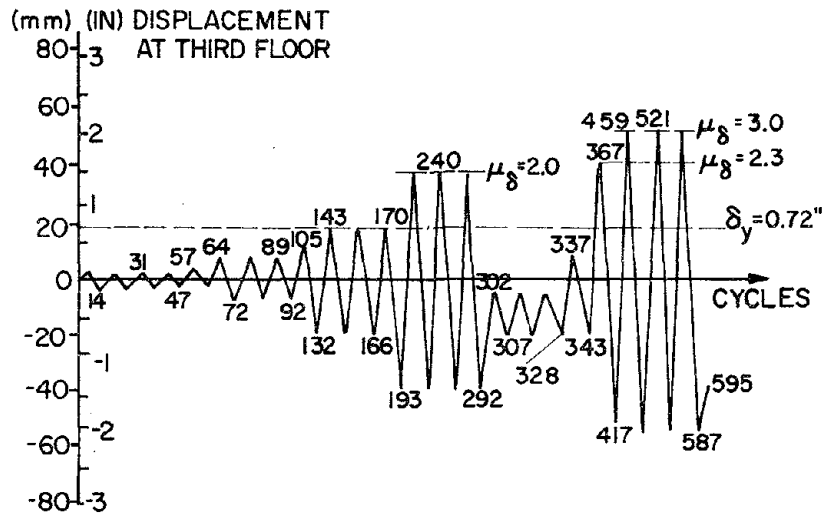


(b) Displacement History

FIG. 4.16 LOADING PROGRAM--SPECIMEN SW8 VIRGIN + SW8 EPOXY-REPAIRED\*



(a) Loading History



(b) Displacement History

FIG. 4.17 LOADING PROGRAM--SPECIMEN SW8 R<sub>2</sub>



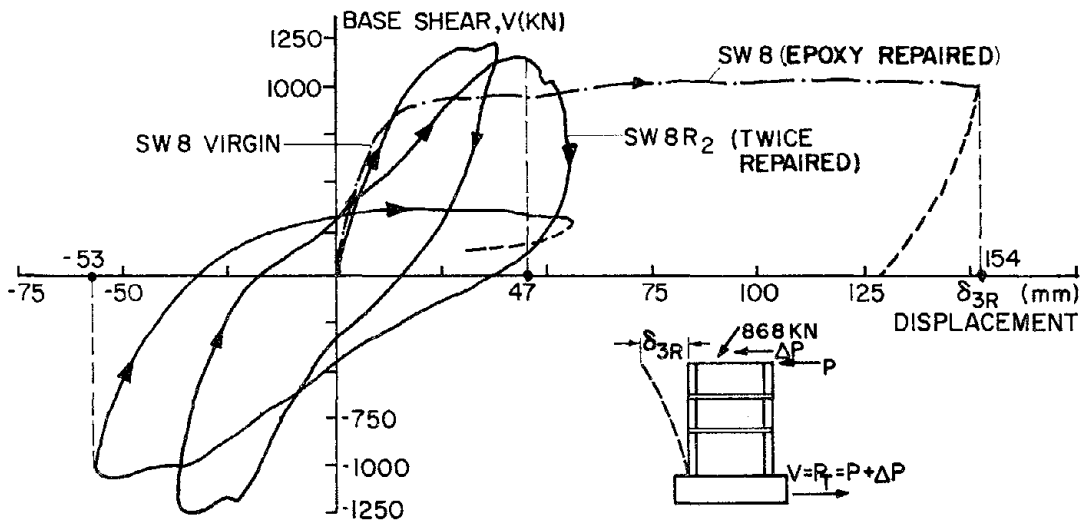


FIG. 4.18 TOTAL LATERAL LOAD,  $V$ , VS. THIRD-FLOOR RELATIVE DISPLACEMENT ENVELOPE,  $\delta_{3R}$ —SPECIMEN SW8: VIRGIN, EPOXY-REPAIRED, TWICE-REPAIRED

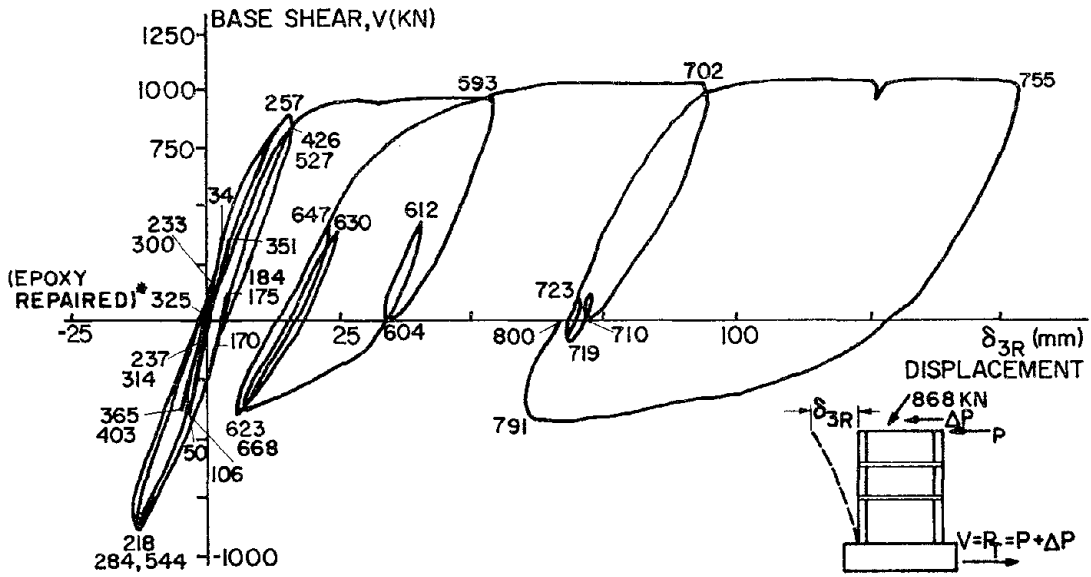


FIG. 4.19 TOTAL LATERAL LOAD,  $V$ , VS. THIRD-FLOOR RELATIVE DISPLACEMENT,  $\delta_{3R}$ —SPECIMEN SW8: VIRGIN + EPOXY-REPAIRED\*

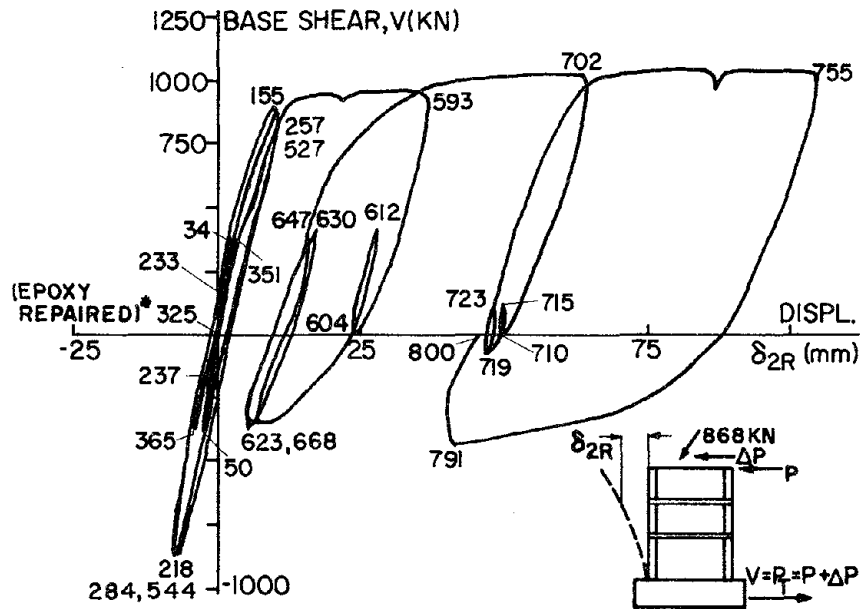


FIG. 4.20 TOTAL LATERAL LOAD,  $V$ , VS. SECOND-FLOOR RELATIVE DISPLACEMENT,  $\delta_{2R}$ ---SPECIMEN SW8: VIRGIN + EPOXY-REPAIRED\*

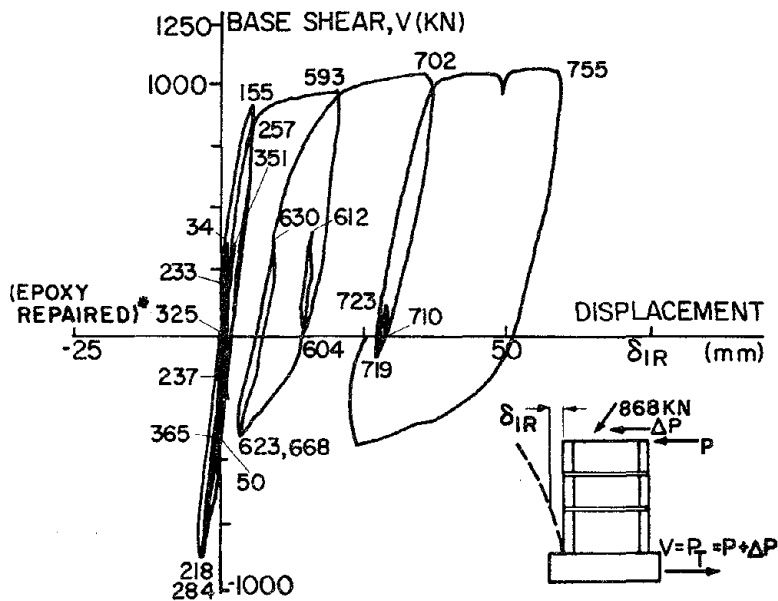


FIG. 4.21 TOTAL LATERAL LOAD,  $V$ , VS. FIRST-FLOOR RELATIVE DISPLACEMENT,  $\delta_{1R}$ ---SPECIMEN SW8: VIRGIN + EPOXY-REPAIRED\*

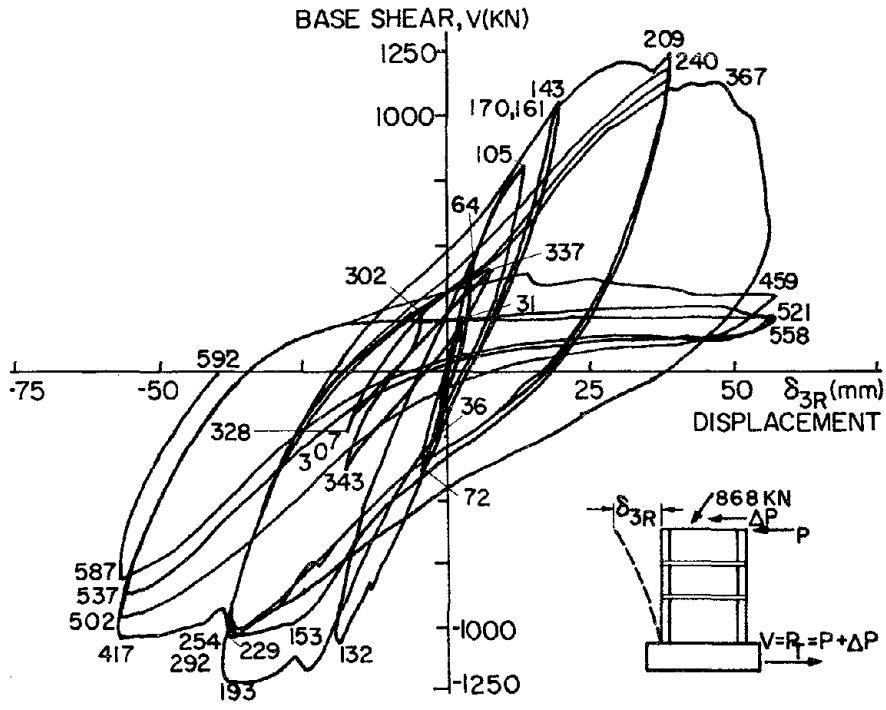


FIG. 4.22 TOTAL LATERAL LOAD, V, VS. THIRD-FLOOR RELATIVE DISPLACEMENT,  $\delta_{3R}$ --SPECIMEN SW8 R<sub>2</sub>

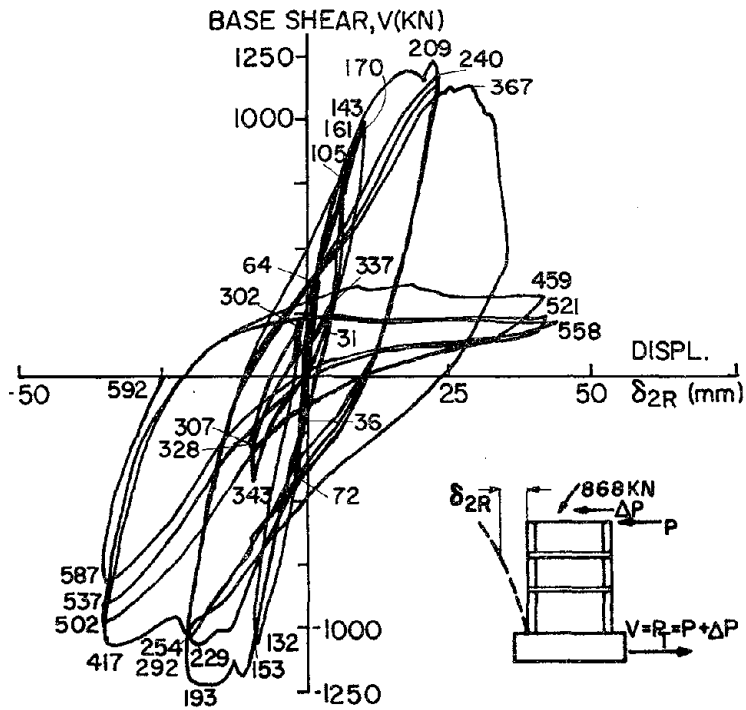


FIG. 4.23 TOTAL LATERAL LOAD, V, VS. SECOND-STORY RELATIVE DISPLACEMENT,  $\delta_{2R}$ --SPECIMEN SW8 R<sub>2</sub>

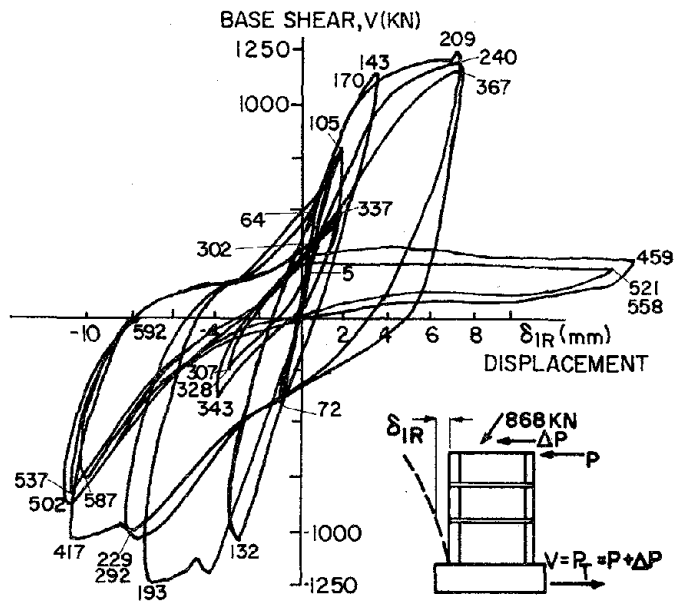


FIG. 4.24 TOTAL LATERAL LOAD, V, VS. FIRST-STORY LATERAL DISPLACEMENT,  $\delta_{1R}$ ---SPECIMEN SW8 R<sub>2</sub>

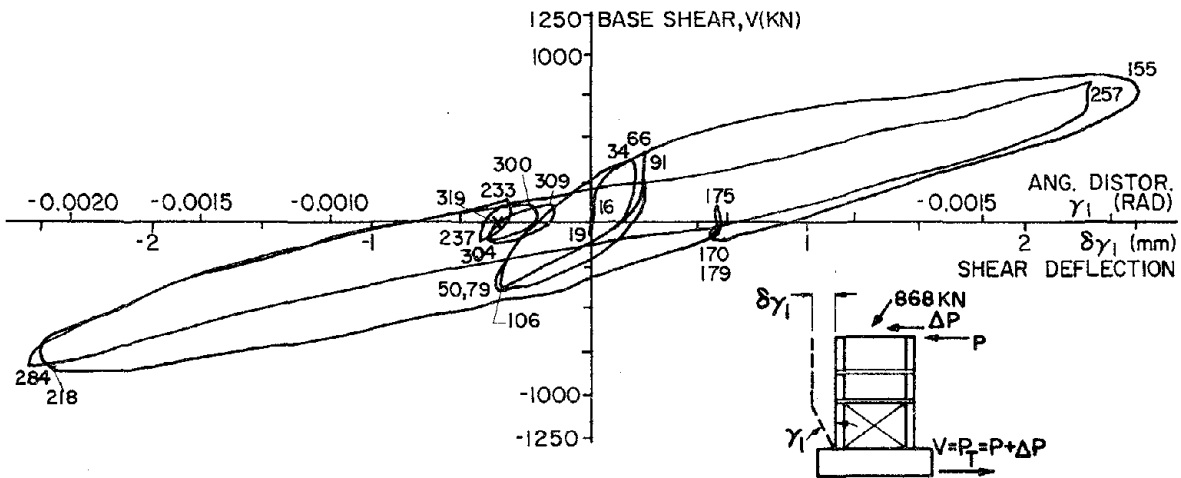


FIG. 4.25 TOTAL LATERAL LOAD, V, VS. FIRST-STORY SHEAR DISTORTION,  $\gamma_1$ ---SPECIMEN SW8 VIRGIN

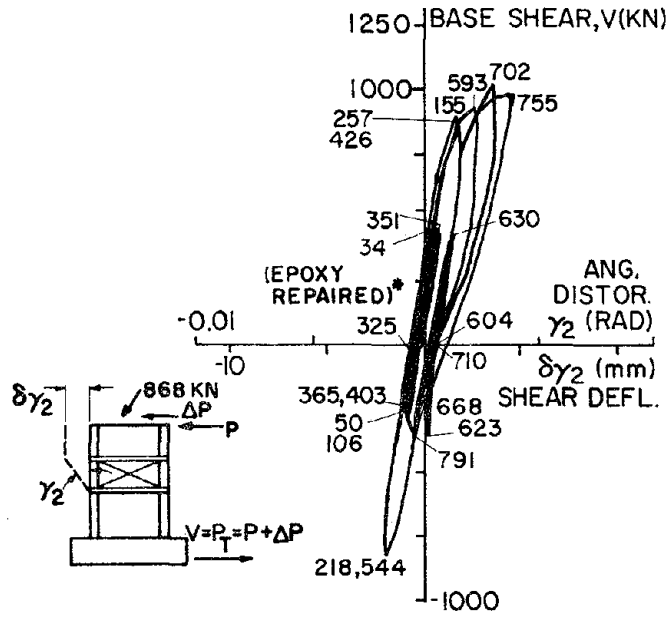


FIG. 4.26 TOTAL LATERAL LOAD,  $V$ , VS. SECOND-STORY SHEAR DISTORTION,  $\gamma_2$ -- SPECIMEN SW8: VIRGIN + EPOXY REPAIRED\*

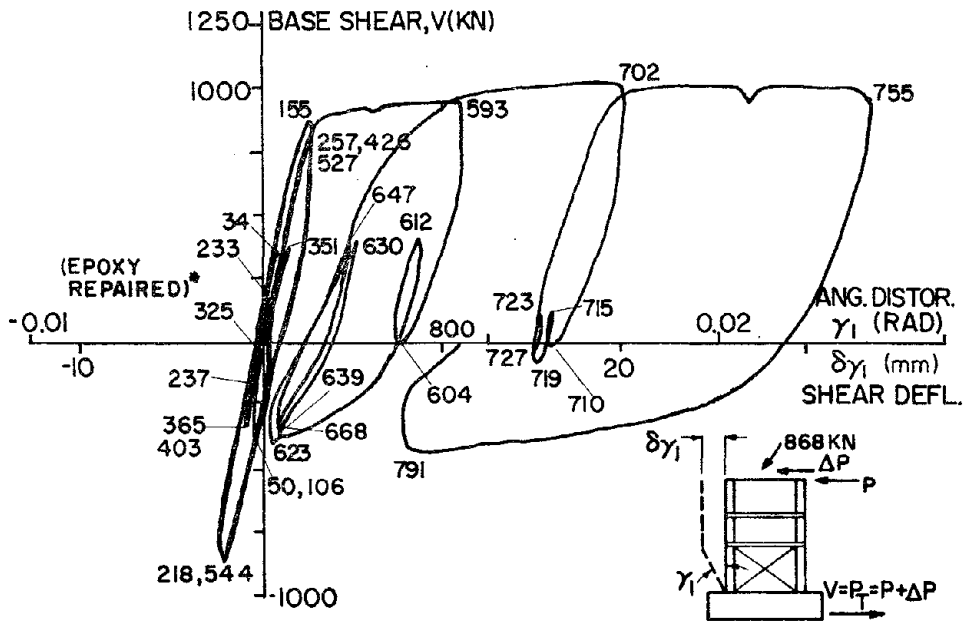


FIG. 4.27 TOTAL LATERAL LOAD,  $V$ , VS. FIRST-STORY SHEAR DISTORTION,  $\gamma_1$ --SPECIMEN SW8: VIRGIN + EPOXY-REPAIRED\*

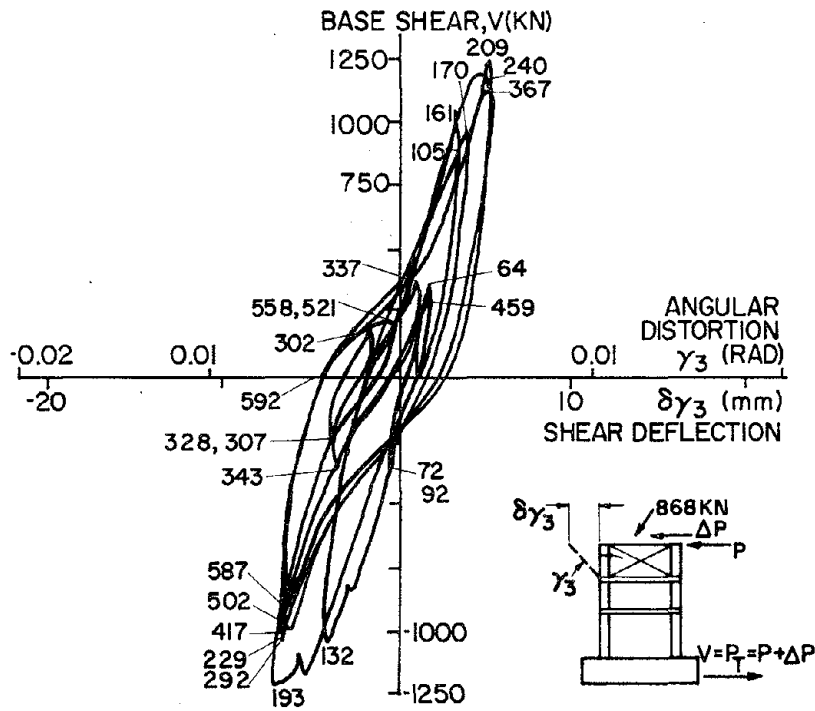


FIG. 4.28 TOTAL LATERAL LOAD, V, VS. THIRD-STORY SHEAR DISTORTION,  $\gamma_3$ --SPECIMEN SW8 R<sub>2</sub>

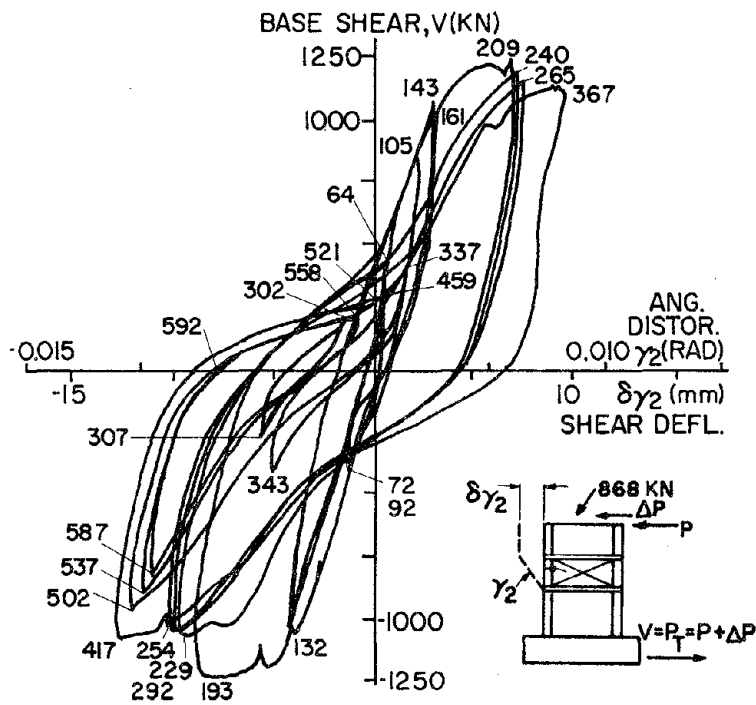


FIG. 4.29 TOTAL LATERAL LOAD, V, VS. SECOND-STORY SHEAR DISTORTION,  $\gamma_2$ --SPECIMEN SW8 R<sub>2</sub>

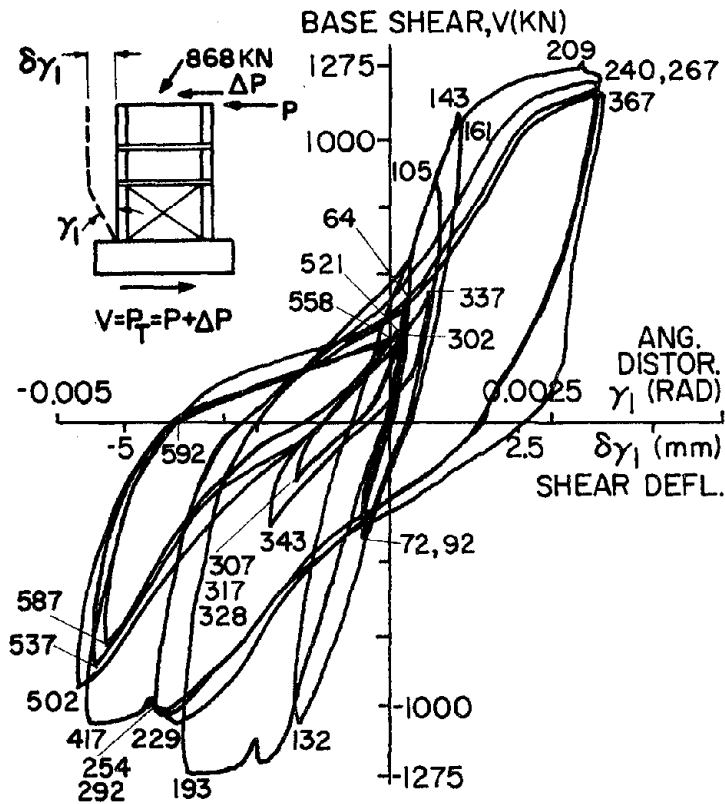


FIG. 4.30 TOTAL LATERAL LOAD, V, VS. FIRST-STORY SHEAR DISTORTION,  $\gamma_1$ --SPECIMEN SW8 R<sub>2</sub>

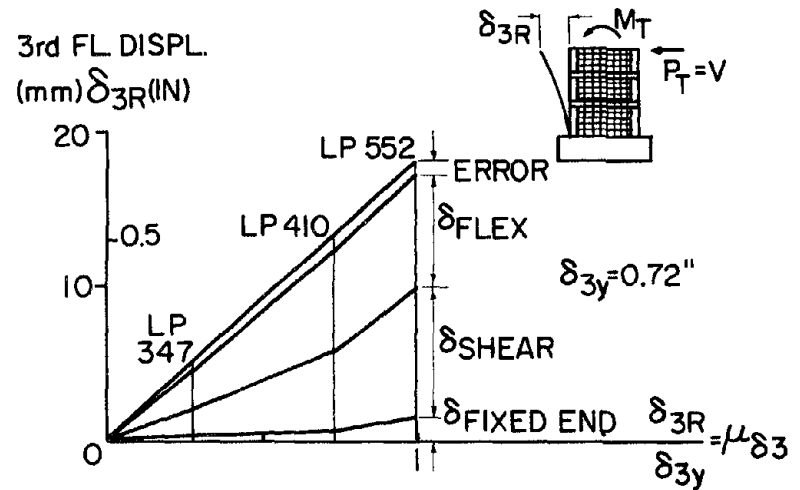


FIG. 4.31 VARIATION OF DISPLACEMENT COMPONENTS WITH DUCTILITY (THIRD STORY)--SPECIMEN SW7 VIRGIN

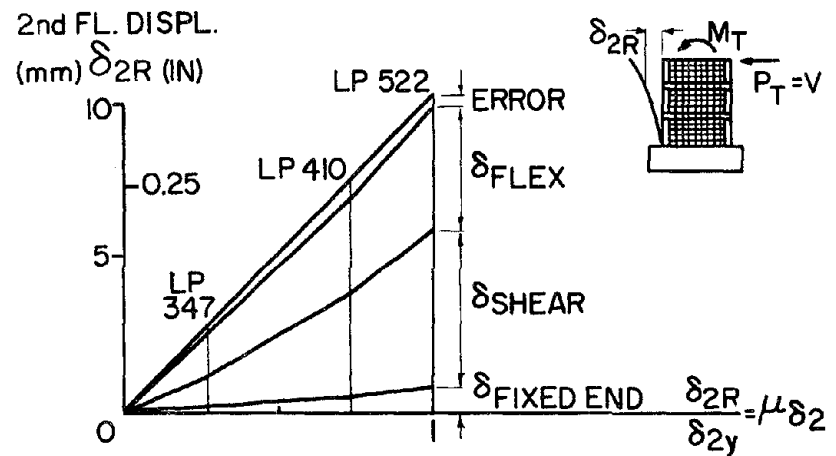


FIG. 4.32 VARIATION OF DISPLACEMENT COMPONENTS WITH DUCTILITY (SECOND STORY)--SPECIMEN SW7 VIRGIN

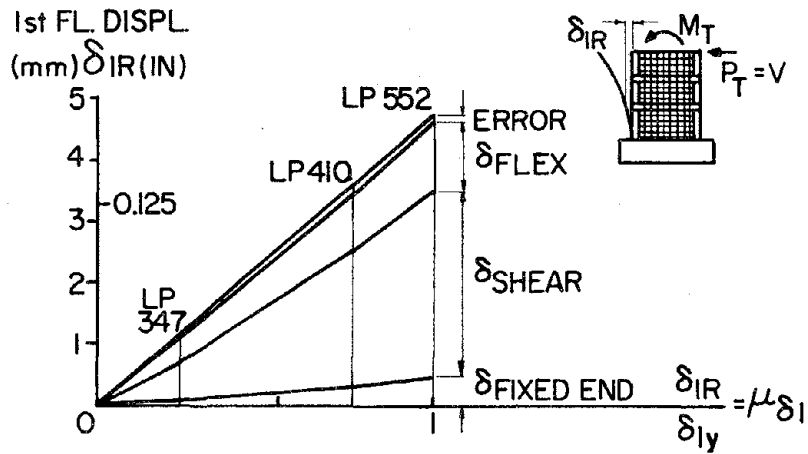


FIG. 4.33 VARIATION OF DISPLACEMENT COMPONENTS WITH DUCTILITY (FIRST STORY)--SW7 VIRGIN

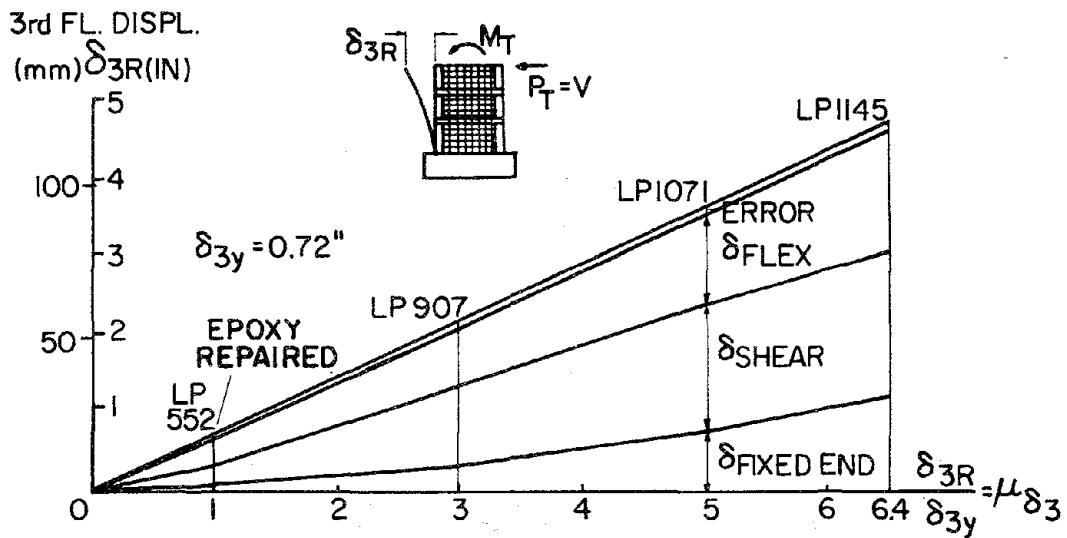


FIG. 4.34 VARIATION OF DISPLACEMENT COMPONENTS WITH DUCTILITY (THIRD STORY)--SW7 VIRGIN AND SW7 EPOXY-REPAIRED



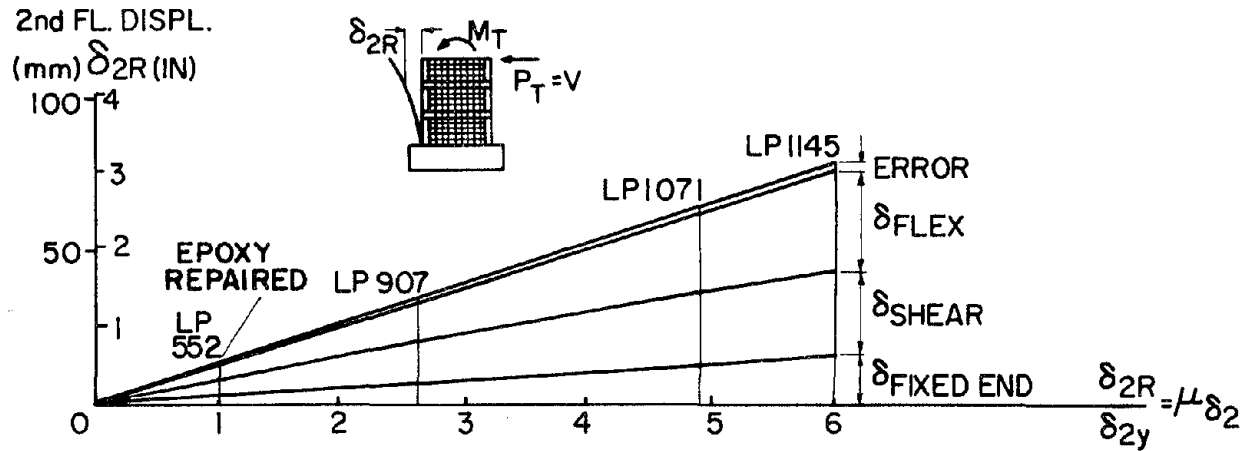


FIG. 4.35 VARIATION OF DISPLACEMENT COMPONENTS WITH DUCTILITY (SECOND STORY)-- SPECIMENS SW7 VIRGIN AND SW7 EPOXY-REPAIRED

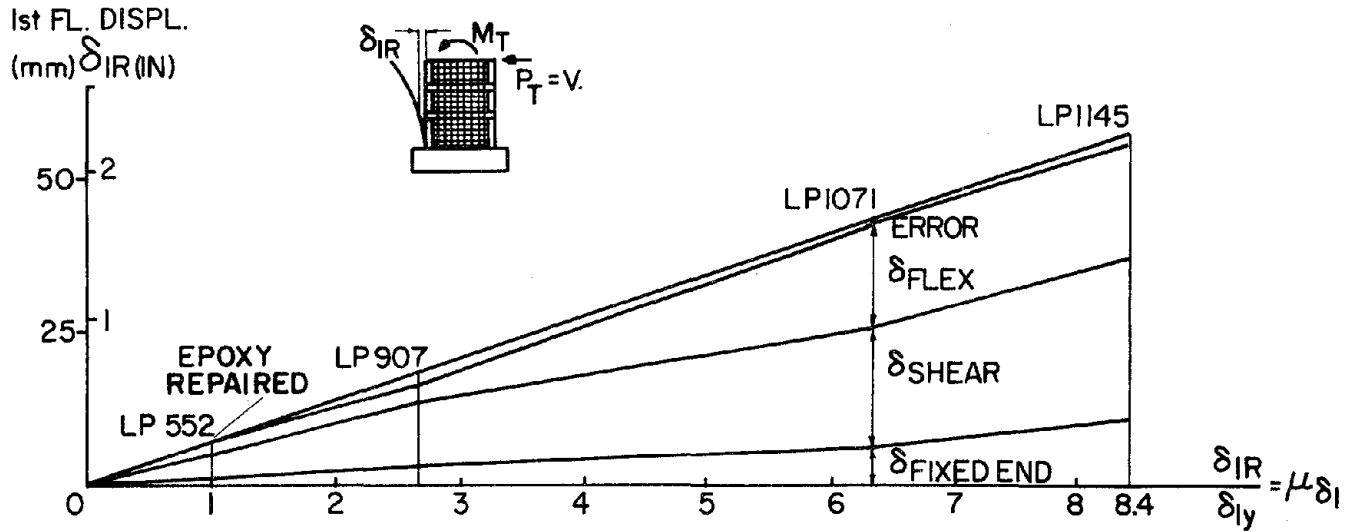


FIG. 4.36 VARIATION OF DISPLACEMENT COMPONENTS WITH DUCTILITY (FIRST STORY)-- SPECIMEN SW7 VIRGIN AND SW7 EPOXY-REPAIRED\*

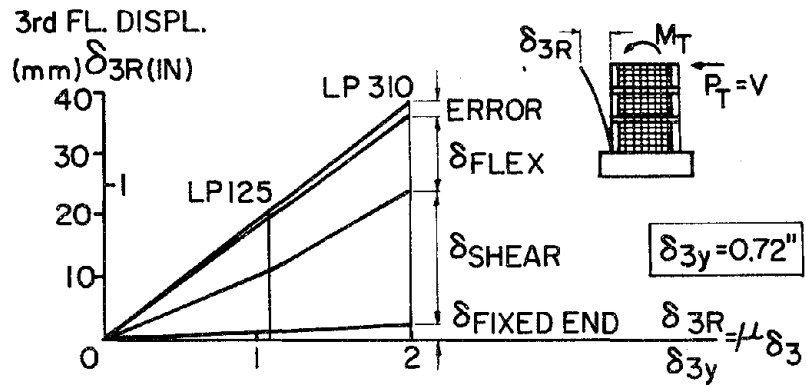


FIG. 4.37 VARIATION OF DISPLACEMENT COMPONENTS WITH DUCTILITY (THIRD STORY)--SPECIMEN SW7 R<sub>2</sub>

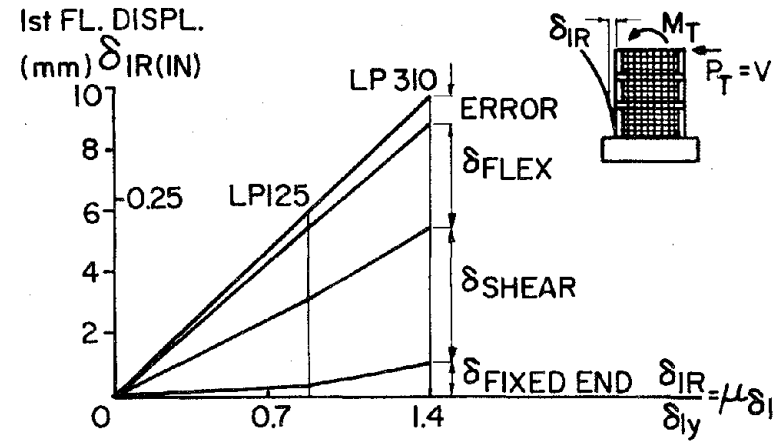


FIG. 4.39 VARIATION OF DISPLACEMENT COMPONENTS WITH DUCTILITY (FIRST STORY)--SPECIMEN SW7 R<sub>2</sub>

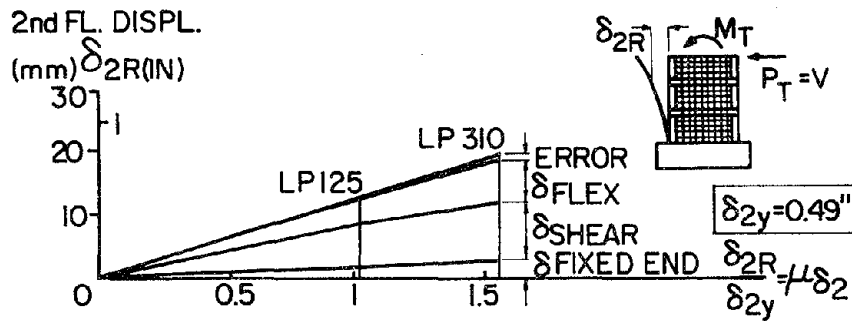


FIG. 4.38 VARIATION OF DISPLACEMENT COMPONENTS WITH DUCTILITY (SECOND STORY)--SPECIMEN SW7 R<sub>2</sub>

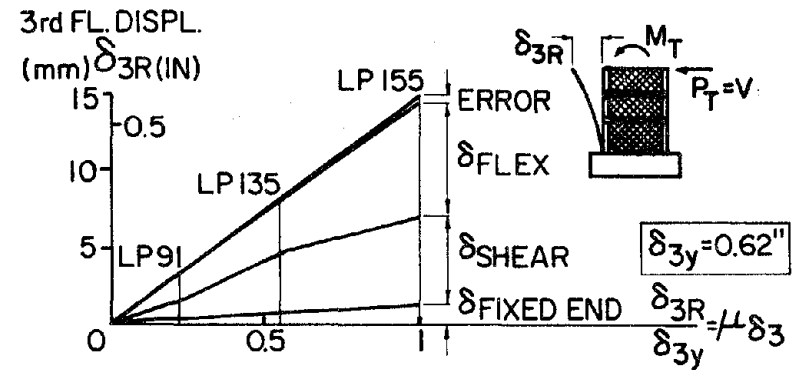


FIG. 4.40 VARIATION OF DISPLACEMENT COMPONENTS WITH DUCTILITY (THIRD STORY)--SPECIMEN SW8 VIRGIN

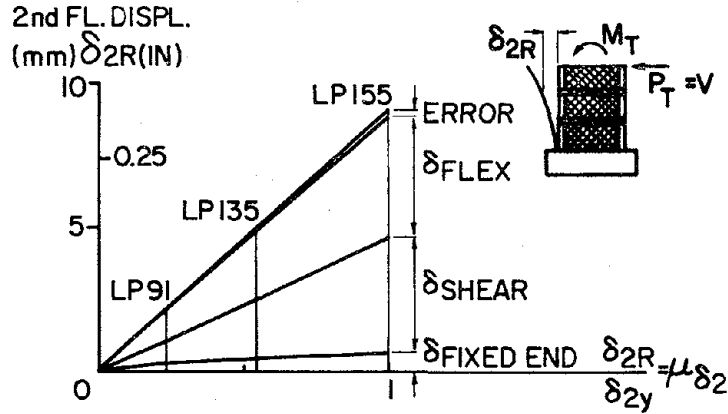


FIG. 4.41 VARIATION OF DISPLACEMENT COMPONENTS WITH DUCTILITY (SECOND STORY)--SPECIMEN SW8 VIRGIN

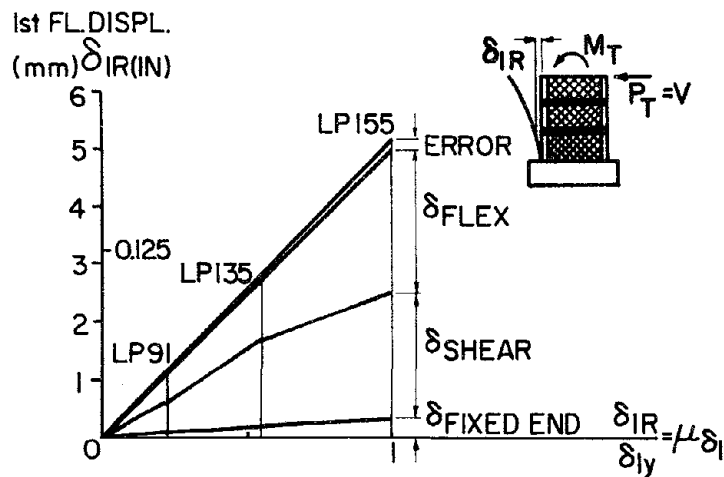


FIG. 4.42 VARIATION OF DISPLACEMENT COMPONENTS WITH DUCTILITY (FIRST STORY)--SPECIMEN SW8 VIRGIN

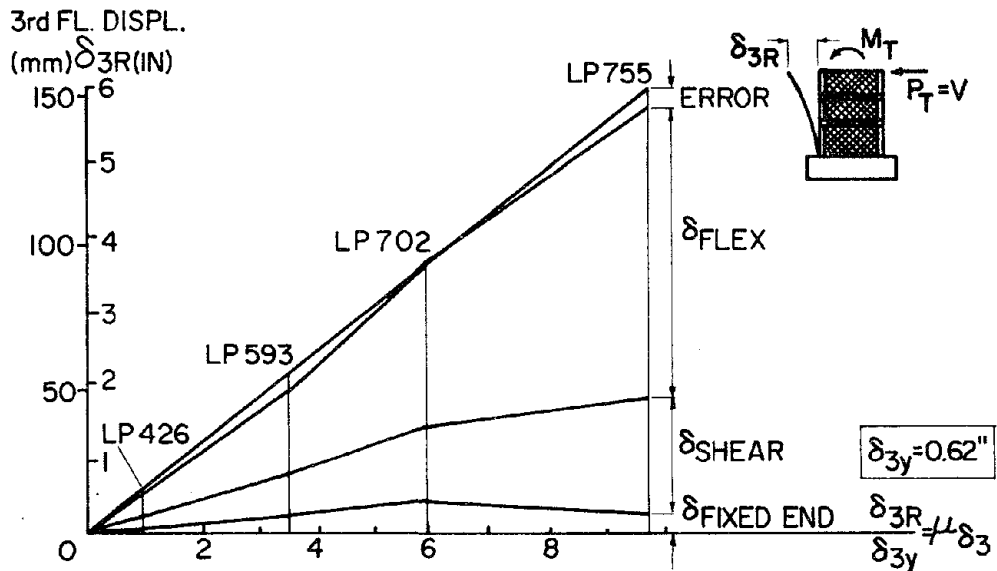


FIG. 4.43 VARIATION OF DISPLACEMENT COMPONENTS WITH DUCTILITY (THIRD STORY)--SPECIMEN SW8 VIRGIN + EPOXY-REPAIRED

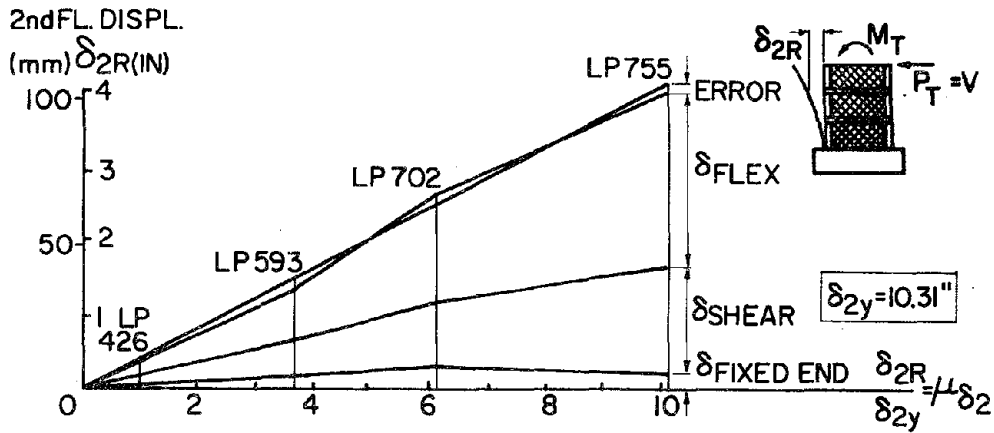


FIG. 4.44 VARIATION OF DISPLACEMENT COMPONENTS WITH DUCTILITY (SECOND STORY)--SPECIMEN SW8 VIRGIN + EPOXY-REPAIRED

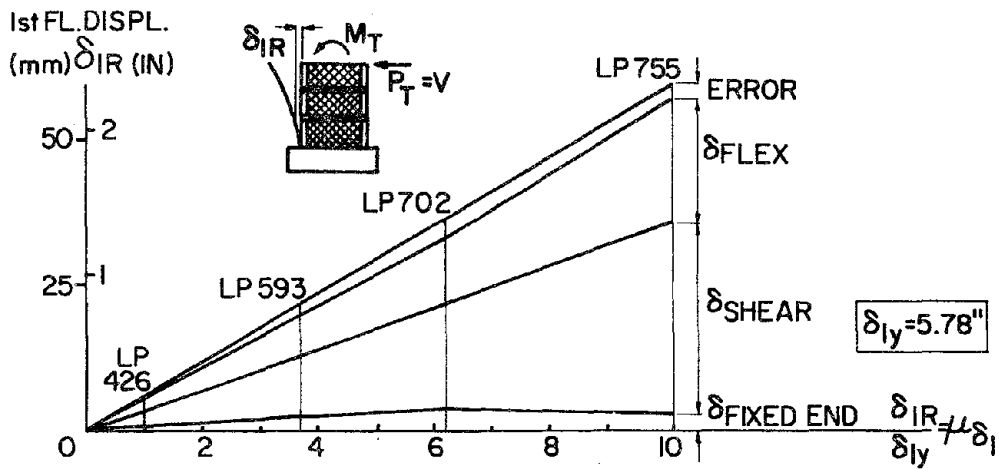


FIG. 4.45 VARIATION OF DISPLACEMENT COMPONENTS WITH DUCTILITY (FIRST STORY)--SPECIMEN SW8 VIRGIN + EPOXY-REPAIRED

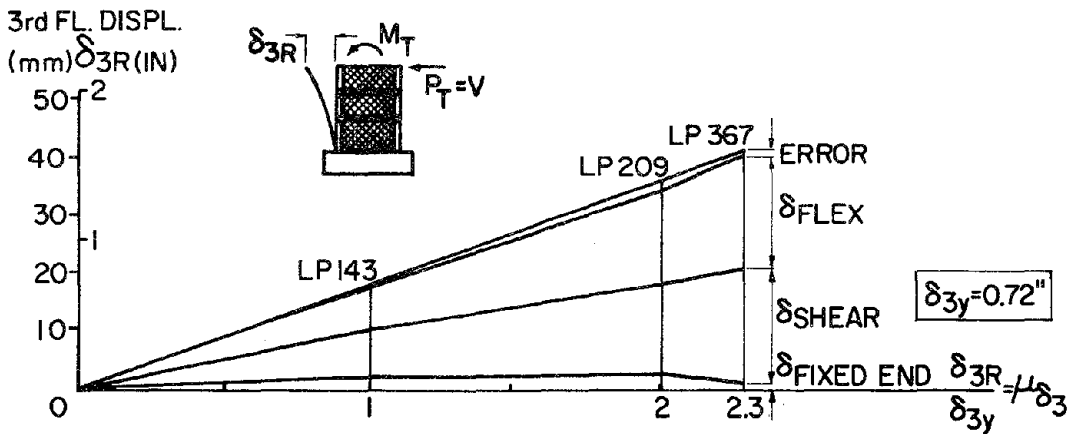


FIG. 4.46 VARIATION OF DISPLACEMENT COMPONENTS WITH DUCTILITY (THIRD STORY)--SPECIMEN SW8 R<sub>2</sub>

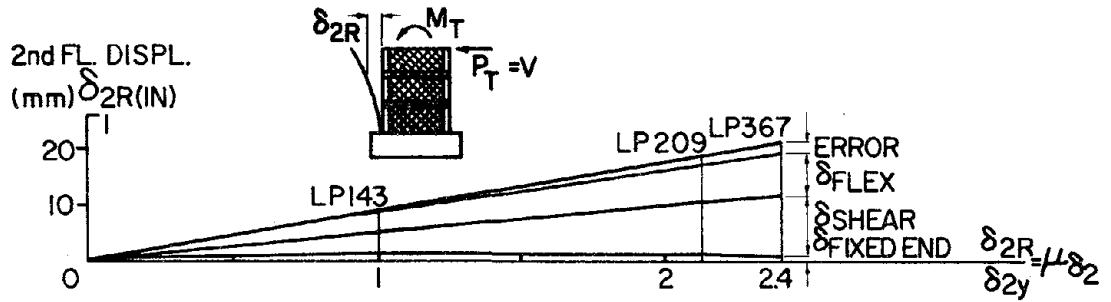


FIG. 4.47 VARIATION OF DISPLACEMENT COMPONENTS WITH DUCTILITY (SECOND STORY)--SPECIMEN SW8 R<sub>2</sub>

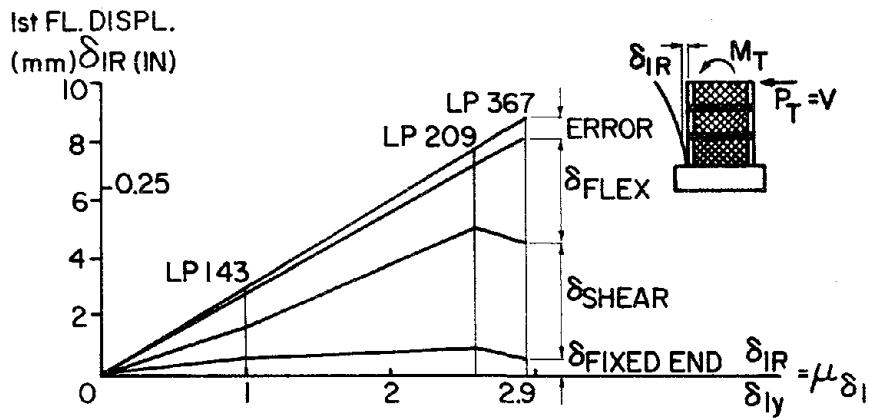


FIG. 4.48 VARIATION OF DISPLACEMENT COMPONENTS WITH DUCTILITY (FIRST STORY)--SPECIMEN SW8 R<sub>2</sub>

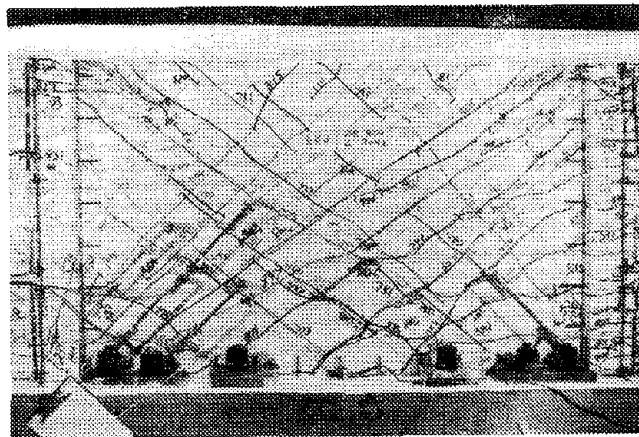


FIG. 4.49 EXCESSIVE CRACKING AT FIRST-STORY LEVEL OF SPECIMEN SW7 EPOXY-REPAIRED. LP 904,  $\mu_{\delta} = 3$

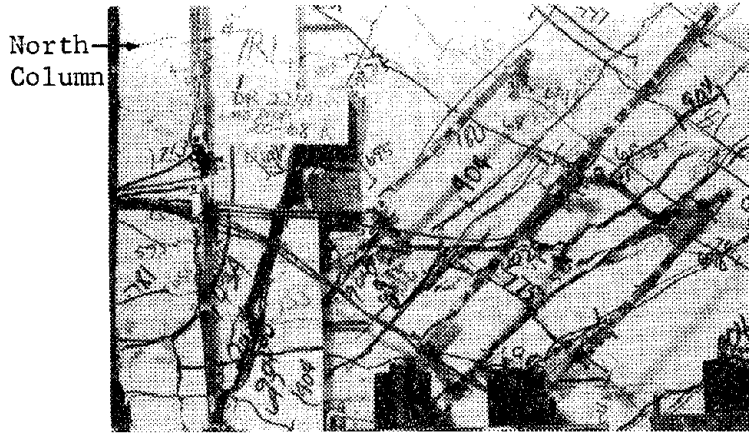


FIG. 4.50 CRUSHING OF CONCRETE IN THE NORTH CORNER OF FIRST-STORY WALL PANEL OF SPECIMEN SW7 EPOXY-REPAIRED. LP 1145,  $\mu_{\delta} = 6.4$

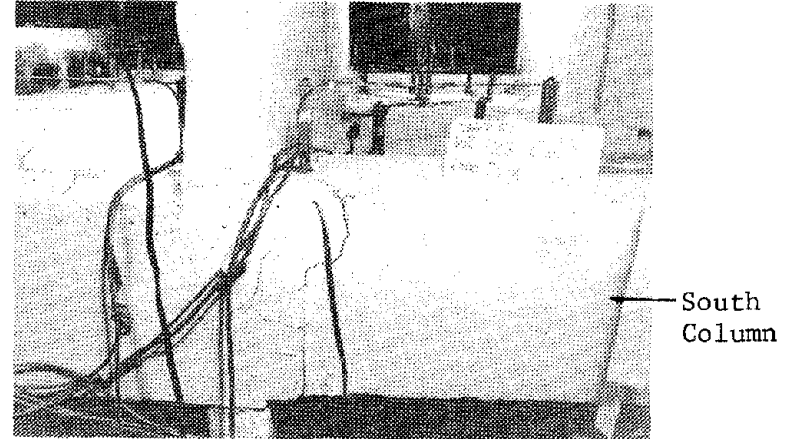


FIG. 4.51 CRACK AT BASE OF SECOND-STORY SOUTH COLUMN OF SPECIMEN SW7 R<sub>2</sub>. LP 125,  $\delta_{3R} = 1''$

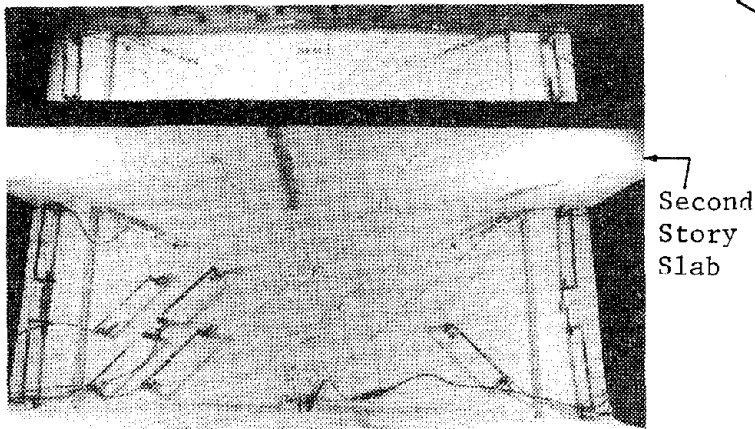


FIG. 4.52 DIAGONAL CRACKS IN SECOND-STORY WALL PANEL OF SPECIMEN SW7 R<sub>2</sub>. LP 125,  $\delta_{3R} = 1''$

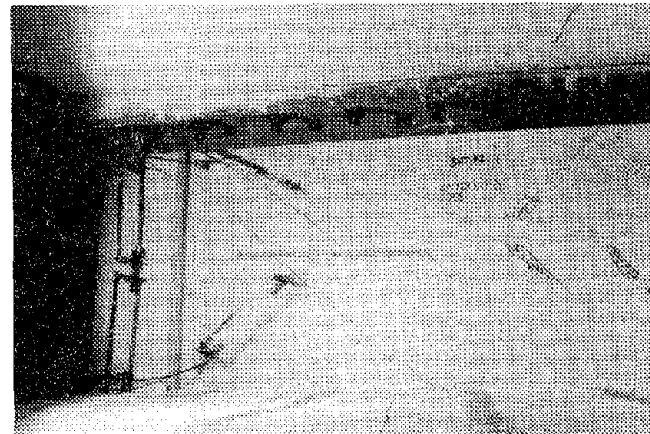


FIG. 4.53 DIAGONAL CRACKING AND LOCALIZED CONCRETE CRUSHING OF THIRD-STORY WALL PANEL OF SPECIMEN SW7 R<sub>2</sub>. LP 159,  $\delta_{3R} = 1''$

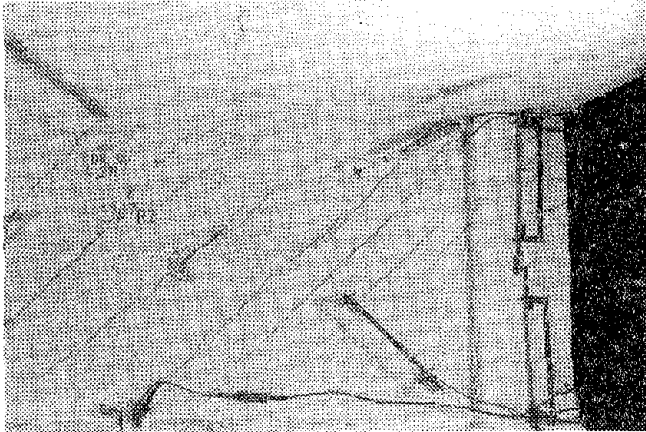


FIG. 4.54 DIAGONAL CRACKING AND LOCALIZED CONCRETE CRUSHING OF SECOND-STORY WALL PANEL OF SPECIMEN SW7 R<sub>2</sub>. LP 310,  $\delta_{3R} = 1\ 1/2"$ ,  $\mu_{\delta} = 2$ .

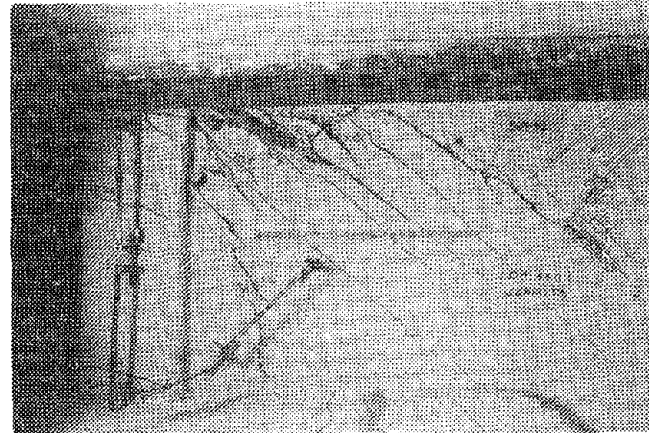


FIG. 4.55 CRACKS EXTENDING FROM UPPER NORTH CORNER OF THIRD-STORY WALL PANEL TO FACE OF SECOND-STORY SLAB OF SPECIMEN SW7 R<sub>2</sub>. LP 450.



FIG. 4.56 SPALLING OF CRUSHED CONCRETE IN UPPER NORTH CORNER OF THIRD-STORY WALL PANEL OF SPECIMEN SW7 R<sub>2</sub>. LP 450.

△N

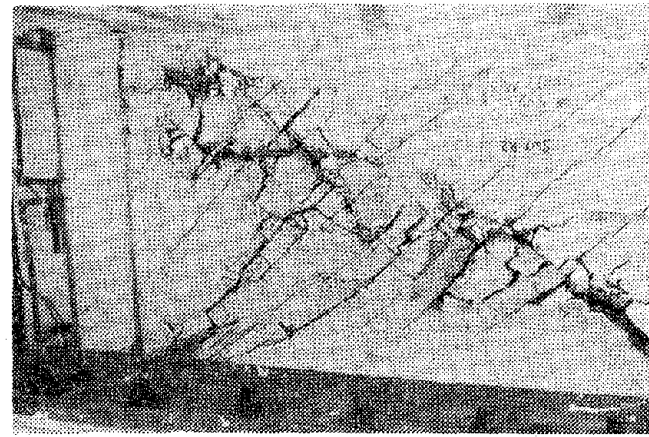


FIG. 4.57 FAILURE ZONE: THIRD-STORY WALL PANEL OF SPECIMEN SW7 R<sub>2</sub>. EXCESSIVE CRUSHING OF CONCRETE AND BUCKLING OF PANEL REINFORCEMENT. LP 547,  $\mu_{\delta} = 3$ .



FIG. 4.58 FAILURE ZONE: THIRD-STORY WALL PANEL OF SPECIMEN SW7 R<sub>2</sub>. EXPOSED AND BUCKLED PANEL REINFORCEMENT. END OF TEST.

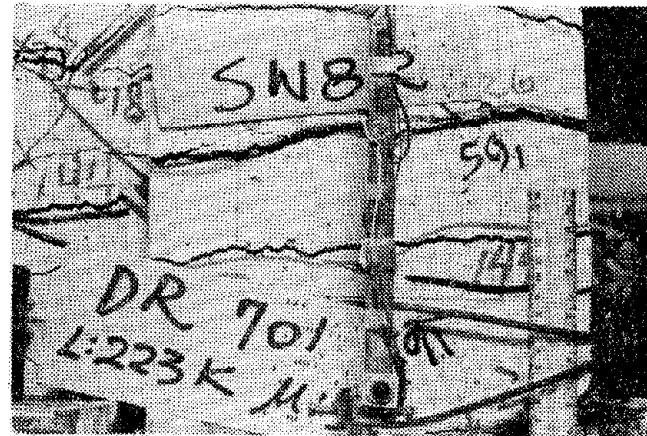


FIG. 4.59 WIDE CRACKS IN THE FIRST-STORY LEVEL OF THE SOUTH COLUMN OF SPECIMEN SW8 R<sub>1</sub>. LP 701,  $\delta_{3R} = 3.7''$ ,  $\mu_{\delta} = 5.9$ .

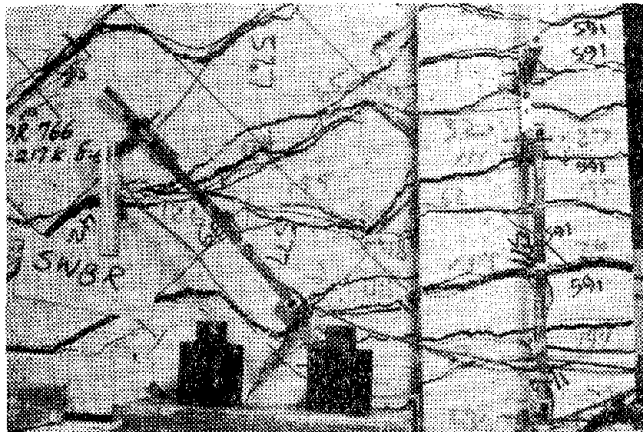


FIG. 4.60 FURTHER WIDENING OF CRACKS IN FIRST-STORY LEVEL OF SOUTH COLUMN OF SPECIMEN SW8 R<sub>1</sub>. PROPAGATION OF CRACKS INTO WALL PANEL. LP 766,  $\delta_{3R} = 6''$ ,  $\mu_{\delta} = 9.75$ .

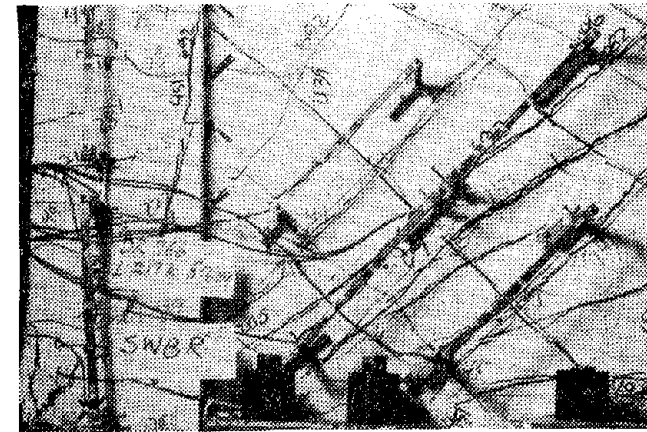


FIG. 4.61 CRUSHING OF CONCRETE AT BASE OF FIRST-STORY NORTH COLUMN OF SPECIMEN SW8 R<sub>1</sub>. LP 766,  $\delta = 6''$ ,  $\mu_{\delta} = 9.75$ .





FIG. 4.62 LOADING TO THE SOUTH AFTER FAILURE OF SPECIMEN SW8 R<sub>1</sub>. CRUSHING OF CONCRETE COVER AT BASE OF FIRST-STORY SOUTH COLUMN. BUCKLING OF WALL-PANEL REINFORCEMENT AND FRACTURE OF SPIRAL. LP 800. END OF EXPERIMENT.

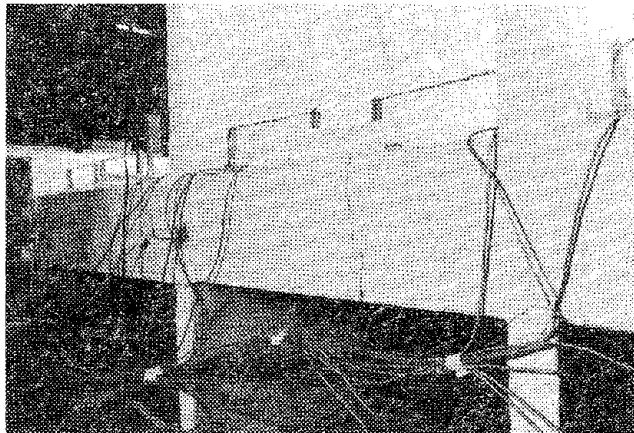


FIG. 4.63 APPEARANCE OF FIRST MAJOR CRACKS AT SECOND-STORY LEVEL OF SOUTH COLUMN OF SPECIMEN SW8 R<sub>2</sub>. LP 142,  $\mu_{\delta} = 1$ .

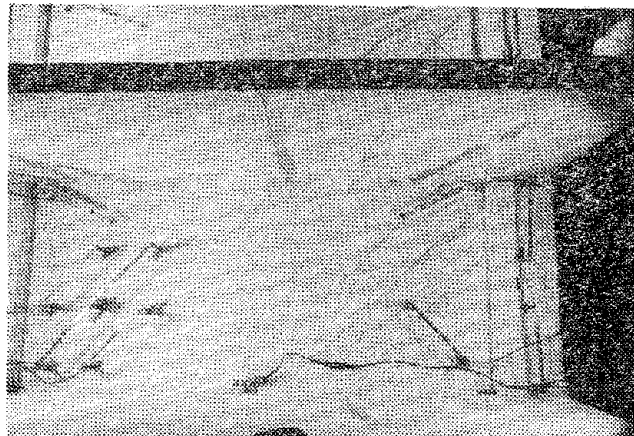
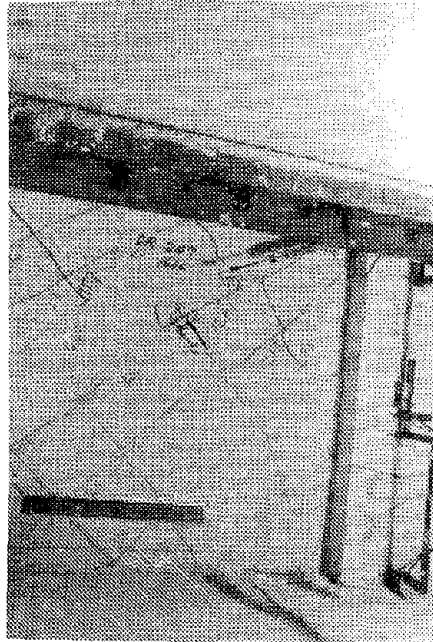
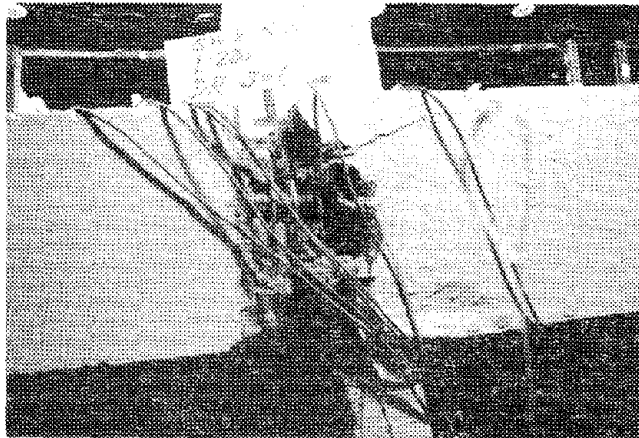


FIG. 4.64 DIAGONAL CRACKING IN SECOND-STORY WALL PANEL OF SPECIMEN SW8 R<sub>2</sub>. LP 142,  $\mu_{\delta} = 1$ .



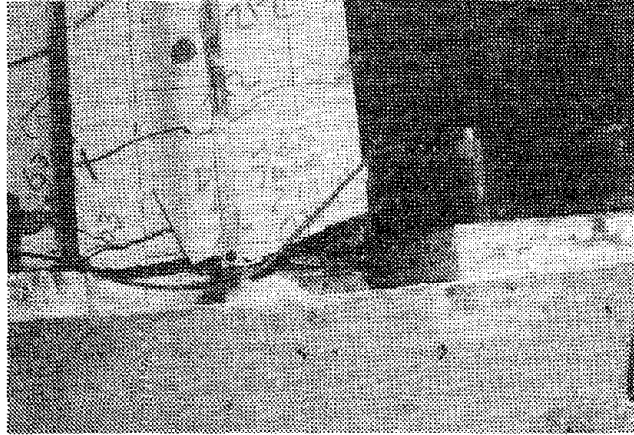
South

FIG. 4.65 LOCALIZED CRUSHING OF CONCRETE AND BUCKLING OF REINFORCEMENT IN THIRD-STORY WALL PANEL OF SPECIMEN SW8 R<sub>2</sub>. LP 247,  $\mu_{\delta} = 2$ .

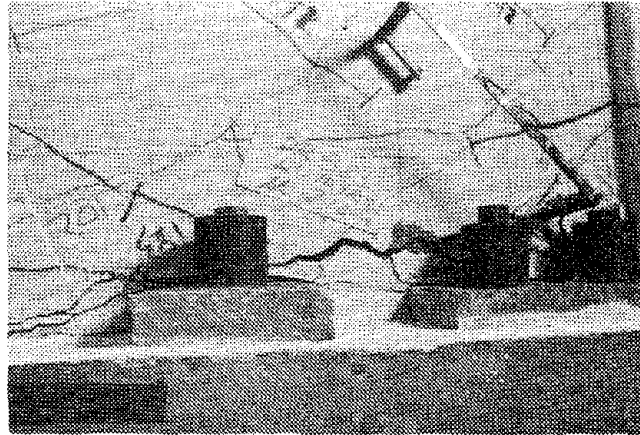


South  
Column

FIG. 4.66 FAILURE OF CONCRETE COVER AT TOP OF FIRST-STORY SOUTH COLUMN OF SPECIMEN SW8 R<sub>2</sub>. LP 361.



(a) Wide Crack Initiated at Base of South Column due to Tension Failure of Longitudinal Reinforcement



(b) Propagation of Crack into First-Story Wall Panel Adjacent to Foundation

FIG. 4.67 SPECIMEN SW8 R<sub>2</sub>. LP 383,  $\mu_{\delta} = 2.18$ .

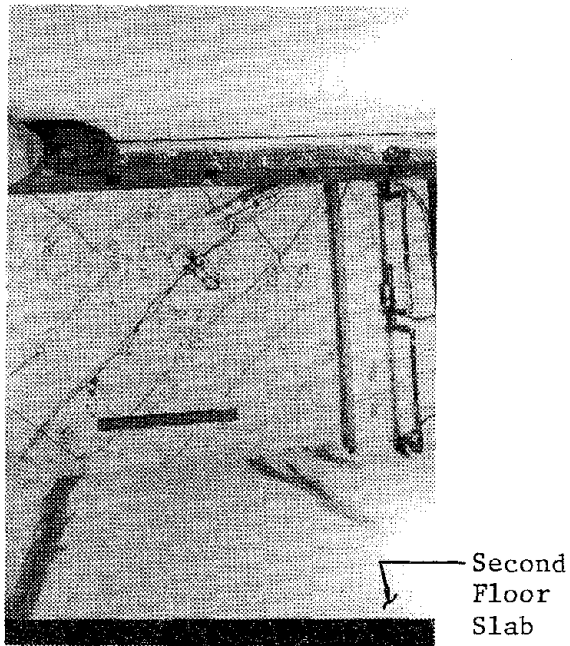


FIG. 4.68 INCREASED LOCALIZED CRUSHING OF CONCRETE IN THIRD-STORY WALL PANEL, ACCOMPANIED BY BUCKLING OF WALL-PANEL REINFORCEMENT OF SPECIMEN SW8 R<sub>2</sub>. LP 383,  $\mu_{\delta} = 2.18$ .

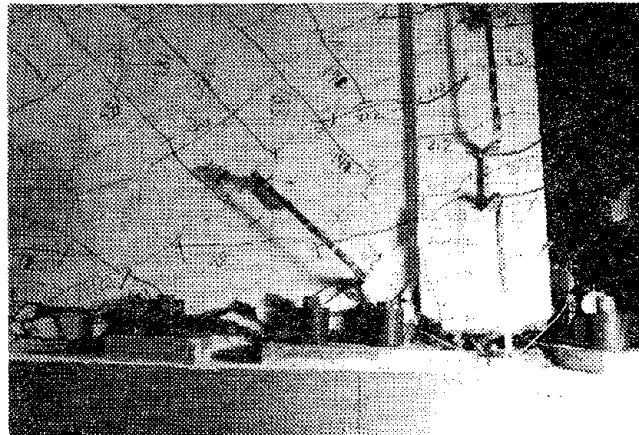


FIG. 4.69 SPECIMEN SW8 R<sub>2</sub> AFTER FAILURE, LP 558. FAILURE OF LONGITUDINAL REINFORCEMENT AT BASE OF FIRST-STORY SOUTH COLUMN AS WELL AS FAILURE OF FIRST-STORY WALL-PANEL REINFORCEMENT.

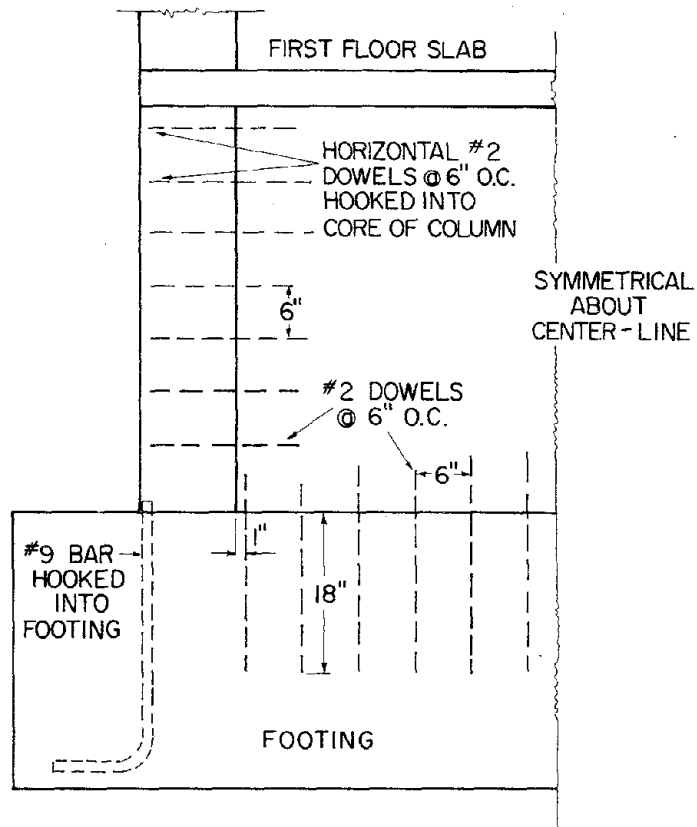


FIG. 5.1 DOWELS ORIGINALLY PLACED AT FIRST-STORY LEVEL TO FACILITATE STRENGTHENING OF SPECIMEN SW7

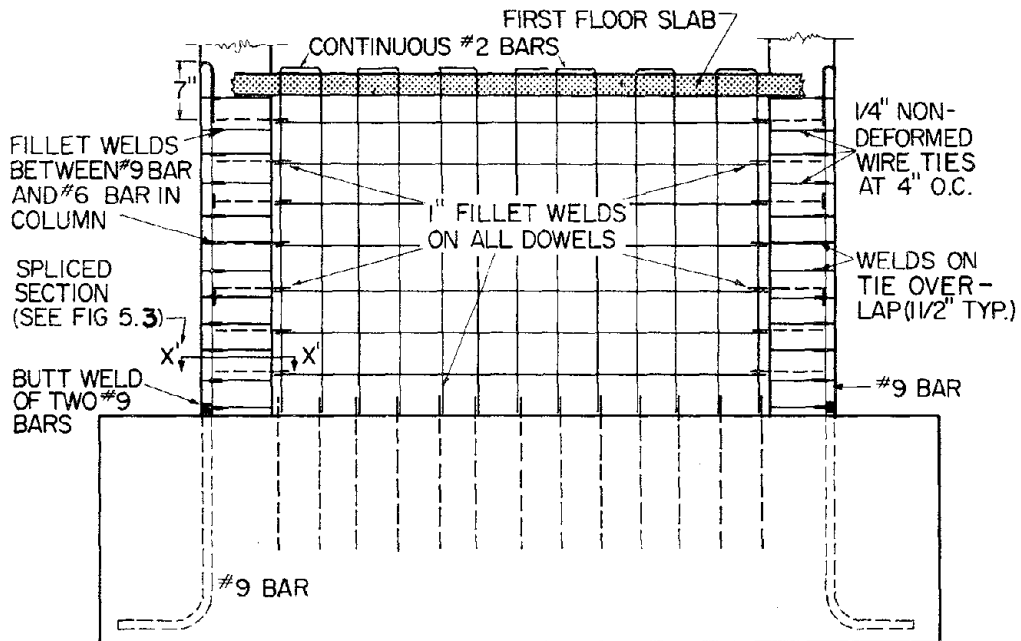
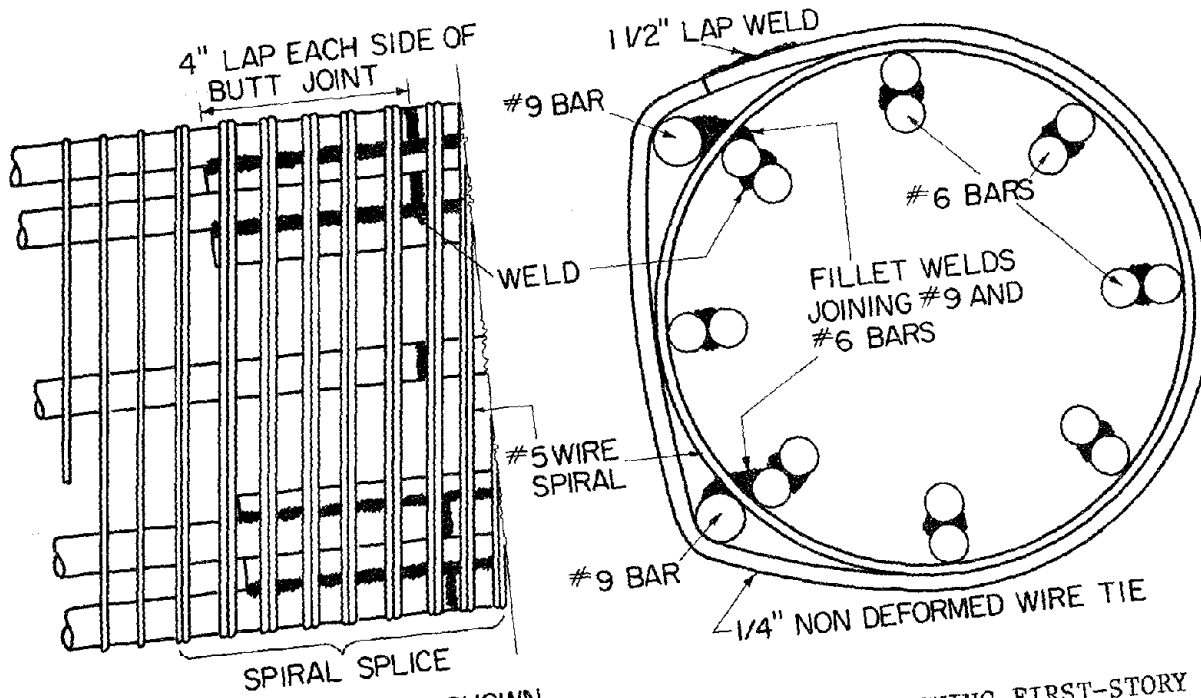


FIG. 5.2 FIRST-STORY REPAIRS ON SPECIMEN SW7 AFTER FAILURE OF SPECIMEN SW7 EPOXY-REPAIRED.



#9 BAR AND STIRRUP NOT SHOWN  
 FIG. 5.3 SECTION X'-X (FIG. 5.2)--SPlice DETAIL SHOWING FIRST-STORY COLUMN REPAIRS ON SPECIMEN SW7 AFTER FAILURE OF SPECIMEN SW7 EPOXY-REPAIRED

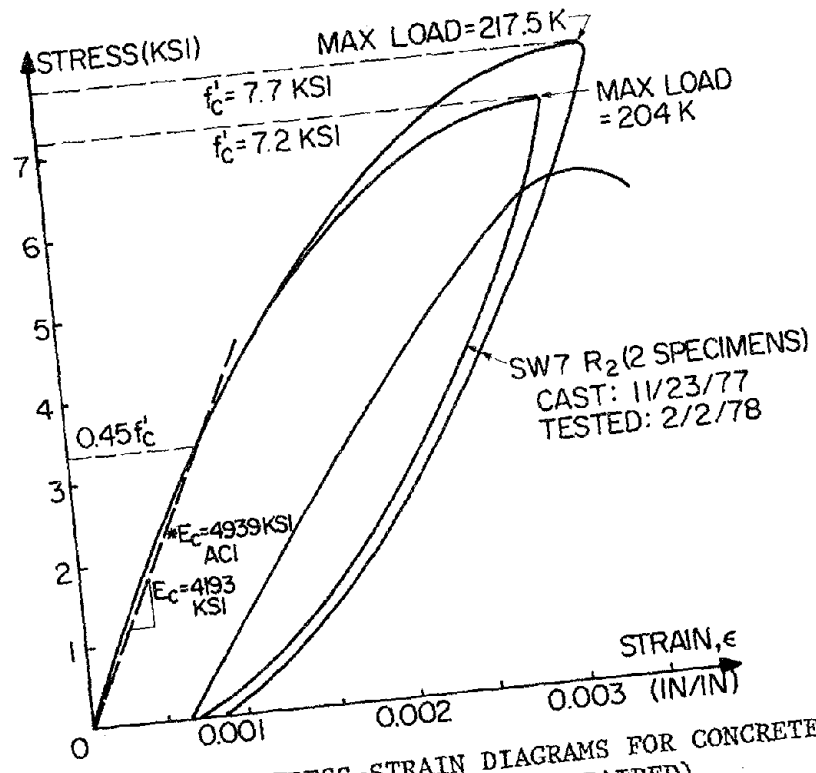


FIG. 5.4 STRESS-STRAIN DIAGRAMS FOR CONCRETE SPECIMENS--SPECIMEN SW7 R<sub>2</sub> (REPAIRED)

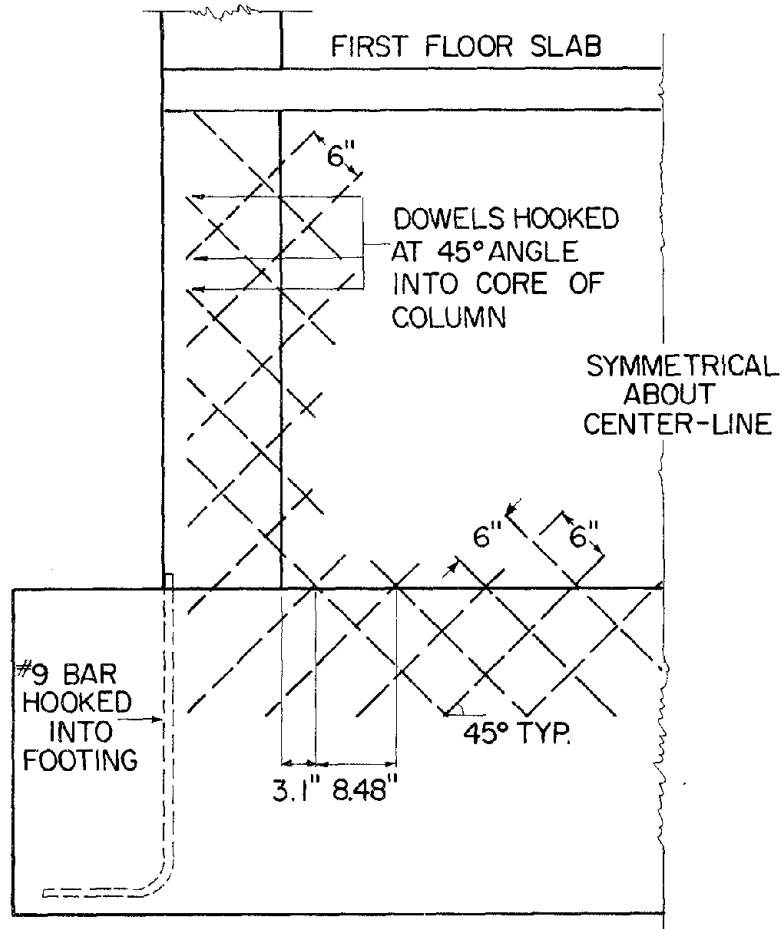


FIG. 5.5 VIEW SHOWING PLACEMENT OF REPAIR STEEL AT FIRST-STORY LEVEL--SPECIMEN SW8 VIRGIN

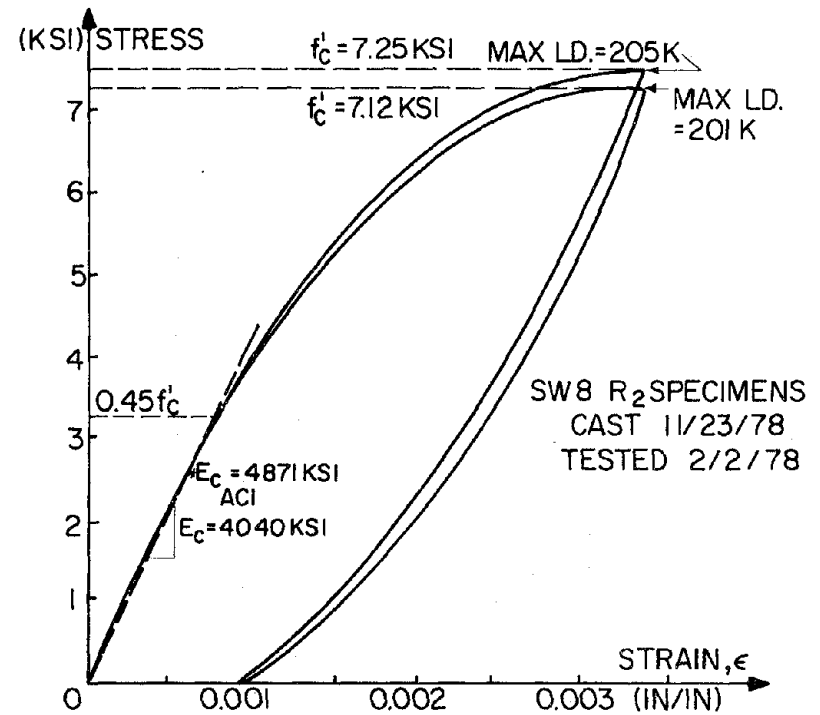


FIG. 5.6 STRESS-STRAIN DIAGRAMS FOR CONCRETE SPECIMENS--SPECIMEN SW8 R<sub>2</sub> (REPAIRED)

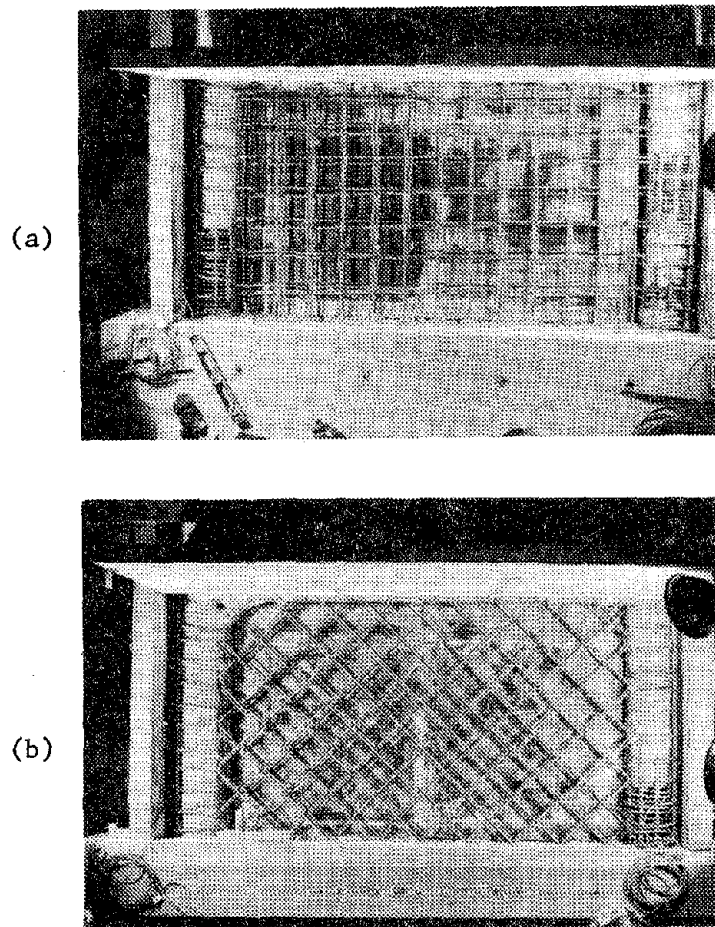


FIG. 5.7 REPAIRING AND STRENGTHENING TECHNIQUES FOR FIRST STORIES OF SPECIMENS SW7  $R_1$  AND SW8  $R_1$ .\*

\*NOTE: REMOVAL OF CONCRETE IN FIRST-STORY WALL PANELS AS WELL AS CRUSHED CONCRETE IN COLUMN CORES; PLACING OF NEW OUTER MATS OF WALL-PANEL STEEL; STRENGTHENING OF COLUMNS BY ADDITIONAL LONGITUDINAL REINFORCEMENT ON OUTER EDGES AS WELL AS ADDITIONAL LATERAL REINFORCEMENT; ALL BUCKLED OR BROKEN PARTS OF REINFORCEMENT WERE STRAIGHTENED OR REMOVED BEFORE REINFORCEMENT WAS ADDED.

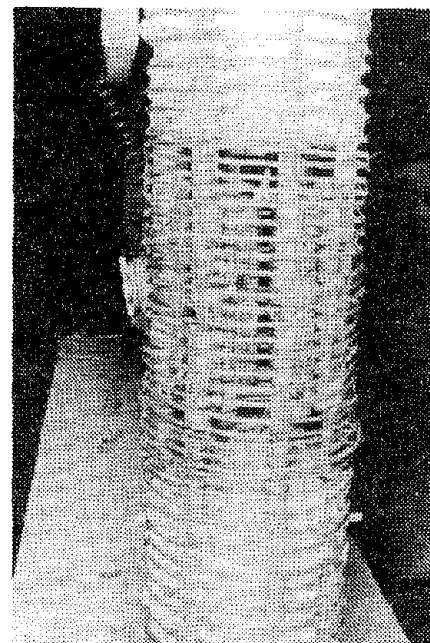


FIG. 5.8 REPAIRING AND STRENGTHENING TECHNIQUES FOR SPECIMENS SW7 AND SW8. (WELDED SPLICE OF LONGITUDINAL REINFORCEMENT IN FIRST-STORY COLUMNS)



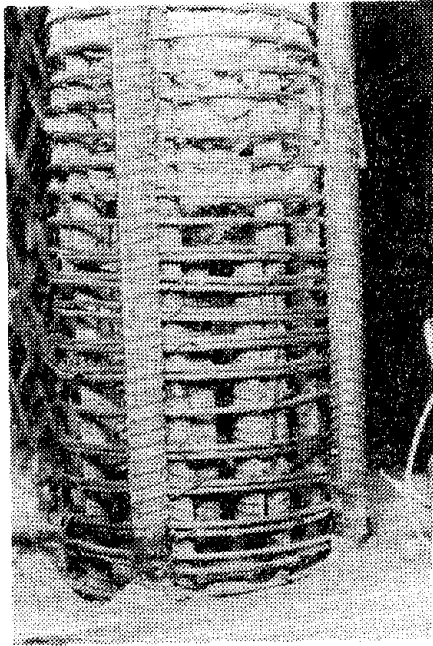
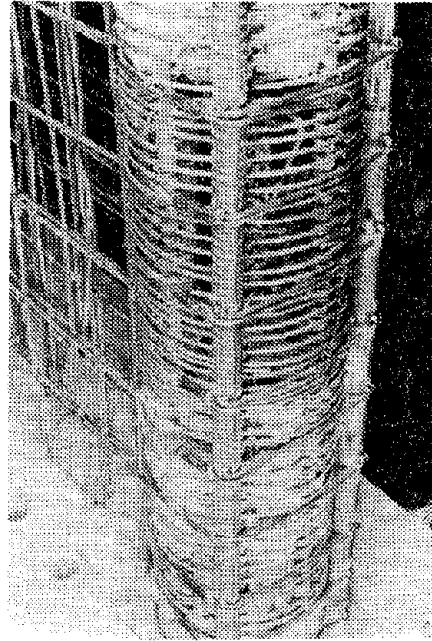
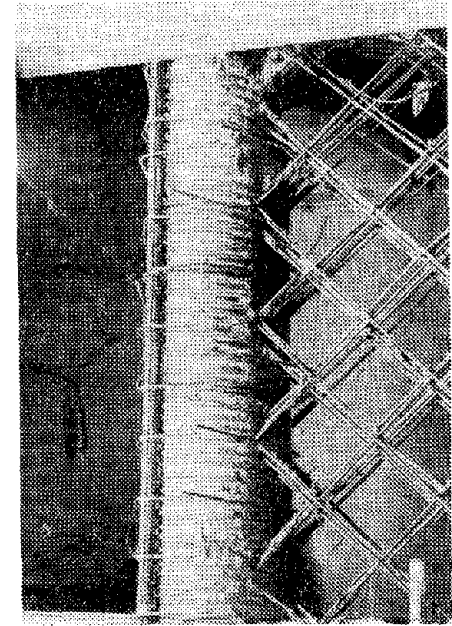


FIG. 5.9 REPAIRING AND STRENGTHENING TECHNIQUES FOR SPECIMENS SW7 AND SW8. (TWO NO. 9 BARS BUTT WELDED ON OUTER EDGES AT BASE OF FIRST-STORY COLUMNS; BARS EXTEND TO FIRST-FLOOR SLAB)



(a)



(b)

FIG. 5.10 REPAIRING AND STRENGTHENING TECHNIQUES FOR SPECIMENS SW7 AND SW8. NOTE: ADDED OUTER MATS OF WALL-PANEL REINFORCEMENT; WELDED STIRRUPS AT 6" O.C. AROUND NO. 9 BARS AND ORIGINAL COLUMNS.

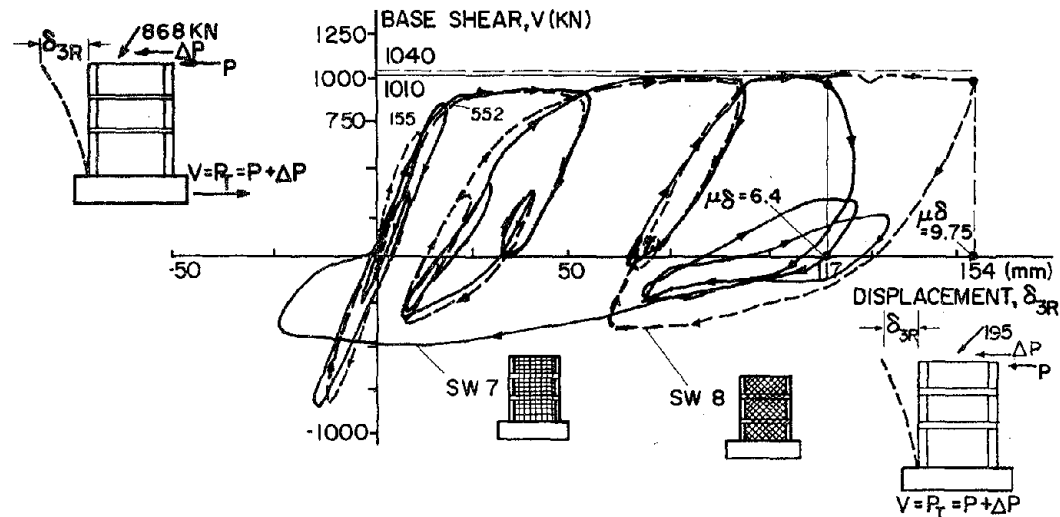


FIG. 6.1 EFFECT OF ARRANGEMENT OF WALL REINFORCEMENT ON THE LOAD-DISPLACEMENT RELATIONSHIP--MONOTONIC LOADING. SPECIMENS SW7 AND SW8 EPOXY-REPAIRED.

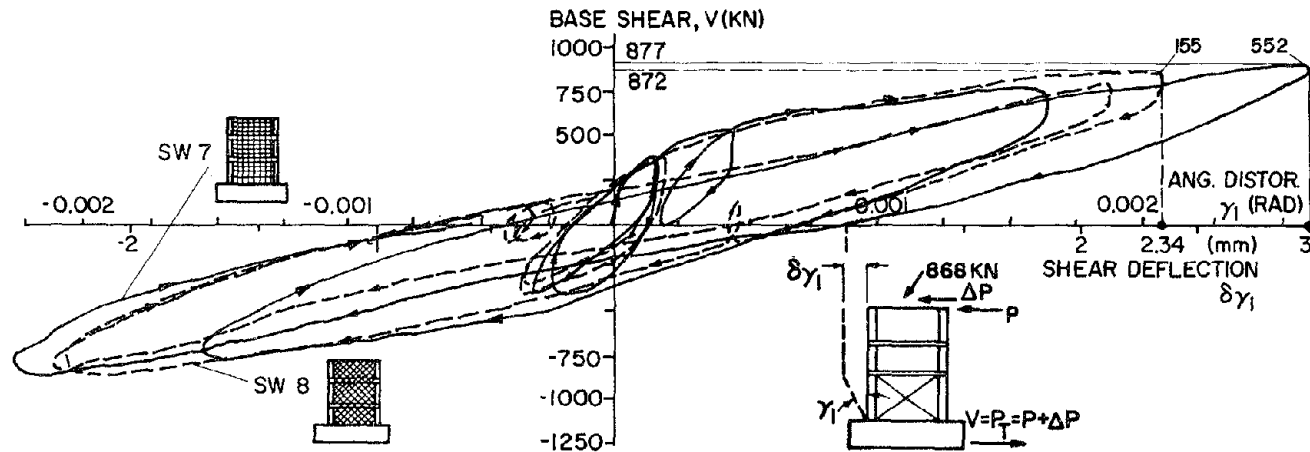


FIG. 6.2 EFFECT OF ARRANGEMENT OF REINFORCEMENT ON AMOUNT OF FIRST-STORY SHEAR DISTORTION. SPECIMENS SW7 AND SW8 VIRGIN. (SEE FIGS. 4.12(a) AND 4.25)

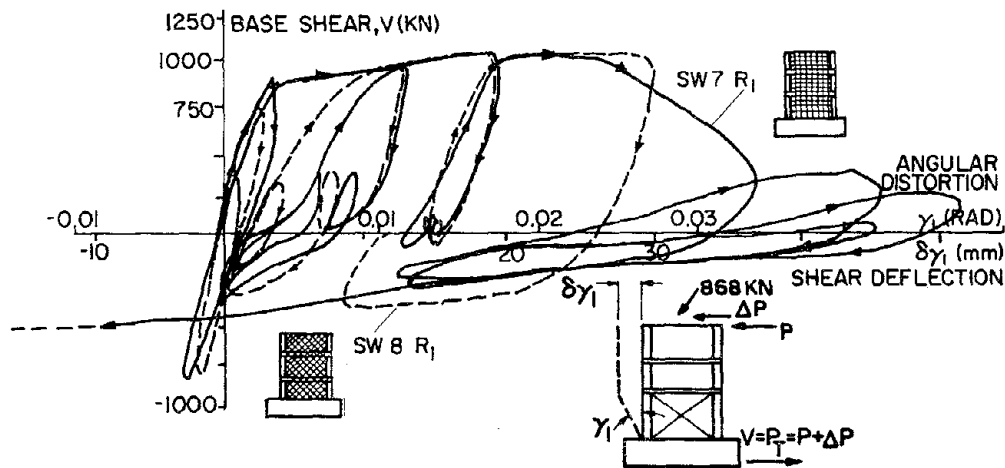


FIG. 6.3 EFFECT OF ARRANGEMENT OF REINFORCEMENT ON AMOUNT OF FIRST-STORY SHEAR DISTORTION--MONOTONIC LOADING. SPECIMENS SW7 R<sub>1</sub> AND SW8 R<sub>1</sub>.

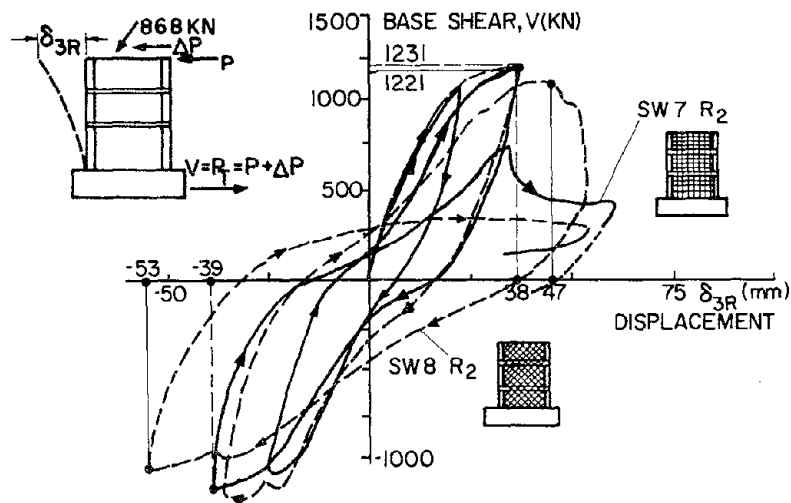


FIG. 6.4 EFFECT OF ARRANGEMENT OF REINFORCEMENT ON LOAD-DISPLACEMENT RELATIONSHIP--CYCLIC LOADING. SPECIMENS SW7 R<sub>2</sub> AND SW8 R<sub>2</sub>

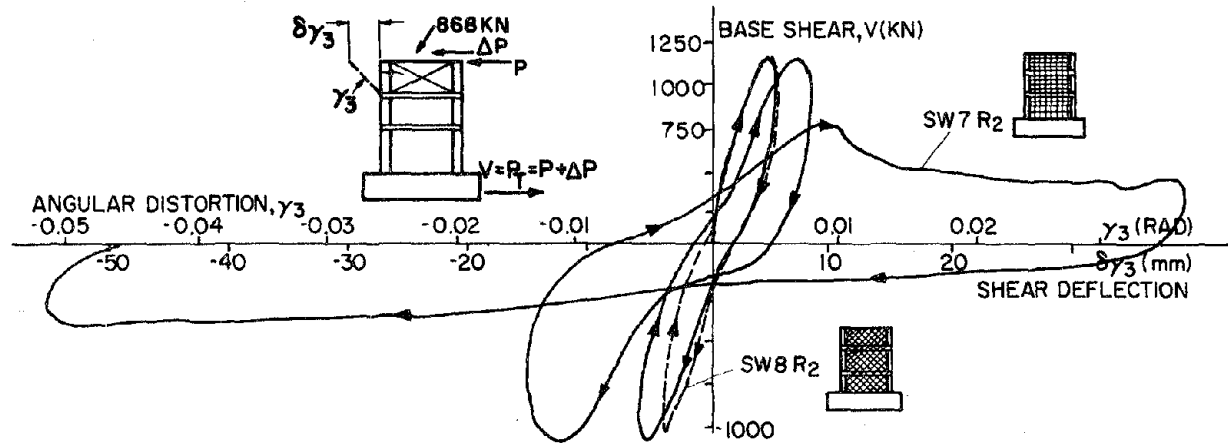


FIG. 6.5 EFFECT OF ARRANGEMENT OF REINFORCEMENT ON AMOUNT OF THIRD-STORY SHEAR DISTORTION--CYCLIC LOADING. SPECIMENS SW7 R<sub>2</sub> AND SW8 R<sub>2</sub>

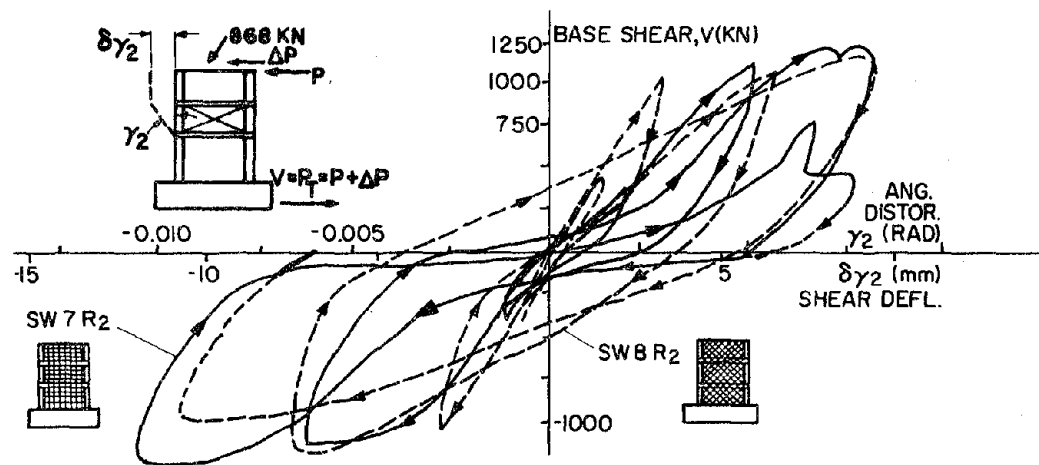


FIG. 6.6 EFFECT OF ARRANGEMENT OF REINFORCEMENT ON THE AMOUNT OF SECOND-STORY SHEAR DISTORTION--CYCLIC LOADING. SPECIMENS SW7 R<sub>2</sub> AND SW8 R<sub>2</sub>





EARTHQUAKE ENGINEERING RESEARCH CENTER REPORTS

NOTE: Numbers in parenthesis are Accession Numbers assigned by the National Technical Information Service; these are followed by a price code. Copies of the reports may be ordered from the National Technical Information Service, 5285 Port Royal Road, Springfield, Virginia, 22161. Accession Numbers should be quoted on orders for reports (PB --- ---) and remittance must accompany each order. Reports without this information were not available at time of printing. Upon request, EERC will mail inquirers this information when it becomes available.

- EERC 67-1 "Feasibility Study Large-Scale Earthquake Simulator Facility," by J. Penzien, J.G. Bouwkamp, R.W. Clough and D. Rea - 1967 (PB 187 905)A07
- EERC 68-1 Unassigned
- EERC 68-2 "Inelastic Behavior of Beam-to-Column Subassemblages Under Repeated Loading," by V.V. Bertero - 1968 (PB 184 888)A05
- EERC 68-3 "A Graphical Method for Solving the Wave Reflection-Refraction Problem," by H.D. McNiven and Y. Mengi - 1968 (PB 187 943)A03
- EERC 68-4 "Dynamic Properties of McKinley School Buildings," by D. Rea, J.G. Bouwkamp and R.W. Clough - 1968 (PB 187 902)A07
- EERC 68-5 "Characteristics of Rock Motions During Earthquakes," by H.B. Seed, I.M. Idriss and F.W. Kiefer - 1968 (PB 188 338)A03
- EERC 69-1 "Earthquake Engineering Research at Berkeley," - 1969 (PB 187 906)All
- EERC 69-2 "Nonlinear Seismic Response of Earth Structures," by M. Dibaj and J. Penzien - 1969 (PB 187 904)A08
- EERC 69-3 "Probabilistic Study of the Behavior of Structures During Earthquakes," by R. Ruiz and J. Penzien - 1969 (PB 187 886)A06
- EERC 69-4 "Numerical Solution of Boundary Value Problems in Structural Mechanics by Reduction to an Initial Value Formulation," by N. Distefano and J. Schujman - 1969 (PB 187 942)A02
- EERC 69-5 "Dynamic Programming and the Solution of the Biharmonic Equation," by N. Distefano - 1969 (PB 187 941)A03
- EERC 69-6 "Stochastic Analysis of Offshore Tower Structures," by A.K. Malhotra and J. Penzien - 1969 (PB 187 903)A09
- EERC 69-7 "Rock Motion Accelerograms for High Magnitude Earthquakes," by H.B. Seed and I.M. Idriss - 1969 (PB 187 940)A02
- EERC 69-8 "Structural Dynamics Testing Facilities at the University of California, Berkeley," by R.M. Stephen, J.G. Bouwkamp, R.W. Clough and J. Penzien - 1969 (PB 189 111)A04
- EERC 69-9 "Seismic Response of Soil Deposits Underlain by Sloping Rock Boundaries," by H. Dezfulian and H.B. Seed 1969 (PB 189 114)A03
- EERC 69-10 "Dynamic Stress Analysis of Axisymmetric Structures Under Arbitrary Loading," by S. Ghosh and E.L. Wilson 1969 (PB 189 026)A10
- EERC 69-11 "Seismic Behavior of Multistory Frames Designed by Different Philosophies," by J.C. Anderson and V. V. Bertero - 1969 (PB 190 662)A10
- EERC 69-12 "Stiffness Degradation of Reinforcing Concrete Members Subjected to Cyclic Flexural Moments," by V.V. Bertero, B. Bresler and H. Ming Liao - 1969 (PB 202 942)A07
- EERC 69-13 "Response of Non-Uniform Soil Deposits to Travelling Seismic Waves," by H. Dezfulian and H.B. Seed - 1969 (PB 191 023)A03
- EERC 69-14 "Damping Capacity of a Model Steel Structure," by D. Rea, R.W. Clough and J.G. Bouwkamp - 1969 (PB 190 663)A06
- EERC 69-15 "Influence of Local Soil Conditions on Building Damage Potential during Earthquakes," by H.B. Seed and I.M. Idriss - 1969 (PB 191 036)A03
- EERC 69-16 "The Behavior of Sands Under Seismic Loading Conditions," by M.L. Silver and H.B. Seed - 1969 (AD 714 982)A07
- EERC 70-1 "Earthquake Response of Gravity Dams," by A.K. Chopra - 1970 (AD 709 640)A03
- EERC 70-2 "Relationships between Soil Conditions and Building Damage in the Caracas Earthquake of July 29, 1967," by H.B. Seed, I.M. Idriss and H. Dezfulian - 1970 (PB 195 762)A05
- EERC 70-3 "Cyclic Loading of Full Size Steel Connections," by F.P. Popov and R.M. Stephen - 1970 (PB 213 545)A04
- EERC 70-4 "Seismic Analysis of the Charaima Building, Caraballeda, Venezuela," by Subcommittee of the SEAONC Research Committee: V.V. Bertero, P.F. Fratessa, S.A. Mahin, J.H. Sexton, A.C. Scordelis, E.L. Wilson, L.A. Wyllie, H.B. Seed and J. Penzien, Chairman - 1970 (PB 201 455)A06

- EERC 70-5 "A Computer Program for Earthquake Analysis of Dams," by A.K. Chopra and P. Chakrabarti - 1970 (AD 723 994)A05
- EERC 70-6 "The Propagation of Love Waves Across Non-Horizontally Layered Structures," by J. Lysmer and L.A. Drake 1970 (PB 197 896)A03
- EERC 70-7 "Influence of Base Rock Characteristics on Ground Response," by J. Lysmer, H.B. Seed and P.B. Schnabel 1970 (PB 197 897)A03
- EERC 70-8 "Applicability of Laboratory Test Procedures for Measuring Soil Liquefaction Characteristics under Cyclic Loading," by H.B. Seed and W.H. Peacock - 1970 (PB 198 016)A03
- EERC 70-9 "A Simplified Procedure for Evaluating Soil Liquefaction Potential," by H.B. Seed and I.M. Idriss - 1970 (PB 198 009)A03
- EERC 70-10 "Soil Moduli and Damping Factors for Dynamic Response Analysis," by H.B. Seed and I.M. Idriss - 1970 (PB 197 869)A03
- EERC 71-1 "Koyna Earthquake of December 11, 1967 and the Performance of Koyna Dam," by A.K. Chopra and P. Chakrabarti 1971 (AD 731 496)A06
- EERC 71-2 "Preliminary In-Situ Measurements of Anelastic Absorption in Soils Using a Prototype Earthquake Simulator," by R.D. Borcherdt and P.W. Rodgers - 1971 (PB 201 454)A03
- EERC 71-3 "Static and Dynamic Analysis of Inelastic Frame Structures," by F.L. Porter and G.H. Powell - 1971 (PB 210 135)A06
- EERC 71-4 "Research Needs in Limit Design of Reinforced Concrete Structures," by V.V. Bertero - 1971 (PB 202 943)A04
- EERC 71-5 "Dynamic Behavior of a High-Rise Diagonally Braced Steel Building," by D. Rea, A.A. Shah and J.G. Bouwkamp 1971 (PB 203 584)A06
- EERC 71-6 "Dynamic Stress Analysis of Porous Elastic Solids Saturated with Compressible Fluids," by J. Ghaboussi and E. L. Wilson - 1971 (PB 211 396)A06
- EERC 71-7 "Inelastic Behavior of Steel Beam-to-Column Subassemblages," by H. Krawinkler, V.V. Bertero and E.P. Popov 1971 (PB 211 335)A14
- EERC 71-8 "Modification of Seismograph Records for Effects of Local Soil Conditions," by P. Schnabel, H.B. Seed and J. Lysmer - 1971 (PB 214 450)A03
- EERC 72-1 "Static and Earthquake Analysis of Three Dimensional Frame and Shear Wall Buildings," by E.L. Wilson and H.H. Dovey - 1972 (PB 212 904)A05
- EERC 72-2 "Accelerations in Rock for Earthquakes in the Western United States," by P.B. Schnabel and H.B. Seed - 1972 (PB 213 100)A03
- EERC 72-3 "Elastic-Plastic Earthquake Response of Soil-Building Systems," by T. Minami - 1972 (PB 214 868)A08
- EERC 72-4 "Stochastic Inelastic Response of Offshore Towers to Strong Motion Earthquakes," by M.K. Kaul - 1972 (PB 215 713)A05
- EERC 72-5 "Cyclic Behavior of Three Reinforced Concrete Flexural Members with High Shear," by E.P. Popov, V.V. Bertero and H. Krawinkler - 1972 (PB 214 555)A05
- EERC 72-6 "Earthquake Response of Gravity Dams Including Reservoir Interaction Effects," by P. Chakrabarti and A.K. Chopra - 1972 (AD 762 330)A08
- EERC 72-7 "Dynamic Properties of Pine Flat Dam," by D. Rea, C.Y. Liaw and A.K. Chopra - 1972 (AD 763 928)A05
- EERC 72-8 "Three Dimensional Analysis of Building Systems," by E.L. Wilson and H.H. Dovey - 1972 (PB 222 438)A06
- EERC 72-9 "Rate of Loading Effects on Uncracked and Repaired Reinforced Concrete Members," by S. Mahin, V.V. Bertero, D. Rea and M. Atalay - 1972 (PB 224 520)A08
- EERC 72-10 "Computer Program for Static and Dynamic Analysis of Linear Structural Systems," by E.L. Wilson, K.-J. Bathe, J.E. Peterson and H.H. Dovey - 1972 (PB 220 437)A04
- EERC 72-11 "Literature Survey - Seismic Effects on Highway Bridges," by T. Iwasaki, J. Penzien and R.W. Clough - 1972 (PB 215 613)A19
- EERC 72-12 "SHAKE-A Computer Program for Earthquake Response Analysis of Horizontally Layered Sites," by P.B. Schnabel and J. Lysmer - 1972 (PB 220 207)A06
- EERC 73-1 "Optimal Seismic Design of Multistory Frames," by V.V. Bertero and H. Kamil - 1973
- EERC 73-2 "Analysis of the Slides in the San Fernando Dams During the Earthquake of February 9, 1971," by H.B. Seed, K.L. Lee, I.M. Idriss and F. Makdisi - 1973 (PB 223 402)A14



- EERC 73-3 "Computer Aided Ultimate Load Design of Unbraced Multistory Steel Frames," by M.B. El-Hafez and G.H. Powell 1973 (PB 248 315)A09
- EERC 73-4 "Experimental Investigation into the Seismic Behavior of Critical Regions of Reinforced Concrete Components as Influenced by Moment and Shear," by M. Celebi and J. Penzien - 1973 (PB 215 884)A09
- EERC 73-5 "Hysteretic Behavior of Epoxy-Repaired Reinforced Concrete Beams," by M. Celebi and J. Penzien - 1973 (PB 239 568)A03
- EERC 73-6 "General Purpose Computer Program for Inelastic Dynamic Response of Plane Structures," by A. Kanaan and G.H. Powell - 1973 (PB 221 260)A08
- EERC 73-7 "A Computer Program for Earthquake Analysis of Gravity Dams Including Reservoir Interaction," by P. Chakrabarti and A.K. Chopra - 1973 (AD 766 271)A04
- EERC 73-8 "Behavior of Reinforced Concrete Deep Beam-Column Subassemblages Under Cyclic Loads," by O. Küstü and J.G. Bouwkamp - 1973 (PB 246 117)A12
- EERC 73-9 "Earthquake Analysis of Structure-Foundation Systems," by A.K. Vaish and A.K. Chopra - 1973 (AD 766 272)A07
- EERC 73-10 "Deconvolution of Seismic Response for Linear Systems," by R.B. Reimer - 1973 (PB 227 179)A08
- EERC 73-11 "SAP IV: A Structural Analysis Program for Static and Dynamic Response of Linear Systems," by K.-J. Bathe, E.L. Wilson and F.E. Peterson - 1973 (PB 221 967)A09
- EERC 73-12 "Analytical Investigations of the Seismic Response of Long, Multiple Span Highway Bridges," by W.S. Tseng and J. Penzien - 1973 (PB 227 816)A10
- EERC 73-13 "Earthquake Analysis of Multi-Story Buildings Including Foundation Interaction," by A.K. Chopra and J.A. Gutierrez - 1973 (PB 222 970)A03
- EERC 73-14 "ADAP: A Computer Program for Static and Dynamic Analysis of Arch Dams," by R.W. Clough, J.M. Raphael and S. Mojtahedi - 1973 (PB 223 763)A09
- EERC 73-15 "Cyclic Plastic Analysis of Structural Steel Joints," by R.B. Pinkney and R.W. Clough - 1973 (PB 226 843)A08
- EERC 73-16 "QUAD-4: A Computer Program for Evaluating the Seismic Response of Soil Structures by Variable Damping Finite Element Procedures," by I.M. Idriss, J. Lysmer, R. Hwang and H.B. Seed - 1973 (PB 229 424)A05
- EERC 73-17 "Dynamic Behavior of a Multi-Story Pyramid Shaped Building," by R.M. Stephen, J.P. Hollings and J.G. Bouwkamp - 1973 (PB 240 718)A06
- EERC 73-18 "Effect of Different Types of Reinforcing on Seismic Behavior of Short Concrete Columns," by V.V. Bertero, J. Hollings, O. Küstü, R.M. Stephen and J.G. Bouwkamp - 1973
- EERC 73-19 "Olive View Medical Center Materials Studies, Phase I," by B. Bresler and V.V. Bertero - 1973 (PB 235 986)A06
- EERC 73-20 "Linear and Nonlinear Seismic Analysis Computer Programs for Long Multiple-Span Highway Bridges," by W.S. Tseng and J. Penzien - 1973
- EERC 73-21 "Constitutive Models for Cyclic Plastic Deformation of Engineering Materials," by J.M. Kelly and P.P. Gillis 1973 (PB 226 024)A03
- EERC 73-22 "DRAIN - 2D User's Guide," by G.H. Powell - 1973 (PB 227 016)A05
- EERC 73-23 "Earthquake Engineering at Berkeley - 1973," (PB 226 033)A11
- EERC 73-24 Unassigned
- EERC 73-25 "Earthquake Response of Axisymmetric Tower Structures Surrounded by Water," by C.Y. Liaw and A.K. Chopra 1973 (AD 773 052)A09
- EERC 73-26 "Investigation of the Failures of the Olive View Stairtowers During the San Fernando Earthquake and Their Implications on Seismic Design," by V.V. Bertero and R.G. Collins - 1973 (PB 235 106)A13
- EERC 73-27 "Further Studies on Seismic Behavior of Steel Beam-Column Subassemblages," by V.V. Bertero, H. Krawinkler and E.P. Popov - 1973 (PB 234 172)A06
- EERC 74-1 "Seismic Risk Analysis," by C.S. Oliveira - 1974 (PB 235 920)A06
- EERC 74-2 "Settlement and Liquefaction of Sands Under Multi-Directional Shaking," by R. Pyke, C.K. Chan and H.B. Seed 1974
- EERC 74-3 "Optimum Design of Earthquake Resistant Shear Buildings," by D. Ray, K.S. Pister and A.K. Chopra - 1974 (PB 231 172)A06
- EERC 74-4 "LUSH - A Computer Program for Complex Response Analysis of Soil-Structure Systems," by J. Lysmer, T. Udaka, H.B. Seed and R. Hwang - 1974 (PB 236 796)A05

- EERC 74-5 "Sensitivity Analysis for Hysteretic Dynamic Systems: Applications to Earthquake Engineering," by D. Ray 1974 (PB 233 213)A06
- EERC 74-6 "Soil Structure Interaction Analyses for Evaluating Seismic Response," by H.B. Seed, J. Lysmer and R. Hwang 1974 (PB 236 519)A04
- EERC 74-7 Unassigned
- EERC 74-8 "Shaking Table Tests of a Steel Frame - A Progress Report," by R.W. Clough and D. Tang - 1974 (PB 240 669)A03
- EERC 74-9 "Hysteretic Behavior of Reinforced Concrete Flexural Members with Special Web Reinforcement," by V.V. Bertero, E.P. Popov and T.Y. Wang - 1974 (PB 236 797)A07
- EERC 74-10 "Applications of Reliability-Based, Global Cost Optimization to Design of Earthquake Resistant Structures," by E. Vitiello and K.S. Pister - 1974 (PB 237 231)A06
- EERC 74-11 "Liquefaction of Gravelly Soils Under Cyclic Loading Conditions," by R.T. Wong, H.B. Seed and C.K. Chan 1974 (PB 242 042)A03
- EERC 74-12 "Site-Dependent Spectra for Earthquake-Resistant Design," by H.B. Seed, C. Ugas and J. Lysmer - 1974 (PB 240 953)A03
- EERC 74-13 "Earthquake Simulator Study of a Reinforced Concrete Frame," by P. Hidalgo and R.W. Clough - 1974 (PB 241 944)A13
- EERC 74-14 "Nonlinear Earthquake Response of Concrete Gravity Dams," by N. Pal - 1974 (AD/A 006 583)A06
- EERC 74-15 "Modeling and Identification in Nonlinear Structural Dynamics - I. One Degree of Freedom Models," by N. Distefano and A. Rath - 1974 (PB 241 548)A06
- EERC 75-1 "Determination of Seismic Design Criteria for the Dumbarton Bridge Replacement Structure, Vol. I: Description, Theory and Analytical Modeling of Bridge and Parameters," by F. Baron and S.-H. Pang - 1975 (PB 259 407)A15
- EERC 75-2 "Determination of Seismic Design Criteria for the Dumbarton Bridge Replacement Structure, Vol. II: Numerical Studies and Establishment of Seismic Design Criteria," by F. Baron and S.-H. Pang - 1975 (PB 259 408)A11 (For set of EERC 75-1 and 75-2 (PB 259 406))
- EERC 75-3 "Seismic Risk Analysis for a Site and a Metropolitan Area," by C.S. Oliveira - 1975 (PB 248 134)A09
- EERC 75-4 "Analytical Investigations of Seismic Response of Short, Single or Multiple-Span Highway Bridges," by M.-C. Chen and J. Penzien - 1975 (PB 241 454)A09
- EERC 75-5 "An Evaluation of Some Methods for Predicting Seismic Behavior of Reinforced Concrete Buildings," by S.A. Mahin and V.V. Bertero - 1975 (PB 246 306)A16
- EERC 75-6 "Earthquake Simulator Study of a Steel Frame Structure, Vol. I: Experimental Results," by R.W. Clough and D.T. Tang - 1975 (PB 243 981)A13
- EERC 75-7 "Dynamic Properties of San Bernardino Intake Tower," by D. Rea, C.-Y. Liaw and A.K. Chopra - 1975 (AD/A008 406) A05
- EERC 75-8 "Seismic Studies of the Articulation for the Dumbarton Bridge Replacement Structure, Vol. I: Description, Theory and Analytical Modeling of Bridge Components," by F. Baron and R.E. Hamati - 1975 (PB 251 539)A07
- EERC 75-9 "Seismic Studies of the Articulation for the Dumbarton Bridge Replacement Structure, Vol. 2: Numerical Studies of Steel and Concrete Girder Alternates," by F. Baron and R.E. Hamati - 1975 (PB 251 540)A10
- EERC 75-10 "Static and Dynamic Analysis of Nonlinear Structures," by D.P. Mondkar and G.H. Powell - 1975 (PB 242 434)A08
- EERC 75-11 "Hysteretic Behavior of Steel Columns," by E.P. Popov, V.V. Bertero and S. Chandramouli - 1975 (PB 252 365)A11
- EERC 75-12 "Earthquake Engineering Research Center Library Printed Catalog," - 1975 (PB 243 711)A26
- EERC 75-13 "Three Dimensional Analysis of Building Systems (Extended Version)," by E.L. Wilson, J.P. Hollings and H.H. Dovey - 1975 (PB 243 989)A07
- EERC 75-14 "Determination of Soil Liquefaction Characteristics by Large-Scale Laboratory Tests," by P. De Alba, C.K. Chan and H.B. Seed - 1975 (NUREG 0027)A08
- EERC 75-15 "A Literature Survey - Compressive, Tensile, Bond and Shear Strength of Masonry," by R.L. Mayes and R.W. Clough - 1975 (PB 246 292)A10
- EERC 75-16 "Hysteretic Behavior of Ductile Moment Resisting Reinforced Concrete Frame Components," by V.V. Bertero and E.P. Popov - 1975 (PB 246 388)A05
- EERC 75-17 "Relationships Between Maximum Acceleration, Maximum Velocity, Distance from Source, Local Site Conditions for Moderately Strong Earthquakes," by H.B. Seed, R. Murarka, J. Lysmer and I.M. Idriss - 1975 (PB 248 172)A03
- EERC 75-18 "The Effects of Method of Sample Preparation on the Cyclic Stress-Strain Behavior of Sands," by J. Mulilis, C.K. Chan and H.B. Seed - 1975 (Summarized in EERC 75-28)

- EERC 75-19 "The Seismic Behavior of Critical Regions of Reinforced Concrete Components as Influenced by Moment, Shear and Axial Force," by M.B. Atalay and J. Penzien - 1975 (PB 258 842)A11
- EERC 75-20 "Dynamic Properties of an Eleven Story Masonry Building," by R.M. Stephen, J.P. Hollings, J.G. Bouwkamp and D. Jurukovski - 1975 (PB 246 945)A04
- EERC 75-21 "State-of-the-Art in Seismic Strength of Masonry - An Evaluation and Review," by R.L. Mayes and R.W. Clough 1975 (PB 249 040)A07
- EERC 75-22 "Frequency Dependent Stiffness Matrices for Viscoelastic Half-Plane Foundations," by A.K. Chopra, P. Chakrabarti and G. Dasgupta - 1975 (PB 248 121)A07
- EERC 75-23 "Hysteretic Behavior of Reinforced Concrete Framed Walls," by T.Y. Wong, V.V. Bertero and E.P. Popov - 1975
- EERC 75-24 "Testing Facility for Subassemblages of Frame-Wall Structural Systems," by V.V. Bertero, E.P. Popov and T. Endo - 1975
- EERC 75-25 "Influence of Seismic History on the Liquefaction Characteristics of Sands," by H.B. Seed, K. Mori and C.K. Chan - 1975 (Summarized in EERC 75-28)
- EERC 75-26 "The Generation and Dissipation of Pore Water Pressures during Soil Liquefaction," by H.B. Seed, P.P. Martin and J. Lysmer - 1975 (PB 252 648)A03
- EERC 75-27 "Identification of Research Needs for Improving Aseismic Design of Building Structures," by V.V. Bertero 1975 (PB 248 136)A05
- EERC 75-28 "Evaluation of Soil Liquefaction Potential during Earthquakes," by H.B. Seed, I. Arango and C.K. Chan - 1975 (NUREG 0026)A13
- EERC 75-29 "Representation of Irregular Stress Time Histories by Equivalent Uniform Stress Series in Liquefaction Analyses," by H.B. Seed, I.M. Idriss, F. Makdissi and N. Banerjee - 1975 (PB 252 635)A03
- EERC 75-30 "FLUSH - A Computer Program for Approximate 3-D Analysis of Soil-Structure Interaction Problems," by J. Lysmer, T. Udaka, C.-F. Tsai and H.B. Seed - 1975 (PB 259 332)A07
- EERC 75-31 "ALUSH - A Computer Program for Seismic Response Analysis of Axisymmetric Soil-Structure Systems," by E. Berger, J. Lysmer and H.B. Seed - 1975
- EERC 75-32 "TRIP and TRAVEL - Computer Programs for Soil-Structure Interaction Analysis with Horizontally Travelling Waves," by T. Udaka, J. Lysmer and H.B. Seed - 1975
- EERC 75-33 "Predicting the Performance of Structures in Regions of High Seismicity," by J. Penzien - 1975 (PB 248 130)A03
- EERC 75-34 "Efficient Finite Element Analysis of Seismic Structure - Soil - Direction," by J. Lysmer, H.B. Seed, T. Udaka, R.N. Hwang and C.-F. Tsai - 1975 (PB 253 570)A03
- EERC 75-35 "The Dynamic Behavior of a First Story Girder of a Three-Story Steel Frame Subjected to Earthquake Loading," by R.W. Clough and L.-Y. Li - 1975 (PB 248 841)A05
- EERC 75-36 "Earthquake Simulator Study of a Steel Frame Structure, Volume II - Analytical Results," by D.T. Tang - 1975 (PB 252 926)A10
- EERC 75-37 "ANSR-I General Purpose Computer Program for Analysis of Non-Linear Structural Response," by D.P. Mondkar and G.H. Powell - 1975 (PB 252 386)A08
- EERC 75-38 "Nonlinear Response Spectra for Probabilistic Seismic Design and Damage Assessment of Reinforced Concrete Structures," by M. Murakami and J. Penzien - 1975 (PB 259 530)A05
- EERC 75-39 "Study of a Method of Feasible Directions for Optimal Elastic Design of Frame Structures Subjected to Earthquake Loading," by N.D. Walker and K.S. Pister - 1975 (PB 257 781)A06
- EERC 75-40 "An Alternative Representation of the Elastic-Viscoelastic Analogy," by G. Dasgupta and J.L. Sackman - 1975 (PB 252 173)A03
- EERC 75-41 "Effect of Multi-Directional Shaking on Liquefaction of Sands," by H.B. Seed, R. Pyke and G.R. Martin - 1975 (PB 258 781)A03
- EERC 76-1 "Strength and Ductility Evaluation of Existing Low-Rise Reinforced Concrete Buildings - Screening Method," by T. Okada and B. Bresler - 1976 (PB 257 906)A11
- EERC 76-2 "Experimental and Analytical Studies on the Hysteretic Behavior of Reinforced Concrete Rectangular and T-Beams," by S.-Y.M. Ma, E.P. Popov and V.V. Bertero - 1976 (PB 260 843)A12
- EERC 76-3 "Dynamic Behavior of a Multistory Triangular-Shaped Building," by J. Petrovski, R.M. Stephen, E. Gartenbaum and J.G. Bouwkamp - 1976 (PB 273 279)A07
- EERC 76-4 "Earthquake Induced Deformations of Earth Dams," by N. Serff, H.B. Seed, F.I. Makdissi & C.-Y. Chang - 1976 (PB 292 065)A08

- EERC 76-5 "Analysis and Design of Tube-Type Tall Building Structures," by H. de Clercq and G.H. Powell - 1976 (PB 252 220) A10
- EERC 76-6 "Time and Frequency Domain Analysis of Three-Dimensional Ground Motions, San Fernando Earthquake," by T. Kubo and J. Penzien (PB 260 556)A11
- EERC 76-7 "Expected Performance of Uniform Building Code Design Masonry Structures," by R.L. Mayes, Y. Omote, S.W. Chen and R.W. Clough - 1976 (PB 270 098)A05
- EERC 76-8 "Cyclic Shear Tests of Masonry Piers, Volume 1 - Test Results," by R.L. Mayes, Y. Omote, R.W. Clough - 1976 (PB 264 424)A06
- EERC 76-9 "A Substructure Method for Earthquake Analysis of Structure - Soil Interaction," by J.A. Gutierrez and A.K. Chopra - 1976 (PB 257 783)A08
- EERC 76-10 "Stabilization of Potentially Liquefiable Sand Deposits using Gravel Drain Systems," by H.B. Seed and J.R. Booker - 1976 (PB 258 820)A04
- EERC 76-11 "Influence of Design and Analysis Assumptions on Computed Inelastic Response of Moderately Tall Frames," by G.H. Powell and D.G. Row - 1976 (PB 271 409)A06
- EERC 76-12 "Sensitivity Analysis for Hysteretic Dynamic Systems: Theory and Applications," by D. Ray, K.S. Pister and E. Polak - 1976 (PB 262 859)A04
- EERC 76-13 "Coupled Lateral Torsional Response of Buildings to Ground Shaking," by C.L. Kan and A.K. Chopra - 1976 (PB 257 907)A09
- EERC 76-14 "Seismic Analyses of the Banco de America," by V.V. Bertero, S.A. Mahin and J.A. Hollings - 1976
- EERC 76-15 "Reinforced Concrete Frame 2: Seismic Testing and Analytical Correlation," by R.W. Clough and J. Gidwani - 1976 (PB 261 323)A08
- EERC 76-16 "Cyclic Shear Tests of Masonry Piers, Volume 2 - Analysis of Test Results," by R.L. Mayes, Y. Omote and R.W. Clough - 1976
- EERC 76-17 "Structural Steel Bracing Systems: Behavior Under Cyclic Loading," by E.P. Popov, K. Takanashi and C.W. Roeder - 1976 (PB 260 715)A05
- EERC 76-18 "Experimental Model Studies on Seismic Response of High Curved Overcrossings," by D. Williams and W.G. Godden - 1976 (PB 269 548)A08
- EERC 76-19 "Effects of Non-Uniform Seismic Disturbances on the Dumbarton Bridge Replacement Structure," by F. Baron and R.E. Hamati - 1976 (PB 282 981)A16
- EERC 76-20 "Investigation of the Inelastic Characteristics of a Single Story Steel Structure Using System Identification and Shaking Table Experiments," by V.C. Matzen and H.D. McNiven - 1976 (PB 258 453)A07
- EERC 76-21 "Capacity of Columns with Splice Imperfections," by E.P. Popov, R.M. Stephen and R. Philbrick - 1976 (PB 260 378)A04
- EERC 76-22 "Response of the Olive View Hospital Main Building during the San Fernando Earthquake," by S. A. Mahin, V.V. Bertero, A.K. Chopra and R. Collins - 1976 (PB 271 425)A14
- EERC 76-23 "A Study on the Major Factors Influencing the Strength of Masonry Prisms," by N.M. Mostaghel, R.L. Mayes, R. W. Clough and S.W. Chen - 1976 (Not published)
- EERC 76-24 "GADFLEA - A Computer Program for the Analysis of Pore Pressure Generation and Dissipation during Cyclic or Earthquake Loading," by J.R. Booker, M.S. Rahman and H.B. Seed - 1976 (PB 263 947)A04
- EERC 76-25 "Seismic Safety Evaluation of a R/C School Building," by B. Bresler and J. Axley - 1976
- EERC 76-26 "Correlative Investigations on Theoretical and Experimental Dynamic Behavior of a Model Bridge Structure," by K. Kawashima and J. Penzien - 1976 (PB 263 388)A11
- EERC 76-27 "Earthquake Response of Coupled Shear Wall Buildings," by T. Srichatrapimuk - 1976 (PB 265 157)A07
- EERC 76-28 "Tensile Capacity of Partial Penetration Welds," by E.P. Popov and R.M. Stephen - 1976 (PB 262 899)A03
- EERC 76-29 "Analysis and Design of Numerical Integration Methods in Structural Dynamics," by H.M. Hilber - 1976 (PB 264 410)A06
- EERC 76-30 "Contribution of a Floor System to the Dynamic Characteristics of Reinforced Concrete Buildings," by L.E. Malik and V.V. Bertero - 1976 (PB 272 247)A13
- EERC 76-31 "The Effects of Seismic Disturbances on the Golden Gate Bridge," by F. Baron, M. Arikan and R.E. Hamati - 1976 (PB 272 279)A09
- EERC 76-32 "Infilled Frames in Earthquake Resistant Construction," by R.E. Klingner and V.V. Bertero - 1976 (PB 265 892)A13

- UCB/EERC-77/01 "PLUSH - A Computer Program for Probabilistic Finite Element Analysis of Seismic Soil-Structure Interaction," by M.P. Romo Organista, J. Lysmer and H.B. Seed - 1977
- UCB/EERC-77/02 "Soil-Structure Interaction Effects at the Humboldt Bay Power Plant in the Ferndale Earthquake of June 7, 1975," by J.E. Valera, H.B. Seed, C.F. Tsai and J. Lysmer - 1977 (PB 265 795)A04
- UCB/EERC-77/03 "Influence of Sample Disturbance on Sand Response to Cyclic Loading," by K. Mori, H.B. Seed and C.K. Chan - 1977 (PB 267 352)A04
- UCB/EERC-77/04 "Seismological Studies of Strong Motion Records," by J. Shoja-Taheri - 1977 (PB 269 655)A10
- UCB/EERC-77/05 "Testing Facility for Coupled-Shear Walls," by L. Li-Hyung, V.V. Bertero and E.P. Popov - 1977
- UCB/EERC-77/06 "Developing Methodologies for Evaluating the Earthquake Safety of Existing Buildings," by No. 1 - B. Bresler; No. 2 - B. Bresler, T. Okada and D. Zisling; No. 3 - T. Okada and B. Bresler; No. 4 - V.V. Bertero and B. Bresler - 1977 (PB 267 354)A08
- UCB/EERC-77/07 "A Literature Survey - Transverse Strength of Masonry Walls," by Y. Omote, R.L. Mayes, S.W. Chen and R.W. Clough - 1977 (PB 277 933)A07
- UCB/EERC-77/08 "DRAIN-TABS: A Computer Program for Inelastic Earthquake Response of Three Dimensional Buildings," by R. Guendelman-Israel and G.H. Powell - 1977 (PB 270 693)A07
- UCB/EERC-77/09 "SUBWALL: A Special Purpose Finite Element Computer Program for Practical Elastic Analysis and Design of Structural Walls with Substructure Option," by D.Q. Le, H. Peterson and E.P. Popov - 1977 (PB 270 567)A05
- UCB/EERC-77/10 "Experimental Evaluation of Seismic Design Methods for Broad Cylindrical Tanks," by D.P. Clough (PB 272 280)A13
- UCB/EERC-77/11 "Earthquake Engineering Research at Berkeley - 1976," - 1977 (PB 273 507)A09
- UCB/EERC-77/12 "Automated Design of Earthquake Resistant Multistory Steel Building Frames," by N.D. Walker, Jr. - 1977 (PB 276 526)A09
- UCB/EERC-77/13 "Concrete Confined by Rectangular Hoops Subjected to Axial Loads," by J. Vallenias, V.V. Bertero and E.P. Popov - 1977 (PB 275 165)A06
- UCB/EERC-77/14 "Seismic Strain Induced in the Ground During Earthquakes," by Y. Sugimura - 1977 (PB 284 201)A04
- UCB/EERC-77/15 "Bond Deterioration under Generalized Loading," by V.V. Bertero, E.P. Popov and S. Viathanatepa - 1977
- UCB/EERC-77/16 "Computer Aided Optimum Design of Ductile Reinforced Concrete Moment Resisting Frames," by S.W. Zagajski and V.V. Bertero - 1977 (PB 280 137)A07
- UCB/EERC-77/17 "Earthquake Simulation Testing of a Stepping Frame with Energy-Absorbing Devices," by J.M. Kelly and D.F. Tsztoo - 1977 (PB 273 506)A04
- UCB/EERC-77/18 "Inelastic Behavior of Eccentrically Braced Steel Frames under Cyclic Loadings," by C.W. Roeder and E.P. Popov - 1977 (PB 275 526)A15
- UCB/EERC-77/19 "A Simplified Procedure for Estimating Earthquake-Induced Deformations in Dams and Embankments," by F.I. Makdisi and H.B. Seed - 1977 (PB 276 820)A04
- UCB/EERC-77/20 "The Performance of Earth Dams during Earthquakes," by H.B. Seed, F.I. Makdisi and P. de Alba - 1977 (PB 276 821)A04
- UCB/EERC-77/21 "Dynamic Plastic Analysis Using Stress Resultant Finite Element Formulation," by P. Lukkunapvasit and J.M. Kelly - 1977 (PB 275 453)A04
- UCB/EERC-77/22 "Preliminary Experimental Study of Seismic Uplift of a Steel Frame," by R.W. Clough and A.A. Huckelbridge 1977 (PB 278 769)A08
- UCB/EERC-77/23 "Earthquake Simulator Tests of a Nine-Story Steel Frame with Columns Allowed to Uplift," by A.A. Huckelbridge - 1977 (PB 277 944)A09
- UCB/EERC-77/24 "Nonlinear Soil-Structure Interaction of Skew Highway Bridges," by M.-C. Chen and J. Penzien - 1977 (PB 276 176)A07
- UCB/EERC-77/25 "Seismic Analysis of an Offshore Structure Supported on Pile Foundations," by D.D.-N. Liou and J. Penzien 1977 (PB 283 180)A06
- UCB/EERC-77/26 "Dynamic Stiffness Matrices for Homogeneous Viscoelastic Half-Planes," by G. Dasgupta and A.K. Chopra - 1977 (PB 279 654)A06
- UCB/EERC-77/27 "A Practical Soft Story Earthquake Isolation System," by J.M. Kelly, J.M. Eiding and C.J. Derham - 1977 (PB 276 814)A07
- UCB/EERC-77/28 "Seismic Safety of Existing Buildings and Incentives for Hazard Mitigation in San Francisco: An Exploratory Study," by A.J. Meltsner - 1977 (PB 281 970)A05
- UCB/EERC-77/29 "Dynamic Analysis of Electrohydraulic Shaking Tables," by D. Rea, S. Abedi-Hayati and Y. Takahashi 1977 (PB 282 569)A04
- UCB/EERC-77/30 "An Approach for Improving Seismic - Resistant Behavior of Reinforced Concrete Interior Joints," by B. Galunic, V.V. Bertero and E.P. Popov - 1977 (PB 290 870)A06

UCB/EERC-78/01 "The Development of Energy-Absorbing Devices for Aseismic Base Isolation Systems," by J.M. Kelly and D.F. Tsztsoo - 1978 (PB 284 978)A04

UCB/EERC-78/02 "Effect of Tensile Prestrain on the Cyclic Response of Structural Steel Connections, by J.G. Bouwkamp and A. Mukhopadhyay - 1978

UCB/EERC-78/03 "Experimental Results of an Earthquake Isolation System using Natural Rubber Bearings," by J.M. Eidinger and J.M. Kelly - 1978 (PB 281 686)A04

UCB/EERC-78/04 "Seismic Behavior of Tall Liquid Storage Tanks," by A. Niwa - 1978 (PB 284 017)A14

UCB/EERC-78/05 "Hysteretic Behavior of Reinforced Concrete Columns Subjected to High Axial and Cyclic Shear Forces," by S.W. Zagajeski, V.V. Bertero and J.G. Bouwkamp - 1978 (PB 283 858)A13

UCB/EERC-78/06 "Inelastic Beam-Column Elements for the ANSR-I Program," by A. Riahi, D.G. Row and G.H. Powell - 1978

UCB/EERC-78/07 "Studies of Structural Response to Earthquake Ground Motion," by O.A. Lopez and A.K. Chopra - 1978 (PB 282 790)A05

UCB/EERC-78/08 "A Laboratory Study of the Fluid-Structure Interaction of Submerged Tanks and Caissons in Earthquakes," by R.C. Byrd - 1978 (PB 284 957)A08

UCB/EERC-78/09 "Model for Evaluating Damageability of Structures," by I. Sakamoto and B. Bresler - 1978

UCB/EERC-78/10 "Seismic Performance of Nonstructural and Secondary Structural Elements," by I. Sakamoto - 1978

UCB/EERC-78/11 "Mathematical Modelling of Hysteresis Loops for Reinforced Concrete Columns," by S. Nakata, T. Sproul and J. Penzien - 1978

UCB/EERC-78/12 "Damageability in Existing Buildings," by T. Blejwas and B. Bresler - 1978

UCB/EERC-78/13 "Dynamic Behavior of a Pedestal Base Multistory Building," by R.M. Stephen, E.L. Wilson, J.G. Bouwkamp and M. Button - 1978 (PB 286 650)A08

UCB/EERC-78/14 "Seismic Response of Bridges - Case Studies," by R.A. Imbsen, V. Nutt and J. Penzien - 1978 (PB 286 503)A10

UCB/EERC-78/15 "A Substructure Technique for Nonlinear Static and Dynamic Analysis," by D.G. Row and G.H. Powell - 1978 (PB 288 077)A10

UCB/EERC-78/16 "Seismic Risk Studies for San Francisco and for the Greater San Francisco Bay Area," by C.S. Oliveira - 1978

UCB/EERC-78/17 "Strength of Timber Roof Connections Subjected to Cyclic Loads," by P. Gülkan, R.L. Mayes and R.W. Clough - 1978

UCB/EERC-78/18 "Response of K-Braced Steel Frame Models to Lateral Loads," by J.G. Bouwkamp, R.M. Stephen and E.P. Popov - 1978

UCB/EERC-78/19 "Rational Design Methods for Light Equipment in Structures Subjected to Ground Motion," by J.L. Sackman and J.M. Kelly - 1978 (PB 292 357)A04

UCB/EERC-78/20 "Testing of a Wind Restraint for Aseismic Base Isolation," by J.M. Kelly and D.E. Chitty - 1978 (PB 292 833)A03

UCB/EERC-78/21 "APOLLO - A Computer Program for the Analysis of Pore Pressure Generation and Dissipation in Horizontal Sand Layers During Cyclic or Earthquake Loading," by P.P. Martin and H.B. Seed - 1978 (PB 292 835)A04

UCB/EERC-78/22 "Optimal Design of an Earthquake Isolation System," by M.A. Bhatti, K.S. Pister and E. Polak - 1978 (PB 294 735)A06

UCB/EERC-78/23 "MASH - A Computer Program for the Non-Linear Analysis of Vertically Propagating Shear Waves in Horizontally Layered Deposits," by P.P. Martin and H.B. Seed - 1978 (PB 293 101)A05

UCB/EERC-78/24 "Investigation of the Elastic Characteristics of a Three Story Steel Frame Using System Identification," by I. Kaya and H.D. McNiven - 1978

UCB/EERC-78/25 "Investigation of the Nonlinear Characteristics of a Three-Story Steel Frame Using System Identification," by I. Kaya and H.D. McNiven - 1978

UCB/EERC-78/26 "Studies of Strong Ground Motion in Taiwan," by Y.M. Hsiung, B.A. Bolt and J. Penzien - 1978

UCB/EERC-78/27 "Cyclic Loading Tests of Masonry Single Piers: Volume 1 - Height to Width Ratio of 2," by P.A. Hidalgo, R.L. Mayes, H.D. McNiven and R.W. Clough - 1978

UCB/EERC-78/28 "Cyclic Loading Tests of Masonry Single Piers: Volume 2 - Height to Width Ratio of 1," by S.-W.J. Chen, P.A. Hidalgo, R.L. Mayes, R.W. Clough and H.D. McNiven - 1978

UCB/EERC-78/29 "Analytical Procedures in Soil Dynamics," by J. Lysmer - 1978

- UCB/EERC-79/01 "Hysteretic Behavior of Lightweight Reinforced Concrete Beam-Column Subassemblages," by B. Forzani, E.P. Popov, and V.V. Bertero - 1979
- UCB/EERC-79/02 "The Development of a Mathematical Model to Predict the Flexural Response of Reinforced Concrete Beams to Cyclic Loads, Using System Identification," by J.F. Stanton and H.D. McNiven - 1979
- UCB/EERC-79/03 "Linear and Nonlinear Earthquake Response of Simple Torsionally Coupled Systems," by C.L. Kan and A.K. Chopra - 1979
- UCB/EERC-79/04 "A Mathematical Model of Masonry for Predicting Its Linear Seismic Response Characteristics," by Y. Mengi and H.D. McNiven - 1979
- UCB/EERC-79/05 "Mechanical Behavior of Lightweight Concrete Confined by Different Types of Lateral Reinforcement," by M.A. Manrique, V.V. Bertero and E.P. Popov - 1979
- UCB/EERC-79/06 "Static Tilt Tests of a Tall Cylindrical Liquid Storage Tank," by R.W. Clough and A. Niwa - 1979
- UCB/EERC-79/07 "The Design of Steel Energy Absorbing Restrainers and Their Incorporation Into Nuclear Power Plants for Enhanced Safety: Volume 1 - Summary Report," by P.N. Spencer, V.F. Zackay, and E.R. Parker - 1979
- UCB/EERC-79/08 "The Design of Steel Energy Absorbing Restrainers and Their Incorporation Into Nuclear Power Plants for Enhanced Safety: Volume 2 - The Development of Analyses for Reactor System Piping," "Simple Systems" by M.C. Lee, J. Penzien, A.K. Chopra, and K. Suzuki "Complex Systems" by G.H. Powell, E.L. Wilson, R.W. Clough and D.G. Row - 1979
- UCB/EERC-79/09 "The Design of Steel Energy Absorbing Restrainers and Their Incorporation Into Nuclear Power Plants for Enhanced Safety: Volume 3 - Evaluation of Commercial Steels," by W.S. Owen, R.M.N. Pelloux, R.O. Ritchie, M. Faral, T. Ohhashi, J. Toplosky, S.J. Hartman, V.F. Zackay, and E.R. Parker - 1979
- UCB/EERC-79/10 "The Design of Steel Energy Absorbing Restrainers and Their Incorporation Into Nuclear Power Plants for Enhanced Safety: Volume 4 - A Review of Energy-Absorbing Devices," by J.M. Kelly and M.S. Skinner - 1979
- UCB/EERC-79/11 "Conservatism In Summation Rules for Closely Spaced Modes," by J.M. Kelly and J.L. Sackman - 1979

- UCB/EERC-79/12 "Cyclic Loading Tests of Masonry Single Piers Volume 3 - Height to Width Ratio of 0.5," by P.A. Hidalgo, R.L. Mayes, H.D. McNiven and R.W. Clough - 1979
- UCB/EERC-79/13 "Cyclic Behavior of Dense Coarse-Grained Materials in Relation to the Seismic Stability of Dams," by N.G. Banerjee, H.B. Seed and C.K. Chan - 1979
- UCB/EERC-79/14 "Seismic Behavior of Reinforced Concrete Interior Beam-Column Subassemblages," by S. Viathanatepa, E.P. Popov and V.V. Bertero - 1979
- UCB/EERC-79/15 "Optimal Design of Localized Nonlinear Systems with Dual Performance Criteria Under Earthquake Excitations," by M.A. Bhatti - 1979
- UCB/EERC-79/16 "OPTDYN - A General Purpose Optimization Program for Problems with or without Dynamic Constraints," by M.A. Bhatti, E. Polak and K.S. Pister - 1979
- UCB/EERC-79/17 "ANSR-II, Analysis of Nonlinear Structural Response, Users Manual," by D.P. Mondkar and G.H. Powell - 1979
- UCB/EERC-79/18 "Soil Structure Interaction in Different Seismic Environments," A. Gomez-Masso, J. Lysmer, J.-C. Chen and H.B. Seed - 1979
- UCB/EERC-79/19 "ARMA Models for Earthquake Ground Motions," by M.K. Chang, J.W. Kwiatkowski, R.F. Nau, R.M. Oliver and K.S. Pister - 1979
- UCB/EERC-79/20 "Hysteretic Behavior of Reinforced Concrete Structural Walls," by J.M. Vallenias, V.V. Bertero and E.P. Popov - 1979
- UCB/EERC-79/21 "Studies on High-Frequency Vibrations of Buildings I: The Column Effects," by J. Lubliner - 1979
- UCB/EERC-79/22 "Effects of Generalized Loadings on Bond Reinforcing Bars Embedded in Confined Concrete Blocks," by S. Viathanatepa, E.P. Popov and V.V. Bertero - 1979
- UCB/EERC-79/23 "Shaking Table Study of Single-Story Masonry Houses, Volume 1: Test Structures 1 and 2," by P. Gülkan, R.L. Mayes and R.W. Clough - 1979
- UCB/EERC-79/24 "Shaking Table Study of Single-Story Masonry Houses, Volume 2: Test Structures 3 and 4," by P. Gülkan, R.L. Mayes and R.W. Clough - 1979
- UCB/EERC-79/25 "Shaking Table Study of Single-Story Masonry Houses, Volume 3: Summary, Conclusions and Recommendations," by R.W. Clough, R.L. Mayes and P. Gülkan - 1979



- UCB/EERC-79/26 "Recommendations for a U.S.-Japan Cooperative Research Program Utilizing Large-Scale Testing Facilities," by U.S.-Japan Planning Group - 1979
- UCB/EERC-79/27 "Earthquake-Induced Liquefaction Near Lake Amatitlan, Guatemala," by H.B. Seed, I. Arango, C.K. Chan, A. Gomez-Masso and R. Grant de Ascoli - 1979
- UCB/EERC-79/28 "Infill Panels: Their Influence on Seismic Response of Buildings," by J.W. Axley and V.V. Bertero - 1979
- UCB/EERC-79/29 "3D Truss Bar Element (Type 1) for the ANSR-II Program," by D.P. Mondkar and G.H. Powell - 1979
- UCB/EERC-79/30 "2D Beam-Column Element (Type 5 - Parallel Element Theory) for the ANSR-II Program," by D.G. Row, G.H. Powell and D.P. Mondkar
- UCB/EERC-79/31 "3D Beam-Column Element (Type 2 - Parallel Element Theory) for the ANSR-II Program," by A. Riahi, G.H. Powell and D.P. Mondkar - 1979
- UCB/EERC-79/32 "On Response of Structures to Stationary Excitation," by A. Der Kiureghian - 1979
- UCB/EERC-79/33 "Undisturbed Sampling and Cyclic Load Testing of Sands," by S. Singh, H.B. Seed and C.K. Chan - 1979
- UCB/EERC-79/34 "Interaction Effects of Simultaneous Torsional and Compressional Cyclic Loading of Sand," by P.M. Griffin and W.N. Houston - 1979
- UCB/EERC-80/01 "Earthquake Response of Concrete Gravity Dams Including Hydrodynamic and Foundation Interaction Effects," by A.K. Chopra, P. Chakrabarti and S. Gupta - 1980
- UCB/EERC-80/02 "Rocking Response of Rigid Blocks to Earthquakes," by C.S. Yim, A.K. Chopra and J. Penzien - 1980
- UCB/EERC-80/03 "Optimum Inelastic Design of Seismic-Resistant Reinforced Concrete Frame Structures," by S.W. Zagajeski and V.V. Bertero - 1980
- UCB/EERC-80/04 "Effects of Amount and Arrangement of Wall-Panel Reinforcement on Hysteretic Behavior of Reinforced Concrete Walls," by R. Iliya and V.V. Bertero - 1980

